THE MICROSTRUCTURAL EVOLUTION OF ALUMINUM DURING THE COURSE OF HIGH TEMPERATURE CREEP

BY

RICHARD G. CONNELL, JR.

A Dissertation Presented to the Graduate Council
of the University of Florida
in Partial Fulfillment of the Requirements for the
Degree of Doctor of Philosophy

UNIVERSITY OF FLORIDA

1973

74-9590

CONNELL, Richard Grant, Jr., 1938-
THE MICROSTRUCTURAL EVOLUTION OF ALUMINUM DURING THE COURSE OF HIGH TEMPERATURE CREEP.

The University of Florida, Ph.D., 1973
Engineering, metallurgy

University Microfilms, A XEROX Company, Ann Arbor, Michigan

© 1974

RICHARD GRANT CONNELL, Jr.

ALL RIGHTS RESERVED

To my wife, Linda, and children,

Deborah and Richard

ACKNOWLEDGEMENTS

The author wishes to express his gratitude to the members of his supervisory committee for their service on the committee and for their guidance during his course of study. In particular, the author is indebted to Dr. Frederick N. Rhines for his continuous interest in the research and for the many hours of discussion related to hot deformation. Discussions with Professors Robert T. DeHoff, Ellis D. Verink, Jr., and Robert E. Reed-Hill were of significant benefit and are hereby acknowledged.

It is with gratitude that the author acknowledges the financial support of the Engineering and Industrial Experiment Station at the University of Florida, under whose sponsorship a majority of this research was conducted.

TABLE OF CONTENTS

		Page
ACKNOWLEDGEMENTS		iv
LIST OF TABLES		viii
LIST OF FIGURES		x
ABSTRACT		xx
CHAPTER		
I	INTRODUCTION	1
	1.1. Scope of the Research	2
	1.2. The Scientific Background for the Research	2
II	EXPERIMENTAL TECHNIQUES	58
	2.1. The Material	58
	2.2. Fabrication of Creep Specimens	60
	2.3. Creep Testing	67
	2.4. Metallographic Techniques	73
III	OBSERVATIONS AND RESULTS	87
	3.1. Observations of Surface Features	90
	3.2. The Development of Substructure	99
	3.3. Grain Boundary Serrations Formed During Creep	117
	3.4. Relations Between Grain Boundary Serrations and the Subgrain Morphology	120
	3.5. The Nature of Subgrain Rows	124
	3.6. The Effect of Grain Boundaries on Deformation	166
	3.7. The Microstructural Evolution During Creep I: Results from Constant Load and Constant Temperature Creep Tests	167

TABLE OF CONTENTS (continued)

CHAPTER		Page
III	(continued)	
	3.8. The Microstructural Evolution During Creep II: Results from Variable Load and Temperature Creep Tests	287
	3.9. The Evidence for Shear Along Subgrain Boundaries	382
	3.10. A Summary of the Observations and Results	400
IV	DISCUSSION	408
	4.1. Grain Boundaries and Deformation .	412
	4.2. A Schematic Representation of High Temperature Creep	428
	4.3. The Microstructural Evolution with Respect to the Schematic Representation of Hot Deformation .	434
V	CONCLUSIONS	453
VI	FUTURE WORK	456
	6.1. The Kinetics of Shearing Along Subgrain Boundaries	456
	6.2. A Correlation Between the Onset of Tertiary Creep and Microstructure	457
	6.3. The Effects of Minor Alloying Additions to Aluminum Upon the Kinetics of Sub-boundary Shearing .	458
	6.4. The Effects of Subgrain Structures Produced by Creep Upon the Mechanical Properties at Ordinary Temperatures	460
APPENDIX		
I	EQUATIONS FOR THE TIME DEPENDENCE OF STRAIN DURING PRIMARY CREEP	462
II	SOLUTIONS FOR ELECTROPOLISHING AND ANODIZING	463
III	THE PHOTOENGRAVING PROCESS	464

TABLE OF CONTENTS (continued)

APPENDIX		Page
IV	LIST OF SPECIMENS AND DEFORMATION CONDITIONS	465
V	WORK SHEET FOR THE CALCULATION OF STATISTICAL TOLERANCE LIMITS ON THE MEAN OF N_L	470
VI	FORTRAN IV PROGRAM FOR CALCULATING THE MEAN VALUES OF N_L AND THE TOLERANCE LIMITS	471
VII	QUANTITATIVE METALLOGRAPHIC DATA FOR SPECIMEN S3-12	473
VIII	A GEOMETRIC CONCEPT OF GRAIN BOUNDARIES	478
IX	CALCULATIONS OF THE LENGTH OF DISLOCATION LINE WHICH PRODUCES EXTERNAL SHAPE CHANGE AND THE LENGTH OF DISLOCATION LINE STORED IN SUB-BOUNDARIES	513
BIBLIOGRAPHY		517
BIOGRAPHICAL SKETCH		528

LIST OF TABLES

Table		Page
I	Chemical Analysis of Aluminum	59
II	Planes Corresponding to Surface Bands and Boundaries Between Subgrain Rows . . .	147
III	Etch Pit Measurements: Grain #1	149
IV	Etch Pit Measurements: Grain #2	150
V	Etch Pit Measurements: Grain #3	151
VI	Etch Pit Measurements: Grain #10	152
VII	Etch Pit Measurements: Grain #5	153
VIII	The Creep Testing Conditions for the Evaluation of the Microstructural Evolution During Creep	169
IX	The Conditions of Creep Testing and Secondary Creep Rates	171
X	Assumed Activation Energies, ΔH; Stress Sensitivity Constants, n; Intercepts, log A; and Sums of the Squares of the Deviations, $\Sigma(\log ZH_i - \log \tilde{ZH}_i)^2$	173
XI	Specimens, Creep Conditions, and Microstructural Parameters	178
XII	The Rates of Subgrain Boundary Formation During the Creep of Aluminum	207
XIII	Assumed Activation Energies, ΔH; Stress Sensitivity Constants, m; Intercepts, log B; and Sums of the Squares of the Deviations, $\Sigma(\log C_i - \log \tilde{C}_i)^2$	209

LIST OF TABLES (continued)

Table		Page
XIV	Specimens, Creep Conditions, Strain, and $f_{SGR}/f_{SG}-f_{SGR}$	235
XV	Creep Testing Conditions for the Preliminary Experiments	290
XVI	Creep Testing Conditions, Strain Rates and Microstructural Parameters for Specimens Tested Under Conditions of Stepped Variations in Stress and Temperature	319
XVII	Creep Tests of Specimen S5-30	393
IV-1	Specimens Creep Tested Under Conditions of Constant Load and Constant Temperature	465
IV-2	Specimens Tested at Constant Strain Rate	467
IV-3	Specimens Creep Tested Under Conditions of Variable Load and Variable Temperature.	468
VII-1	Lineal Intercept Counts	473
VII-2	Counts of Grains Containing Subgrains and Subgrain Rows, and the Angles Between Subgrain Rows and the Tensile Axis	476

LIST OF FIGURES

Figure		Page
1	Shear stress versus shear strain for f.c.c. single crystals	53
2	Flow sheet for the fabrication of Series 1 creep specimens	61
3	Flow sheet for the fabrication of Series 3 creep specimens	62
4	Flow sheet for the fabrication of Series 4 specimens	63
5	Flow sheet for the fabrication of Series 5 creep specimens	64
6	Creep specimen dimensions.	65
7	A photomicrograph of the square grid photoengraved on the sides of some creep specimens	66
8	Schematic diagram of creep testing apparatus	68
9	Creep specimen, grips and hanger rods . .	69
10	Mounted metallographic specimens	74
11	Automatic mechanical polishing apparatus	76
12	Anodizing cell	77
13	Schematic microstructure of a creep strained specimen	81
14	Schematic diagram of smooth and serrated grain boundary serrations, based upon the period and amplitude of serrations	83

LIST OF FIGURES (continued)

Figure		Page
15	Intercepts of a test line with grain boundaries	84
16	Surface bands in specimen 4 tested at 200°C under an initial stress of 1,000 psi for 18.98 hours	92
17	Surface bands in specimen S1-2 tested at 200°C under an initial stress of 1,000 psi for 24.05 hours to a strain of 0.049	94
18	Surface bands in specimen S1-6 tested at 200°C under an initial stress of 1,000 psi for 12.03 hours to a strain of 0.032	95
19	Surface bands in specimen S3-6 tested at 425°C under an initial stress of 150 psi for 4 hours to a strain of 0.016 . . .	96
20	Surface structure of specimen S3-18 tested at 275°C under an initial stress of 800 psi for 5.38 hours to a strain of 0.176	98
21	Microstructures of creep specimens	102
22	Microstructures of creep specimens tested at 425°C	103
23	Microstructures of creep specimens tested at 350°C	105
24	Microstructures of creep specimens tested at 275°C	107
25	Microstructures of creep specimens tested at 200°C under an initial stress of 800 psi	109
26	Microstructures of fine-grained creep specimens tested at 200°C under an initial stress of 1,000 psi	110

LIST OF FIGURES (continued)

Figure		Page
27	Microstructures of coarse-grained creep specimens tested at 200°C under an initial stress of 1,000 psi	111
28	Microstructures of creep specimens tested at 200°C under an initial stress of 1,200 psi	112
29	Microstructures of creep specimens tested at a nominal temperature of 130°C	113
30	Microstructures of specimens tested at room temperature at constant strain rates	114
31	Microstructures illustrating wavy and dentate grain boundary serrations	119
32	The microstructure of specimen S5-7 illustrating well-defined subgrain rows in adjacent grains and very sharp, dentate grain boundary serrations	122
33	The microstructure of specimen S1-4 illustrating that the boundaries around a single grain, "A," may be smooth, "S," wavy, "W," or dentate, "D."	123
34	Position of metallographic specimen with respect to the geometry of creep specimens	126
35	The microstructure of specimen S1-8 illustrating the alternating shading of subgrain rows as observed under polarized light	128
36	Photomicrographs showing the subgrain row pattern in specimen S5-7	134
37	The orientation of subgrain rows in specimen S5-7	135
38	Stereographic plots of planes (AB and AC) corresponding to boundaries separating subgrain rows	136

LIST OF FIGURES (continued)

Figure		Page
39	Strip-wood model illustrating the three-dimensional nature of subgrain rows . . .	138
40	The microstructure of specimen S5-7 showing subgrain rows and etch pits which indicate crystallographic orientation	140
41	Traces of surface bands on specimen S5-8 . .	144
42	Subgrain row traces in specimen S5-8 . . .	145
43	Stereographic projection of the orientation of grain #1 and the planes determined from the traces of surface bands and from the traces of subgrain rows	154
44	Stereographic projection of the orientation of grain #2 and the planes determined from the traces of surface bands and from the traces of subgrain rows . . .	155
45	Stereographic projection of the orientation of grain #3 and the planes determined from the traces of surface bands and from the traces of subgrain rows . . .	156
46	Stereographic projection of the orientation of grain #10 and the planes determined from the traces of surface bands and from the traces of subgrain rows . . .	157
47	Stereographic projection of the orientation of grain #5 and the planes determined from the traces of surface bands . .	158
48	Photomicrographs showing the alignment between surface bands and subgrain rows .	164
49	$\Sigma(\log ZH_i - \log \tilde{} ZH_i)^2$ versus ΔH	174
50	Log ZH ($ZH = \dot{\varepsilon}\, e^{\Delta H/RT}$) versus log σ (σ = stress (psi))	175
51	Grain boundary area, $S_{V(GB)}$, versus time, t.	184

LIST OF FIGURES (continued)

Figure		Page
52	Grain boundary area, $S_{V(GB)}$, versus strain, ε	192
53	Subgrain boundary area, $S_{V(SGB)}$, versus time, t	200
54	$\Sigma(\log C_i - \log \tilde{C}_i)^2$ versus ΔH	210
55	Log C ($C = \dot{S}_{V(SGB)} e^{\Delta H/RT}$) versus log σ (σ = stress (psi))	211
56	Subgrain boundary area, $S_{V(SGB)}$, versus strain, ε	213
57	Fraction of grains containing subgrains, f_{SG}, and fraction of grains containing subgrain rows, f_{SGR}, versus time, t	221
58	Fraction of grains containing subgrains, f_{SG}, and fraction of grains containing subgrain rows, f_{SGR}, versus strain, ε	227
59	Histograms showing the distribution of the angles between subgrain rows and the tensile axis	236
60	Fraction of the grain boundary area which is serrated, $\tilde{S}_V/S_{V(GB)}$, versus time, t	247
61	Fraction of the grain boundary area which is serrated, $\tilde{S}_V/S_{V(GB)}$, versus strain, ε	253
62	Fraction of grain boundary area which is serrated, $\tilde{S}_V/S_{V(GB)}$, versus fractions of grains which contain subgrains, f_{SG}, subgrain rows, f_{SGR}, and only subgrains of random morphology, $f_{SG}-f_{SGR}$	261
63	The change in grain boundary anisotropy, $e_g(f)-e_g(i)$, versus time, t	273
64	The change in grain boundary anisotropy, $e_g(f)-e_g(i)$, versus strain, ε	281

LIST OF FIGURES (continued)

Figure		Page
65	Strain, ε, and temperature, T, versus time, t, for specimen S5-5	291
66	Strain, ε, and temperature, T, versus time, t, for specimen S5-6	292
67	Strain, ε, and temperature, T, versus time, t, for specimen S5-7	293
68	Strain, ε, and temperature, T, versus time, t, for specimen S5-9	294
69	Strain, ε, and temperature, T, versus time, t, for specimen S5-11	295
70	Strain, ε, and temperature, T, versus time, t, for specimen S5-12	296
71	Strain, ε, and temperature, T, versus time, t, for specimen S5-13	297
72	Microstructure of specimen S5-5 illustrating subgrain rows and dentate grain boundary serrations	300
73	Microstructure of specimen S5-6 illustrating wavy grain boundary serrations and the random morphology of subgrains	304
74	Microstructure of specimen S5-7 illustrating subgrain rows and dentate grain boundary serrations	307
75	Microstructure of specimen S5-9 illustrating subgrain rows and grain boundary serrations	310
76	Microstructure of specimen S5-11 illustrating the subgrain structure and grain boundary serrations developed during 24 hours of creep at 300°C under an initial stress of 450 psi	313

LIST OF FIGURES (continued)

Figure		Page
77	Microstructure of specimen S5-12 showing that no observable subgrain structure was developed during 24 hours of creep at 200°C under an initial stress of 450 psi	314
78	Microstructure of specimen S5-13 illustrating the subgrain structure and grain boundary serrations developed in a stepped temperature creep test under an initial stress of 450 psi	315
79	Strain, ε, and temperature T, versus time, t, for specimen S5-38	326
80	Strain, ε, and temperature, T, versus time, t, for specimen S5-31	327
81	Strain, ε, and temperature, T, versus time, t, for specimen S5-43	328
82	Strain, ε, and temperature, T, versus time, t, for specimen S5-45	329
83	Strain, ε, and temperature, T, versus time, t, for specimen S5-40	330
84	Strain, ε, and temperature, T, versus time, t, for specimen S5-41	331
85	Strain, ε, and temperature, T, versus time, t, for specimen S5-42	332
86	Strain, ε, and temperature, T, versus time, t, for specimen S5-44	333
87	Strain, ε, and temperature, T, versus time, t, for specimen S5-39	334
88	Grain boundary area, $S_{v(GB)}$, versus time, t	336
89	Subgrain boundary area, $S_{v(SGB)}$, versus time, t	340

LIST OF FIGURES (continued)

Figure		Page
90	Fraction of grains containing subgrains, f_{SG}, versus time, t	343
91	Microstructures illustrating the effects of precreep upon subgrain structure	346
92	Fraction of grains containing subgrain rows, f_{SGR}, versus time, t, for specimens of the first experiment	350
93	Fraction of the grain boundary area which is serrated, $\tilde{S}_V/S_{V(GB)}$, versus time, t	354
94	Fraction of the grain boundary area which is serrated, $\tilde{S}_V/S_{V(GB)}$, versus fractions of grains containing subgrains, f_{SG}, subgrain rows, f_{SGR}, and the random morphology of subgrains, f_{SG}-f_{SGR}	357
95	Histograms showing the distribution of angles between subgrain rows and the tensile axis	361
96	Change in grain boundary anisotropy, $e_g(f)$-$e_g(i)$, versus time, t	365
97	Laue x-ray diffraction photograph from specimen S5-38	368
98	Laue x-ray diffraction photograph from specimen S5-31	369
99	Laue x-ray diffraction photograph from specimen S5-43	370
100	Laue x-ray diffraction photograph from specimen S5-45	371
101	Laue x-ray diffraction photographs from specimen S5-40	372
102	Laue x-ray diffraction photograph from specimen S5-41	374

LIST OF FIGURES (continued)

Figure		Page
103	Laue x-ray diffraction photograph from specimen S5-42	375
104	Laue x-ray diffraction photograph from specimen S5-44	376
105	Laue x-ray diffraction photograph of specimen S5-39	377
106	Photomicrographs showing the alignment of subgrain rows and ledges in the edge of a creep specimen	384
107	Photomicrograph showing the ledge in the edge of a creep specimen produced by grain boundary shear	387
108	Photomicrograph showing surface bands aligned with shear steps in a photo-engraved grid	388
109	Photographs of a three-dimensional model of a serrated grain boundary	389
110	Displacement of surface reference scratches in specimen S5-30	394
111	Microstructure of specimen S5-30 after test	401
112	Grain boundary shearing as an adjustment required by a violation of the condition of contiguity	417
113	The development of subgrain rows	420
114	Three-dimensional lattice bending and the formation of sub-boundaries . . .	422
115	Shearing along the boundaries separating subgrain rows	425
116	Three-dimensional view of bi-directional shearing to produce dentate grain boundary serrations	427
117	Block diagram of the schematic representation of high temperature creep . . .	429

LIST OF FIGURES (continued)

Figure		Page
VIII-1	Twist boundary formed by rotating one-half of a crystal with respect to the other through an angle, ρ	479
VIII-2	Two-dimensional grain sheared to form a tilt orientation with respect to the plane of the boundary interface .	481
VIII-3	The formation of a simple tilt boundary by joining two grains which have been sheared oppositely	482
VIII-4	Single tilts (a) and (b), and a skew (c) of a crystal with respect to the plane of the boundary interface	483
VIII-5	Geometric difference between a twist boundary (a) and a skew boundary (b) . .	485
VIII-6	Combinations of tilts and a skew of a crystal with respect to the plane of the boundary interface	486
VIII-7	Classification of tilt boundaries . . .	487
VIII-8	Combinations of symmetrical and non-symmetrical tilts in forming a grain boundary	490
VIII-9	Stereographic projections showing the differences in the orientations of the conjoint crystals with respect to the plane of the boundary interface	494
VIII-10	Stereographic plots of grain boundaries corresponding to those shown in Figure VIII-8	498
VIII-11	Stereographic plot of the boundary formed between two simple cubic crystals by double symmetrical tilting .	504
VIII-12	Stereographic plots of the orientations of conjoint grains relative to the plane of the boundary interface . .	506

Abstract of Dissertation Presented to the Graduate Council of the University of Florida in Partial Fulfillment of the Requirements for the Degree of Doctor of Philosophy

THE MICROSTRUCTURAL EVOLUTION OF ALUMINUM DURING THE COURSE OF HIGH TEMPERATURE CREEP

By

Richard G. Connell, Jr.

March, 1973

Chairman: Dr. Frederick N. Rhines
Major Department: Materials Science and Engineering

In polycrystalline metals it is well recognized that the microstructures which develop during the course of hot deformation are more inhomogeneous than those produced by equivalent amounts of deformation at ordinary temperatures. As the microstructure evolves during the course of hot deformation from that of an initially annealed state to that of a typical hot deformed structure, the grain boundaries, as observed in metallographically prepared surfaces, assume paths which alternate sharply back and forth across their originally smooth contours. With large amounts of strain, the grain boundaries attain a distinctively dentate form.

A detailed investigation of the microstructural evolution during the hot creep of aluminum was made to determine the relations that exist between the formation of dentate grain boundary serrations and the mechanisms involved in

high temperature creep. Quantitative metallographic techniques were employed to evaluate the microstructures produced by increasing amounts of creep strain at several temperatures between 100°C and 425°C under various initial applied stresses from 150 to 4,000 psi. The microstructures produced during creep were retained for metallographic evaluation by quenching the creep specimens from the temperature of deformation while the loading was maintained.

Concurrent with the evolution of the microstructure in aluminum during high temperature creep, subgrain rows gradually form within grains until all of the grains contain subgrain rows. When the rows are first formed, the crystallographic misorientation across the boundaries separating the rows of subgrains is small; with the progress of deformation it increases until the sub-boundaries represent misorientations equivalent to those of ordinary grain boundaries. When the misorientation across the sub-boundaries becomes large, and subgrain rows exist in grains on opposite sides of common grain boundaries, the grain boundaries take on an appearance which is dentate in form. Late in the progress of creep, shearing occurs along the boundaries separating subgrain rows.

Based upon the results of this research, and upon considerations of the constraints to deformation imposed by the presence of grain boundaries, it is proposed that the dentate grain boundary serrations formed during the hot creep of

aluminum are the result of macroscopic shearing which occurs along the boundaries of subgrain rows. This shearing is cooperative across grain boundaries.

Shear along the boundaries separating subgrain rows and formation of dentate grain boundary serrations commences concurrently with the onset of tertiary creep. Further, sub-boundary shearing is viewed as a recovery process. Therefore, it is proposed that an additional amount of recovery associated with sub-boundary shearing contributes to an accelerating creep rate and the beginning of third-stage creep.

CHAPTER I

INTRODUCTION

The way in which a polycrystalline metal responds by plastic deformation to an enduring stress at an elevated temperature depends upon the way in which the microstructure is altered during the course of deformation. The temperature and the stress control the microstructural evolution; and, in turn, the microstructural evolution controls the plastic response of the metal.

Initiation of the present research was prompted because little is known of the mechanisms by which metals deform at high temperature except that there exist important differences between the plastic response at high temperature and that at ordinary temperature. It is generally agreed upon that metals at high temperature deform rather more inhomogeneously than at ordinary temperatures. Further, the great rate-sensitivity of hot working metals may be explained partially by the competition that develops between work hardening and thermal recovery. The effects of inhomogeneous deformation and thermal recovery are both manifested, at least in part, by changes in the microstructure during deformation. Therefore, a logical approach to investigate the mechanisms by which metals deform is to monitor the

microstructural evolution during the course of hot deformation and to study its interrelations amongst the plastic response of the metal and the parameters of the deformation: stress, temperature, strain and strain rate.

1.1. Scope of the Research

A major portion of this research is confined to a study of the microstructural evolution which takes place concurrently with the high temperature creep of high purity aluminum. A special emphasis has been placed upon discovering the mechanism by which dentate grain boundary serrations form during hot working. From the outset it was believed that such an approach would lead to a significantly more complete understanding of hot deformation in terms of the shear which results in microscopic shape changes and the nature of the internal disorder left behind by the various hot deformation processes. As a result of the present research, these objectives have been realized.

1.2. The Scientific Background for the Research

The current research, confined primarily to a study of the microstructural evolution during the course of high temperature creep, has required a background of scientific knowledge in several metallurgical subject areas. In addition to the obvious topics dealing with the historical

background and the phenomenological nature of creep, six other subjects are reviewed in the ensuing sections. These six subjects -- the microstructural features of slip, the microstructural features of deformation bands and kink bands, the formation of subgrains, the formation of grain boundary serrations, grain boundary sliding* and dynamic recovery -- are all important to the research because each in some way is connected to the interrelation between microstructural evolution during creep and the mechanical response of a metal to the various parameters of deformation: stress, temperature, strain and strain rate.

1.2.1. A Brief Historical Review

The beginning of a scientific approach to the subject of hot deformation dates back to just before the turn of the century and the discovery of the crystallinity of metals. Among notable contributors to an understanding of the crystalline nature of metals were Stead [1], Desch [2], Humfrey [3], Rosenhain and Humfrey [4] and Osmond and Cartaud [5].

Since this early work, the concepts of deformation have progressed through three overlapping periods: 1898 to the present, crystallographic slip; 1910 to the early 1920's, the amorphous metal hypothesis; late 1940's to the present,

---

*The term "grain boundary sliding" is used in this dissertation in order to maintain consistency with the literature; however, the author believes the term to be misleading in that it implies that shear occurs along the grain boundary interface rather than in a layer of material adjacent to the interface.

microstructural and atomistic views of deformation. The concepts of crystallographic slip began development with Mügge's [6,7,8] study of slip lines in relation to crystallographic planes. In the face-centered-cubic metals -- copper, gold, silver and lead -- he found that slip followed {111} planes. Simultaneously, Ewing and Rosenhain [9,10] discovered slip in lead and proposed block movements which accompany deformation.

The amorphous metal hypothesis had its beginning in the work of Beilby [11], who, upon studying the earlier work of Lord Rayleigh on polished metal surfaces, first ascribed a hardening effect to a highly distorted structure. The amorphous metal hypothesis was extended by Rosenhain along with several other investigators [4,12-17] to the structure of grain boundaries. The observation that grain boundaries resist deformation was taken as evidence for the presence of a hard, deformation resistant structure cementing together individual grains in an aggregate. Rosenhain and Ewen [14] found that intergranular fractures could be produced in lead, tin, gold and bismuth under very small stresses at temperatures from 3° to 20°C below the melting point. The authors believed that such an observation could be accounted for only by a layer of amorphous material along the grain boundary surfaces. At very high temperatures such an amorphous film would behave in a viscous manner when subjected to small stresses. Further support of this concept was obtained when "intercrystalline fractures" were

observed in low carbon steels which had been ruptured at elevated temperatures [4].

Chappell [18] in his study of transcrystalline fractures in low carbon steels postulated that what often appeared as intergranular fractures at high temperatures may in fact be the result of fracture along paths separating grain fragments. Thus, the suggestion was that grains became fragmented during hot deformation and that these fragments were cemented together by an amorphous cement. The rupture was presumed to result from fracture through the amorphous cement.

In 1916, Howe [19] summarized the state of knowledge concerning the types of motion which occur within polycrystalline metals during deformation. Howe's classification of the types of motion is given as follows:

Types of Motion

Fluid			
Block	Noncrystalline	Intergranular	Movement of irregular grain fragments
	Crystalline	Slip	
		Twinning	Annealing (broad twins)
			Mechanical (Neumann lamellae or narrow twins)

In making the distinction between fluid motion and block motion, Howe made the following statement in connection with fluid motion:

> So with steam expanding in a cylinder, with glass on the pontil, clay on the potter's wheel, and putty and dough when kneaded, ubiquitous stress causing ubiquitous and almost necessarily irregular shear. [19, p. 293]

Block movement, on the other hand, was believed by Howe to consist of the motion of whole blocks of structure which in themselves remained intact throughout relative movement with respect to one another. Jefferies [20] proposed the concept of the equicohesive temperature in relation to the viscous behavior of grain boundaries at high temperature. The equicohesive temperature was defined as that temperature above which the cohesion in amorphous regions adjacent to grain boundaries was less than that of crystalline metal. Hence, above the equicohesive temperature viscous flow along the grain boundaries would occur. In relation to the behavior of grain boundaries during deformation at elevated temperatures, the viscous nature of an amorphous grain boundary cement persisted to the early 1920's and the beginnings of x-ray diffraction.

The advent of dislocation theory, the early application of the electron microscope to the study of metals [16], the confirmation of the existence of subgrains and Mott's [21] ideas of polygonization ushered in the current period of research in which deformation is investigated primarily in terms of the microstructure and dislocation mechanisms.

1.2.2. The Phenomenological Nature of Creep

The first creep tests at ordinary temperature for long duration (33 months) were made by Vicat [22]. Mechanical properties of metals at high temperature and under varying rates of loading became of considerable interest at the turn of the century. Hanson [23] contributed important information in showing that at elevated temperatures coarse-grained aluminum was more creep resistant than fine-grained metal. That creep occurs in three stages was demonstrated by McVetty [24], who also proposed a mathematical formulation of creep curves.

1.2.2.1. Primary creep

In the first stage of creep, called primary creep, the creep rate diminishes with time, indicating that hardening processes are active. Andrade [25] found for primary creep that the creep strain is proportional to the one-third root of the time according to the equation:

$$l = l_o(1 + \beta t^{1/3}) e^{kt} , \qquad (1)$$

where l is the measured length of the specimen at time t, l_o is the initial length of the specimen, t is the time and β and k are constants. Such an expression has been found to be generally applicable in expressing primary creep behavior. Other equations have been proposed to express the primary creep strain in terms of time and/or the instantaneous strain rate. Some of the important contributors in this

area are Cottrell and Aytekin [26], Garofalo [27] and de Lacombe [28]. Their equations are given in Appendix I.

It is now generally held that the hardening developed during primary creep is related to substructural changes that take place [29,30]. The development of a cell structure and the "entanglement of dislocations" presumably contribute significantly to hardening. As primary creep progresses the original dislocation "entanglements" disperse and a well-defined subgrain structure begins to form. The subgrain boundaries formed by the in situ precipitation of dislocations (polygonization) into walls result in a more or less stable substructure. Polygonization, at least in metals with high stacking fault energies, aluminum for example, requires that dislocations must climb to surmount the stress fields of dislocation pile-ups and glide to stable positions in the subgrain boundary as proposed by Mott [21].

1.2.2.2. Secondary creep

Second stage, or secondary creep, is defined as that creep deformation which proceeds at a substantially constant rate. This implies that the rate of thermal softening (recovery) is just great enough to balance the rate of work hardening.

Several empirical mathematical expressions are of common use in expressing the dependence of the secondary creep rate upon stress and temperature. McQueen [31], in a review paper on deformation mechanisms in hot working, has

summarized these expressions. For low stresses, the power law,

$$\dot{\varepsilon} = A\,\sigma^{N}\,e^{(-\Delta H/RT)} \quad , \tag{2}$$

where $\dot{\varepsilon}$ is the strain rate, σ is the stress, ΔH is the apparent activation energy, R is the gas constant, T is the absolute temperature and A and N are constants, is of general applicability in fitting creep data, but is not suitable for the results of hot working. A modified power law,

$$\dot{\varepsilon} = A'\,\sigma^{n} \quad , \tag{3}$$

where $\dot{\varepsilon}$ is the strain rate, σ is the stress, n is a function of temperature and A' is a constant has been used to fit secondary creep data and has often been used for the results of hot working experiments. The reciprocal of n increases linearly from about 0.04 to 0.2 as the temperature increases from 0.55 T_m to 0.9 T_m, respectively.

An exponential equation of the form

$$\dot{\varepsilon} = A''\,e^{(\beta\sigma)}\,e^{(-\Delta H/RT)} \quad , \tag{4}$$

where $\dot{\varepsilon}$, σ, ΔH, R and T have their usual meanings, and A'' and β are constants, is of use in analyzing the results of creep and hot working data at high stresses. Deviations from linearity in plots log $\dot{\varepsilon}$ versus σ at high stresses, however, create difficulties in the determination of apparent activation energies.

A more general expression, the hyperbolic sine equation,

$$\dot{\varepsilon} = A''' [\sinh(\alpha\sigma)]^{n'} e^{(-\Delta H/RT)} , \qquad (5)$$

where $\dot{\varepsilon}$, σ, ΔH, R and T have their usual meanings and A''', α and n' constants, can be applied to creep and hot working data over wide ranges of strain rate and stress. At high stress, equation (5) is a good approximation of the exponential equation, equation (4), and at low stress, it is a good approximation to the power equation, equation (2).

In comparing creep data at different stresses and temperatures, the Zener-Hollomon parameter,

$$Z = \dot{\varepsilon} e^{\Delta H/RT} , \qquad (6)$$

where $\dot{\varepsilon}$, ΔH, R and T have their usual meanings, has been widely employed. By plotting the Zener-Hollomon parameter, Z, versus the stress, σ, on logarithmic scales, a straight line is obtained, the slope of which is the exponent, N, in the power law equation, equation (3).

Methods for analyzing combined primary and secondary creep data have been considered by Conway and Mullikin [32]. They proposed an equation of the form

$$\varepsilon = a + bt^{1/3} + ct^{2/3} + dt , \qquad (7)$$

where ε is the strain rate, t is the time, and a, b, c and d are constants. This equation, applied to the creep data

from arc-cast tungsten tested at 2400°C under a stress of 800 psi, proved to better express the creep strain as a function of time than did the equations of Andrade [25], de Lacombe [28], Cottrell and Aytekin [26] or Garofalo [27].

Secondary creep (constant strain rate) demands that there exist a balance between work hardening and recovery. The behavior of the subgrain structure during secondary creep has been taken as an indicator of the rate of recovery. There is evidence that the subgrain size developed during steady state creep is strongly stress dependent [33-35]. Barrett et al. [36] have indicated that the subgrain size is constant during the course of steady state creep. Subgrain size is not importantly related to temperature as long as the temperature is above that required for recovery [33, 34]. That the subgrain size remains constant implies that lattice dislocations must be continuously precipitated in subgrain boundaries.

Metals with high stacking fault energies polygonize readily during creep; metals with low stacking fault energies reduce their energy and soften through recrystallization [37]. It seems reasonable to expect recrystallization to occur when the driving force for recrystallization cannot be lowered at a sufficiently rapid rate by other recovery processes. Lead, for example, under certain creep conditions apparently recrystallizes almost continuously during secondary creep [38,39].

Under extremely small stresses, it has been proposed by Nabarro [40] and Herring [41] that, when the temperature is sufficiently high, creep proceeds primarily by the stress directed diffusion of vacancies. According to the model proposed, plastic flow results when material is transported by self-diffusion from grain boundaries under compressive stresses to boundaries under tensile stresses. Harper et al. [42] indicate that low stress creep arises from a process involving the motion of dislocations. These investigators found that at low stresses the creep rates were about three orders of magnitude greater than could be accounted for by Nabarro-Herring diffusional creep. Further, similar creep behavior was observed in single crystals, which, according to the diffusional creep model, would not occur because of the lack of grain boundaries. The authors believed that the motion of jogged screw dislocations could well account for the creep behavior of aluminum under very small stresses. At stresses below 13.5 psi the creep rate in aluminum was found to increase linearly with the applied stress.

1.2.2.3. Tertiary creep

Third stage, or tertiary, creep is characterized by a period of accelerating elongation prior to rupture. The accelerating strain rate has been most commonly related to a reduction in the cross-section of the specimen, either by necking or by the presence of internal cavities developed first at grain boundary quadruple points or triple lines.

Third stage creep and its accelerating creep rate was correlated to a reduction in cross-section by Andrade [43]. Early investigations by Howe [44] of the strength of creep tested copper and silver showed that low temperature creep produced irreparable damage to the metal. Even annealing subsequent to creep testing did not repair the damage sustained during creep. Therefore, structural changes in the metal itself during secondary creep are suspect in leading to a change in the response of the metal to its loading, and, hence, to the onset of tertiary creep.

Nemy and Rhines [45], in studying the creep behavior of aluminum alloy 52S-O (5052-0), found that creep at 400°C under a stress of 1,500 psi produced no internal cavities even when creep had progressed well into the third stage. Some specimens were subjected to creep testing long enough to produce a well-defined neck, remachined to remove the neck and again creep tested under identical conditions of temperature and stress. When these specimens were retested, the creep rate proceeded at an accelerating rate much as if the initial test had been continued. This experiment produced conclusive evidence that neither necking of the specimen nor internal cavities were responsible for the onset of tertiary creep. Tensile tests of similar specimens after creep showed a progressive loss in tensile strength. The authors pointed out that these results were reminiscent of Howe's observations, and support the concept of "creep

damage." At the present, the nature of the microstructural features which are connected with "creep damage" are not known.

1.2.3. The Microstructural Features of Slip

Since the early work of Mügge [6-8] and Ewing and Rosenhain [9,10] on the relationships between slip and deformation, the concepts of slip have evolved through the amorphous metal hypothesis to the current concepts of dislocation theory.

Slip is manifested in two forms as observed on the polished surfaces of deformed metal crystals:

1. Slip bands, observable at low magnifications, have spacings and displacements of the order of one to ten microns. In appearance they may be straight, wavy, forked, continuous or discontinuous.

2. Slip lines, whose observation usually requires the magnification and resolution capabilities of an electron microscope, represent spacings and displacements on the order of several angstroms to one micron.

Heidenreich and Shockley [46] were the first to establish that slip bands consist of lamallae of fine slip lines. It has been observed that, with progressive deformation, coarse slip bands develop from a fine slip structure [47-49].

In aluminum deformed at slow strain rates in the temperature range 20° to 350°C, Wood and Rachinger [50] have demonstrated that as the temperature of deformation is raised, the slip bands observed on polished surfaces become less sharply defined, more wavy in appearance and fewer in number. Coincident with these changes, x-ray diffraction

studies showed that at the lowest temperature (20°C) the structure developed was like that of a cold worked metal; at an intermediate temperature (200°C), a subgrain structure developed; and at the highest temperature (350°C), a substructure approaching the size of individual grains developed.

Servi and Grant [51], investigating the slip band spacing on the surfaces of creep deformed aluminum specimens, found that the average spacing between slip bands decreased linearly with increasing stress and was independent of the temperature.

In an earlier research, Hanson and Wheeler [52] had observed that aluminum deformed in creep for 252 hours at 250°C under a stress of 2,800 pounds per square inch elongated without the formation of coarse slip bands. On the basis of this observation, they postulated that deformation occurred by uniform slip too fine to be observed with the optical microscope. McLean [48,53], some twenty years later, followed up this postulate and studied in detail the surface markings on aluminum deformed in creep. Both interference and phase contrast optical microscopy were employed. The major findings of this investigation were

1. The existence of fine slip lines between coarse slip bands was confirmed.

2. The extension due to prominent slip contributed less than one-half to the total extension. Most of the remaining extension was ascribed to fine slip.

3. The number of prominent slip bands and the amount of slip within each band increases with increasing grain size and/or stress.

4. The fraction of the total extension contributed by prominent slip bands increases with increasing grain size and with increasing stress.

5. A connection between prominent slip bands and fine slip bands was emphasized; the former were simply those positions where fine slip occurred in an intensified fashion.

In the face-centered-cubic metals, slip deviates from the ideal, the major deviation being cross-slip [54]. Slip lines corresponding to slip on a {111} plane are ideally straight; however, they sometimes follow zig-zag steps when the slip is locally altered to a conjugate {111} slip plane. The two slip planes share a common slip direction. Cahn [54], Ogilvie and Boas [55], Gifkins [31] and McLean [48] have observed cross-slip in aluminum.

Maddin et al. [56,57] have identified prominent and intimate cross-slip. Prominent cross-slip usually appears as a zig-zag pattern, while intimate cross-slip is distinguished by the visibility, at high magnifications, of fine slip elements connecting the main slip bands. At low magnifications intimate cross-slip often appears as overlapping discontinuous slip bands.

Cahn [54] has shown that in aluminum low temperatures of deformation favor intimate cross-slip, whereas high temperatures (500°C) favor prominent cross-slip. At room temperature increasing amounts of extension greatly increases the amount of intimate cross-slip. The electron microscopic studies of Trotter [58] on the slip of aluminum during creep confirmed the

existence of cross-slip as previously observed by optical techniques. Using replica techniques, Trotter found that slip zones do not consist of parallel slip lamellae as discovered by Heidenreich and Shockley [46], rather they consist of intimate segments of primary and cross-slip. The directions of such shear zones do not coincide with the trace of the slip plane, in fact, they may be rather far removed from it. Slip bands formed at high temperatures often appear as broad, wavy lines.

A number of researchers [54,59-62] have investigated the continuity of slip at grain boundaries, and it is apparent that slip cannot proceed across grain boundaries without a change in direction. The continuity of slip lines at a boundary observed on a two-dimensional surface is coincidental. In three dimensions, for the continuity of slip lines to exist at more than a point on a grain boundary surface requires that slip planes in conjoint crystals meet at the boundary in a line. Such would be the case for simple tilt boundaries.

The inhomogeneity of deformation as observed by the inhomogeneity of slip has been pointed out by Urie and Wain [63] for the plastic deformation of coarse-grained aluminum, and by Gifkins [39] for the creep of lead. The evidence presented by Urie and Wain suggests that grain to grain constraints play an important role in the way in which individual grains deform. The strength of grain to grain constraints in

retarding deformation is apparently related to the misorientation between neighboring grains. Gifkins [39] proposed that the inhomogeneous deformation within grains assists relative grain movements in lead. High creep rates tend to favor inhomogeneous deformation within grains. Slip lines were observed in two or three directions within one grain, and inhomogeneity was observed as clusters of slip lines within isolated portions of individual grains.

1.2.4. The Formation of Subgrains

Conclusive proof for the existence of subgrains was provided by the work of Lacombe and Beaujard [59], in which etch-figures were used to study deformed polycrystalline aluminum. The etch-figure study was supported by x-ray back-reflection patterns, and it was found that subelements within a single grain were misoriented by small angles, usually of the order of 15 to 30 minutes.

The formation of subgrain structures during the course of creep was first observed in iron by Jenkins and Mellor [64], and since then they have been observed in many other metals. Evidence for the formation of subgrains during the course of creep or hot deformation has been found in aluminum [65-67], α-iron [64], nickel [37], iron-3.1 percent silicon [68], zinc [69,70], cadmium [71], magnesium [72,73], tin [74], lead [75], a tin-antimony alloy [76], noibium [77] and copper [78,79].

1.2.4.1. The effect of stacking-fault energy

Metals which form subgrains during the course of creep or hot deformation are usually those which have high stacking-fault energies. Hardwick and Tegart [37], for instance, in comparing the hot deformation microstructures of aluminum, nickel and lead, found that both aluminum and nickel formed subgrains and that lead showed no evidence of a subgrain structure. Metals which rapidly polygonize do not, in general, recrystallize during creep. Therefore, it seems that polygonization and recrystallization are competitive processes, and that the relative strengths of each of these processes is dependent upon the stacking-fault energy. If the stacking-fault energy is high, polygonization is favored.

1.2.4.2. The size of subgrains

Recovery by polygonization, a process which requires prior lattice bending, is regarded as the rate-controlling mechanism of the high temperature creep of aluminum. The size of the subgrains has been assumed to be a measure of the rate of recovery. During primary creep, subgrains form and attain an equilibrium size which is dependent upon the temperature and the strain rate [80-83]. The stable subgrain size increases with increasing temperature and decreases with increasing strain rate, or stress, in the case of creep. In creep testing, the temperature and the stress are independent variables; however, they are related in a

unique manner to the strain rate. Jonas et al. [80] claim that this is true only after a stable subgrain size is attained, as is the case for secondary creep. Sherby and Dorn [84] suggested that the size of the subgrains is the same for a given stress, regardless of the temperature. The strain rate of secondary creep, then, must assume a value related to the subgrain size which is related strongly to the stress and weakly to the temperature. It is the balance between work hardening and recovery (by polygonization) which results in a given stable subgrain size. The greater the rate of working, the greater is the rate of recovery required to balance the work hardening. The greater the rate of recovery, the smaller is the stable subgrain size. Therefore, a stable subgrain size is responsible for the relationship among the strain rate, the stress and the temperature. Raising the temperature or decreasing the stress, subsequent to achieving secondary creep, causes the subgrain size to increase to a new equilibrium value [82,84]. This new equilibrium subgrain size dictates a new secondary creep rate. On the other hand, if the temperature is decreased or the stress is increased, the equilibrium subgrain size becomes smaller and the steady state creep rate is dependent upon the smaller subgrain size.

For creep deformation to proceed at a constant rate, a balance between the rates of work hardening and recovery must be maintained. If polygonization is the rate-controlling

process, then the presence of a stable subgrain size during secondary creep implies that dislocations are removed from the lattice by continuous precipitation in pre-existing subgrain boundaries. Such a concept may seem untenable, because as dislocations are added to subgrain boundaries, the angular misorientations across the boundaries would increase and intuitively result in a hardening effect. Thus, the creep rate would diminish. Two alternatives to this problem exist: (1) the subgrain size remains constant, but their boundaries continuously disperse and reform at an equilibrium spacing [85]; or (2) the subgrain size decreases concurrent with increases in the angular misorientations of the subgrains.

McQueen et al. [85], after investigating the hot extrusion of aluminum, proposed that the subgrain structure developed during steady state hot deformation may not be stable, but only the average size of the subgrains remains constant. These authors contend that subgrain boundaries must continuously reform at equilibrium spacing following their disorganization by a high flux of dislocations. In addition to finding that the subgrain size remains constant during deformation, it was proposed that the misorientation between subgrains is small and remains constant. In this way a constant dislocation density is maintained during steady state deformation.

Voznesensky and Rosenberg [86] monitored the size of subgrains in nickel throughout the course of creep, and found that as rupture is approached, there is a continuous refinement of the subgrains. They also discovered that the degree of crystallographic misorientation between neighboring subgrains increases with increasing deformation.

1.2.4.3. Subgrain boundaries

In the last two decades there has been considerable disagreement over the amount of crystallographic misorientation which may exist across a subgrain boundary between conjugate subgrains. McLean [87-89], Servi et al. [90], Wood and Rachinger [50] and Ramsey [69] have all favored the development of large angles of misorientations between adjacent subgrains. Misorientations as large as 16.6° have been measured by McLean [87] in creep deformed aluminum. Small angles of misorientation have been favored by Garofalo et al. [91], Hammad and Nix [92] and by McQueen et al. [85]. Green et al. [93], in tantalum creep tested at 1900°C under a stress of 500 psi up to a strain of 16 percent, found no misorientation angles between adjacent subgrains greater than 0.5 degrees.

Walls of edge dislocations have been shown by Cahn [94] to form upon heating bent aluminum single crystals. The observation coincides with the views of Mott [21], and leads to the conclusion that, in the most elementary case, subgrain boundaries represent simple tilt misorientations between

subgrains. Cottrell [95] summarizes the characteristics of subgrain boundaries formed during creep, noting that the similarities between subgrain structures formed during creep and those formed upon annealing cold worked metals suggest that the subgrain boundaries form in simple tilt walls by climb and glide of edge dislocations. Objections to this view have been raised by Wood and his associates [50,66, 96,97] and are restated by Cottrell [95] in the following quote:

> 1. The sub-structures produced during creep form at a lower temperature than in the usual polygonization experiments, and appear to form directly during the deformation without an intermediate stage during which the lattice is continuously bent.
>
> 2. The sub-boundaries form an irregular, polyhedral network instead of parallel planes with a definite crystallographic orientation.

These objections, based upon the studies of subgrains formed during creep, appear to point out two conclusions about the nature of the substructure formed during creep. First, it seems that the formation of subgrain boundaries in creep is accelerated by the action of the enduring applied stress. Second, since the boundaries between subgrains do not follow definite crystallographic orientations, the boundaries must in themselves be rather complex in terms of their dislocation content. Such complexity may result from the operation of several slip systems within each grain, and when dislocations from these various slip systems come together in planes, it is not difficult to understand

that the resultant boundary may be rather complex. A recent investigation by Orlová and Čadek [78] on the origin of the dislocation substructure during the high temperature creep of copper, shows that under certain creep conditions subgrain boundaries are formed not only perpendicular to the slip direction, but also in the primary slip planes. The latter boundaries were found to represent twist misorientation angles of up to 20 minutes.

1.2.4.4. Subgrain rows

Bands or rows of subgrains have been observed by several investigators [26,48,68,98,99] to form within grains during the course of creep. McLean [48] has shown qualitatively that slip lines observed on the surface of aluminum creep specimens are related to the internal subgrain structure. Rows or bands of subgrains correspond to rather irregularly curved slip lines which lie between very prominent slip bands. The subgrains, separated by prominent slip bands, have significantly different crystallographic orientations, as observed by polarized light microscopy, on opposite sides of the prominent slip bands. Bands of subgrains were observed in aluminum specimens crept at 200°C under stresses in the range of 666 to 1,500 psi to total extensions as large as 50 percent [87]. The bands of subgrains were described as polygonization bands and were thought to coincide with previously formed deformation bands with rather poorly defined boundaries. McLean [26] proposed

that the boundaries of deformation bands representing localized bending provided the necessary sites for subgrain-like boundaries to form through the climb and glide of dislocations. Ramsey [98] observed in creep deformed aluminum that subgrains formed within kink bands resulting in a banded structure of subgrains. When no prominent slip bands were observed on the surface of specimens (slow rates of deformation) subgrains did not appear preferentially in bands. Lytton et al. [68], in studying the creep behavior of (100) [001]-oriented polycrystalline iron-3.1 percent silicon, found that when the orientation of the grains with respect to the tensile axis was favorable for the predominate operation of a single slip system, dislocation pile-ups formed in rows and with concurrent recovery during creep. The development of polygonized boundaries in parallel rows resulted. Initially dislocation pile-ups and polygonized rows formed adjacent to grain boundaries. The parallel bands of dislocation walls were aligned with primary <111> slip directions, whereas the polygonized rows were formed perpendicular to these slip directions. Commercial purity aluminum deformed at 410°C at a strain rate of $2.7 \times 10^{-1} sec^{-1}$ and subsequently annealed at the same temperature for nine seconds developed elongated grains with bands of subgrains. The bands of subgrains were oriented at about 45 degrees to the tensile axis [99]. Serrations in the grain boundaries were observed at positions where the subgrain bands

intersected the grain boundaries. Further, Evans and Dunston [99] found that the subgrain bands were extremely stable during further annealing after deformation. This, no doubt, was due to the stability of the boundaries which separated the subgrain bands. These boundaries were found to represent misorientations of 7 or 8 degrees, while the boundaries separating subgrains along the length of the bands represented misorientations of only about one-half degree.

1.2.5. The Microstructural Features of Deformation Bands and Kink Bands

The appearance of deformation bands is associated with turbulent flow. Intuitively, it seems that easy glide should give way to turbulent flow, when a crystal attains an orientation such that two or more slip systems are stressed approximately to the same level [100]. Results on brass confirm this behavior; however, in aluminum easy glide ceases long before symmetrical orientations are reached. Deformation at elevated temperatures should tend to further restrict the occurrence of easy glide in aluminum because of the thermal activation of secondary slip systems; thus, turbulent flow should predominate. Barrett and Levenson [101], in studying the structure of polycrystalline aluminum after compression, discovered parallel bands extending across entire grains. When the bands first became visible they were straight, and the orientation difference across the boundaries of a band was on the order of only a few degrees.

As the amount of deformation increased, the bands became curved and the orientation differences across their boundaries increased. Such bands are not to be confused with twins, because the band boundaries tend to increase misorientation with increasing deformation. The material on each side of a band boundary has a cube plane in common, and the bands follow (100) planes or possibly some other planes in the [001] zone. Further, these authors observed that the bands apparently have different widths when observed under different conditions of illumination, a phenomenum which they ascribe to a more or less continuous range of orientations across narrow regions at the boundaries of bands. This feature of deformation bands was further supported by Gay and Honeycombe [102] when they observed asterisms in Laue patterns in cases where the incident x-ray beam straddled a deformation band. Honeycombe [103,104] demonstrated that the lattice is rotated within deformation bands formed in aluminum.

The primary features of deformation bands as discovered by Honeycombe [103,104], Cahn [54] and Chen and Mathewson [105] are as follows:

1. After only a few percent of strain, bands appear on the surfaces of crystals as waves with sharp crests. As the amount of deformation increases, the bands become forked and less regular.

2. The lattice within bands is rotated with respect to the lattice outside the bands.

3. In slightly deformed crystals, the plane of the deformation band is invariably perpendicular to a <110> slip direction to within a few degrees. As the deformation is increased, the plane of the band becomes rotated away from its original position by an angle, θ. The angle, θ, is approximately equal to the rotation of the crystal lattice of the band. The axis of rotation of the band lies in the slip plane normal to the slip direction.

4. Most of the deformation bands form at the start of deformation and persist throughout the process, increasing in rotation as the amount of deformation increases.

5. The initially formed slip lines cross deformation bands, altering direction only to the extent of the lattice curvature across the band. Slip lines formed later in deformation do not cross deformation bands. Short segments of slip bands on intersecting slip systems are formed within the bands.

6. Deformation bands represent inhomogeneous deformation. Material on either side of a deformation band may differ in strain by as much as 5 percent.

7. Crystals which deform (in tension) in double slip from the beginning of deformation do not form observable deformation bands. Barrett [106] found that when iron crystals were compressed with their <100> or <111> axes parallel to the compression axis, no bands resulted.

8. Specimens deformed by pure bending or shear do not form deformation bands.

9. Grain boundaries have no apparent effect upon the formation of bands.

A double fiber texture, <111>+<001>, has been produced in extruded single crystals of aluminum by Reed and McHargue [107]. The resultant texture had a strong <111> component and a weak <001> component; their relative strengths depended upon the temperature of deformation and the initial

orientation of the single crystal. The authors attributed the observed effects of temperature and initial orientation upon the resultant texture to the formation and interaction of deformation bands.

Recently Mitchell et al. [108] and Ahearn et al. [109] have described a new kind of deformation band in copper-aluminum solid solution alloys. The experimental observations establish that polyslip-oriented single crystals form deformation bands when they undergo avalanches of single slip during an abrupt relaxation process.

Cottrell [100] cites the tendency to use the term "kink band" in place of "deformation band," because of their crystallographic similarities. A kink band represents opposing localized lattice bending at the parallel boundaries of the band which, according to Hess and Barrett [110], results from the gradual and progressive rotation of the lattice. Kink bands are usually associated with the hexagonal-close-packed metals, and are viewed as being produced by organized slip on many parallel planes. The plane about which the kink forms is called the "kink plane." It is normal to the slip direction and symmetrically oriented with respect to the slip planes on either side of the sharp bend.

Cahn [54] has produced evidence of subgrains within deformation bands, and Mott [21] proposed that the boundaries of deformation bands are preferred sites for polygonization.

1.2.6. The Formation of Grain Boundary Serrations

Grain boundary serrations, the dentate or wavy offsets produced in grain boundaries during the course of hot deformation, have been observed in a wide variety of metals and alloys deformed at elevated temperatures over a range of strain rates encompassing those commonly encountered in creep and hot deformation. The metals which reportedly form grain boundary serrations are nickel [111-114], nickel-copper alloys [112], nickel-aluminum alloys [112], nichrome [114], austenitic stainless steel [115], magnesium [73,116], uranium [117], lead [39], aluminum [53,87,118-121], aluminum-magnesium alloys [120,122], an aluminum-20 percent zinc alloy [123] and niobium [77].

The main characteristics of grain boundary serrations and the hot working conditions under which they form are generally agreed upon. There exists a temperature range of hot working in which serrations form. Below a certain critical temperature, usually associated with that required for recovery, serrations either do not form, or they are of such a small size that they are unresolvable by the ordinary techniques of optical microscopy. Above a rather higher temperature they become destroyed by recrystallization during the course of hot working [111]. On the other hand, Gifkins [39] believes that grain boundary serrations formed in lead may be the results of recrystallized grains formed along grain boundaries. Serrations become more sharply defined with increasing temperatures and increasing amounts of

deformation [111,113,115,124] within the temperature interval of their formation. The appearance of grain boundary serrations vary depending upon the temperature and the rate of deformation [113]. Low temperatures and fast rates of working favor sharp serrations with more or less straight sides, while higher temperatures and slow rates of working favor a less sharp form of serrations which impart a wavy appearance to the grain boundary. Smeal [114] has reported that serrations become less pronounced as the grain size is increased.

The size and/or spacing of serrations along a grain boundary have been associated with the slip spacing [120], or with the subgrain structure [51,119,123,124]. Photomicrographs in the papers by McLean [53,87,118] show an association between grain boundary serrations and subgrains in creep deformed aluminum. This observation was also made by Presland and Hutchinson [73], Brumner and Grant [120], Evans and Dunston [99] and Brinson and Argent [77]. That there exists an association between grain boundary serrations and subgrains has led some researchers [39,120] to attribute the formation of serrations to the migration of grain boundaries. When a newly formed subgrain boundary impinges upon a grain boundary, the angles between the grain boundary and the subgrain boundary are nearly 90 degrees. The surface tension of the subgrain boundary causes the migration of grain boundary segments from their original positions towards the line of the subgrain boundary, resulting

in more nearly equilibrium angles at the juncture between the subgrain boundary and the two grain boundary segments. This mechanism accounts for the observation that the apex of a serration is often joined to a subgrain boundary. Walter and Cline [121] attribute the formation of serrations to grain boundary migration into the shear zone adjacent to a shearing grain boundary, but they do not connect the migration with the existence of subgrain boundaries. Mullendore and Grant [124] subscribe to the concept that grain boundary migration results in serrations. They have been led to the conclusion, by the studies of grain boundary sliding in polycrystals and bicrystals of an aluminum-2 percent magnesium alloy, that grain boundary displacements can be the result of slip crossing the grain boundary. Sliding along the boundary between two conjugate grains represents an unresolved component of shear when slip in one grain changes direction in crossing the grain boundary. When such a process occurs in the vicinity of a serration peak, a dislocation accumulation is built up on one side of the boundary. The result of the dislocation accumulation produces complex strain fields around the serration peak and causes the grain boundary to migrate, thus altering the form of the serration peak. Even a slightly irregular boundary represents an unstable condition in the presence of grain boundary sliding, and growth, or at least alterations, of the serrations should occur as long as appreciable

grain boundary sliding occurs. By this model, the authors have avoided the necessity of requiring the surface tension of subgrain boundaries to provide the driving force for grain boundary migration.

Rows or bands of subgrains were observed in aluminum by Evans and Dunston [99] and in niobium by Brinson and Argent [77]. The original grain boundaries were serrated at intersections of subgrain rows or bands with the boundaries, the size of the serrations being equal to the width of the subgrain bands. It is of particular interest that the bands of subgrains observed by Evans and Dunston were oriented at nearly 45 degrees to the tensile axis.

A model of crystal deformation during creep has been proposed by McLean [87] and extended [118] to show that crystal deformation controls grain boundary shear. Rows of subgrains can be accounted for by this model. The operation of the model is best described by the following sequence of steps:

1. Initially the lattice planes are flat.

2. During primary creep, some dislocations approach the boundary and, in becoming immobile, produce deformation bands. Others form deformation bands elsewhere in the crystal.

3. During the course of secondary creep, polygonization occurs first near the grain boundaries, then in whole crystals. Sub-boundaries form along the boundaries of deformation bands, resulting in what McLean calls "polygonization bands."

4. Late in secondary creep, subgrain boundaries form within the "polygonization bands," segmenting the bands into subgrains; hence, subgrain bands.

5. Further deformation causes the subgrains within the "polygonization bands" to rotate with respect to each other, resulting in shear along subgrain and grain boundaries.

The model does not account for the spasmodic behavior of grain boundary sliding, nor for the formation of grain boundary serrations. Had the author considered the possible occurrence of long range shear along the boundaries between adjacent polygonization bands, then, at least in principle, the formation of grain boundary serrations would have been explained.

1.2.7. Grain Boundary Sliding

Sliding upon mutual interfaces of metal crystals was reported as early as 1913 by Rosenhain and Humfrey [4] for α-iron. Observations of grain boundary sliding led Andrade [43] to believe that grain boundaries possessed a capacity for viscous sliding which could be at least partly responsible for the constant strain rate behavior of secondary creep. Some two decades after its demise in the mid-1920's, Kê [125] revived the amorphous metal hypothesis in studying the stress relaxation across grain boundaries, an effect which he ascribed to a viscous behavior of the grain boundaries. He concluded from his investigations that the viscosity of grain boundaries corresponds to that of a supercooled liquid metal. However, McLean and Farmer [74] pointed out that the

viscosity of liquid metals under supercooled conditions would result in grain boundary sliding rates many times greater than those observed experimentally.

Wood et al. [67] were the first to conclude that adjacent subgrains may move relative to one another by sliding along their mutual boundaries. Their conclusion was based upon the following three observations:

1. Subgrain boundaries become observable as surface relief between neighboring subgrains.
2. X-ray reflections from subgrains show displacements after further deformation.
3. Scribe marks across subgrain boundaries become displaced as the result of shear along subgrain boundaries.

The authors also concluded that the shape of grains may change during hot deformation by deformation within subgrains as well as by internal block movements of the subgrains relative to one another. McLean [87] also presented evidence that subgrain boundary sliding does occur.

Grain boundary sliding has been linked with grain boundary migration and crystal deformation. In high purity aluminum, Chang and Grant [119] observed spasmodic sliding of grain boundaries and connected the rest periods between sliding periods with grain boundary migration. Sliding along grain boundaries was found to occur through a thickness of material adjacent to, and on both sides of, the grain boundary. It was concluded that grain boundary sliding causes localized deformation within grains as evidenced

by "folds" at grain boundary triple junctions opposite the shearing boundary, and by the appearance of subgrains whose boundaries intercept the boundaries which have sheared. The strain produced in primary creep was attributed primarily to initial grain boundary sliding.

Gifkins [39,126], investigating the creep of lead, also associated grain boundary sliding with grain boundary migration. He presumed that, in addition to grain boundary migration, inhomogeneous deformation within grains also aided grain boundary sliding. Because sheared grain boundaries in lead often exhibited steps, Gifkins believed that alternate shearing and migration of the boundary occurred.

1.2.7.1. The contribution of sliding to total deformation

The first attempt to discover the contribution of grain boundary sliding to the total creep extension was made by Rachinger [127]. In creep tested aluminum, internal grains elongated very little while the surface grains elongated to a marked degree. Rachinger attributed the effect to grain boundary sliding. That the internal grains remained equiaxed suggested that grain boundary sliding was the predominant mode of creep deformation within the bulk of the specimen. The exterior surfaces of the specimen apparently suffered little deformation from grain boundary sliding. The contribution of grain boundary sliding to total extension was found to be greater the lower the stress and the higher

the temperature, up to a temperature above which extensive grain growth occurred (350°C). Grain boundary shear may account for as little as 6 percent or as much as 95 percent of the total deformation, depending upon whether measurements were made at the surface or within the bulk of the creep specimen, respectively.

Davies et al. [128] measured the contribution of grain boundary sliding to the total creep strain in high purity (99.97 percent) polycrystalline gold. Measurements made on the surface of creep specimens tested at 395°C showed that the contribution was as high as 67 percent at a stress of 2,225 psi. The contribution decreased linearly with increasing stress at this temperature to about 8 percent at a stress of 5,650 psi.

The work of Rachinger [127] has been reconfirmed by Davies et al. [129] who found, in nickel, that the contribution of grain boundary sliding to the total strain was smaller at the surface than in the interior of creep specimens. Additional experiments with gold, nickel, copper and aluminum showed that the ratio of the contribution of grain boundary sliding at the surface to that measured in the interior of creep specimens was always less than unity. The ratios obtained were as follows: aluminum, 0.67; nickel, 0.82; copper, 0.89; and gold, 0.93. The smaller the ratio, the greater is the difference between the surface and interior measurements. All specimens were tested at the

same homologous temperature and within the same order of magnitude of the strain rate. The authors suggest that the variations in the contribution of grain boundary sliding to the total strain reported in the literature may be due, in part, to surface effects in large-grained specimens. Typical values of the contributions of grain boundary sliding to the total creep strain are: aluminum, 0.15 [74]; nickel, 0.35 [65]; copper, 0.50 [130]; and gold, 0.67 [128].

Measurements of the contribution of grain boundary sliding to the total deformation in aluminum creep tested between 337°C and 474°C, made by Fazan et al. [131], indicated that the contribution may be between 65 and 95 percent of the total creep strain. The value of grain boundary sliding obtained for the same total strain was found to be independent of temperature. The apparent activation energy for grain boundary sliding was found to be between 35 and 38.5 Kcal/mole, a value which agrees with earlier determination [34,132,133]. Since the apparent activation energy for grain boundary sliding is nearly equal to that for the creep process as a whole, it was concluded that the rate controlling processes for grain boundary sliding were identical with those for creep.

In several papers [48,53,87,118] McLean had shown that the relative contribution of grain boundary sliding to the total strain was independent of the temperature at a constant stress, but decreased with increasing stress at a constant

temperature. In this regard, the results of Fazan et al. [131] were in total agreement with those of McLean. Harper et al. [42], in studying grain boundary sliding during the creep of aluminum, found that the ratio of grain boundary sliding to the total strain was not only independent of the temperature, but also independent of the strain. Contrary to these results, Brunner and Grant [120] discovered that with increasing temperature, the contribution of grain boundary sliding to the total elongation begins near the equicohesive temperature, reaches a maximum, then decreases with further increase in temperature or decrease in strain. They also found that the contribution of grain boundary sliding to the total strain is insensitive to grain size over a rather wide range of grain sizes. In contradiction to the work of Harper et al. [42], the ratio of the strain due to grain boundary sliding to the total strain was markedly affected by the amount of strain, the ratio being greater in the early stages of creep and diminishing with increasing strain. Moreover, Brunner and Grant [120] connected grain boundary sliding with grain boundary migration, and suggested that the formation of grain boundary serrations impedes the progress of grain boundary sliding as the strain increases. Barrett et al. [134] suggest that, in the creep of copper, an increase in the secondary creep rate as the grain size is decreased below 0.1 mm in average diameter may be attributable to an increased contribution of grain boundary sliding to the total creep strain.

McLean [48,53,87,118] and Brunner and Grant [135] have derived equations for the contribution of grain boundary sliding to the total extension. McLean's derivation is based upon a statistical average of the amount of shear on many grain boundaries and is applicable to fine grain materials, whereas the equation derived by Brunner and Grant considers contributions for single grain boundaries. Stevens [136] has reviewed the equations used by various researchers [48,127,128,131,137-141] to express the contribution of grain boundary sliding to the total creep extension. The author indicates that the previously derived equations usually involve doubtful assumptions, are not rigorously derived or are often in serious error. However, Rachinger's equation and the way in which he applied it [127] seems to be the most suitable and easily applied for the measurement of grain boundary contributions at the surfaces of creep specimens.

1.2.7.2. Mechanisms of grain boundary sliding

In the last two decades, the studies of grain boundary sliding have produced a great variation in the observed characteristics of the sliding process. Consequently, the mechanisms proposed for grain boundary sliding also are varied. The following paragraphs review briefly some of the more prominent studies and the proposed mechanisms.

It has been postulated by Feltham [142] that grain boundary sliding is dependent upon crystal deformation; and

that this deformation, in turn, is dependent upon recovery. Recovery was viewed by the author to consist of the "melting" of regions of good crystallographic fit between neighboring grains. The regions of good fit were considered as barriers to both dislocation motion and grain boundary sliding as first proposed by Mott [143]. The concept of "melting" coincides with viscous behavior during grain boundary sliding.

Crussard and Friedel [144] suggested that grain boundary sliding takes place along the boundary by the movement of partial dislocations in planes parallel to the boundary. Dislocations approaching a grain boundary which acts as a barrier to dislocation motion dissociate into partials and move parallel to the boundary. Such a concept supports the observation that sliding occurs within a thickness of material adjacent to the boundary. On the other hand, it appears generally untenable because in the high stacking fault metals, such as aluminum, partial dislocations do not readily form.

McLean and Farmer [74] have proposed that in grain boundary sliding there exists a viscous flow such that as the temperature decreases, the viscosity of the grain boundary increases. However, in considering the viscosity of a supercooled liquid metal layer at the grain boundary, they pointed out that the layer of supercooled liquid would predict a sliding rate many times faster than those observed experimentally. To overcome this difficulty, it was considered that sliding may be inhibited at low temperatures by

the formation of ledges in the grain boundaries produced by plastic deformation of the grains. Such ledges were viewed to be large on an atomic scale. In order for sliding to proceed, these ledges must be sheared through. At high temperature, crystal slip was presumed to aid grain boundary sliding. At low temperatures, where the deforming stresses are high, the number of active slip sources increases sharply; but the proportion of these sources which assist sliding presumably decreases. Thus, at low temperatures grain boundary sliding was not believed to be controlled by crystal deformation, because most of the slip goes into forming ledges in the grain boundary which has a retarding effect upon grain boundary sliding.

Macroscopic grain boundary sliding is the result of many small-scale shears, each of approximately the same magnitude, according to the ideas of Couling and Roberts [137]. Macroscopic shear is at least partially blocked by the elastic behavior at grain boundary triple junctions. Elastic recovery of the macroscopic shear in the reverse sense was thought to be prevented by grain boundary migration which was regarded as a recovery mechanism. Once such a recovery process takes place, the boundary is again free to shear. Hence, the concept that grain boundary sliding occurs intermittently and alternately with boundary migration was supported.

A part of the grain boundary sliding, that which results from activated sites near the grain boundary, was attributed

by Tung and Maddin [145] to a component of displacement parallel to the boundary surface. The activated sites correspond to regions properly oriented for crystal shear in a direction parallel to the boundary. Regions of poor crystallographic fit between the grains were believed to constitute barriers to boundary shear. These authors proposed that the regions of poor fit are removed by diffusional processes which they identified as grain boundary migration. The idea of poor fit described by Tung and Maddin appears to be counter to the proposals of Mott [143].

Martin et al. [146], from a study of grain boundary sliding in β-brass, concluded that grain deformation was the controlling factor in the rate of grain boundary sliding. In addition, they demonstrated that the creep rate at high temperatures was controlled by the resistance of grains to deformation, rather than by the resistance of grain boundaries to shear.

Grain boundary sliding in oriented tricrystals was investigated by Weinberg [147]. It was confirmed that the rate of sliding is dependent upon the grain boundary misorientation angle. As the angle of misorientation increased, so did the rate of sliding. Boundaries with less than five degrees of misorientation did not shear. Grain boundary shear was observed to be confined to one side of the boundary and it occurred in successive layers adjacent to the boundary, each layer being further removed from the boundary.

The author attributed this observed behavior to grain boundary migration. It was also observed that sliding occurred without overall deformation of the grains; however, as sliding progressed, the regions adjacent to the grain boundaries became rather severely deformed.

Gifkins [148], incorporating various features of several of the aforementioned mechanisms for grain boundary sliding, suggested a mechanism based upon the existence of subgrain boundaries adjacent to shearing boundaries and upon the movement of dislocations by climb and glide in close proximity to the grain boundary. Dislocations from within the subgrains adjacent to the grain boundary either precipitate in the subgrain boundaries or pile up against the grain boundary. The dislocations in the pile-ups move toward the boundary by climb and glide and in the process create a deficiency of vacancies. To replenish the vacancy deficiency, vacancies diffuse from the boundary toward the climbing dislocations, thus establishing a vacancy flow along the boundary toward the climbing dislocations. Vacancy flow in the grain boundary is suggestive of a high degree of disorder or possibly as "melting" as proposed by Mott [143]. A vacancy flow in the grain boundary is regarded as causing relaxation of the boundary which allows grain boundary sliding to progress. After climb, dislocations are more uniformly distributed along the grain boundary, a condition which Gifkins believed was favorable for grain boundary

migration. Migration was thought to occur once sliding had ceased.

By applying a direct shear stress to the boundaries in aluminum bicrystals, Biscondi and Goux [149] investigated the characteristics of grain boundary shear. They found evidence which suggests that two regions of behavior exist with respect to the initiation of sliding, depending upon a critical temperature or stress. For a given stress (or temperature) there exists a critical temperature (or stress) below which sliding begins only after an incubation period. The critical conditions of stress and/or temperature which separate the two regions of behavior depend upon the purity of the metal and the angular misorientation between the conjugate grains. The higher the purity and the smaller the misorientation angle, the greater is the critical temperature (or stress) for a given stress (or temperature). Grain boundary sliding was observed to occur in alternate periods of rapid displacement and rest. Grain boundary migration was associated with the rest periods and was found to vary in degree from point to point along the boundary. For a constant stress, the logarithm of the initial sliding rate decreases linearly with the inverse of the absolute temperature, within the temperature region where an incubation period exists. The heat of activation for sliding was found to be dependent upon the misorientation angle; the smaller the misorientation, the greater the heat of activation.

Horton et al. [150] observed that grain boundary sliding occurs in zinc bicrystals in the temperature range 320° to 390°C within the existence of slip in both of the conjugate grains. Sliding apparently did not occur within a layer of material adjacent to the grain boundary, but was rather sharply defined at the grain boundary interface. Because a band of subgrains was observed next to sheared grain boundaries, the authors suggested that, during the course of sliding, dislocations are ejected from the boundary into the conjugate grains. Grain boundary migration was observed and its direction and degree appeared to be associated with the subgrain structure. It was proposed that the rate of grain boundary sliding depends upon the ease with which dislocations can be absorbed by the conjugate grains. As the substructure develops adjacent to the boundary during creep, the rate of dislocation absorption becomes increasingly slower; thus, the rate of grain boundary sliding becomes diminished.

Walter and Cline [121] investigated grain boundary sliding in aluminum at 315°C using constant strain rate (10^{-4} sec^{-1}) tensile tests. Sliding occurred continuously, and when the amount of deformation became great enough for deformation bands and subgrains to be clearly observed, sliding ceased. Migration of the grain boundaries occurred spasmodically, and in such directions as to accommodate the changing stresses created by the grain boundary shear.

Migration also ceased about the same time as did grain boundary sliding. The authors believed that even slight curvatures of grain boundaries might result in shear zones adjacent to grain boundaries and provide a driving force for grain boundary migration.

When grain boundary sliding occurs along boundaries which are not planar -- and, indeed, grain boundaries are seldom perfectly planar -- it is reasonable to expect that some other process might be occurring concurrently with sliding. Raj and Ashby [151] have considered some of these other processes, which they call accommodation processes, in detail. Underlying their work is the assumption that it is the accommodation process which controls the rate of sliding, rather than any intrinsic property of the boundary itself. The accommodation may be purely elastic, diffusional, or it may involve plastic flow by dislocation processes. Regardless of the accommodation process, there exists some upper limit to which it can operate. When this limit is attained, sliding along irregular boundaries ceases. The particular nature of the accommodation and its limit of operation then control the rate and extent of sliding, respectively.

Slide hardening in aluminum has been linked to the occurrence and extent of crystal deformation by Beevers et al. [152]. Small additions of copper to aluminum decreased the slide hardening effect and promoted increased rates of grain boundary sliding.

Horton [153], as the result of grain boundary sliding experiments with bicrystal specimens of zinc, aluminum and aluminum containing small additions of copper in solid solution, has reported several important features of slide hardening. It was found that:

1. The rates of sliding and crystal creep deformation have the same time and temperature dependencies, but behave differently with respect to the stress and to alloying copper with aluminum.

2. If a power law stress dependence of the creep rate is assumed ($\dot{\varepsilon} \propto \sigma^n$), then the exponent n for sliding is greater than unity but less than that for crystal deformation.

3. At low stresses, where sliding occurs without macroscopically observable crystal deformation, sliding is not affected by additions of copper to aluminum.

4. At intermediate shear stresses, copper additions to aluminum decrease the rate of crystal deformation and increase the rate of sliding.

5. Tests made at constant shear rates indicate that the rate of sliding is linearly proportional to the shear stress developed, and the ratio of the amount of sliding to the shear stress increases with increasing temperature.

From these observations it was concluded that grain boundary sliding is not controlled by crystal deformation in any unique way. Horton proposes that grain boundary sliding is controlled by slide hardening, a process which is apparently independent of the rate of crystal deformation.

McLean [154] has developed a two-dimensional model for grain boundary sliding which considers the rate of sliding

in terms of dislocations meeting a grain boundary and then moving along the boundary by a series of climb and glide processes. Coincident with these processes, vacancies are either emitted from or absorbed by the boundary during the course of sliding. The model also takes into account the orientations of conjugate grains and the orientation of the boundary surface with respect to the tensile axis. Apparently, the assumption of continuous sliding was made. This is contrary to the findings of a majority of other investigators.

Another recent model for high temperature low stress creep has been proposed by Stevens [155]. The creep strain is attributed to grain boundary sliding and diffusional transport. None of the strain results from dislocation mechanisms. Grain boundary sliding is viewed as an accommodation mechanism which maintains continuity of the metal at grain boundaries in addition to contributing large amounts of strain to the total creep strain. Calculations based upon the model predicts that 60 percent of the total strain results from grain boundary sliding.

Much of the variation in the observed characteristics of grain boundary sliding and in the mechanisms based upon these characteristics, no doubt, arises because of differences in investigative techniques. In spite of the wide variation, there exists some majority agreement on several points listed below:

1. Grain boundary sliding proceeds spasmodically in alternate periods of rapid displacement and periods of rest.

2. Grain boundary sliding is controlled in degree and overall rate by the rate and extent of crystal deformation.

3. The misorientation between conjugate crystals influences the average rate of grain boundary shear. The greater the misorientation, the greater is the rate of sliding.

4. Grain boundary sliding occurs within a layer of materials adjacent to the boundary interface.

5. Grain boundary migration accompanies grain boundary sliding.

6. The contribution of grain boundary sliding to total creep strain is significantly large.

That grain boundary migration is associated with sliding as part of the same phenomenon seems most doubtful. Grain boundary migration has been observed in polycrystalline specimens, in tricrystals and in bicrystals which have been stressed so as to apply bending moments or stress concentrations to the grain boundary. Therefore, it is likely that grain boundary sliding has not been effectively isolated from the operation of other processes by such experiments.

The classic paper of Rhines et al. [156] on the subject of grain boundary sliding in aluminum bicrystals describes the essential characteristics of the phenomenon as it occurs essentially free of other processes. A summary of these characteristics is given in the following statements:

1. There exists an incubation period prior to the onset of sliding. Short induction periods are associated with large orientation differences between the conjugate grains, high

temperatures and large stresses. The onset of sliding is abrupt regardless of the length of the induction period.

2. Grain boundary sliding occurs spasmodically in alternating periods of rapid shear and periods of rest. Such behavior is not influenced by temperature surges or mechanical shock.

3. As sliding progresses, the displacement surges become smaller and the rest periods become longer.

4. The direction of sliding coincides with the direction of the maximum resolved shear stress in the plane of the grain boundary.

5. Sliding occurs in a layer of material adjacent to and only on one side of the grain boundary. Subgrains formed within this zone are rotated relative to each other through greater angles than elsewhere.

6. Sliding is not uniform along the full length of the grain. It may occur not only to different extent, but also at different times along the boundary.

7. The average grain boundary displacement is proportional to the cube root of time.

8. Grain boundary sliding follows an Arrhenius behavior as does the creep of individual grains.

9. The overall rate of sliding increases with the angular misorientation between grains.

10. Grain boundary migration was not observed.

11. Crystal deformation precedes the onset of grain boundary sliding and continues throughout the course of creep testing.

Based upon these observed characteristics of grain boundary sliding, the authors proposed that during the incubation period, slip, impinging on the boundary surface, causes localized bending all along the boundary. At some

point, enough energy has been stored for a recovery process to occur. When the recovery takes place, the layer of material adjacent to the grain boundary becomes softer. When this layer of material coincides with a direction of high resolved shear stress, yielding parallel to the grain boundary occurs until the material has again become hardened. This process continues throughout creep in a repetitive fashion.

1.2.8. Dynamic Recovery

Dynamic recovery is that portion of recovery operative during deformation which is strongly stress dependent. At low temperatures it is the predominate form of recovery; while at higher temperatures, usually above $T/T_m = 0.5$, it is superimposed upon the thermally activated recovery processes. The thermally activated recovery processes are those which are responsible for the softening obtained prior to recrystallization in the heating of prestrained metals.

The concepts of dynamic recovery in terms of dislocation mechanisms have been described thoroughly in three papers: Seeger [157], Seeger et al. [158], and Haasen [159]. Based upon these papers, a brief description of dynamic recovery as it applies to aluminum follows.

Dynamic recovery at ambient temperatures is associated with the onset of Stage III deformation as shown in the shear stress versus shear strain curve for face-centered-cubic single crystals, Figure 1. The high stresses attained

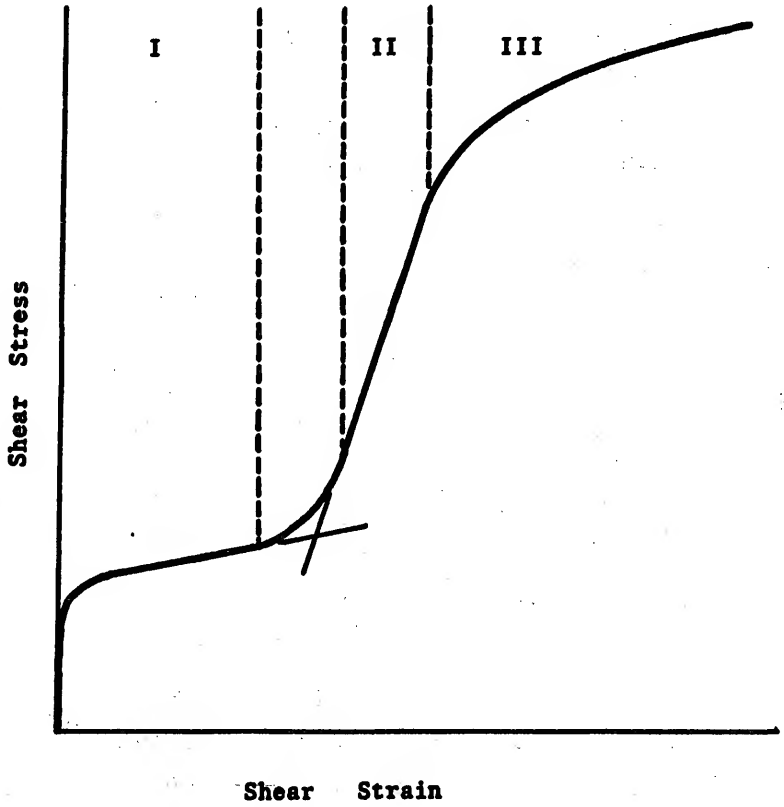

Figure 1. Shear stress versus shear strain for F.C.C. single crystals.

at the end of Stage II, which represents work hardening, cause slip dislocations to surmount obstacles, thus reducing the rate of work hardening. At room temperature, aluminum exhibits no Stage I and very little Stage II behavior, indicating that dynamic recovery occurs almost at the beginning of deformation. That aluminum exhibits recovery at temperatures well below those required for thermally activated recovery processes is attributable to its very high stacking-fault energy. In terms of dislocation behavior, a high stacking-fault energy means that dislocations do not readily dissociate into partials; therefore they may cross-slip with ease.

Two processes have been postulated for dynamic recovery in face-centered-cubic metals: cross-slip of screw dislocations and the collapse of Lomer-Cottrell dislocations which act as barriers to screw dislocation movement. The former process, that of cross-slip, is favored because theoretical calculations show that the activation energy for cross-slip is always smaller than that for the collapse of Lomer-Cottrell dislocations. Further supporting evidence for the cross-slip process based upon surface observations of face-centered-cubic metals deformed into Stage III has been provided. From the onset of Stage III, the amount of cross-slip observed at the surface continuously increases with increasing deformation. Such a theory explains why aluminum at room temperature begins Stage III at very low

stresses. These low stresses are too small to account for a significant number of dislocation pile-ups, hence work hardening (Stage II) does not occur.

In contrast to single crystals, dislocation pile-ups and attendant work hardening do form in polycrystalline aluminum deformed at room temperature. Evidence that these pile-ups do exist after deformation is observed by polygonization during heating subsequent to deformation. This implies that grain boundaries offer barriers to dislocation movement, and that the barriers must be of such a nature as to impart bending to the lattice. A similar situation, as previously described in Section 1.2.4, occurs in the pure bending of single crystals which polygonize upon heating [94].

With reference to Seeger's paper [157], it has been proposed that cold working into Stage III may result in near tilt boundaries of edge dislocations when edge dislocation segments are left behind in the cross-slip plane by the annihilation of opposing screw dislocation segments. Parallel sets of such edge dislocation segments represent bending which, with addition deformation, may form the parallel boundaries of deformation bands. Elastic interactions amongst the edge dislocations would then tend to align them into well-formed tilt boundaries. Geometrically, these tilt boundaries would be much like boundaries formed through thermally activated polygonization. In summary, if

a metal recovers easily at the temperature of deformation by the cross-slip process, it is then possible for rather sharp sub-boundaries to be formed without the operation of thermally activated recovery processes.

During the course of high temperature creep, dynamic recovery is superimposed upon the more commonly thought of thermally activated recovery process of polygonization. Because of the ease with which aluminum polygonizes during high temperature deformation, it has been the recent trend of some researchers [29,31,82,85,94,160-163] to attribute dynamic recovery to polygonization as it arises from the thermally activated processes. Mukherjee et al. [29] have considered cross-slip to be included in dynamic recovery processes in that, along with dislocation climb, it may play a role in the development of subgrain boundaries through polygonization.

The proposals of McQueen [31] and McQueen et al. [85, 161] that the subgrain boundaries developed during the hot working of aluminum are not stable, but go through repeated processes of dispersion and reformation, "repolygonization" [85], may be yet another process of dynamic recovery.

It has been shown that recovery during hot working [80] or under the action of an applied stress during the heating of prestrained specimens [84,164] produces greater softening than can be accounted for by static recovery.

Embury et al. [165], in studying the substructures of various cold worked ferrous alloys and copper, have found that the face-centered-cubic metals do not harden as readily as do the body-centered-cubic ones, a fact they attribute to dynamic recovery during working.

Langford and Cohen [166,167] have attributed a portion of the dynamic recovery in the drawing of iron wires to dislocation annihilation and a loss of cell wall area to cell coalescence. The motion of the cell walls under the applied stresses accounts for the annihilation of dislocations.

In commercial purity aluminum (1100) deformed by rapid compression at temperatures between 400° and 500°C, McQueen and Hockett [168] have observed that the subgrain structure developed during deformation resists subsequent recrystallization. This observation suggests that the degree of recovery during deformation was large; thus, there is little remaining driving force for recrystallization.

CHAPTER II

EXPERIMENTAL TECHNIQUES

The experimental techniques employed in this research have been many and varied. Those techniques which were used most widely are described in detail in this chapter, while those used only for special experiments are described in appropriate sections of Chapter III, Observations and Results.

2.1. The Material

High purity aluminum was chosen as the material for this research, because it is easily fabricated into test specimens, it is easily prepared for metallography, it requires no protective atmosphere at high temperatures, it readily develops grain boundary serrations during hot deformation and it deforms without forming twins. The metal was obtained in the form of twenty-five-pound pigs, intended as remelt stock, from Consolidated Aluminum Company, Jackson, Tennessee. An analysis furnished by the vendor is shown in Table I.

The level of the impurities was believed to be low enough not to greatly affect the microstructure developed during hot deformation.

Table I

Chemical Analysis of Aluminum

Element	Weight Percent
Al	99.9980
Si	0.0003
Fe	0.0009
Cu	0.0001
Mg	0.0005
Ca	0.0002

2.2. Fabrication of Creep Specimens

Creep specimens were fabricated from the as-cast aluminum by milling slabs from the pigs, rolling in three stages with intermediate anneals, machining the specimens, grinding the surfaces, and final annealing. Several series of specimens were prepared for creep or tensile testing in this way with some variations as outlined in the flow sheets given in Figures 2 through 5.

After the final anneal each specimen was electropolished and anodized so that lineal intercept counts could be made for the determination of the initial grain boundary area and initial grain boundary anisotropy. Formulae of solutions for electropolishing and anodizing are given in Appendix II. Anodizing rendered the microstructure sensitive to polarized light which facilitated the lineal intercept counting. A drawing showing the dimensions of the creep specimens is given in Figure 6.

Following the quantitative metallographic counting, the specimens were again electropolished to remove the anodized film. A photoengraved grid was etched on the sides of some specimens as reference marks for observations of surface deformation. A spacing of 1.01×10^{-2} inches separated the lines of the square grid. Appendix III gives the details of the photoengraving process using commercially available materials. A photomicrograph of the photoengraved grid is shown in Figure 7.

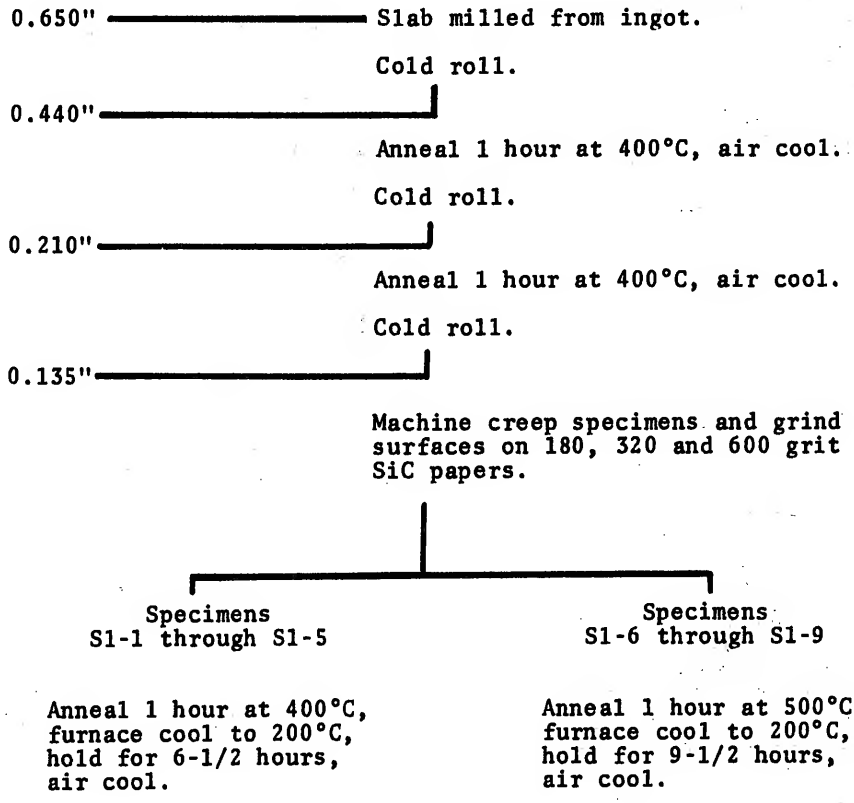
0.650"
Slab milled from ingot.
Cold roll.
0.440"
Anneal 1 hour at 400°C, air cool.
Cold roll.
0.210"
Anneal 1 hour at 400°C, air cool.
Cold roll.
0.135"
Machine creep specimens and grind surfaces on 180, 320 and 600 grit SiC papers.
Specimens S1-1 through S1-5
Specimens S1-6 through S1-9
Anneal 1 hour at 400°C, furnace cool to 200°C, hold for 6-1/2 hours, air cool.
Anneal 1 hour at 500°C, furnace cool to 200°C, hold for 9-1/2 hours, air cool.

Electropolish (Electropolishing Solution #1)
Anodize
Quantitative Metallography (Grain Boundary Area)
Electropolish (Electropolishing Solution #1)

Figure 2. Flow sheet for the fabrication of Series 1 creep specimens.

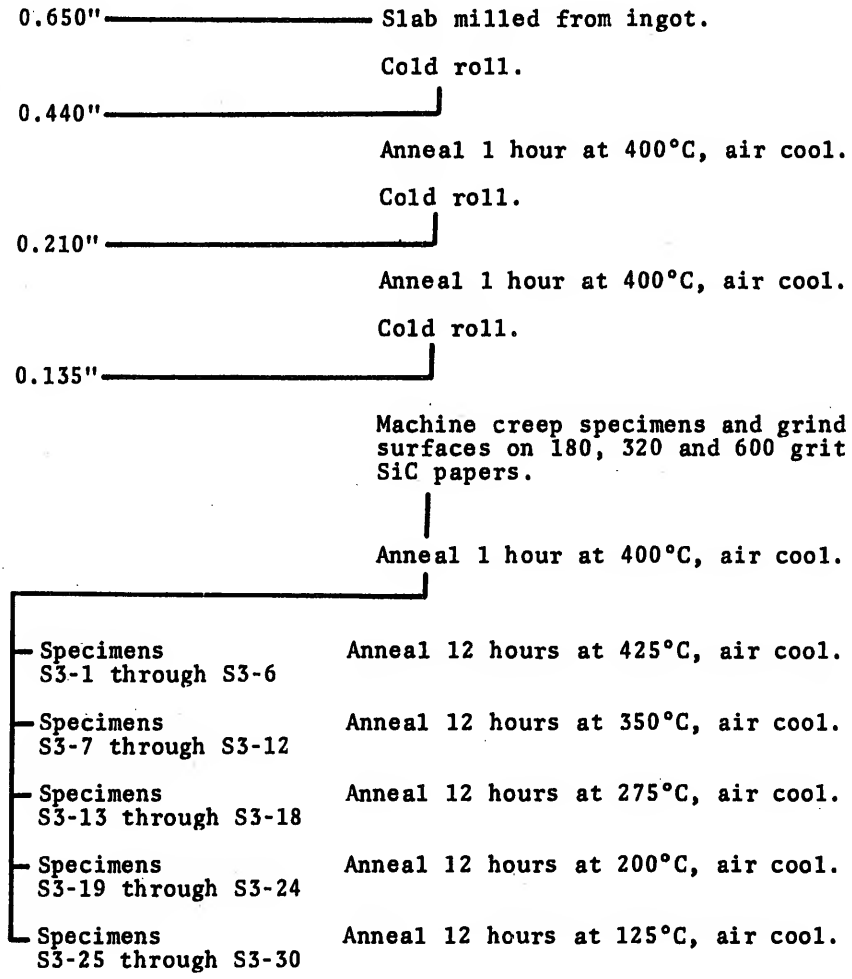
0.650"
Slab milled from ingot.
Cold roll.
0.440"
Anneal 1 hour at 400°C, air cool.
Cold roll.
0.210"
Anneal 1 hour at 400°C, air cool.
Cold roll.
0.135"
Machine creep specimens and grind surfaces on 180, 320 and 600 grit SiC papers.
Anneal 1 hour at 400°C, air cool.
Specimens S3-1 through S3-6
Anneal 12 hours at 425°C, air cool.
Specimens S3-7 through S3-12
Anneal 12 hours at 350°C, air cool.
Specimens S3-13 through S3-18
Anneal 12 hours at 275°C, air cool.
Specimens S3-19 through S3-24
Anneal 12 hours at 200°C, air cool.
Specimens S3-25 through S3-30
Anneal 12 hours at 125°C, air cool.
Electropolish (Electropolishing Solution #2)
Anodize
Quantitative Metallography (Grain Boundary Area)
Electropolish (Electropolishing Solution #2)

Figure 3. Flow sheet for the fabrication of Series 3 creep specimens.

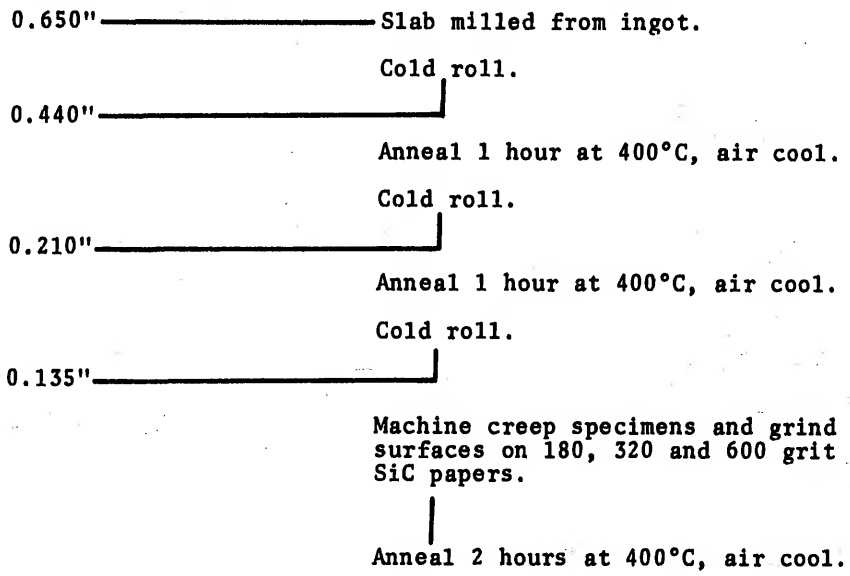
0.650"
Slab milled from ingot.
Cold roll.
0.440"
Anneal 1 hour at 400°C, air cool.
Cold roll.
0.210"
Anneal 1 hour at 400°C, air cool.
Cold roll.
0.135"
Machine creep specimens and grind surfaces on 180, 320 and 600 grit SiC papers.
Anneal 2 hours at 400°C, air cool.
Electropolish (Electropolishing Solution #2)

Figure 4. Flow sheet for the fabrication of Series 4 specimens.

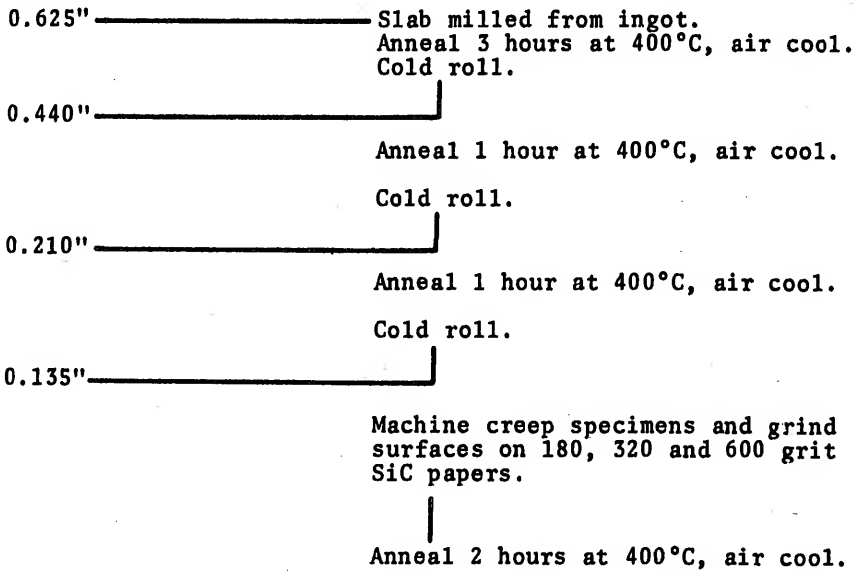
0.625"
Slab milled from ingot.
Anneal 3 hours at 400°C, air cool.
Cold roll.
0.440"
Anneal 1 hour at 400°C, air cool.
Cold roll.
0.210"
Anneal 1 hour at 400°C, air cool.
Cold roll.
0.135"
Machine creep specimens and grind surfaces on 180, 320 and 600 grit SiC papers.
Anneal 2 hours at 400°C, air cool.

Electropolish (Electropolishing Solution #2)
Anodize
Quantitative Metallography (Grain Boundary Area)
Electropolish (Electropolishing Solution #2)

Figure 5. Flow sheet for the fabrication of Series 5 creep specimens.

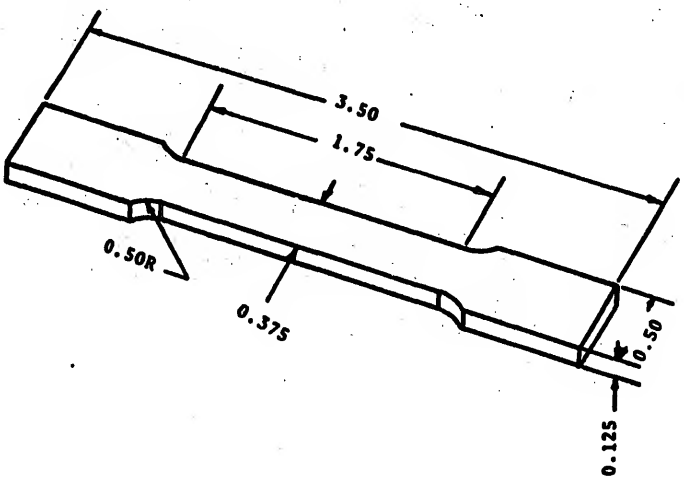

Figure 6. Creep specimen dimensions. Dimensions are in inches.

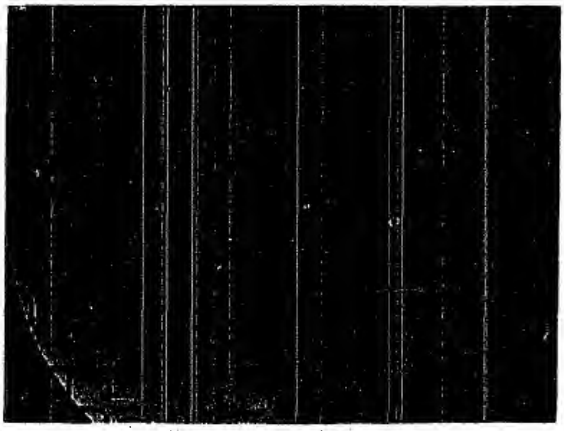

25X

Figure 7. A photomicrograph of the square grid photo-engraved on the sides of some creep specimens.

2.3. Creep Testing

2.3.1. Creep Testing Apparatus

Air furnaces for creep testing, constructed in the laboratory, feature two-layer non-inductive windings of 18 gage Kanthal-A resistance wire wound on impervious mullite tubes. The inside dimensions of the furnace were 2 inches in diameter by 24 inches in length. A side viewing port at midlength of the furnace tube permitted observation of the specimen during creep testing. Both ends of the furnace and the viewing port were open to the air. A schematic diagram in Figure 8 shows the methods employed for supporting and loading the specimen and the provisions made for quenching the specimen at the termination of a creep test. Stainless steel all-thread rod was used for upper and lower hanger rods. Specimen grips were also fabricated from stainless steel. Hanger rods, grips and a specimen are shown in the photograph of Figure 9. The specimens were loaded into the furnace from the bottom by pulling the assembly of both hanger rods, grips and specimens up into the furnace with an overhead chain. The upper hanger was supported by a clevis block resting on two steel angles above the furnace. Loading was accomplished by hanging a three-pound coffee can containing the desired weight of lead shot on the lower hanger rod. After loading the specimen a quench tank was placed beneath the weight and filled with tap water.

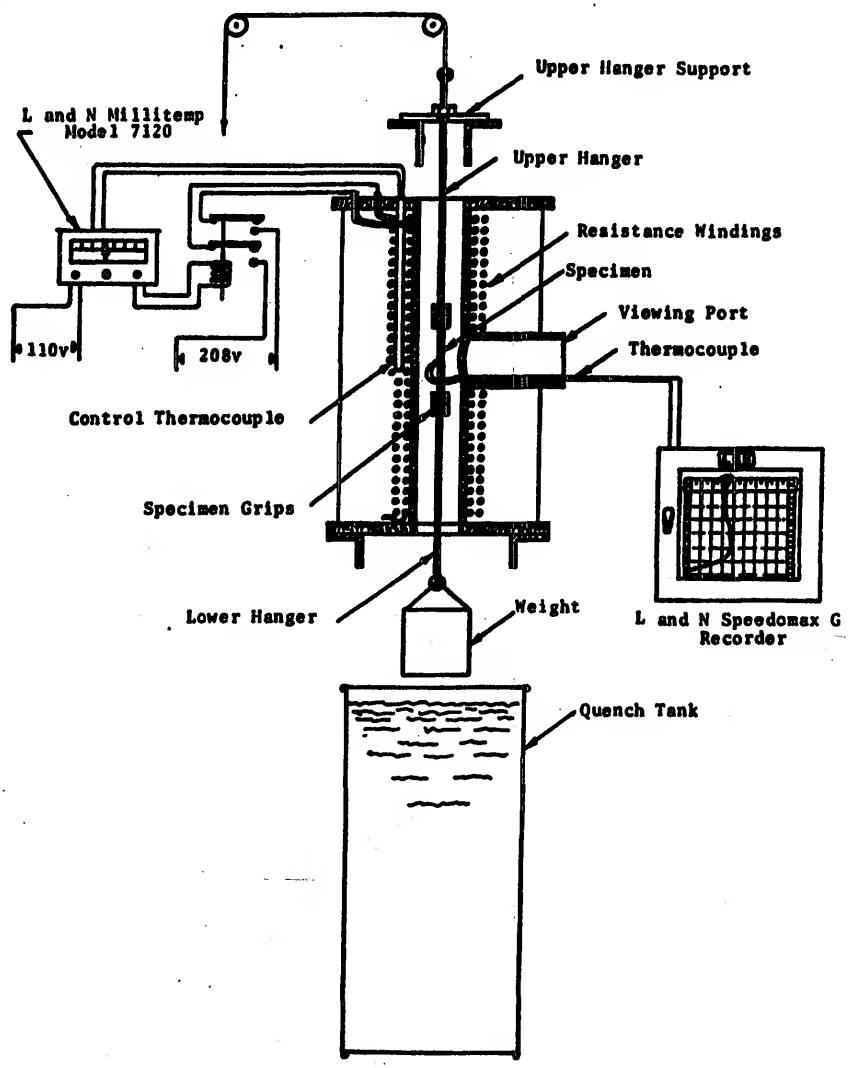

Figure 8. Schematic diagram of creep testing apparatus.

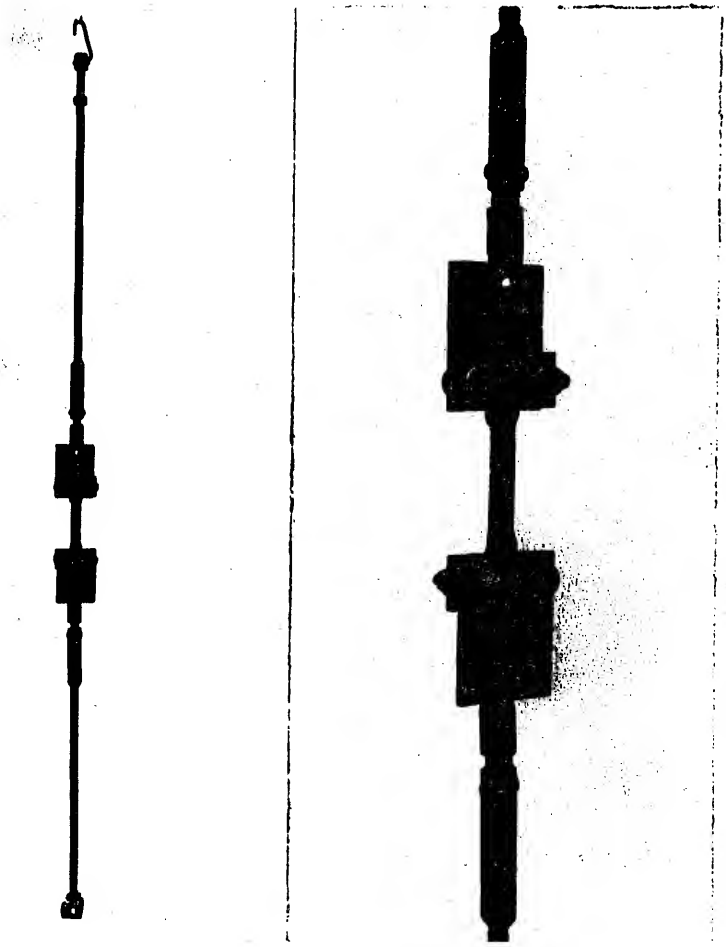

Figure 9. Creep specimen, grips and hanger rods.

The temperature of the furnace was controlled by a Leeds and Northrup Model 7120 Millitemp controller connected to a chromel alumel thermocouple. Measurement of the specimen temperature was made using a chromel-alumel thermocouple in contact with the specimen surface. The thermocouple was connected either to a Leeds and Northrup Model 8690 Potentiometer or a Leeds and Northrup Speedomax G recording potentiometer. The specimen temperature was maintained within ±5°C of the desired temperature. It was found that the temperature along the length of the specimen varied no more than ±5°C.

2.3.2. Creep Testing Sequence

Two types of creep tests were made using the apparatus described in the preceding section; one in which the temperature and load remained constant throughout the duration of the test, and one in which either or both the temperature and the load was altered during the test. The sequence of steps in performing tests under constant temperature and constant temperature was as follows:

1. The furnace was heated to the desired temperature.
2. The specimen was loaded into the furnace and allowed to heat to the testing temperature.
3. The load was applied to the specimen.
4. At the end of the test, the upper support was released and the specimen was lowered with the load still applied into the quench tank by means of the overhead chain.

The sequence of steps in performing tests under conditions of variable temperature and variable load was as follows:

1. The specimen was loaded into a cold furnace.
2. The load was applied to the specimen.
3. Power was applied to the furnace and the temperature allowed to rise to and equilibrate at the set point.
4. To increase or decrease the temperature, the set point on the controller was adjusted accordingly and the temperature of the furnace was allowed to increase or decrease to the new set point.
5. In cases where the load was to be increased or decreased simultaneously with a temperature change, the load was increased or decreased simultaneously with changing the set point of the controller.
6. At the end of the test, the upper support was released and the specimen was lowered with load still applied into the quench tank by means of the overhead chain.

Quenching specimens under load at the end of a creep test was accomplished within a time period of one second after the specimen passed out of the furnace. In cases when rupture of the creep specimen terminated the creep test, the lower portion of the specimen was immediately quenched. The time between rupture and immersion of the specimen in water was calculated to be 0.35 seconds.

2.3.3. Measurement of Strain

Throughout this research the use of the term strain was taken as the engineering strain, i.e., the change in length of the specimen divided by the original length. For

creep specimens tested under conditions of constant temperature and constant load, the strain was calculated from the change in length between two reference scratches on the specimen surface. When creep specimens were tested under conditions of variable temperature and variable load, the strain was periodically measured using a time-lapse photographic technique. A motor-driven Nikon Photomic FTN camera fitted with an extension bellows and a 135 mm lens was focused on the surface of the specimen in order to periodically photograph reference scratches on the surface of the specimen. The camera was activated by a clock-motor intervalometer set for one exposure per hour. More frequent exposures could be made by manually activating the camera. The distances between the images of the reference scratches on negatives obtained in this manner were measured and the strain calculated.

2.3.4. The Specimens and Their Testing Conditions

Specimens from Series 1, 3, 4 and 5 were tested under various conditions of loading and temperature. A complete list of these specimens and their conditions of deformation is given in Appendix IV.

2.4. Metallographic Techniques

Metallographic techniques employed in this research were especially developed to facilitate rapid preparation of polished surfaces with a high degree of reproducibility and a minimum of manual effort. Quantitative metallographic measurements were standardized and statistical methods for computing tolerance limits were employed. The following several sections describe the procedures employed.

2.4.1. Metallographic Preparation

Sections about 1-1/4 inches long were cut with a jeweler's saw from the center of the gage length of the creep specimens and mounted so that a surface parallel to one side of the specimen could be ground and polished. Specially designed specimen mounts, 2 inches in diameter, were cast from Caulk NuWeld dental plastic. Electrical contact was made with copper alligator clips fastened to the specimens and cast into the mounting material. A photograph of a mounted specimen in Figure 10 shows the physical configuration of the mount which was designed to be used with an automatic mechanical polishing device. Each specimen was ground on 180, 320 and 600 grit SiC abrasive papers using a solution of four parts of water and one part of a commercial liquid hand soap (Franklin's 40 % Liquid Hand Soap or Spence Liquid Hand Soap No. 40). The specimens were polished using a slurry containing one level tablespoon of

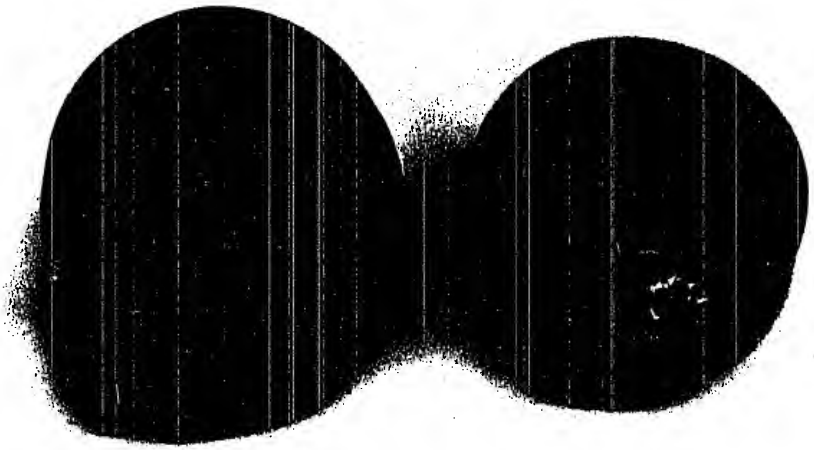

Figure 10. Mounted metallographic specimens.

AB 1200 mesh emery, 300 ml commercial liquid hand soap (Franklin's 40% Liquid Hand Soap or Spence Liquid Hand Soap No. 40) and 900 ml of water on an AB microcloth. In both grinding and polishing, a specially constructed automatic polishing device mounted on a Geoscience Unipol polisher was used. The polishing device utilized a 20 rpm synchronous motor and friction drive to rotate the specimen about an axis normal to the surface of the polishing wheel. A 1,400 gm weight resting on the specimen mount applied a dead load to the specimen. The speed of the polishing wheel was adjusted to about 150 rpm. The abrasive slurry was dripped onto the polishing wheel just ahead of the specimen position. The essential features of the polishing apparatus are shown in the photograph in Figure 11. About twenty minutes polishing time after grinding was required to produce a highly polished abrasive-free surface. Following mechanical polishing, the specimens were electrolytically polished and anodized in a polycarbonate cell using the solution for anodizing listed in Appendix II. The specimen to cathode distance was 1 inch. A photograph of the anodizing cell is shown in Figure 12. In addition to leaving behind an anodized film which renders the microstructure sensitive to polarized light, the anodizing procedure also lightly electropolished the surface, removing any residual fine scratches left behind by mechanical polishing. A major advantage of this metallographic preparation is that the

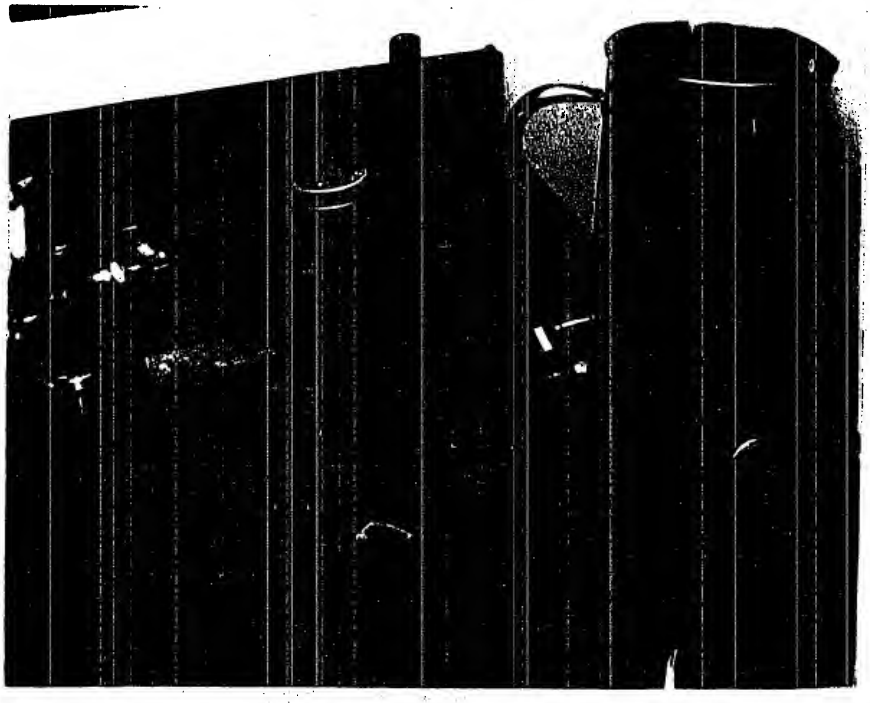

Figure 11. Automatic mechanical polishing apparatus.

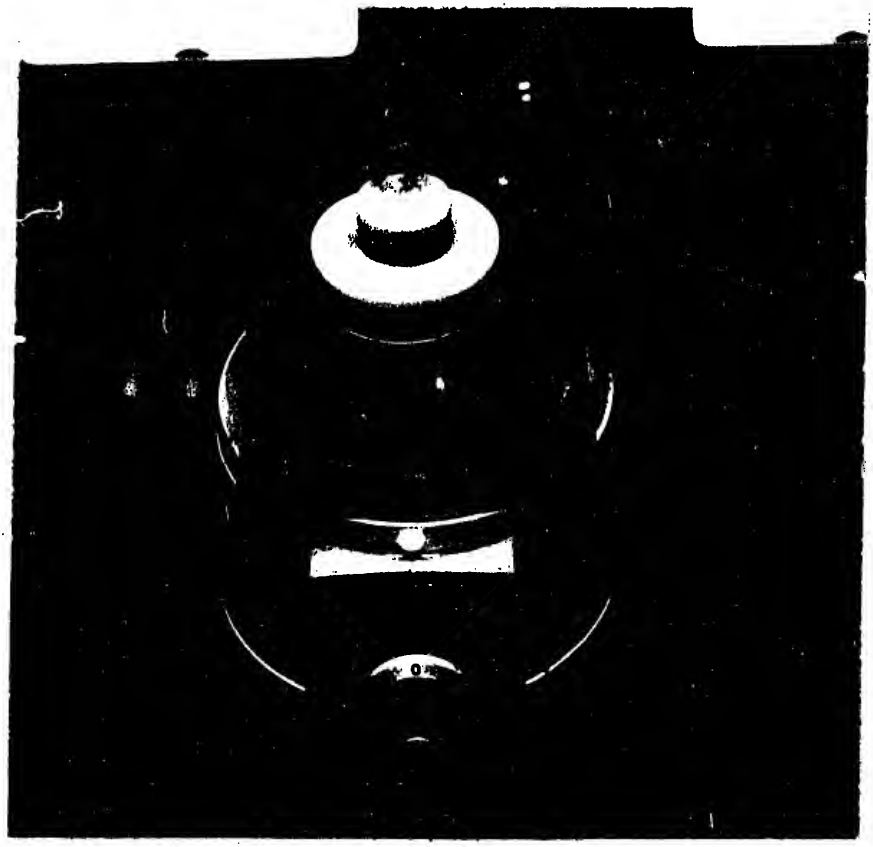

Figure 12. Anodizing cell.

prepared surfaces remain suitable for metallographic examination for several days without special storage precautions. If for any reason a specimen required repolishing, the hard, abrasion-resistant anodized film was first removed by immersing the specimen for 1 minute in an aqueous solution containing 10 volume percent of hydrofluoric acid.

2.4.2. Quantitative Metallography

For all of the metallographic work in this research, both photographic and quantitative metallography, a Bausch and Lomb Research II Metallograph was used. This instrument is superior to other available instruments for polarized light examination because of the high contrast afforded by the employment of a Foster calcite prism which maintains a precisely fixed relation between polarizing and analyzing filters. With this sort of design, the specimen must be rotated in order to affect the various polarized extinctions due to the variations in surface orientations of the specimen. A single drawback to the design, however, is that very often not all of the microstructural features may be observed at any one rotational setting of the specimen. For this reason, it was necessary, during quantitative metallographic counting, to rotate the specimen to observe all the features, then reposition the specimen in the proper reference to the test line or grid to make the necessary counts. Such rotations of the specimen during counting were extremely tedious and time-consuming because of the care that was necessary to reindex the specimen after each rotation.

Quantitative metallographic measurements were made on the microstructures of creep specimens before and after testing. The measurements made prior to creep testing consisted of lineal intercept measurements in the longitudinal, $(N_L)_L$, and transverse, $(N_L)_T$, directions for the determination of the initial grain boundary area, $S_{V(GB)}$, and the initial value of grain boundary anisotropy, $e_g(i)$. All lineal intercept measurements were made at a 25X magnification and the length of the test line was 1.16 mm. Initial measurements were taken from 100 areas for the longitudinal direction and from 100 areas for the transverse direction. For the determination of the initial grain boundary area per unit volume, both the longitudinal and transverse readings were used. Grain boundary anisotropy was calculated according to the methods of Rachinger [128] from the relation:

$$e_g = \left(\frac{(N_L)_T}{(N_L)_L}\right)^{2/3} - 1 \qquad (8)$$

where e_g is the anisotropy factor, and $(N_L)_T$ and $(N_L)_L$ are the number of intercepts per unit length of test line in the transverse and longitudinal directions, respectively. When $e_g = 0$, the grains are equiaxed; when $e_g < 0$, the grains are wider than they are long; and when $e_g > 0$, the grains are longer than they are wide.

Final quantitative metallographic measurements of boundary area per unit volume, those measurements made after

creep testing, included the total boundaries, $S_{V(TOT)}$; the smooth grain boundaries, $\bar{S}_V$; the serrated grain boundaries, $\tilde{S}_V$; the grain boundaries, $S_{V(GB)} = \bar{S}_V + \tilde{S}_V$; and the subgrain boundaries, $S_{V(SGB)} = S_{V(TOT)} - S_{V(GB)}$. As with the initial measurements, the magnification was 25X and the length of the test line was 1.16 mm. The final grain boundary anisotropy, $e_g(f)$, was also calculated. Fifty areas were measured for each of the longitudinal and transverse directions.

A schematic drawing in Figure 13 illustrates how the intercept measurements were made. Based upon this drawing, the reader will see that the test line of length L intercepts 16 total boundaries, 4 smooth grain boundaries, 2 serrated grain boundaries, 6 grain boundaries (smooth and serrated) and 10 subgrain boundaries. The values of N_L for the area are as follows.

$$(N_L)_{TOT} = 16/L$$

$$\bar{N}_L = 4/L$$

$$\tilde{N}_L = 2/L$$

$$N_{L(GB)} = 6/L$$

$$N_{L(SGB)} = 10/L$$

From a basic relationship in quantitative metallography, the surface area of boundary per unit volume is equal to twice the number of intercepts per unit length of test line, or

$$S_V = 2N_L \qquad (9)$$

Figure 13. Schematic microstructure of a creep strained specimen.

The criterion used to distinguish between serrated and unserrated grain boundaries was based upon visual discrimination of the amplitude versus the period of the serrations. When the amplitude was greater than one-fourth of the period, the grain boundary was considered to be serrated; and when the amplitude was less than one-fourth of the period, the grain boundary was considered to be smooth. A sketch in Figure 14 shows schematically the differences between serrated and smooth grain boundaries. Measurements were made at a magnification of 25X and thus are limited by the resolution obtainable at that magnification. Based upon the average resolution of the human eye (0.11 mm at a distance of 250 mm), the smallest serrations which would constitute a serrated grain boundary would have an amplitude of 4.4×10^{-3} mm (1.73×10^{-4} inches) and a period of 1.76×10^{-2} mm (6.92×10^{-4} inches).

It was frequently observed in specimens with small amounts of creep strain that segments of a grain boundary connecting two triple junctions were serrated while other segments were smooth. For this reason, in making lineal intercept measurements, the intercepts were classified according to serrated or smooth, depending upon the appearance of the grain boundary in the vicinity of the intercept. Examples of the classifications are given in Figure 15.

Statistical tolerance limits were applied to the mean values of N_L, $\hat{N}_L$, at a 95 percent confidence level. A work

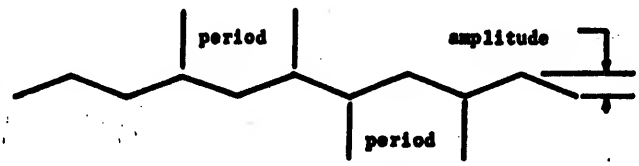

Smooth: amplitude < 1/4 period

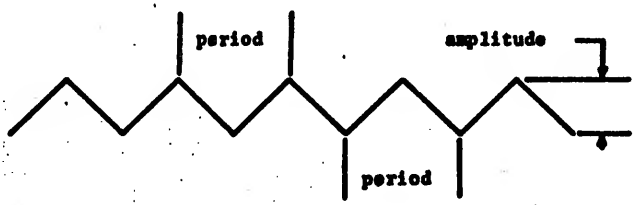

Serrated: amplitude > 1/4 period

Figure 14. Schematic diagram of smooth and serrated grain boundary serrations, based upon the period and amplitude of serrations.

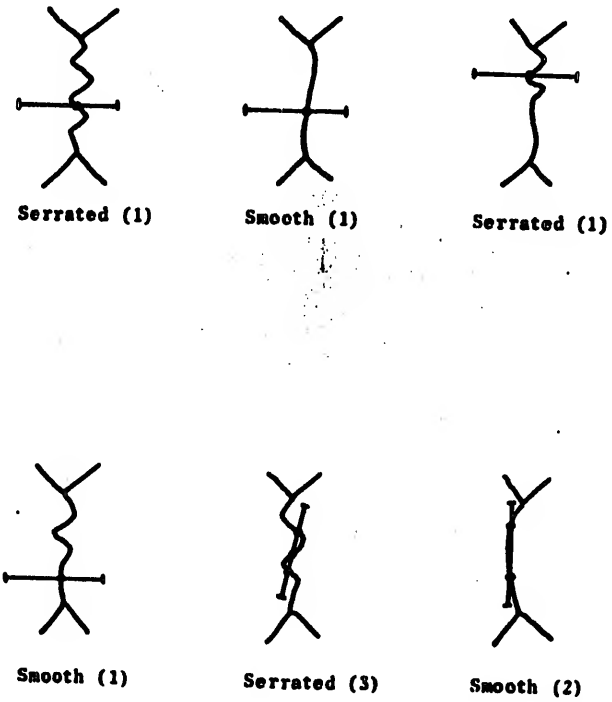

Figure 15. Intercepts of a test line with grain boundaries.

sheet for the calculation is given in Appendix V. A Fortran IV Program was used in the IBM 360 computer to calculate the mean values of N_L and the applicable tolerance limits. The program is given in Appendix VI.

Still another set of measurements were made on the creep specimens after creep testing. These measurements were made to determine the fractions of the number of grains which contained no subgrains, subgrains and subgrain rows. The angles between the length dimension of the subgrain rows and the tensile axis were also measured. One hundred neighboring grains were counted and a record was kept of the number of grains containing no evidence of subgrains, the number of grains containing subgrains but no subgrain rows (random subgrain morphology) and the number of grains containing subgrain rows. For those grains containing subgrain rows, the angle between the length dimension of the rows and the tensile axis was measured and recorded. From these measurements the several parameters obtained were the fraction of grains containing subgrains (both subgrains and subgrain rows), f_{SG}; the fraction of grains containing subgrain rows, f_{SGR}; and the fraction of grains containing subgrains but no subgrain rows, f_{SG}-f_{SGR}. These parameters were used to trace the development of the subgrain structure during the course of high temperature creep. The measurement of the angles between subgrain rows and the tensile axis made it possible to determine the distribution of angles

that subgrain rows make with the tensile axis, in terms of the number of grains.

To illustrate how the fraction counts were obtained, refer to the schematic microstructure of Figure 13. In this schematic, 21 grains are wholly contained within the field. Seven of these grains contain subgrains but no subgrain rows and 7 contain subgrain rows. The fractions computed are:

$$f_{SG} = 14/21 = 0.67$$

$$f_{SGR} = 7/21 = 0.33$$

$$f_{SG}-f_{SGR} = 7/21 = 0.33$$

These three fractions along with the following quantitative metallographic parameters were used to monitor the microstructural evaluation during secondary creep:

1. the grain boundary area, $S_{V(GB)}$.
2. the subgrain boundary area, $S_{V(SGB)}$.
3. the fraction of the grain boundary area which is serrated, $\tilde{S}_V/S_{V(GB)}$.
4. the change in grain boundary anisotropy, $e_g(f)-e_g(i)$, where $e_g(f)$ is the grain boundary anisotropy after creep testing and $e_g(i)$ is the grain boundary anisotropy before testing.

An example of the quantitative metallographic data obtained from creep specimens after testing is given for specimen 53-12 in Appendix VII.

CHAPTER III

OBSERVATIONS AND RESULTS

Noticeable changes in the microstructure of aluminum occur during high temperature creep; and, as a rule, the changes are detectable by visual examination of the microstructure after only a small amount of strain. Most of these changes persist in kind and increase in degree with further creep deformation. The development of subgrain structures and the formation of grain boundary serrations stand out as the most significant of the microstructural changes which occur. As the microstructure evolves during the course of creep, so do the features of the external surfaces of creep specimens. It has become apparent during this research that some of the features developed upon the external surface can be directly related to the underlying microstructure. The evolution of the microstructure is dependent upon the creep testing conditions of temperature and initial stress.

In the following sections of this chapter, the surface and microstructural features developed during creep and the way in which these features evolve as related to temperature and initial stress will be described. The relation between some of the surface features and the underlying

microstructure will also be presented. Evidence will be given to support a proposed mechanism for the formation of grain boundary serrations.

To prepare the reader for the assimilation of the observations and results of this chapter, the following statements list the major points which are presented.

1. Within the range of creep testing conditions of this research, the creep rate and the rate at which subgrain boundary area form as functions of the temperature and the stress obey similar empirical equations.

2. Grain growth occurs early in creep and thereafter the grain size remains constant throughout secondary creep.

3. Two morphologies of subgrain structure and two types of grain boundary serrations form during creep depending upon the temperature, the stress and the amount of strain. Wavy serrations and a random morphology of subgrains are favored by high temperatures, small stresses and small amounts of strain. On the other hand, dentate serrations and subgrain rows are favored by low temperatures, high stresses and large amounts of strain.

4. Microstructural examination and quantitative metallography have shown that an association exists between the wavy form of grain boundary serrations and the random morphology of subgrains, and between dentate serrations and subgrain rows.

5. Regardless of the temperature or stress, when creep had progressed into the third stage, almost all of the grains contained subgrain rows, and a majority of the grain boundary serrations were of the dentate type.

6. In three dimensions subgrain rows lie in planar arrays so that the boundaries separating the rows are oriented parallel

to directions of high resolved stress. The boundaries separating subgrain rows are often complex in terms of dislocation content, but in many areas they approach simple tilt boundaries. The boundaries between subgrain rows may represent rather large crystallographic misorientations, and there is evidence to suggest that the misorientation increases with increasing creep strain. Subgrain rows alternate in crystallographic orientation.

7. The fraction of grain boundary area which is serrated increases with time and strain.

8. Surface bands which bear little resemblance to slip lines form during creep. Boundaries between subgrain rows have been observed to coincide with these surface bands as well as with ledges in the edges of creep specimens and with displacements in grain boundaries.

9. The fraction of grains containing subgrains and the fraction of grains containing subgrain rows increase with time and the amount of strain. Not all grains form subgrains or subgrain rows at the same times or at the same strain.

10. Creep at a low temperature increases the steady state creep rate during subsequent creep testing at a higher temperature. Increasing the amount of creep strain attained during the low temperature creep, either by increasing the stress or by testing for longer times, increases the steady state creep rate during subsequent creep testing at the higher temperature.

11. The presence of grain boundaries exert an influence upon deformation. Effects of their influence have been observed microstructurally in the "blocky" appearance of the substructure and in a variation in the appearance of grain boundary serrations among grain boundaries.

3.1. Observations of Surface Features

During the early part of this research, a great deal of emphasis was placed upon the surface manifestations of deformation during the course of creep. It was originally hoped that this approach would produce evidence of non-crystallographic shear which would be capable of operating across grain boundaries, thus transmitting shear from one grain to another and producing grain boundary serrations. After a number of attempts were made to observe the surface during the progress of creep, it was realized that if non-crystallographic shear crossed grain boundaries it did so only after the surface had become so deformed that its observation was completely masked. The formation of slip bands, the appearance of grain boundaries due to the relative changes in crystallographic orientations of neighboring grains, the progress of grain boundary shear and the development of localized surface kinks at grain boundary triple junctions could all be followed with ease during creep. Microscopic observations of the surfaces after creep, however, provided evidence that rather coarse surface bands which crossed grain boundaries without large changes in direction were developed during secondary creep. Had these bands been the result of slip, then they would not have crossed grain boundaries without significant changes in direction. Often these surface bands were rather wavy, and in some instances they resembled the wavy slip lines

observed in B.C.C. metals. When these bands were observed, slip lines at other directions in the grains were also seen. The slip lines were never observed to be aligned in neighboring grains nor were they seen to cross grain boundaries without regard to differences in crystallographic orientation.

Several photographs which illustrate these bands are given in Figures 16 through 19. The first observation of the surface bands were produced in a coarse-grained specimen (strain annealed) by creep testing at 200°C under an initial stress of 1,000 psi for about 19 hours. The four photomicrographs in Figure 16 illustrate the wavy appearance of the bands, that they cross a grain boundary without a gross change in direction and that they coincide with minor perturbations of the grain boundary. A perturbation of a grain boundary is defined as a slight change in the direction of the boundary from its normally smooth two-dimensional trace. The scanning electron micrograph of Figure 16(d) shows that the disturbance of the grain boundary is not only in the plane of the surface, but also in a direction nearly normal to the surface. It is evident from the scanning electron micrographs that the surface bands observed are not merely cracks in a thin layer of surface oxide, but rather, represent real steps in the surface. The photomicrographs of Figure 17 show rather more straight surface bands in specimen S1-2 tested at 200°C under an initial stress of 1,000

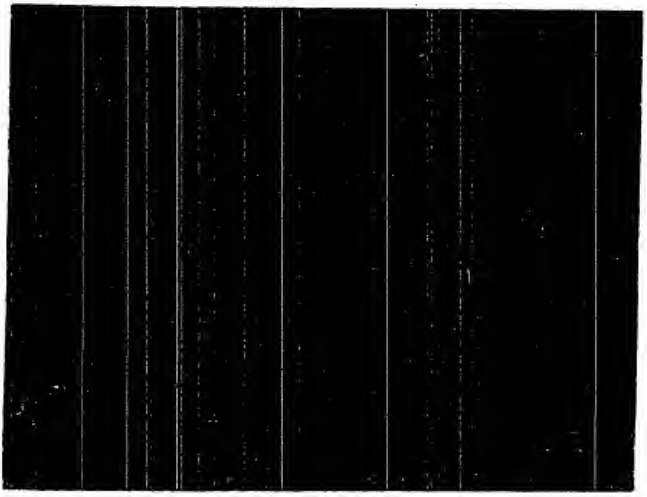

(a) 55X

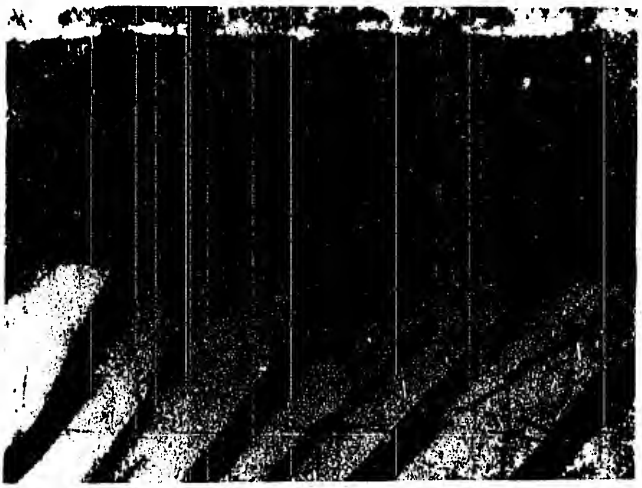

(b) 200X

Figure 16. Surface bands in specimen 4 tested at 200°C under an initial stress of 1,000 psi for 18.98 hours.

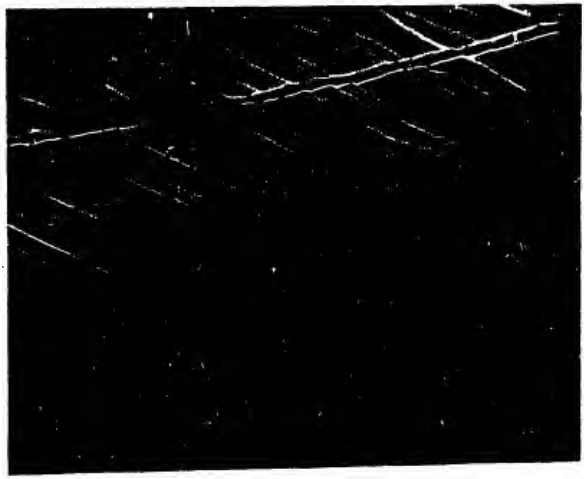

(c) Scanning electron micrograph 58X

(d) Scanning electron micrograph 580X

Figure 16. (continued)

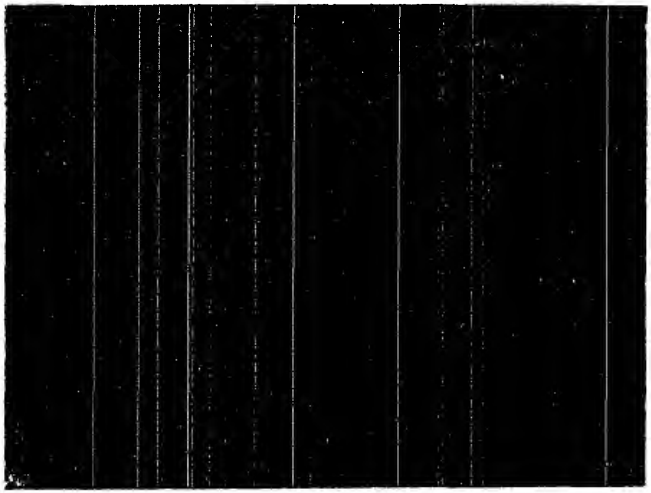

(a) 150X

(b) Scanning electron micrograph 1,000X

Figure 17. Surface bands in specimen S1-2 tested at 200°C under an initial stress of 1,000 psi for 24.05 hours to a strain of 0.049. Arrows indicate position of grain boundary.

40X

Figure 18. Surface bands in specimen S1-6 tested at 200°C under an initial stress of 1,000 psi for 12.03 hours to a strain of 0.032.

110X

Figure 19. Surface bands in specimen S3-6 tested at 425°C under an initial stress of 150 psi for 4 hours to a strain of 0.016.

psi for 24.05 hours to a strain of 0.049. Families of parallel surface bands at nearly right angles to each other are seen in the photomicrograph of Figure 17(a). Note that both sets of bands cross the grain boundary in the center of the field without an apparent change in direction. A scanning electron micrograph in Figure 17(b) shows similar bands crossing a grain boundary. Specimen S1-6 also developed surface bands as shown in the photomicrograph of Figure 18. Specimen S1-6 was tested at 200°C under an initial stress of 1,000 psi for 12.03 hours to a strain of 0.033. Bands developed in a specimen tested at 425°C under an initial stress of 150 psi for 4 hours to a strain of 0.016 are shown in the photomicrograph of Figure 19. Note that the bands are aligned across the grain boundary, but they produced no perceptible disturbance of the grain boundary.

In highly strained creep specimens, the observation of surface bands was complicated by the roughness of the deformed surface. Little information was gained from surface observations of specimens strained more than about 8 percent. Highly deformed surfaces often display a network structure not unlike that of a subgrain structure. Such a network structure on the surface may have a band-like structure as seen in the photomicrograph of specimen S3-18 shown in Figure 20. Specimen S3-18 was tested at 275°C under an initial stress of 800 psi for 5.37 hours to a strain of 0.176. In the grain in the lower left of the field, note

110X

Figure 20. Surface structure of specimen S3-18 tested at 275°C under an initial stress of 800 psi for 5.38 hours to a strain of 0.176.

the band-like surface structure and the overall network appearance of the surface markings. This photomicrograph was taken slightly underfocused to enhance the surface structure.

No quantitative information was obtained concerning the evolution of the surface features with respect to the creep testing conditions of temperature and stress. However, it appears that under a given set of creep testing conditions that surface bands form first after a rather large amount of strain as nearly straight lines which may be aligned in neighboring grains without producing perturbations of the grain boundaries. As the strain increases, the bands become wavy and in crossing grain boundaries they disturb the path of the boundary. At large strains the bands become connected in a network pattern not unlike a subgrain network and produce even further distortion of grain boundaries.

3.2. The Development of Substructure

For the purposes of this research, it has become necessary to define subgrains in terms of the origin of subgrain boundaries rather than upon an arbitrary value of crystallographic misorientation across a subgrain boundary. Simply stated, the definition is:

> A subgrain is a crystalline subdivision of a grain, separated from its neighbors by boundaries which form in situ by the precipitation of dislocations from the lattice.

This definition distinguishes subgrain boundaries from grain boundaries in that grain boundaries come into existence and assume metastable positions through recrystallization and grain growth; whereas, subgrain boundaries are formed at their metastable positions by the alignment of dislocations in boundary walls. The positions at which subgrain boundaries form are controlled by the localized nature of lattice bending. Further, the definition allows subgrain boundaries to be of rather high angle.

3.2.1. Classification of Subgrain Morphologies

The subgrain structures developed during the high temperature creep of aluminum are of two morphologies. The first, which shall be referred to as the random morphology, consists of rather equiaxed subgrains with near equilibrium angles (120°) at boundary triple junctions. The second, which shall be referred to as subgrain rows, consists of rows of subgrains which are often block-like in appearance. The boundaries separating subgrain rows represent greater crystallographic misorientation than do the boundaries between subgrains along the length dimension of the rows. From the overall appearance of subgrain rows, it appears that the boundaries separating subgrain rows make angles of nearly 90° with those separating subgrains along the rows; however, close observation shows that triple junctions of these subgrain boundaries do, in fact, approach angles of 120°. Examples of the random and subgrain row morphologies

are shown in the photomicrographs of Figure 21. The photomicrograph in Figure 21(a) (specimen S3-5, tested at 425°C under an initial stress of 150 psi for 16.17 hours to a total strain of 0.144), displays a microstructure in which the grains are subdivided into subgrains which are rather equiaxed in shape. In Figure 21(b) (a photomicrograph of specimen S1-8, tested at 200°C under an initial stress of 1,000 psi for 96.28 hours to a total strain of 0.131), it is shown that the grains are subdivided into rows in which the angular misorientation across the boundaries separating the rows appears to be rather large as indicated by the contrast difference between adjacent rows. Angular misorientations between subgrains along the length of the rows appear to be somewhat less than that between adjacent rows.

3.2.2. Subgrain Morphology as Affected by Stress, Temperature and Strain

The type of subgrain morphology is related to the creep testing conditions of temperature and initial stress; and, under a given set of creep testing conditions, the morphology is related to the amount of strain. As a generality, low temperature, high stress and large amounts of strain favor the subgrain row morphology. On the other hand, high temperature, low stress and small amounts of strain favor the random subgrain morphology. In Figures 22 through 30 several series of photomicrographs are given which illustrate the relations between subgrain morphology and the variables of temperature, initial stress and strain.

(a) 25X

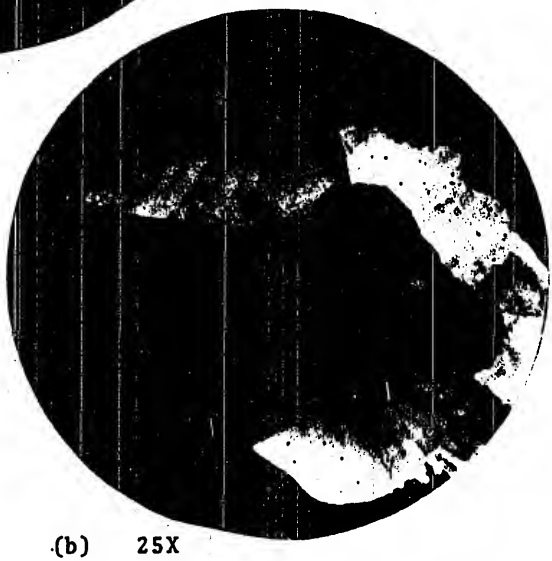

(b) 25X

Figure 21. Microstructures of creep specimens. (a) Specimen S3-5 tested at 425°C under an initial stress of 150 psi to a strain of 0.128. (b) Specimen S1-9 tested at 200°C under an initial stress of 1,000 psi to a strain of 0.131.

(a) S3-6, σ = 150 psi, 25X
t = 4.00 hrs., ϵ = 0.016

(b) S3-3, σ = 150 psi, 25X
t = 7.17 hrs., ϵ = 0.032

(c) S3-5, σ = 150 psi, 25X
t = 16.17 hrs., ϵ = 0.128

Figure 22. Microstructures of creep specimens tested at 425°C.

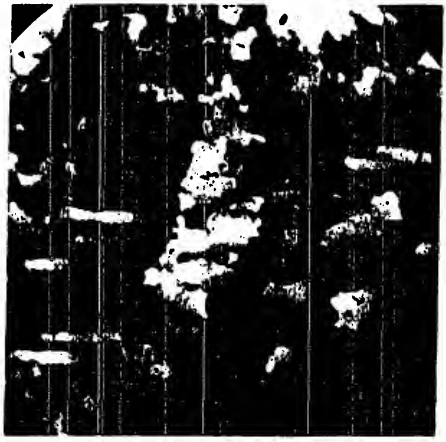

(d) S3-1, σ = 250 psi, 25X
t ≅ 3 hrs., ε = R

(e) S3-2, σ = 400 psi, 25X
t ≅ 0.6 hrs., ε = R

Figure 22. (continued)

(a) S3-10, σ = 280 psi, 25X
t = 4.17 hrs., ε = 0.024

(b) S3-9, σ = 250 psi, 25X
t = 10.00 hrs., ε = 0.064

(c) S3-7, σ = 250 psi, 25X
t = 24.00 hrs., ε = 0.120

Figure 23. Microstructures of creep specimens tested at 350°C.

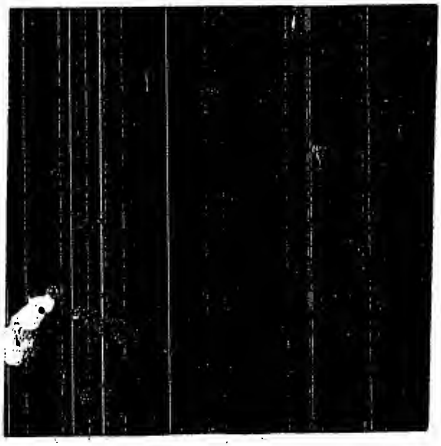

(d) S3-12, σ = 400 psi, 25X
t = 8.83 hrs., ε = 0.288

(e) S3-8, σ = 500 psi, 25X
t ≅ 2 hrs., ε = R

Figure 23. (continued)

(a) S3-13, σ = 400 psi, 25X
t = 4.00 hrs., ε = 0.016

(b) S3-16, σ = 400 psi, 25X
t = 10.02 hrs., ε = 0.016

(c) S3-15, σ = 400 psi, 25X
t = 24.02 hrs., ε = 0.032

Figure 24. Microstructures of creep specimens tested at 275°C.

(d) S3-18, σ = 800 psi, 25X
t = 5.37 hrs., ε = 0.176

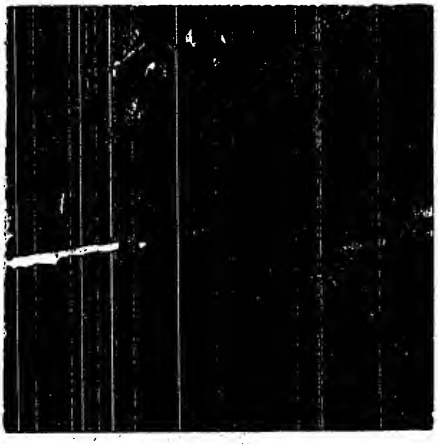

(e) S3-17, σ = 800 psi, 25X
$t \cong 8$ hrs., ε = R

Figure 24. (continued)

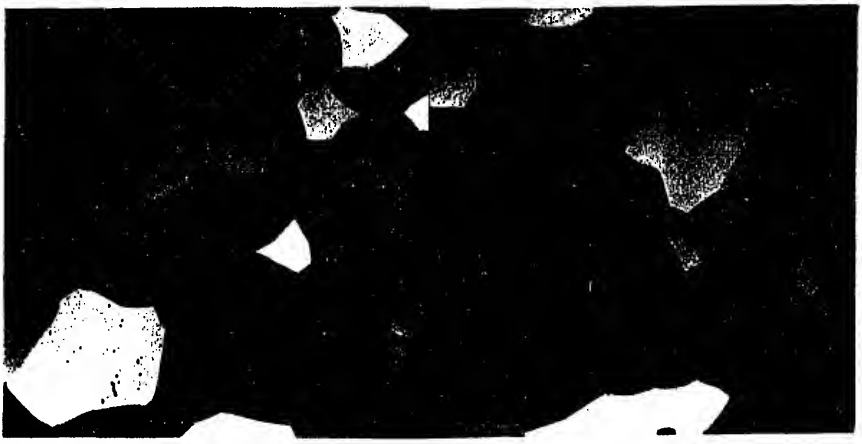

(a) S3-19 25X
t = 4.03 hrs., ε = 0.024

(b) S3-21 25X
t = 24.05 hrs., ε = 0.032

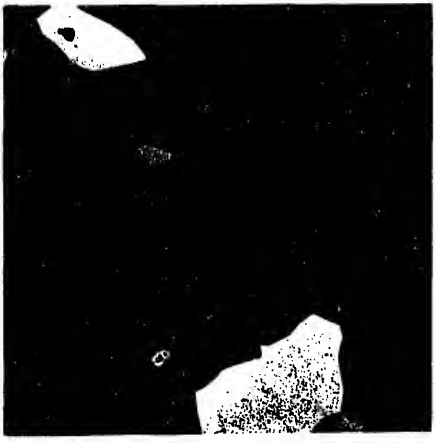

(c) S3-24 25X
t = 10.92 hrs., ε = 0.024

Figure 25. Microstructures of creep specimens tested at 200°C under an initial stress of 800 psi.

(a) S1-1 25X t = 11.85 hrs., ε = 0.025

(b) S1-2 25X t = 24.05 hrs., ε = 0.049

(c) S1-4 25X t = 95.78 hrs., ε = 0.098

(d) S1-5 25X t = 191.90 hrs., ε = 0.148

Figure 26. Microstructures of fine-grained creep specimens tested at 200°C under an initial stress of 1,000 psi.

(a) S1-7 25X (b) S1-8 25X
t = 24.00 hrs., ε = 0.049 t = 96.28 hrs., ε = 0.131

(c) S1-9 25X
t = 192.37 hrs., ε = 0.330

Figure 27. Microstructures of coarse-grained creep specimens tested at 200°C under an initial stress of 1,000 psi.

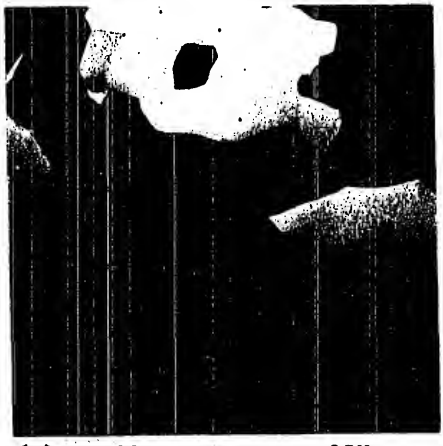

(a) S3-22 25X
t = 10.43 hrs., ε = 0.072

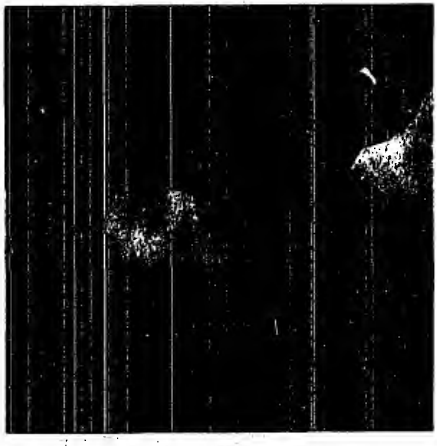

(b) S3-20 25X
t = 23.47 hrs., ε = 0.096

Figure 28. Microstructures of creep specimens tested at 200°C under an initial stress of 1,200 psi.

(a) S3-25, σ = 4,330 psi, 25X
t = 2 min., ε = R,
T = 136°C

(b) S3-28, σ = 4,792 psi, 25X
t = 20 sec., ε = R,
T = 141°C

(c) S3-29, σ = 4,790 psi, 25X
t = 1.75 min., ε = R,
T = 128°C

Figure 29. Microstructures of creep specimens tested at a nominal temperature of 130°C.

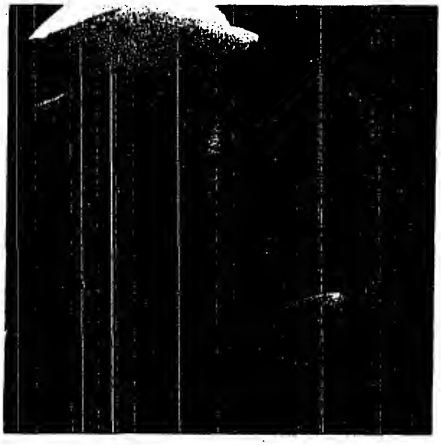

(a) S4-2 25X
$\dot{\varepsilon} = 3.33\ min^{-1}$,
$\varepsilon_R = 0.307$

(b) S4-7 25X
$\dot{\varepsilon} = 2.66 \times 10^{-2} min^{-1}$,
$\varepsilon_R = 0.447$

Figure 30. Microstructures of specimens tested at room temperature at constant strain rates.

The combined effects of temperature and stress upon the subgrain morphology are best seen by comparing the photomicrographs of specimens tested at 425°C under a stress of 150 psi, at 350°C under a stress of 250 psi, and at 200°C under a stress of 1,000 psi, shown in Figures 22 (a through c), 23 (a through c) and 26 (a through d), respectively. From these photomicrographs, it is easily seen that creep testing at 200°C under a stress of 1,000 psi is rather more effective in producing the subgrain row morphology than either of the other two sets of creep testing conditions.

At a given temperature of testing, the influence of stress, strain and strain rate upon the subgrain morphology can be observed by comparing the photomicrographs of specimens tested at 275°C, Figure 24 (a through e). Creep testing under a stress of 400 psi for 24.02 hours to a strain of 0.032 produces only the random morphology of subgrains; but if the stress is increased to 800 psi and testing is carried out to greater amounts of strain, Figure 24 (d and e), the microstructure developed consists primarily of grains divided into subgrain rows. Similar comparisons of the photomicrographs given in Figures 12 and 23 yield like observations. Upon the basis of the above comparisons, it seems that the subgrain morphology is related to temperature, stress and the amount of strain such that low temperature, high stress and large amounts of strain favor the formation of subgrain rows during the creep of aluminum. Because the

strain rate is dependent upon the stress, it would be reasonable to expect that high strain rates would also enhance the formation of subgrain rows. However, evidence to the contrary exists in the comparison of the microstructures of specimens tested at 200°C. The steady state creep rate at 200°C under a stress of 1,200 psi is 3.08×10^{-4} min^{-1} or about 28.5 times greater than the creep rate of 1.08×10^{-5} min^{-1} at 200°C under a stress of 1,000 psi; yet the photomicrographs of Figures 26(c) and 28(b) show that at comparable strains the development of subgrain rows is not as great in the specimen tested under the greater stress and at the faster strain rate. This anomaly in the relation between subgrain morphology and stress (strain rate) may be due in part to small angular misorientations of boundaries between subgrain rows developed at the higher stress and strain rate. It is entirely reasonable to expect that subgrain rows may exist, but the orientation differences between rows is too small to be detected by polarized light microscope.

Tests conducted at 130°C under very high initial stresses and at room temperature under conditions of constant strain rate (tests in tensile machine) produced microstructures with substructures which resemble subgrain rows. Examples of the microstructures produced are given in the photomicrographs of Figures 29 and 30. Although the row structure is very fine and not as well defined as the

subgrain rows developed during high temperature creep, there is evidence, particularly in Figure 29(c),that the row-like substructure is composed of subgrains.

The qualitative results obtained from the microstructures of specimens tested by creep at high temperatures and by constant strain rate at room temperature indicate that the more drastic the deformation, i.e., high stress, high strain and high strain rate, the greater is the tendency to form subgrain rows.

3.3. Grain Boundary Serrations Formed During Creep

From the outset of this research, the formation of grain boundary serrations during the course of high temperature creep has been a subject of major importance. As stated previously, it was thought that grain boundary serrations may be a manifestation of noncrystallographic shear which transmits deformation across grain boundaries without regard to differences in the crystallographic orientations of conjugate grains. Grain boundary serrations developed during the high temperature creep of aluminum have been found to vary in kind and degree depending upon creep testing conditions and the amount of deformation.

3.3.1. Classification of Grain Boundary Serrations

Grain boundary serrations have been found to exist in two forms depending upon the creep testing conditions of

temperature and stress, and upon the amount of strain attained under a given set of creep testing conditions. By their appearance, grain boundary serrations have been classified into two forms: wavy and dentate. Photomicrographs in Figure 31 illustrate the two forms of grain boundary serrations. In the microstructure of specimen S3-7, Figure 31(a), the serrations are wavy in form and are rather large, their dimensions corresponding to the dimensions of the subgrains. The dentate grain boundary serrations shown in Figure 31(b) were developed in specimen S3-2 during creep to rupture at 425°C under an initial stress of 400 psi. In this microstructure, the serrations are very much more "toothy" than those shown in the previous photomicrograph, and the dimensions of these dentate serrations correspond to the dimensions of the subgrain rows.

3.3.3. The Form of Grain Boundary Serrations as Affected by Temperature, Stress and Strain

The relations between the form of grain boundary serrations and the creep testing variables of temperature, stress and strain can be observed qualitatively by referring to Figures 22 through 30. As a rule of thumb, the form of grain boundary serrations to some degree follows the morphology of subgrains as related to the creep testing variables. That is to say, the greater the stress and the amount of strain at a given temperature, the more dentate are the grain boundary serrations; and the smaller the stress and

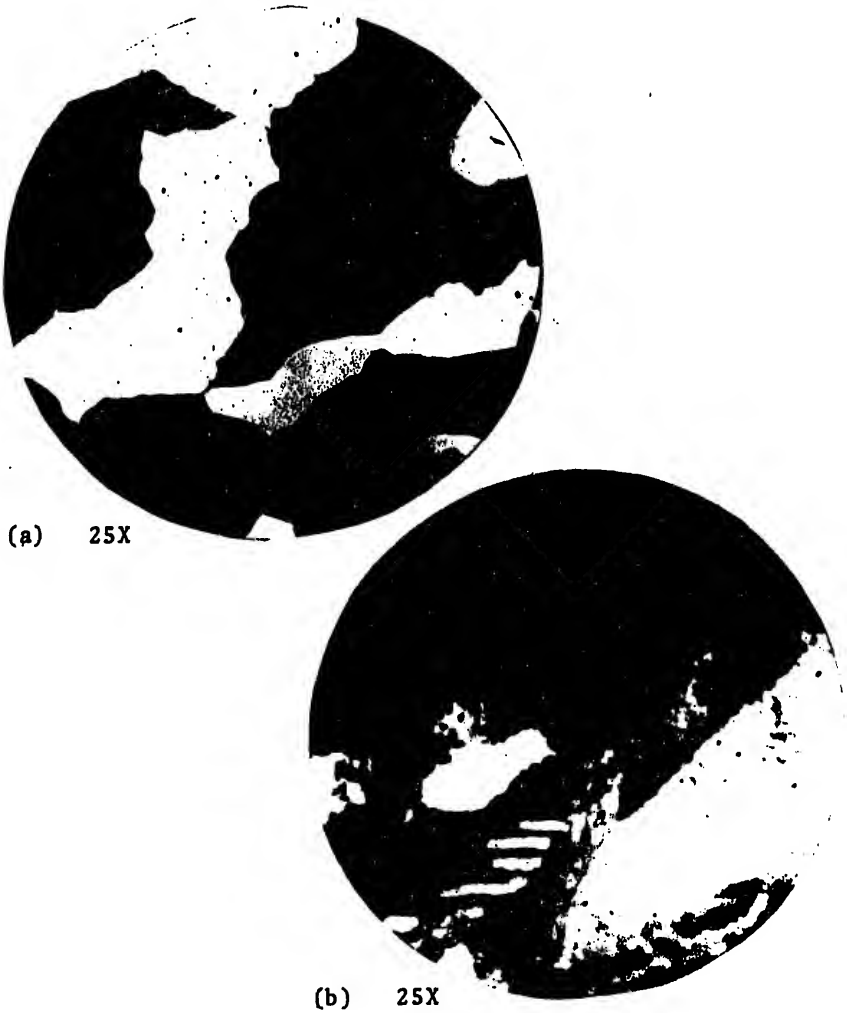

Figure 31. Microstructures illustrating wavy and dentate grain boundary serrations. (a) Wavy grain boundary serrations in specimen S3-7 tested at 350°C under an initial stress of 250 psi to a strain of 0.120. (b) Dentate grain boundary serrations in specimen S3-2 tested at 425°C under an initial stress of 400 psi to rupture.

the amount of strain at a given temperature, the more wavy is the form of the serrations.

3.4. Relations Between Grain Boundary Serrations and the Subgrain Morphology

It is apparent in the photomicrographs of Figures 22 through 30 that the form of the grain boundary serrations is linked to the subgrain morphology. When very dentate serrations are observed, they are always found in microstructures with well-developed subgrain rows. On the other hand, the wavy form of grain boundary serrations is found in microstructures containing the random subgrain morphology and also in microstructures containing the subgrain row morphology. From the microstructural evidence obtained in this research, it is a certainty that dentate serrations are always connected to the subgrain row morphology. Further, it is difficult to rationalize a mechanism by which wavy serrations associated with the random subgrain morphology could become dentate with further deformation without a prior change in the subgrain morphology. A proposed mechanism for the formation of dentate serrations which is to be presented later can account, however, for the transformation of wavy serrations, associated with subgrain rows at small amounts of deformation, into dentate serrations by additional high temperature creep deformation.

An important feature of dentate serrations is that they are the sharpest and have the greatest amplitude when subgrain rows are well aligned across the grain boundaries of conjugate grains. An example of good subgrain row alignment in adjacent grains and very sharp dentate serrations is shown in the photomicrograph of Figure 32.

An often observed microstructural feature in specimens tested well into the regime of secondary creep, particularly at the lower temperatures, is that the boundaries around a single grain may vary widely in their roughness. For example, in the photomicrograph of Figure 33, the boundaries around grain "A" are smooth, wavy and dentate. This observation strongly suggests that the form of the grain boundary separating conjugate grains may be largely dependent upon grain to grain constraints to deformation. It is reasonable to expect that grain to grain constraints have an effect upon the nature of the substructure developed in each grain, and likewise reasonable that such constraints to deformation also partly control the subsequent development of grain boundary serrations. There is no reason to doubt the crystallographic orientations of individual grains and the nature of the applied stress also play important roles in the formation of subgrain structure and grain boundary serrations.

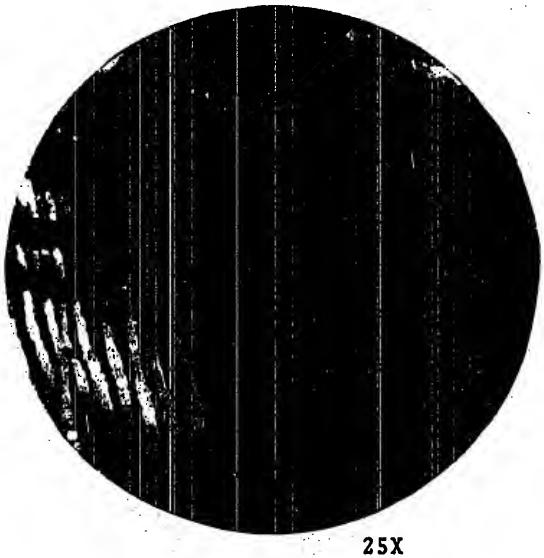

25X

Figure 32. The microstructure of specimen S5-7 illustrating well-defined subgrain rows in adjacent grains and very sharp, dentate grain boundary serrations.

25X

Figure 33. The microstructure of specimen S1-4 illustrating that the boundaries around a single grain, "A," may be smooth, "S," wavy, "W," or dentate, "D."

3.5. The Nature of Subgrain Rows

The correlation between subgrain rows and the dentate form of grain boundary serrations suggests that the existence of subgrain rows may play an important role in the deformation process. For this reason, it was necessary to establish the three-dimensional form of the subgrain rows, to ascertain the relations between their orientations and the tensile axis, to investigate their crystallographic orientations, to establish the nature of the boundaries separating the rows and to determine whether or not there exists any relation between the subgrain rows and surface bands formed during the high temperature creep of aluminum.

Observations which have led to a comprehensive picture of subgrain rows have been obtained by several metallographic techniques involving the study of serial sections, the study of metallographic sections taken at several angles through the volume of creep specimens, the study of etch pits produced in the subgrains and a study of the traces of subgrain rows and surface bands as related to the crystallographic orientation after creep deformation. Results from these various investigative techniques will be presented in the several following paragraphs.

3.5.1. Some Characteristics of Subgrain Rows Discovered from Metallographic Observations of Sides Parallel to the Edges of Creep Specimens

In order to maintain consistency in the nomenclature used to define the relative positions of metallographically prepared surfaces and the geometry of the creep specimens, reference is made to the sketch in Figure 34 which shows a metallographic specimen in relation to a creep specimen with sides and edges labeled.

A frequent observation made during the metallographic examination of surfaces parallel to the sides of creep specimens was that the long dimension of subgrain rows were most often oriented at nearly 45° to the tensile axis. Subgrain rows which appeared to make angles of other than 45° to the tensile axis were also observed, but this observation was most definitely in the minority. A detailed analysis of distribution of subgrain orientations with respect to the tensile axis has shown that this orientation distribution is maintained at all temperatures and stresses, and does not appreciably change with increasing amounts of creep strain. The presentation of the distribution of subgrain row orientations with respect to the tensile axis is reserved for a later section dealing with the microstructural evolution during creep.

Metallographic examination under polarized light has shown that subgrain rows alternate in shading from light to dark. This feature is shown in the photomicrograph of

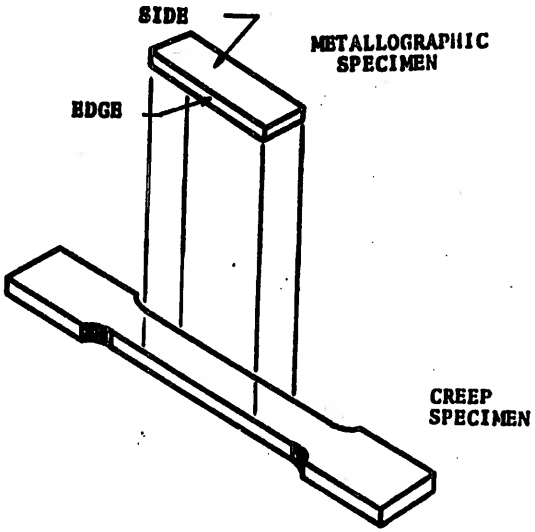

Figure 34. Position of metallographic specimen with respect to the geometry of creep specimens.

Figure 35. The alternating shading under polarized light indicates that the rows have alternating crystallographic orientations. Further proof that the subgrain rows do, in fact, alternate in crystallographic orientation will be given in a later paragraph.

Another observation which further elucidates the nature of subgrain rows and their evolution during the course of high temperature creep is that the rows increase in prominence with increasing amounts of creep strain. Subgrain rows increase in prominence because the contrast differences between adjacent rows becomes greater with increasing strain. A good example of the increasing prominence of subgrain rows can be seen in the photomicrographs of specimens tested at 200°C under an initial stress of 1,000 psi (Figure 26). An increase in the contrast difference among subgrain rows indicates that the angle of misorientation between the rows has also increased. The conclusion to be drawn from this observation is that the angular misorientation across the boundaries separating adjacent subgrain rows increases with increasing creep strain.

3.5.2. The Three-dimensional Nature of Subgrain Rows

The microstructures as observed upon metallographically prepared surfaces parallel to the sides of creep specimens have shown the existence of subgrain rows and some of their basic characteristics. Because observations concerning the row-like morphology of subgrains and their observed 45°

25X

Figure 35. The microstructure of specimen S1-8 illustrating the alternating shading of subgrain rows as observed under polarized light.

orientation with respect to the tensile axis were based upon examinations of two-dimensional surfaces, these observations were open to challenge. Do subgrain rows form in arrays which appear in three dimensions as rows or as plates? In three dimensions, what are the orientation relations between subgrain rows and the tensile axis? These were the two questions raised by the challenge to the validity of the two-dimensional observations. In order to answer these questions, an investigation of the three-dimensional structure was made by employing the serial sectioning technique and by analyzing the traces of subgrain rows upon several surfaces polished at various angles to the tensile axis through the volume of creep specimens.

3.5.2.1. Three-dimensional observations based upon the study of serial sections

Using the automatic polishing and anodizing techniques described previously, a set of 26 parallel serial sections was removed from specimen S5-7. After each section was removed, photomicrographs were made to record the microstructure. Two areas in the specimen which contained pronounced subgrain rows at about 45° to the tensile axis were selected for study. Marker holes drilled into the specimen with a SWG #80 drill bit provide a means by which the photomicrographs of successive serial sections could be aligned, one over the other in a stack, to construct an enlarged three-dimensional model of the microstructure. In polishing

the 26 serial sections, a layer 0.0116 inch thick was removed from the specimen. This thickness was equivalent to about four subgrain dimensions.

It must be stated at this point that a subgrain row is considered to be made up of subgrains, all having nearly identical crystallographic orientations. Under polarized light one subgrain row is distinguished from its neighbor by the contrast in their shading indicating qualitatively the degree of angular misorientation across the boundary separating the rows.

A section by section examination of the three-dimensional microstructure revealed that subgrains, which in two dimensions appeared as rows, also had a row-like structure in three dimensions. In addition to the row-like morphology of the subgrains, the subgrain rows were found to be in planes extending some distance within each grain. In some cases, the planes extended through entire grains and seemed to be aligned with and approximately parallel to similar planes of subgrain rows in adjacent grains. The width and thickness dimensions of subgrain rows did not correspond in general to the dimensions of one subgrain. but,rather, the rows are often observed to contain several subgrains across their width or thickness. It was generally observed that the boundaries separating adjacent subgrain rows were not smooth, but rather "lumpy." The irregularities of the row boundaries followed the boundaries of individual subgrains.

Often during the course of serial sectioning it was found that, as a subgrain row was polished away, another row with a different average crystallographic orientation appeared below it and in the same plane of rows. This observation is consistent with the previously described alternating crystallographic orientations of subgrain rows and shows that they alternate in orientation not only as seen on the surface, but also within the volume of the material.

3.5.2.2. Observations of subgrain row traces on two or more metallographically prepared surfaces

Several metallographic specimens with well-developed subgrain rows were sectioned so that surfaces parallel to their sides and edges could be prepared for metallographic examination. In two specimens, metallographic surfaces were prepared, at various other angles through the specimen.

By examining several metallographic surfaces at different angles through a creep specimen, it was found that, if subgrain rows were seen on one section through a grain, they were also to be seen in other sections through the same grain. This particular feature was observed in at least a dozen grains. The likelihood that subgrain rows could be seen on any arbitrary surface passed through a grain is greatly enhanced if the three-dimensional subgrain structure is row-like rather than plate-like. If the three-dimensional subgrain structure were plate-like, then by sectioning parallel to the plates one would observe no row structure. By

sectioning at a small angle to the plates, one would observe a structure of wide rows. It was quite evident that a three-dimensional plate-like subgrain structure did not exist in any of the grains examined.

A number of grains examined exhibited a crosshatched or checkerboard pattern on one or more of the surfaces through the grain. Such a pattern of subgrains is easily rationalized if one visualizes an orderly stack of 2" x 4" boards and considers that each board represents a row of subgrains. The end view of this stack of lumber has very much the same configuration as an "end-on" view of the three-dimensional subgrain row structure. The checkerboard pattern would be observed in almost any section through a grain of subgrain rows except, of course, those sections which are nearly parallel to the length dimensions of the subgrain rows. Examples of the checkerboard or crosshatched pattern of subgrain rows can be seen in several of the photomicrographs in Figures 22, 23, 24 and 27. A particularly good example is shown by the photomicrograph of Figure 23(e).

Subgrain rows seen on two intersecting surfaces were invariably found to join at the intersection of the two surfaces. The three-dimensional structure of subgrain rows lying in planes is further supported by this observation. If subgrain rows observed in two surfaces meet the intersection of two surfaces, it seems reasonable to expect that the surface traces of the subgrain rows then define a plane

in which the rows lie. This concept is analogous to the two-surface method for the determination of the orientation of slip planes from traces of slip lines on the surfaces of a deformed test specimen.

Regarding the orientation of subgrain rows with respect to the tensile axis, it was found that the planes of subgrain rows were oriented such that the angles between the poles of these planes and the tensile axis were of the order of 40° to 60°. Planes oriented in this way would contain directions with high resolved shear stresses. An example of planes of subgrain rows determined from traces of subgrain rows on intersecting surfaces of creep specimen S5-7 is shown in Figures 36 through 38. Photomicrographs of subgrain rows on surfaces parallel to the side and one edge of specimen S5-7 are shown in Figure 36 (a and b), respectively. Corresponding regions on the two surfaces are indicated on the photomicrographs. The sketch in Figure 37 shows the subgrain row traces measured and the values of the corresponding angles. Note that a rather strong checkerboard pattern is evident on the surface parallel to the edge of the specimen. For this reason, two trace angles were measured. It is also to be pointed out that the surface parallel to the edge of the specimen is 4° from being parallel to the tensile axis. This deviation was taken into account when the orientation of the plane was determined. Stereographic plots of the planes of subgrain rows are given in

(a) 25X

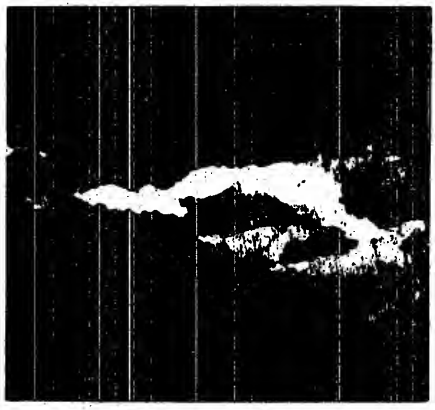

(b) 25X

Figure 36. Photomicrographs showing the subgrain row pattern in specimen S5-7. (a) Subgrain row side traces. (b) Subgrain row edge traces.

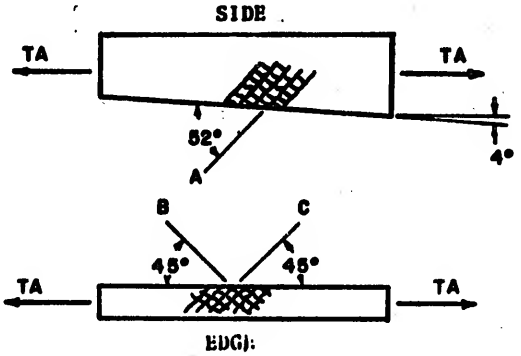

Figure 37. The orientation of subgrain rows in specimen S5-7. Subgrain row traces are indicated by the letters A, B and C. "TA" indicates the direction of the tensile axis. Trace angles are shown.

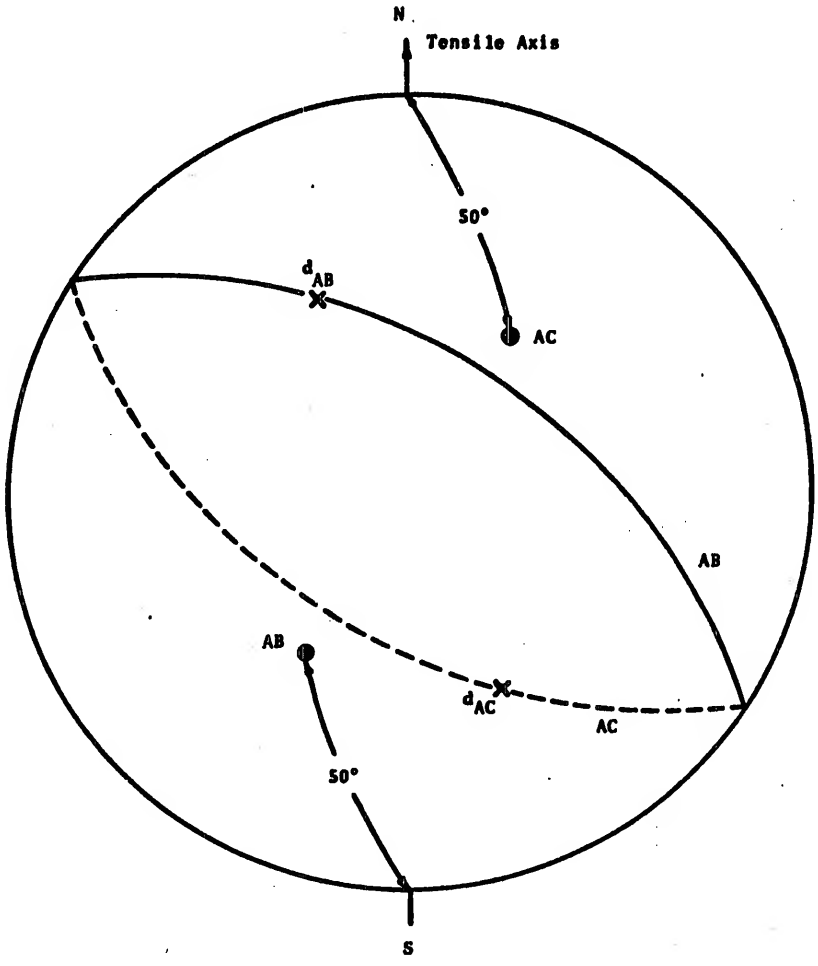

Figure 38. Stereographic plots of planes (AB and AC) corresponding to boundaries separating subgrain rows.

Figure 37, where the planes are indicated both by their poles and their great circles. Planes "AB" and "AC" were obtained from subgrain row traces A, B and C, as shown in Figure 38. Note that the poles of both planes make angles of 50° with the tensile axis and that plane "AB" is normal to plane "AC." The directions in each plane of the maximum resolved shear stress are given by the poles "d_{AB}" and "d_{AC}."

3.5.2.3. A three-dimensional model of the subgrain row structure

In the previous section an analogy was drawn between the subgrain row structure and a stack of lumber. Although this analogy is highly idealized, it does represent fairly well many of the details of the subgrain row structure as observed by the several metallographic techniques. Therefore, a model was constructed of 1/4 inch by 1/4 inch balsa wood strips to illustrate the three-dimensional nature of the subgrain structure. A photograph of the model is shown in Figure 39. The top and sides of the model show subgrain rows in the long dimension, and the crosshatch markings indicate a difference in crystallographic orientation from the unmarked rows. In the front face, row ends form the edges of vertical and horizontal planes of subgrain rows. The end view of the rows illustrates the checkerboard subgrain row described previously.

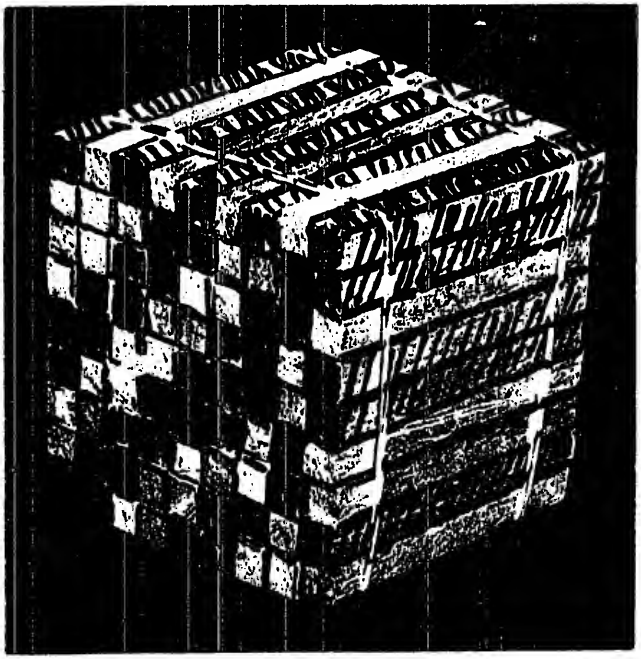

Figure 39. Strip-wood model illustrating the three-dimensional nature of subgrain rows.

3.5.3. The Angular Misorientation Across Subgrain Row Boundaries

In Section 3.5.1, the alternating shading among subgrain rows as seen under polarized light was described. It was presumed that the subgrain rows alternated in crystallographic orientation in a like manner. To verify this, specimens with well-defined subgrain rows were electropolished, etch pitted in Tucker's reagent and anodized. This preparation rendered the subgrain rows visible under polarized light and produced etch pits within each subgrain row. The electropolishing technique used is given in Appendix I as solution #2. Etch pitting was accomplished by immersion of the specimens in Tucker's reagent at 5°C for about 10 seconds. Tucker's reagent consists of 35 percent nitric acid, 61 percent hydrochloric acid and 4 percent hydrofluoric acid. After etch pitting, the specimens were anodized in the usual manner (Appendix I). The photomicrographs shown in Figure 40 show the etch pits in the subgrain row structure in heavily deformed specimen, S5-7. At a magnification of 400X, segments of seven subgrain rows can be seen (Figure 40(a)). In the particular grain shown, the etch pits produced indicated that the (110) plane was nearly parallel to the metallographically prepared surface. By examining the orientations of the [100] directions, which correspond to the center lines at the bottoms of the etch pits, it was found that the crystallographic orientations of the rows were tilted with respect to one another, by

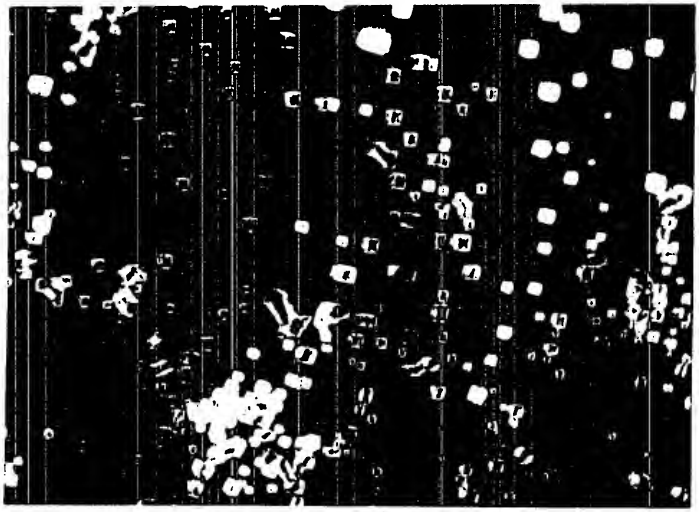

(a) 400X

Figure 40. The microstructure of specimen S5-7 showing subgrain rows and etch pits which indicate crystallographic orientation. The photomicrograph was taken in an un-necked region of the specimen.

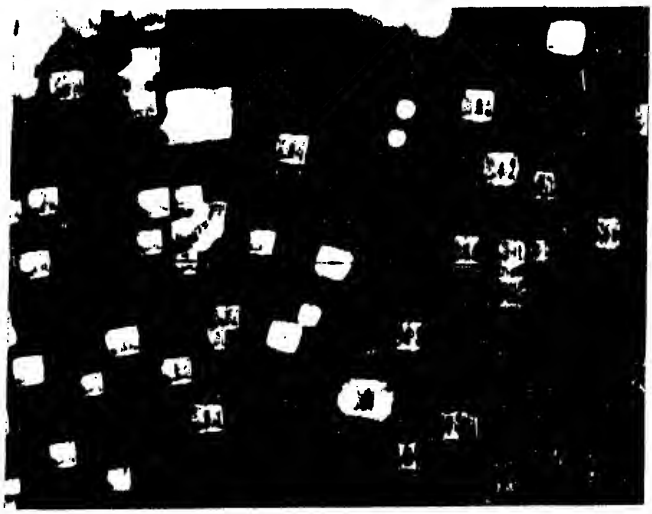

(b) 800X

Figure 40. (continued). Note that lines are drawn parallel to <100> directions.

measurable angles. Further, it was found that orientation of the rows alternated as was first expected. Thus alternating orientations are more easily seen in the higher magnification (800X) photomicrograph of Figure 40(b). Crystallographic tilts between adjacent subgrain rows were surprisingly large. In some instances these tilts were as much as 25°.

Consistent with the idea that early in secondary creep the angular misorientation between rows is small and that the misorientation increases with increasing amounts of creep strain, the misorientations between subgrain rows measured in specimen S1-2, strained to only 4.9 percent at 200°C under an initial stress of 1,000 psi, were of the order of 2.5° to 3.0°.

3.5.4. The Boundaries Between Subgrain Rows and Their Relation to Surface Bands

To establish a connection between the spatial orientation of surface bands and subgrain rows, and to ascertain the nature of the boundaries separating subgrain rows, the orientation relationships among the surface bands developed during creep, the boundaries separating subgrain rows and the crystallographic orientations of individual grains became important. Therefore, a study was made of the orientations of surface band and subgrain rows in relation to the crystallographic orientations in several grains of a large-grained specimen which had been creep tested to rupture. The large

grain size was produced by straining 1 percent at room temperature and annealing at 600°C for 53 hours. Creep testing was performed under an initial stress of 500 psi for 23.5 hours at 116°C, 24.5 hours at 228°C and for about 50 minutes during a temperature increase to 300°C. Rupture of the specimen occurred before the temperature became equilibrated at 300°C. Upon rupture, the lower portion of the specimen was immediately water quenched, and the upper portion was quenched within 15 seconds.

The surface bands developed during the creep test consisted of one or more families of rather straight lines in each grain. These bands were presumed to be associated with slip or some other form of shear. The microstructure consisted of sharply defined subgrain rows in each grain.

Surfaces of the upper portion of the specimen were carefully examined under the microscope and the angles between traces of the surface bands and the tensile axis were measured and recorded for each of the five largest grains. These measurements were made on one side and both edges of the specimen. A schematic diagram indicating the angular measurements is given in Figure 41.

Next, the specimen was mounted and metallographically prepared so that surfaces parallel to the edges and the side previously examined could be observed under the microscope. Angles between the subgrain row traces and the tensile axis were measured on both edges and the surface as shown schematically in Figure 42. In two instances (grains #1 and

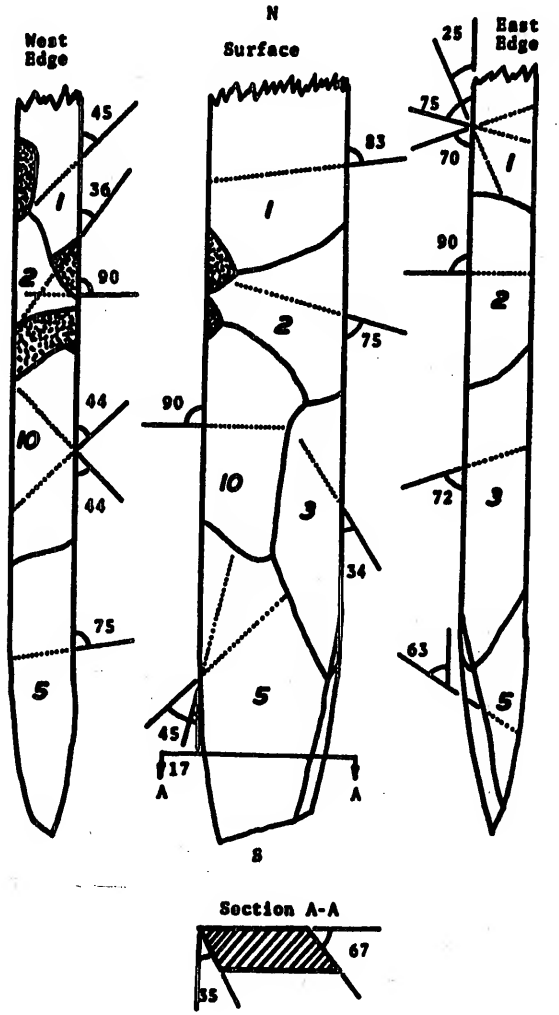

Figure 41. Traces of surface bands on specimen S5-8.

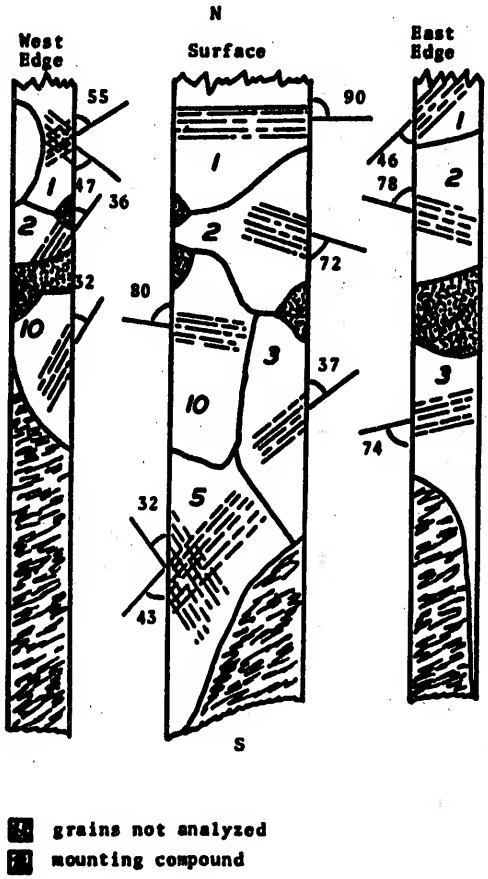

Figure 42. Subgrain row traces in specimen S5-8.

#5), two sets of subgrain rows, making different angles with the tensile axis, appeared to be superimposed upon one another; therefore, both trace angles were measured (see Figure 42).

From the traces of the surface bands and the subgrain rows, planes corresponding to the surface bands and to the boundaries between subgrain rows were obtained by the usual two-surface analysis. These planes are listed in Table II for each of the five largest grains, along with the traces from which they were obtained.

A correspondence between the surface bands and the traces of subgrain rows can be seen by comparing Figures 41 and 42. Note that there exists in grains #1, #2, #3 and #10 an apparent correspondence between some of the surface bands and some subgrain row traces. For instance, in grain #1, plane "D" and plane "F" approximately coincide. Exact angular coincidence of the planes is not realized because of the difficulty in obtaining accurate measurements of the angles between the traces of surface bands and the tensile axis on the very highly distorted surfaces developed during creep.

The crystallographic orientation of each of the five largest grains was determined from the measurement of etch pits according to the methods of Tucker and Murphy [169]. Because of the subgrain structure developed within each grain, no single etch pit was representative of the

Table II

Planes Corresponding to Surface Bands and Boundaries Between Subgrain Rows

Planes	Surface Markings	Subgrain Rows
Grain #1		
A	Surface: 83° - East: 25°	------
B	Surface: 83° - East: 75°	------
C	Surface: 83° - East: 70°	------
D	Surface: 83° - West: 45°	------
E	------	Surface: 90° - East: 46°
F	------	Surface: 90° - West: 55°
G	------	Surface: 90° - West: 47°
Grain #2		
A	Surface: 75° - East: 90° West: 90°	------
B	Surface: 75° - West: 36°	------
C	------	Surface: 72° - East: 78°
D	------	Surface: 72° - West: 36°
Grain #3		
A	Surface: 34° - East: 72°	------
B	------	Surface: 37° - East: 74°
Grain #10		
A	Surface: 90° - West: 44°	------
B	Surface: 90° - West: 44°	------
C	------	Surface: 80° - West: 32°
Grain #5		
A	Surface: 45° - East: 63°	------
B	Surface: 17° - East: 63°	------
C	Surface: 45° - West: 75°	------
D	Surface: 17° - West: 75°	------

orientation of a given grain. For this reason, a number of etch pits (ten or twenty) were measured in each grain and an average orientation was determined. To produce the etch pits, the specimen was first electropolished in Solution #2 (Appendix I) and then immersed in Tucker's reagent at 5°C for about 10 seconds. Following etch pitting the specimen was anodized in the usual manner (Appendix I) to render the microstructure sensitive to polarized light. Angular measurements of the etch pits in the five largest grains are given in Tables III through VII. These tables also include sketches to indicate the configurations of the etch pits, the angles measured and the angles which were either calculated or taken from the tabular data of Tucker and Murphy [169]. In these tables, the word "boundary" inserted in the list of etch pits indicates that measurements were made in adjacent subgrain rows. In all cases, the boundaries across which measurements were made were those separating subgrain rows.

The orientation of each grain is shown by the stereographic plots in Figures 43 through 47. The planes obtained from the traces of surface markings and subgrain rows are also shown in these stereographic plots. They are indicated by their great circles and their poles (square symbols). Planes obtained from the traces of surface markings may correspond to slip planes, may be approximately coincident with the boundary planes of subgrain rows or may have no simple

Table III

Etch Pit Measurements: Grain #1

(Triangular Etch Pits)

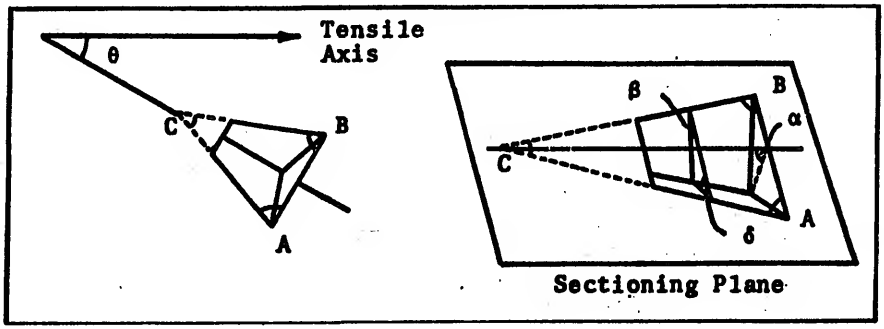

Etch Pit	θ (°)	A (°)	B (°)	C (°)	α (°)	β (°)	δ (°)
1	43	83	82	15	82	47	44
2	42	80	78	22	79	49	44
3	41	86	80	14	85	58	33
4	43	83	84	13	84	43	48
5	43	80	86	14	85	33	58
6	46	86	85	9	86	48	42
7	44	89	88	3	89	55	35
Boundary	(Tilt 5°)						
8	49	89	88	3	89	55	35
9	42	86	83	11	85	53	37
Boundary	(Tilt 3°)						
10	45	86	84	10	85	55	36

Average angles: $\bar{\theta} = 43.8°$, $\alpha = 84.9°$, $\beta = 49°$, $\delta = 41°$

NOTE: From tabular data of Tucker and Murphy [169].

Table IV

Etch Pit Measurements: Grain #2

(Rectangular Etch Pits)

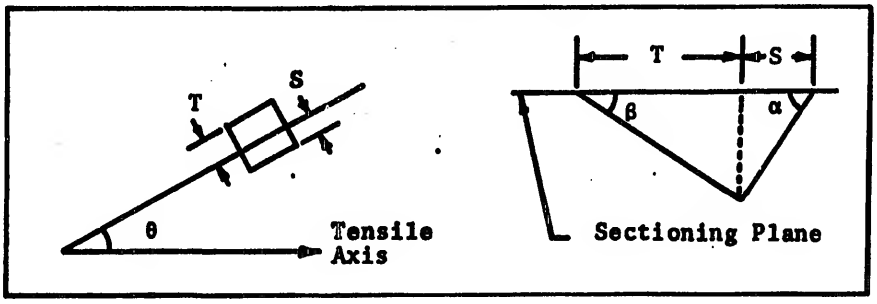

Etch Pit	θ (°)	S	T	S/T
1	85	1.0	5.0	0.200
2	83	1.0	6.0	0.167
3	87	1.0	5.0	0.200
4	84	1.0	5.0	0.200
5	82	1.5	6.5	0.230
6	83	1.0	6.0	0.167
7	86	1.0	6.0	0.167
8	85	1.0	5.0	0.200
9	85	1.0	5.0	0.200
10	84	1.5	6.5	0.230
11	83	1.0	6.0	0.167
12	87	1.0	6.0	0.167
13	83	1.0	5.0	0.200
Boundary	(Tilt 3°)			
14	86	1.0	5.0	0.200
15	83	1.0	5.0	0.200
Boundary	(Tilt 3°)			
16	86	1.0	5.0	0.200
17	87	1.0	5.0	0.200
Boundary	(Tilt 3°)			
18	83	1.0	5.0	0.200
19	85	1.5	6.5	0.230
Boundary	(Tilt 3°)			
20	82	1.5	6.5	0.230

θ (average) = 84.5°; S/T (average = 0.198; T/S (average = 5.050.

$\alpha = \tan^{-1}\sqrt{T/S} = \tan^{-1} 2.25 = 66°$

$\beta = \tan\sqrt{S/T} = \tan^{-1} 0.445 = 24°$

Table V

Etch Pit Measurements: Grain #3

(Square Etch Pits)

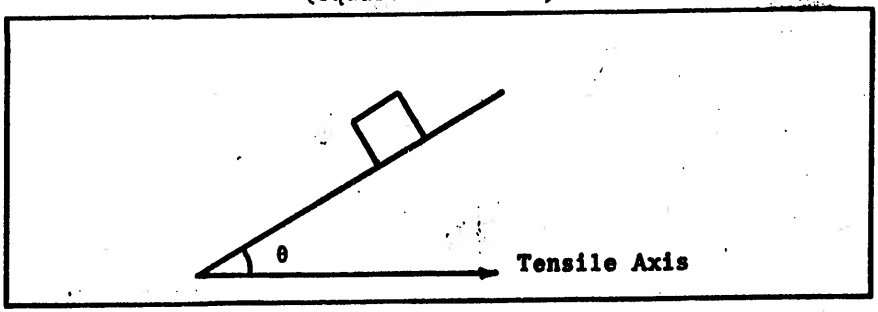

Etch Pit	θ (°)
1	9
2	11
3	1
4	10
5	7
6	10
7	9
Boundary	(Tilt 5°)
8	4
9	8
Boundary	(Tilt 3°)
10	11
11	12
12	10
13	5
14	9
15	10
Boundary	(Tilt 4°)
16	6
17	6
18	8
19	11
Boundary	(Tilt 6°)
20	5

θ (average) = 8.1°

Table VI

Etch Pit Measurements: Grain #10

(Rectangular Etch Pits)

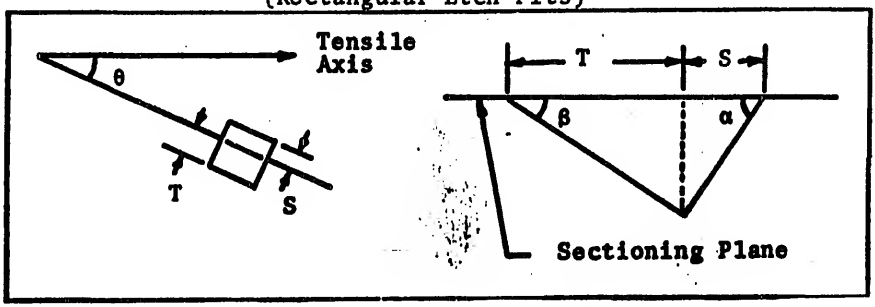

Etch Pit	θ (°)	S	T	S/T
1	44	4.0	6.0	0.667
2	43	2.0	3.0	0.667
3	45	4.0	5.5	0.727
4	38	4.0	6.0	0.667
5	42	2.0	3.0	0.667
6	44	4.0	5.5	0.727
7	47	4.0	6.0	0.667
8	42	3.0	4.5	0.667
9	41	3.0	4.5	0.667
10	39	2.0	3.0	0.667
11	44	3.0	5.0	0.600
12	47	4.0	5.5	0.727
13	43	3.0	4.5	0.667
Boundary	(Tilt 5°)			
14	48	2.0	3.0	0.667
15	46	2.0	3.0	0.667
Boundary	(Tilt 9°)			
16	37	2.0	3.0	0.667
17	45	2.0	3.0	0.667
Boundary	(Tilt 5°)			
18	40	4.0	6.0	0.667
19	47	4.0	6.0	0.667
Boundary	(Tilt 8°)			
20	39	3.0	4.5	0.667

θ (average) = 43°; S/T (average) = 0.673;
T/S (average) = 1.485.

$\alpha = \tan^{-1}\sqrt{T/S} = \tan^{-1} 1.22 = 50.6°$

$\beta = \tan^{-1}\sqrt{S/T} = \tan^{-1} 0.822 = 39.4°$

Table VII

Etch Pit Measurements: Grain #5

(Square Etch Pits)

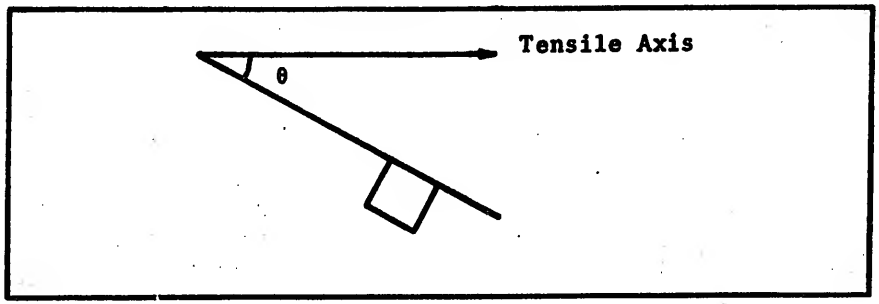

Etch Pit	θ (°)
1	27
Boundary	(Tilt 9°)
2	18
Boundary	(Tilt 6°)
3	24
4	25
Boundary	(Tilt 11°)
5	14
Boundary	(Tilt 10°)
6	24
7	26
Boundary	(Tilt 10°)
8	16
9	28
Boundary	(Tilt 8°)
10	20

θ (average) = 22.2°

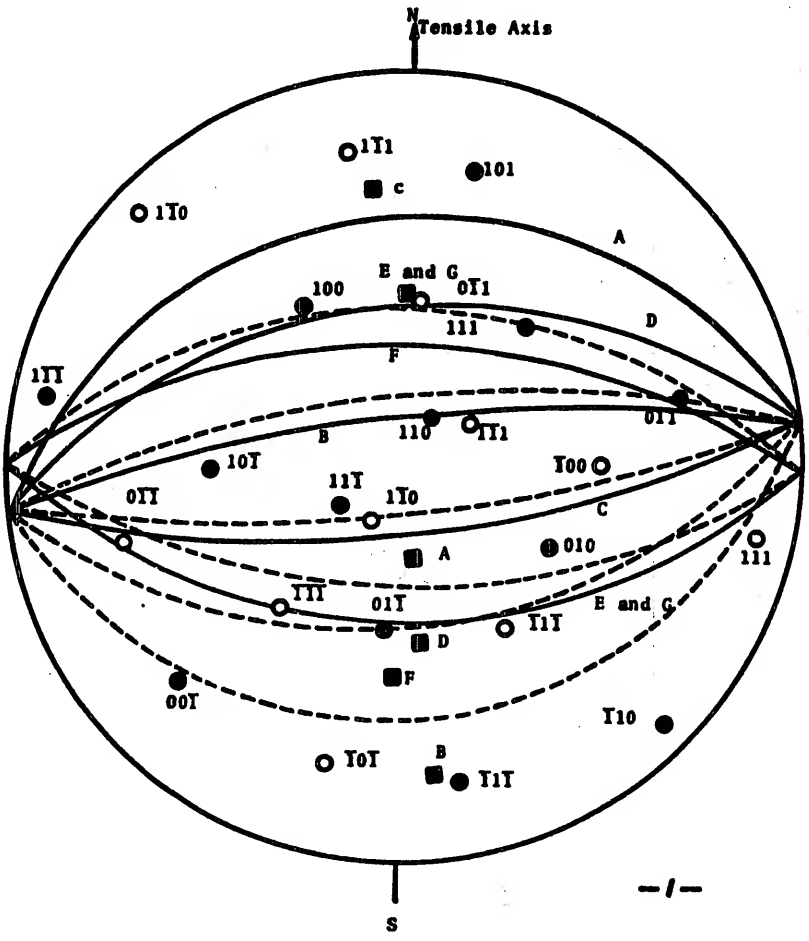

Figure 43. Stereographic projection of the orientation of grain #1 and the planes determined from the traces of surface bands and from the traces of subgrain rows.

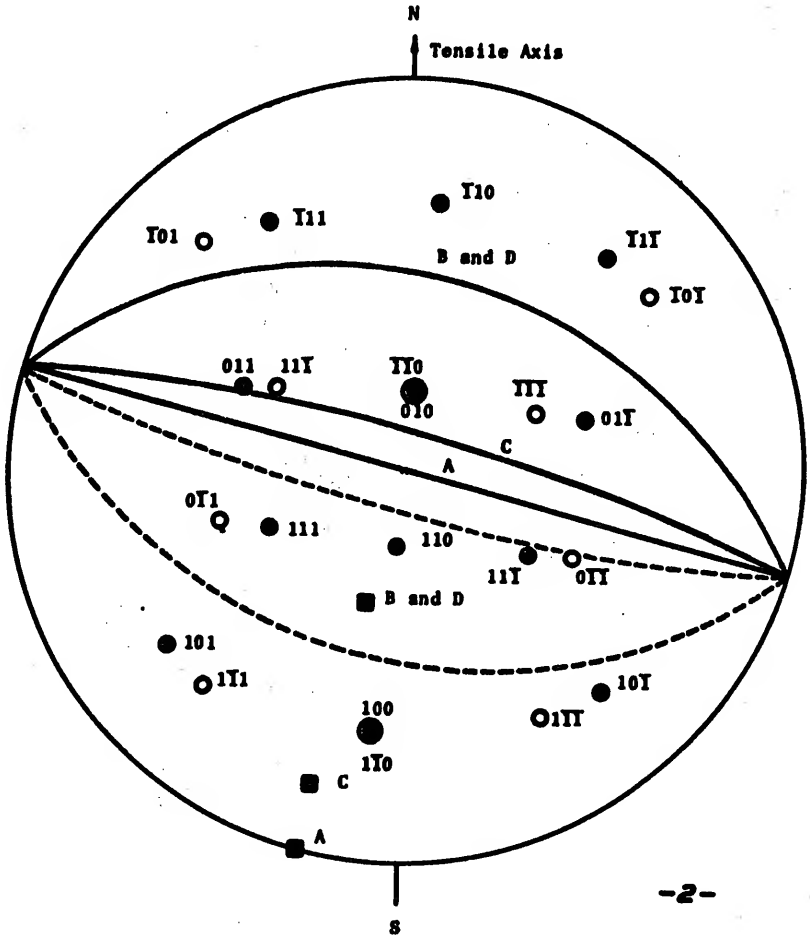

Figure 44. Stereographic projection of the orientation of grain #2 and the planes determined from the traces of surface bands and from the traces of subgrain rows.

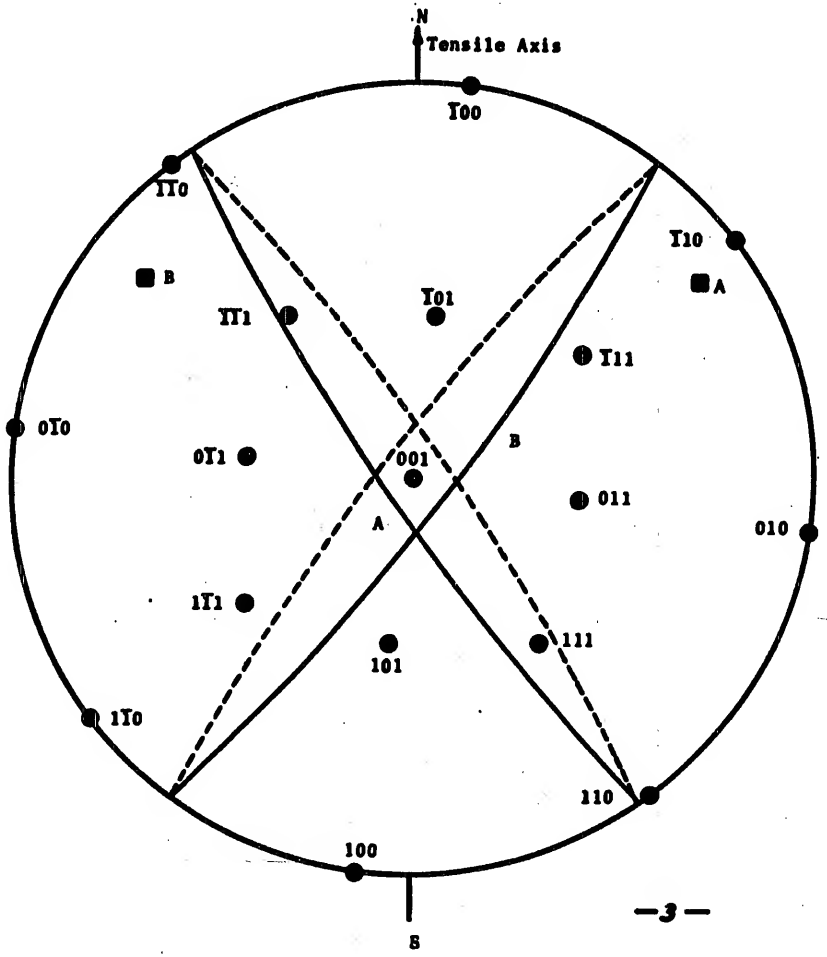

Figure 45. Stereographic projection of the orientation of grain #3 and the planes determined from the traces of surface bands and from the traces of subgrain rows.

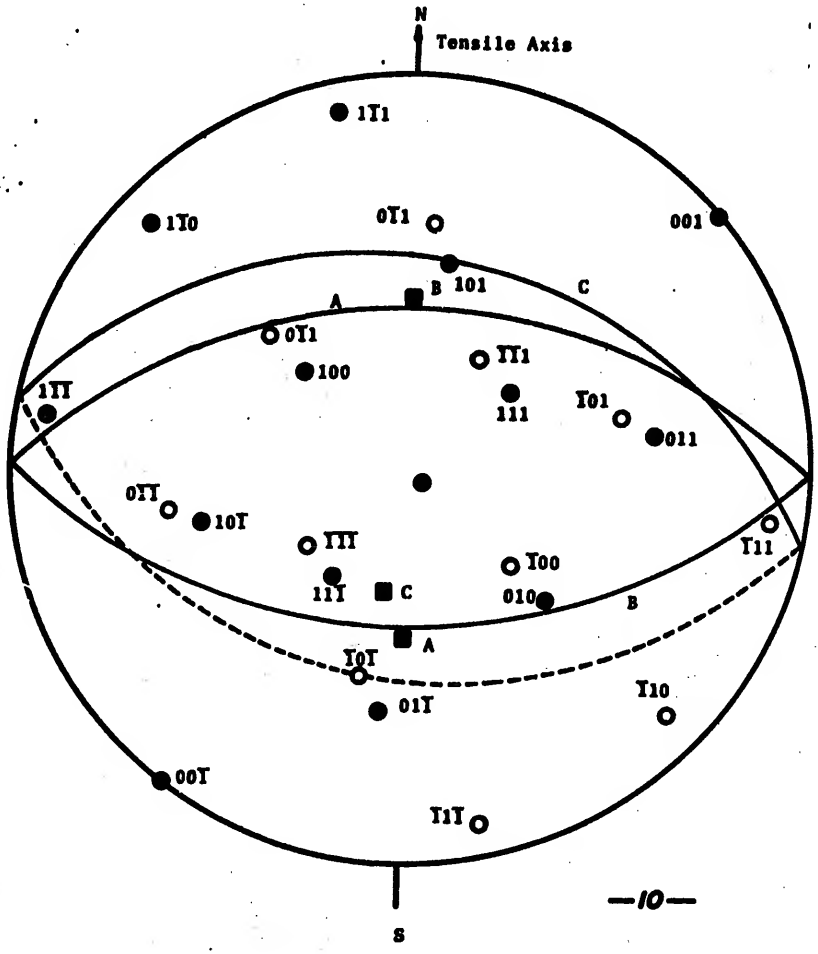

Figure 46. Stereographic projection of the orientation of grain #10 and the planes determined from the traces of surface bands and from the traces of subgrain rows.

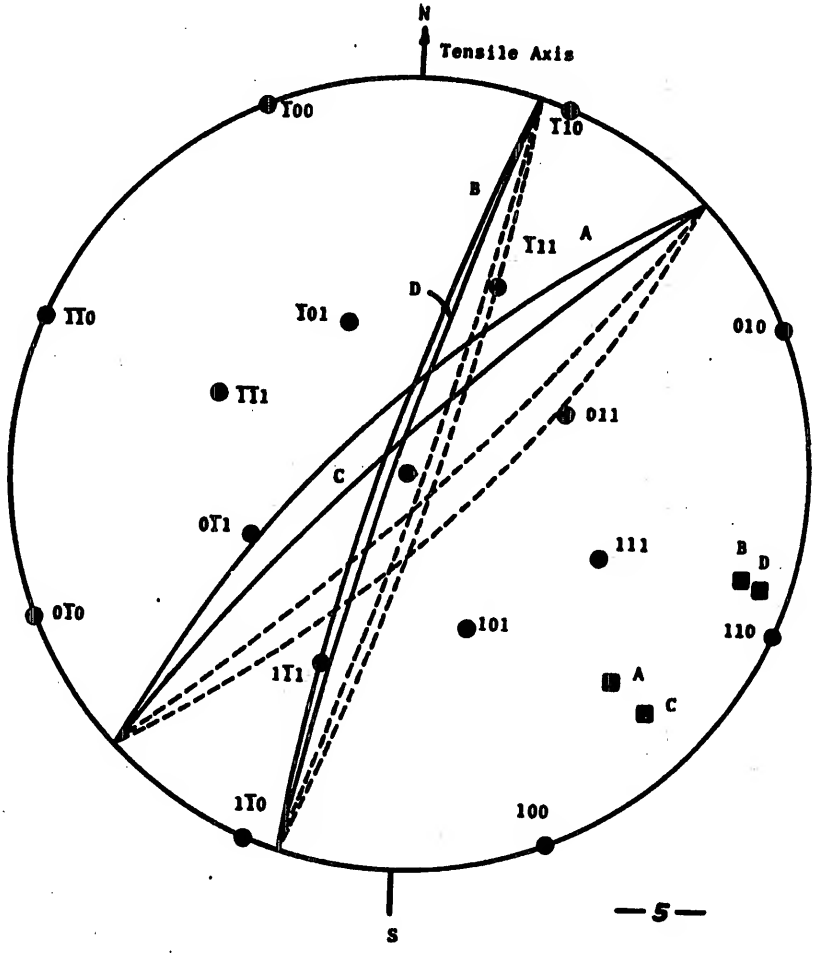

Figure 47. Stereographic projection of the orientation of grain #5 and the planes determined from the traces of surface bands.

relation to the crystallographic orientation. In the latter case, surface bands probably are the result of the interaction among dislocations from several slip systems which are operative during the course of creep. Planes obtained from the traces of subgrain rows represent the average orientation of boundaries between subgrain rows; therefore, it was expected that these planes should be aligned rather closely with planes normal to slip directions, indicating an "average" boundary with a simple tilt character. In general, however, most boundaries between subgrain rows were not simply or exactly related to slip directions, but rather had only approximate geometric correspondence to either slip directions or planes. Such boundaries are no doubt complex and are the result of the alignment of dislocations from several slip systems into a boundary wall.

To present a more detailed picture of the orientations of surface markings and the boundaries between subgrain rows and their relation to crystallographic orientation, the results obtained for each grain will be described individually in the following outline.

Grain #1 (Figure 43):

Plane A (surface bands) shows no simple correlation to either slip planes or slip directions.

Plane B (surface bands) is within 5° of being parallel to the $(\bar{1}1\bar{1})$ slip plane; therefore, surface markings probably are slip bands.

Plane C (surface bands) is within about 20° of being normal to the [101] slip direction.

Plane D (surface bands) is within 8° of being normal to the [01$\bar{1}$] slip direction; therefore, it nearly represents a tilt boundary.

Plane E (subgrain boundary) is nearly normal to the (0$\bar{1}$1) plane and within about 2° of being parallel to the [01$\bar{1}$] and [0$\bar{1}$1] slip directions.

Plane F (subgrain boundary) is nearly coincident with plane D and is within about 11° of being normal to the [01$\bar{1}$] slip direction; therefore, it nearly represents a tilt boundary.

Plane G (subgrain boundary) coincides with plane E.

Grain #2 (Figure 44):

Plane A (surface bands) has no simple correlation to either slip planes or slip directions.

Plane B (surface bands) is within 17° of being normal to the [110] slip direction.

Plane C (subgrain boundary) has no simple correlation to either slip planes or slip directions, but it is within 11° of being coincident with plane A.

Plane D (subgrain boundary) is coincident with plane A.

Grain #3 (Figure 45):

Plane A (surface bands) is within 9° of being normal to the [$\bar{1}$10] slip direction; therefore, it nearly represents a tilt boundary.

Plane B (subgrain boundary) is within 16° of being normal to plane A and is within 18° of being normal to the $[\bar{1}\bar{1}0]$ slip direction.

Grain #10 (Figure 46):

Plane A (surface bands) is within 18° of being normal to the $[01\bar{1}]$ slip direction.

Plane B (surface bands) is within 12° of being normal to the [101] slip direction.

Plane C (subgrain boundary) is within 12° of being coincident with plane A and within 14° of being parallel to the $(11\bar{1})$ slip plane; therefore, the "average" boundary represented by this plane is no doubt of a very complex nature.

Grain #5 (Figure 47):

Plane A (surface bands) has no simple relation to a slip plane, but it does contain the $[0\bar{1}1]$ slip direction.

Plane B (surface bands) is within 9° of being normal to the [110] slip direction.

Plane C (surface bands) is within 10° of being coincident with plane A, but it has no simple relation to either slip planes or slip directions.

Plane D (surface bands) is within 7° of being normal to the [110] slip direction and within 4° of being coincident with plane B.

Although no measurements were made of subgrain row traces on surfaces parallel to the edges of the specimen, it can be seen by comparing Figures 41 and 42 that subgrain row traces do correspond to a trace of surface bands on the surface of the creep specimen.

Further evidence that subgrain rows are related to the surface bands developed during the course of creep was obtained by metallographic examination of the lower portion of the specimen. The specimen was mounted in the usual manner in Caulk NuWeld dental plastic, which in very thin sections is rather transparent. In metallographic preparation, the specimen was not initially ground on SiC papers as was the usual practice but,rather, only polished using 1200 grit emery. As the plastic covering upon the surface of the specimen became thinner with successive polishing, the surface bands became observable under the microscope. Polishing was continued in steps until the plastic was removed from the high spots on the specimen surface and these high spots became polished. Anodizing in the usual manner rendered the microstructure in the high spots sensitive to polarized light. In this way, both surface bands and the subgrain rows could be viewed simultaneously. Successive polishing steps increased the polished area of the specimen so that an increasing fraction of the underlying microstructure could be observed.

It was a general observation that the more pronounced surface bands were aligned with boundaries between subgrain rows. The photomicrographs of Figure 48 show the alignment of subgrain rows with surface bands.

In one instance, the surface bands were found to be perpendicular to underlying subgrain rows. The subgrain structure possessed a weak checkerboard pattern and the surface bands were aligned with one of the orthogonal directions of the subgrain rows. A photomicrograph showing this particular observation is given in Figure 48(b).

Only about one-third of the surface band and subgrain row traces in specimen S5-8 are close (within 10°) to being oriented at 45° to the tensile axis. This seems to be a relatively small proportion compared to measurements of subgrain row orientations in fine-grained creep specimens. It is suspected that the reason for this conflicting observation lies in the much greater effect of the surface upon the deformation of the coarse-grained specimen.

This investigation has yielded several significant results. First, there is evidence that some of the surface bands developed during creep are connected with the underlying subgrain row structure. Second, the "average" boundaries separating subgrain rows are generally complex in terms of their dislocation content. It is to be pointed out, however, that this is a property of the "average" boundary. If individual segments of the boundary separating subgrain

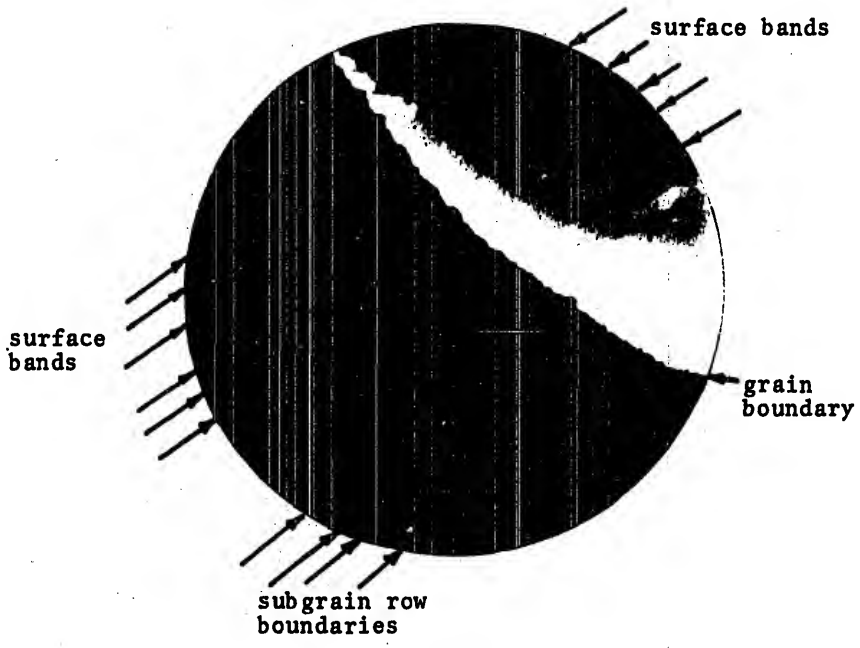

(a) 25X

Figure 48. Photomicrographs showing the alignment between surface bands and subgrain rows.

(b) 25X

Figure 48. (continued).

rows were considered, it is expected that these segments would be rather more simple in dislocation makeup than the "average" boundary. Third, the measurements suggest that in many instances the "average" boundaries between subgrain rows closely represent simple tilt boundaries. Finally, it is important that the "average" boundaries between subgrain rows are not coincident with slip planes. The significance of this final result will become apparent in future sections of this chapter and in the discussion of the results.

3.6. The Effect of Grain Boundaries on Deformation

Regardless of the temperature, stress, strain rate or the amount of strain, the microstructures developed in specimens which were deformed hot or at room temperature all exhibit evidence of the influence of grain boundaries on deformation. During deformation, the grains develop a "blocky" appearance in their substructures. Each "block" may consist of one or more subgrains which have similar orientations. That each block appears to be associated with a given grain boundary or segment of a boundary, suggests that the deformation in any given grain is rather strongly influenced by the presence of its surrounding boundaries. Varying degrees of blockiness can be seen in the microstructures of Figures 22 through 30. A particularly strong effect is shown in Figure 30.

The effects of grain boundaries upon deformation are also manifested in the variation in the sharpness and form of the serrations produced during deformation in the boundaries surrounding single grains, Section 3.4, Figure 33. Variations in the grain boundary serrations of this sort would be difficult to justify if the grain boundaries did not exert an influence upon deformation.

3.7. The Microstructural Evolution During Creep I: Results from Constant Load and Constant Temperature Creep Tests

During the course of creep, it has been observed qualitatively that the microstructures of creep specimens undergo several significant changes with increasing amounts of creep strain and also with variations in temperature and initial stress. These changes in microstructure include grain growth, the formation of subgrains, the formation of rows of subgrains and the formation of serrations in grain boundaries. The primary emphasis of this section is to describe quantitatively the evolution of the microstructure during second stage creep and to correlate this evolution to the formation of grain boundary serrations. The quantization of the microstructural evolution was accomplished by employing basic counting techniques of quantitative metallography to measure parameters which describe the microstructure in specimens tested under the several conditions of temperature and initial stress. As previously described, several specimens

were tested under each set of creep conditions (temperature and stress), the testing of individual specimens differing only in the length of time they were tested. Except as noted, the quantitative metallographic data were obtained from specimens in which necks had not formed.

The ranges of creep testing conditions employed for this portion of the research are given in Table VIII. A number of specimens tested at stresses other than those listed in Table VIII were excluded from the quantitative metallographic evaluation because they either ruptured or necked during creep testing. It was believed that the quantitative metallographic measurements of those specimens which ruptured may be in serious error because their hot deformation microstructures might not be fully preserved by quenching without an applied load. Those specimens which formed necks during creep were observed to exhibit a wide variation in the microstructure. This variation would, no doubt, result in a large statistical spread in the quantitative metallographic measurements and cast a significant degree of doubt upon the validity of these measurements. The listed sets of creep conditions were chosen so that tertiary creep would not commence within a testing interval of twenty-four hours. For a complete listing of the creep conditions of temperature and initial stress, refer to Chapter II, Experimental Techniques.

Table VIII

The Creep Testing Conditions for the Evaluation of the Microstructural Evolution During Creep

Temperature (°C)	Stress (psi)
425	150
350	250; 400
275	400; 800
200	800; 1,000; 1,200

3.7.1. Analysis of Strain Rate versus Temperature and Stress

In the first chapter, it was pointed out that the creep rate during secondary creep usually is dependent upon temperature and stress according to the empirical equation

$$\dot{\varepsilon} = A\sigma^n e^{-\Delta H/RT}, \qquad (10)$$

where $\dot{\varepsilon}$ = strain rate ($d\varepsilon/dt$), A = a constant of the material, σ = stress, n = stress sensitivity constant, ΔH = activation energy for creep, R = gas constant, and T = the absolute temperature.

Although it was not a primary objective of this research to study in depth the relations between strain rate, stress and temperature, it is essential to have at least a semi-quantitative idea of how the strain rate depends upon stress and temperature. The importance of this knowledge will become more apparent in later sections of the chapter where the various parameters which characterize the microstructure are related to the strain, temperature and stress. The conditions of the creep tests and the steady state creep rates obtained are given in Table IX.

In order to determine the values for the constants in the strain rate equation (equation 10), the following statistical scheme was employed.

1. The strain rate equation was divided by $e^{-\Delta H/RT}$ and the logarithm of both sides was taken to result in the form

$$\log(\dot{\varepsilon}\, e^{\Delta H/RT}) = \log A + n \log \sigma, \qquad (11)$$

Table IX

The Conditions of Creep Testing and Secondary Creep Rates

Temperature (°C)	σ (psi)	Specimen Number	$\dot{\varepsilon}$ (min^{-1})
425	150	S3-6 S3-3 S3-5	8.90×10^{-5}
350	250	S3-10 S3-9 S3-7	7.77×10^{-5}
275	400	S3-13 S3-16 S3-15	1.25×10^{-5}
200	800	S3-19 S3-24 S3-21	7.16×10^{-6}
200	1,000	S1-1 S1-2 S1-4 S1-5	1.08×10^{-5}
200	1,000	S1-7 S1-8 S1-9	2.00×10^{-4}
200	1,200	S3-22 S3-20	3.08×10^{-4}

where $(\dot{\varepsilon}\, e^{\Delta H/RT})$ is the Zener-Hollomon parameter (ZH), and A, n and σ have their usual meanings. By plotting the log ZH versus log σ, n becomes the slope and log A the intercept.

2. An assumed value for the activation energy, ΔH, was used to compute values of log ZH for each strain rate. These values were plotted versus the logarithms of the corresponding values of stress, σ.

3. The least squares method was employed to fit a straight line to the plotted values of log ZH and log σ. From the least squares data the values of n and log A were determined. Statistical tolerances were computed for the value of n at a 95 percent confidence level.

4. Steps 2 and 3 were repeated for seven values of ΔH ranging from 30 Kcal/mole to 38 Kcal/mole, inclusive. For each assumed value of ΔH, corresponding values of n and log A were determined.

5. To determine which value of ΔH best fitted the plotted data, the sum of the squares of the deviations between the calculated values of log ZH and the corresponding least squares values of log ZH were computed. The notation for this sum is $\Sigma(\log ZH_i - \log\tilde{}ZH_i)^2$. The smaller the magnitude of this quantity, the better is the correlation between the stress, temperature and strain rate data and the assumed value for ΔH.

Table X lists the values of the activation energy, ΔH, the slope or stress sensitivity constant, n, the intercept, log A, and the values of $\Sigma(\log ZH_i - \log\tilde{}ZH_i)^2$. The assumed values of ΔH plotted versus the corresponding values of $\Sigma(\log ZH_i - \log\tilde{}ZH_i)^2$ are given in the graph of Figure 49. From the graph it can be seen that the assumed value of ΔH = 33 Kcal/mole represents the best fit to the creep data. The graph of log ZH versus log σ for ΔH = 33 Kcal/mole is given in Figure 50.

Table X

Assumed Activation Energies, ΔH; Stress Sensitivity Constants, n; Intercepts, log A; and Sums of the Squares of the Deviations, $\Sigma(\log ZH_i - \log \tilde{} ZH_i)^2$

ΔH Kcal/mole	n	log A	$\Sigma(\log ZH_i - \log \tilde{} ZH_i)^2$
38	7.1568 ± 1.6753	-8.2103	0.8517
36	6.7626 ± 1.6789	-7.9646	0.8553
35	6.5643 ± 1.6830	-7.8287	0.8597
34	6.3662 ± 1.6553	-7.7132	0.8315
33	6.0509 ± 1.7801	-7.2360	0.5622
32	5.9703 ± 1.7040	-7.4643	0.8814
30	5.5761 ± 1.7270	-7.2215	0.9051

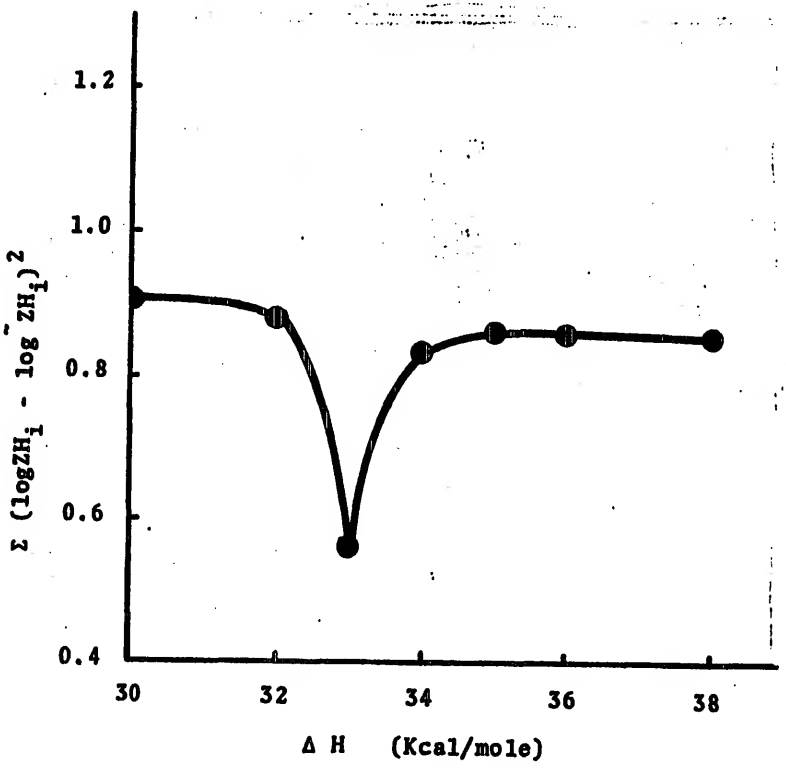

Figure 49. $\Sigma(\log ZH_i - \log \tilde{Z}H_i)^2$ versus ΔH. The parameter ZH is the Zener-Hollomon parameter, $\varepsilon\, e^{\Delta H/RT}$. Log ZH_i is the i^{th} value of log ZH for a given ΔH, and $\log \tilde{Z}H_i$ is the corresponding value of log ZH determined from the least squares straight line. The apparent activation energy is ΔH.

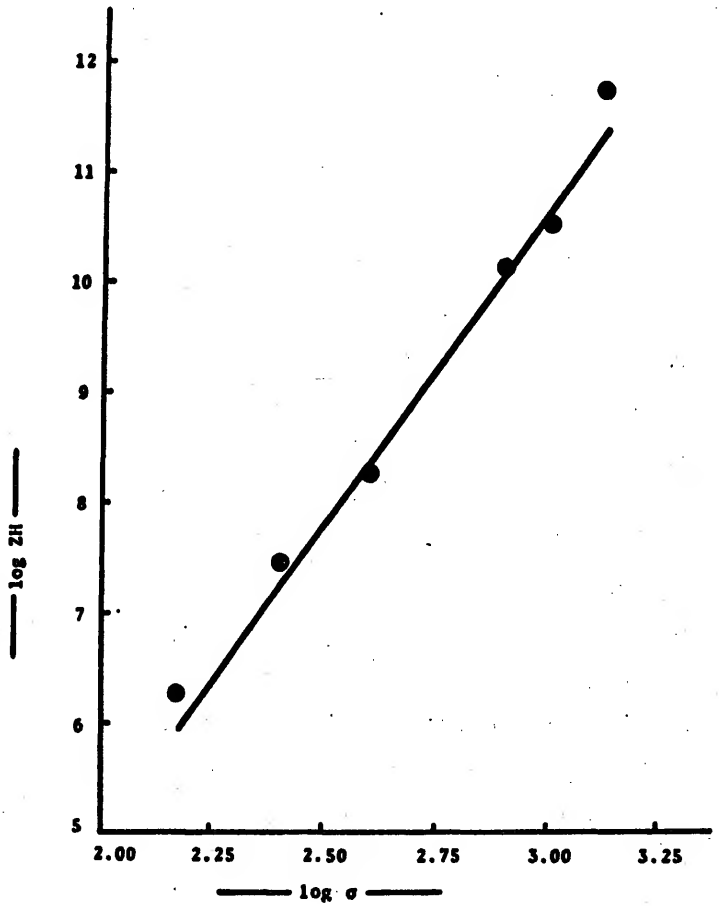

Figure 50. Log ZH ($ZH = \dot{\varepsilon}\, e^{\Delta H/RT}$) versus log σ (σ = stress(psi)).

From the analysis outlined above, it was concluded that the secondary creep rates measured in this portion of the research could be expressed by

$$\dot{\varepsilon} = A\sigma^n e^{-\Delta H/RT} , \qquad (12)$$

where $A = 5.8076 \times 10^{-8}$, $n = 6.0509 \pm 1.7801$, and $\Delta H = 33$ Kcal/mole.

3.7.2. Characterization of the Microstructural Evolution

Metallographic specimens cut from the gage section of each tested creep specimen were prepared for quantitative metallographic evaluation using the automatic mechanical polishing technique described previously. After mechanical polishing the specimens were anodized to render the microstructure sensitive to polarized light. Quantitative metallographic measurements were made according to the scheme outlined in the chapter entitled "Experimental Techniques." From the counted data the parameters listed below were calculated.

1. f_{SG} - the fraction of grains containing subgrains.
2. f_{SGR} - the fraction of grains containing subgrain rows.
3. $f_{SGR(35-55)}$ - the fraction of those grains containing subgrain rows whose rows make angles with the tensile axis in the range of 35° to 55°, inclusive.

4. $S_{V(TOT)}$ - the total boundary area including smooth grain boundaries, serrated boundaries and subgrain boundaries.
5. $\bar{S}_V$ - the boundary area of smooth grain boundaries.
6. $\tilde{S}_V$ - the boundary area of serrated (wavy and dentate) grain boundaries.
7. $S_{V(GB)}$ - the grain boundary area ($\bar{S}_V+\tilde{S}_V$).
8. $S_{V(SGB)}$ - the subgrain boundary area.
9. $e_g(f)-e_g(i)$ - the change in the anisotropy factor.

Table XI gives the initial grain boundary areas $S_{V(GB)}(i)$, the initial anisotropy factors $e_g(i)$, the creep testing conditions, and the values for the nine parameters listed above. The statistical tolerances are given for the data at a confidence level of 95 percent.

The data given in Table XI have been plotted in a series of graphs to show quantitatively the evolution of the microstructure both as a function of time and strain. The following is a list of the parameters which have been chosen to graphically show the microstructural evolution during creep.

1. Grain boundary area, $S_{V(GB)}$.
2. Subgrain boundary area, $S_{V(SGB)}$.
3. The change in grain boundary anisotropy, $e_g(f)-e_g(i)$.
4. The ratio of serrated grain boundary area to the grain boundary area, $\tilde{S}_V/S_{V(GB)}$.
5. The fraction of grains containing subgrains, f_{SG}.
6. The fraction of grains containing subgrain rows, f_{SGR}.
7. The fraction of grains containing only subgrains, $f_{SG}-f_{SGR}$.

Table XI

Specimens, Creep Conditions, and Microstructural Parameters

(a) Specimens and Creep Conditions

Specimen Number	Temp. (T) (°C)	Stress (σ) (psi)	Time (t) (hours)	Strain (ε) (%)
S3-6	425	150	4.00	1.6
S3-3	425	150	7.17	3.2
S3-5	425	150	16.17	14.4
S3-10	350	250	4.17	2.4
S3-9	350	250	10.00	6.4
S3-7	350	250	24.00	12.0
S3-12	350	400	8.83	28.8
S3-13	275	400	4.00	1.6
S3-16	275	400	10.00	1.6
S3-15	275	400	24.00	3.2
S3-18	275	800	5.37	17.6
S3-19	200	800	4.00	2.4
S3-24	200	800	10.92	2.4
S3-21	200	800	24.00	3.2
S1-1	200	1,000	11.85	2.5
S1-2	200	1,000	24.05	4.9
S1-4	200	1,000	95.78	9.8
S1-5	200	1,000	191.90	14.8
S1-7	200	1,000	24.00	4.9
S1-8	200	1,000	96.28	13.1
S1-9	200	1,000	192.37	33.0
S3-22	200	1,200	10.43	7.20
S3-20	200	1,200	23.47	9.60

Table XI (continued)

(b) Specimens, Initial Grain Boundary Area, and Initial Grain Boundary Anisotropy

Specimen Number	$S_{v(GB)}(i)$ (mm^2/mm^3)	$e_g(i)$
S3-6	4.84±0.38	0.01±0.13
S3-3	5.36±0.38	0.07+0.10-0.15
S3-5	4.64±0.36	0.04+0.13-0.11
S3-10	5.84±0.42	-0.02+0.12-0.11
S3-9	5.24±0.44	0.04+0.16-0.12
S3-7	6.26±0.36	0.02+0.10-0.09
S3-12	5.04±0.36	0.02+0.15-0.14
S3-13	6.82±0.44	0.06+0.11-0.10
S3-16	5.42±0.40	0.00±0.12
S3-15	5.18±0.44	0.03+0.14-0.13
S3-18	5.50±0.38	0.07±0.11
S3-19	6.20±0.44	0.09+0.12-0.11
S3-24	4.20±0.36	0.09+0.19-0.17
S3-21	5.28±0.44	0.09+0.14-0.12
S1-1	6.14±0.44	0.21+0.19-0.15
S1-2	5.84±0.40	0.06±0.11
S1-4	5.62±0.44	0.04±0.13
S1-5	5.58±0.38	0.07+0.12-0.11
S1-7	2.38±0.22	0.10+0.02-0.05
S1-8	3.30±0.30	0.06+0.15-0.14
S1-9	2.88±0.26	0.04±0.15
S3-22	5.40±0.40	0.01+0.09-0.13
S3-20	6.46±0.44	0.03±0.11

Table XI (continued)

(c) Specimens and Fractions of Grains Containing Subgrains, Subgrain Rows, and Subgrain Rows Oriented Between 35° and 55° with Respect to the Tensile Axis

Specimen Number	f_{SG}	f_{SGR}	$f_{SGR(35-55)}$
S3-6	0.02	0.00	0.00
S3-3	0.23	0.00	0.00
S3-5	0.55	0.05	0.80
S3-10	0.07	0.02	1.00
S3-9	0.53	0.08	0.75
S3-7	0.74	0.17	0.65
S3-12	1.00	0.14	0.93
S3-13	0.12	0.00	0.00
S3-16	0.23	0.04	0.75
S3-15	0.54	0.09	0.67
S3-18	1.00	0.62	0.79
S3-19	0.15	0.02	1.00
S3-24	0.18	0.00	0.00
S3-21	0.15	0.01	1.00
S1-1	0.14	0.09	0.78
S1-2	0.25	0.20	0.75
S1-4	0.86	0.41	0.68
S1-5	0.89	0.50	0.76
S1-7	0.86	0.34	0.68
S1-8	0.97	0.67	0.61
S1-9	0.99	0.76	0.80
S3-22	0.79	0.38	0.74
S3-20	0.98	0.39	0.77

Table XI (continued)

(d) Specimens and Boundary Area Measurements

Specimen Number	$S_{V(TOT)}$	$\bar{S}_V$	$\tilde{S}_V$	$S_{V(GB)}$
S3-6	4.52±0.46	3.74±0.32	0.06±0.06	3.82±0.32
S3-3	4.08±0.46	3.28±0.26	0.12±0.08	3.32±0.26
S3-5	6.06±0.50	2.24±0.14	0.16±0.04	2.42±0.26
S3-10	4.62±0.60	4.08±0.36	0.08±0.06	4.14±0.36
S3-9	8.22±0.60	2.92±0.32	0.56±0.16	3.46±0.34
S3-7	10.06±0.62	2.40±0.32	0.76±0.18	3.20±0.34
S3-12	18.08±0.72	1.70±0.34	3.12±0.40	4.04±0.46
S3-13	4.32±0.54	3.88±0.52	0.12±0.10	3.96±0.52
S3-16	4.36±0.48	3.66±0.44	0.18±0.10	3.82±0.46
S3-15	5.06±0.46	3.62±0.40	0.34±0.16	3.96±0.42
S3-18	29.82±1.12	0.56±0.20	2.94±0.44	3.46±0.48
S3-19	5.18±0.60	4.86±0.60	0.02±0.04	4.90±0.58
S3-24	4.32±0.50	3.82±0.48	0.24±0.16	4.08±0.48
S3-21	4.38±0.52	3.56±0.48	0.10±0.08	3.68±0.46
S1-1	7.18±0.76	2.40±0.30	1.24±0.22	3.62±0.34
S1-2	13.12±1.04	2.52±0.30	1.50±0.24	3.88±0.34
S1-4	16.20±1.02	1.86±0.28	2.72±0.30	4.54±0.36
S1-5	28.52±1.20	1.06±0.22	3.08±0.32	4.20±0.34
S1-7	9.58±0.96	0.84±0.18	1.50±0.20	2.38±0.24
S1-8	25.94±1.28	0.56±0.14	1.88±0.24	2.42±0.24
S1-9	30.28±1.26	0.28±0.08	2.30±0.28	2.54±0.28
S3-22	9.14±0.94	2.94±0.38	0.32±0.18	3.28±0.40
S3-20	13.82±1.10	2.30±0.40	0.72±0.26	3.02±0.46

Table XI (continued)

(e) Specimens, Subgrain Boundary Area and Change in Grain Boundary Anisotropy

Specimen Number	$S_{v(SGB)}$	$e_g(f)-e_g(i)$
S3-6	0.70*	0.10+0.07-0.03
S3-3	0.76*±0.72	0.06+0.08-0.11
S3-5	3.64*	-0.03+0.11-0.08
S3-10	0.48*	0.00+0.06-0.04
S3-9	5.76*	0.16+0.07-0.09
S3-7	6.86*±0.96	0.12+0.14-0.11
S3-12	14.00 ±0.76	-0.11+0.19-0.05
S3-13	0.32 ±0.16	-0.11+0.19-0.09
S3-16	0.50 ±0.24	0.13+0.19-0.11
S3-15	1.10 ±0.32	0.03+0.10-0.07
S3-18	26.40 ±1.20	0.01+0.20-0.14
S3-19	0.32 ±0.16	0.02+0.18-0.11
S3-24	0.28 ±0.16	-0.09+0.07-0.06
S3-21	0.72 ±0.26	0.19+0.21-0.14
S1-1	3.56*±1.10	0.19+0.09-0.08
S1-2	9.24*±1.38	0.12+0.08-0.07
S1-4	11.66*±1.38	0.11+0.06-0.03
S1-5	24.32*±1.54	0.18+0.09-0.07
S1-7	7.20*±1.20	0.07+0.28-0.09
S1-8	23.52*±1.52	0.21+0.10-0.06
S1-9	27.74*±1.54	0.62+0.27-0.16
S3-22	5.98 ±0.94	0.12+0.19-0.13
S3-20	10.80 ±1.16	0.24+0.34-0.21

*$S_{v(SGB)}$ calculated by subtracting the mean $S_{v(GB)}$ from the mean $S_{v(TOT)}$:

Each of the parameters listed above plotted versus time and strain will be described separately in the following sections.

3.7.2.1. Grain boundary surface area, $S_{v(GB)}$, versus time

In Figure 51 (a through f), grain boundary surface area is plotted as a function of time. The initial value at zero time was taken as the average of the initial values for the specimens tested under the given set of creep conditions. The range of values shown for the initial value was obtained by using as the lower limit the smallest initial grain boundary area minus its statistical tolerance, and as the upper limit the largest initial grain boundary area plus its statistical tolerance.

Within the range of creep testing conditions of this research, the grain boundary area decreases rather markedly within the first few hours of creep to a value which, up to the maximum time of testing, remains essentially unchanged. Such behavior indicates that grain growth occurs rather rapidly during the initial portion of the creep test. After this initial growth, the grain size, on the average, becomes stable for the duration of creep testing. Two exceptions to this behavior are to be pointed out. In creep tests at 425°C under an initial stress of 150 psi, Figure 51(a), the grain boundary surface area continuously decreased up to the time limit of creep testing, 16 hours. A second exception to the

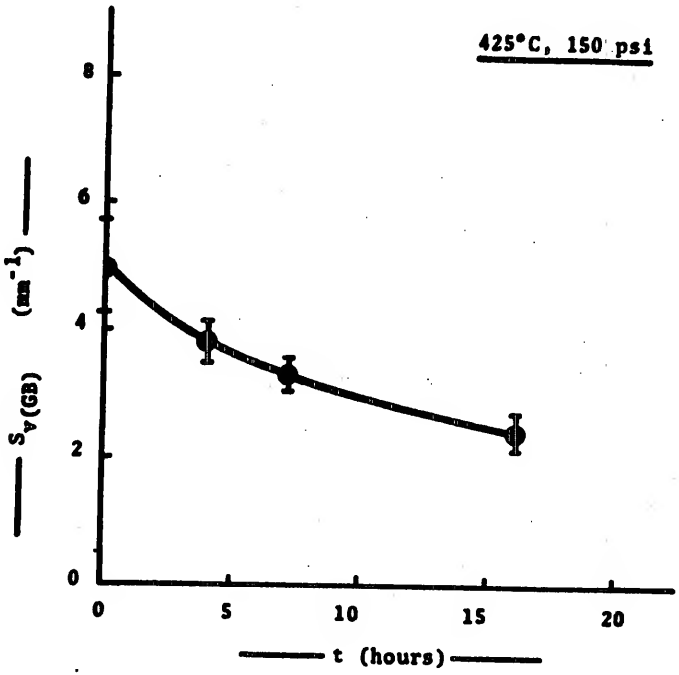

Figure 51. Grain boundary area, $S_{v(GB)}$, versus time, t.

(a) Specimens tested at 425°C under an initial stress of 150 psi.

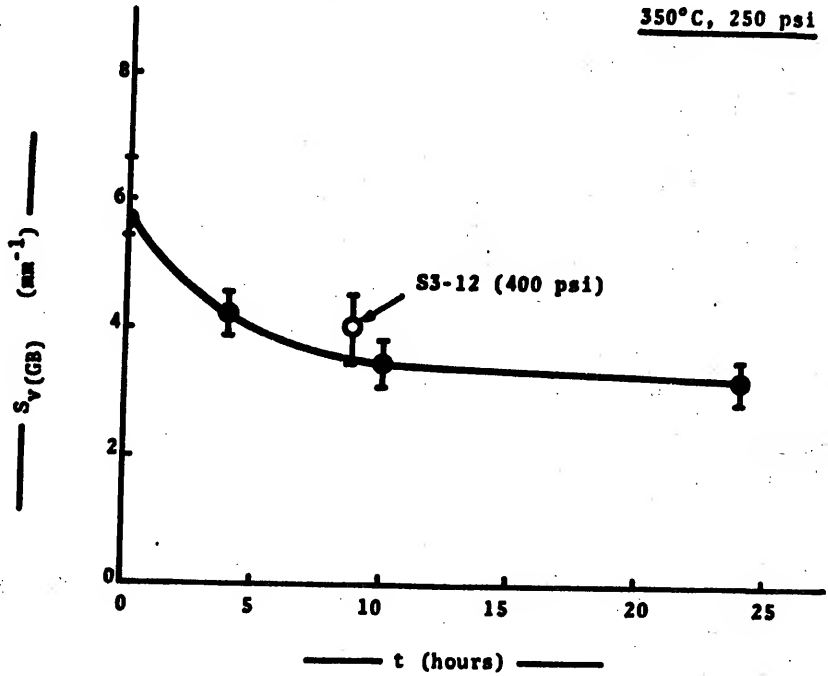

Figure 51. (continued)

(b) Specimens tested at 350°C under initial stresses of 250 and 400 psi.

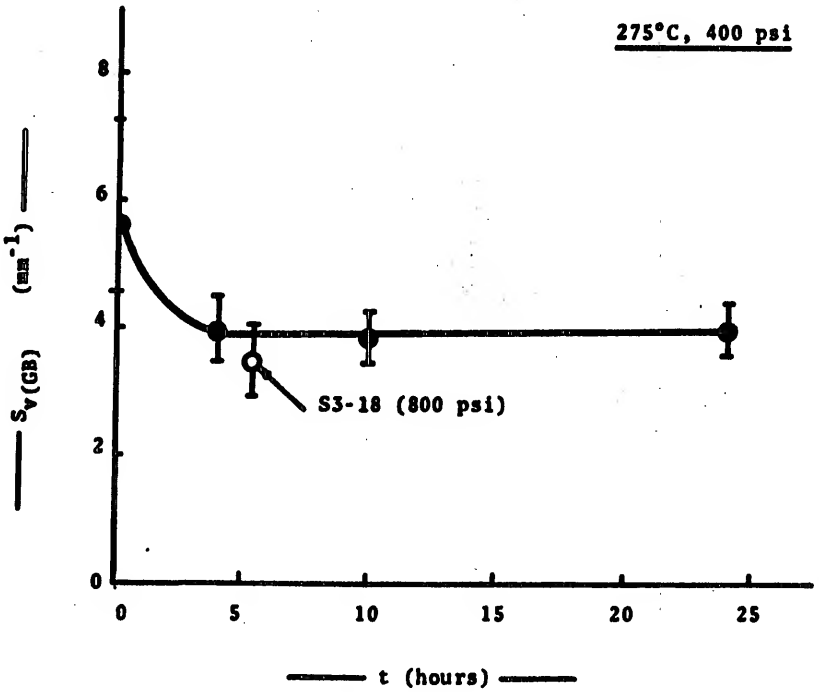

Figure 51. (continued)

(c) Specimens tested at 275°C under initial stresses of 400 and 800 psi.

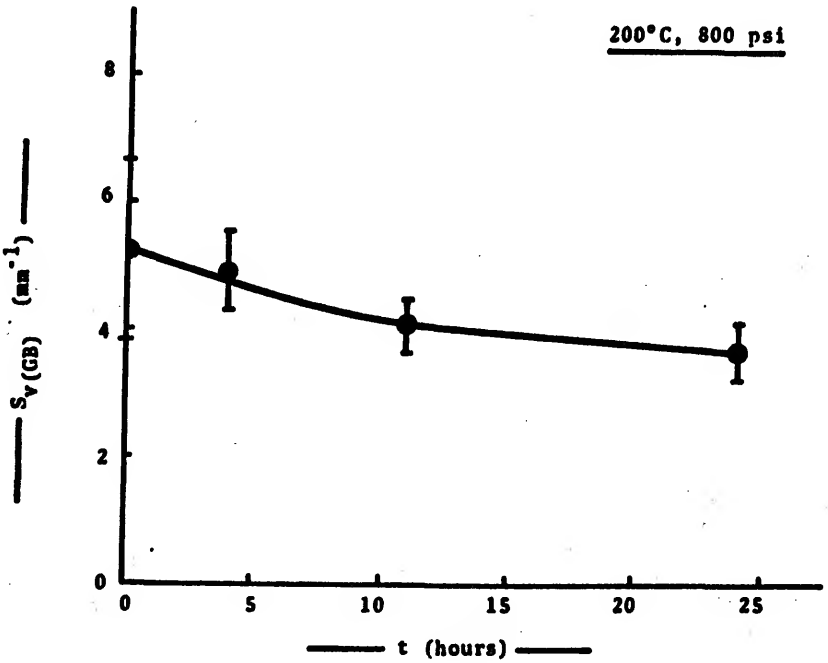

Figure 51. (continued)

(d) Specimens tested at 200°C under an initial stress of 800 psi.

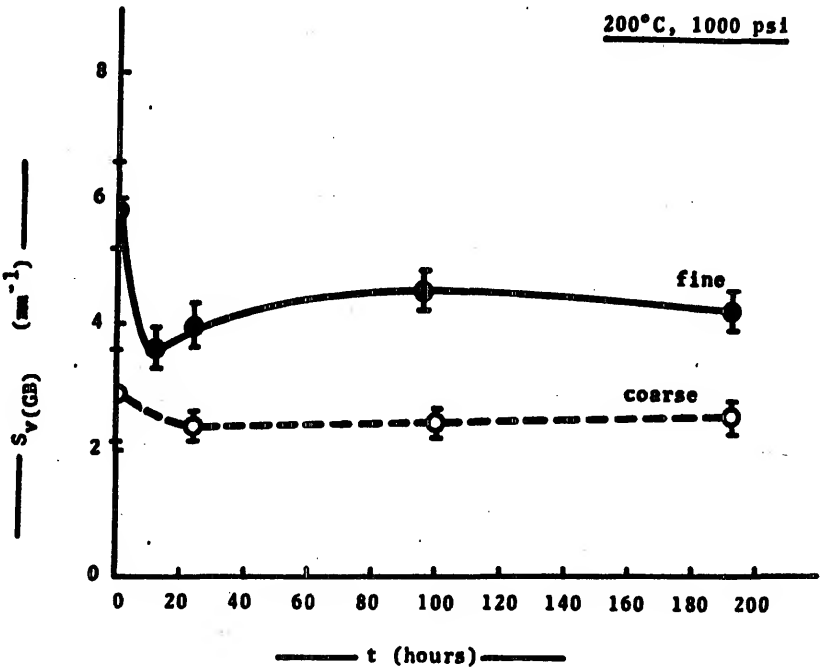

Figure 51. (continued)

(e) Specimens tested at 200°C under an initial stress of 1,000 psi. Dashed line is the curve for coarse-grained specimens; solid line is the curve for fine-grained specimens.

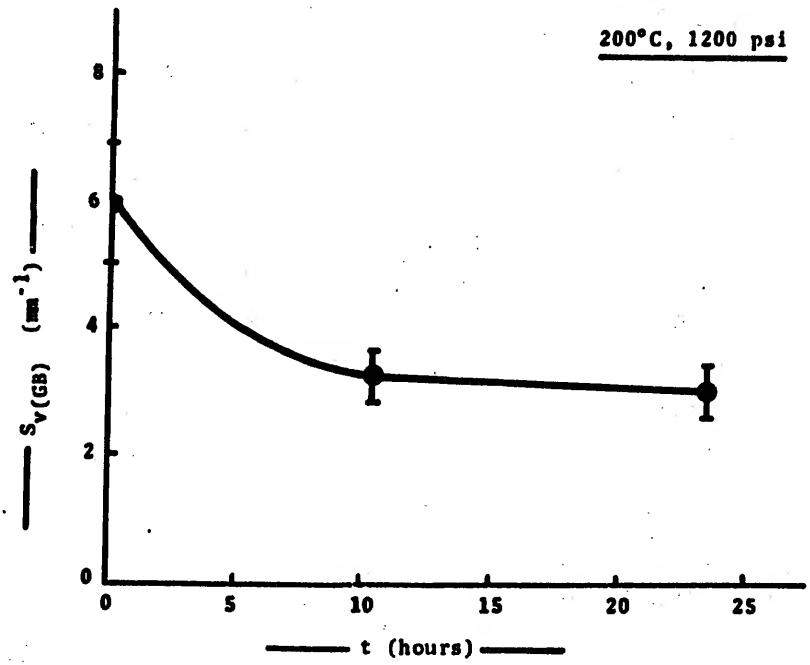

Figure 51. (continued)

(f) Specimens tested at 200°C under an initial stress of 1,200 psi.

general behavior is shown in Figure 51(e), where $S_{v(GB)}$ is plotted versus time for creep tests at 200°C under an initial stress of 1,000 psi for material of two different initial grain sizes. Creep tests under this condition were run for much longer times than those for the several other conditions. Note that for the fine-grained material there is a trend for the grain boundary area to increase slightly and become stable after the initial grain growth. The statistical tolerances indicated on the plotted points show that the behavior is hardly significant; however, the trend does appear to exist. Such behavior can be accounted for only by the formation of new grains during the course of creep. In comparison to the general behavior of initial grain growth, the coarse-grained material did not show a significant initial decrease in grain boundary area.

It seems fortuitous that, for all material having approximately the same initial grain boundary area (between 5 and 6 mm^2/mm^3), the decrease in grain boundary area is nearly the same regardless of the conditions of creep testing. That is, the grain boundary area seems to become stable at a value between 3 and 4 mm^2/mm^3. Further, the initial stress at a given temperature has little effect on the level of the stable grain boundary area. In Figure 51(b), specimen S3-10,tested at 400 psi rather than 250 psi, possesses a grain boundary area not significantly different from similarly tested specimens under the lower initial stress.

A like observation is to be noted in Figure 51(c) in the case of specimen S3-18 tested under an 800 psi initial stress rather than a 400 psi stress. The most tenable explanation for this observation is based upon the effects of the external surfaces of the creep specimen on the grain boundary network. Grain growth occurs continuously with creep until a sufficient portion of the grain boundary surface area intercepts the external surfaces of the specimen. From this point on, further grain growth is inhibited by the surface pinning of the grain boundary network.

3.7.2.2. Grain boundary area, $S_{v(GB)}$, versus strain

The various creep testing conditions result in differing rates of secondary creep; therefore, the previous graphs of grain boundary area versus time do not give any information regarding its change with respect to increasing amounts of creep strain. In Figure 52 (a through f), the grain boundary area, $S_{v(GB)}$, is plotted versus strain for the several sets of creep testing conditions. The evidence for initial grain growth during creep is observed in these graphs. The trends observed in the several graphs suggest that the grain growth occurs within the first 5 percent of strain. By comparing the several graphs, it is readily apparent that, within statistical tolerances, there is no significant difference in the magnitude of grain boundary area decrease among the several sets of creep testing

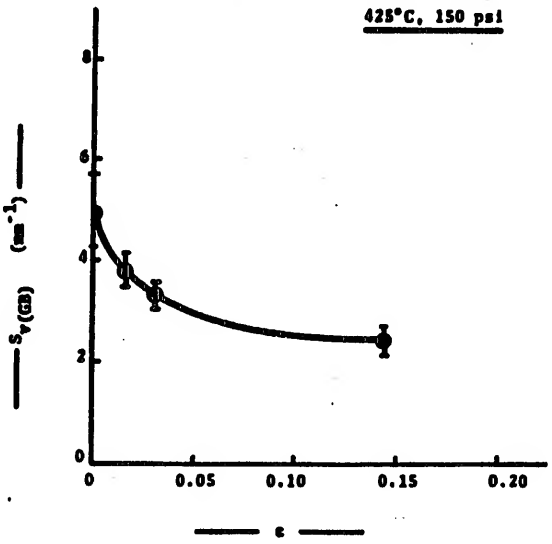

Figure 52. Grain boundary area, $S_{V(GB)}$, versus strain, ε.

(a) Specimens tested at 425°C under an initial stress of 150 psi.

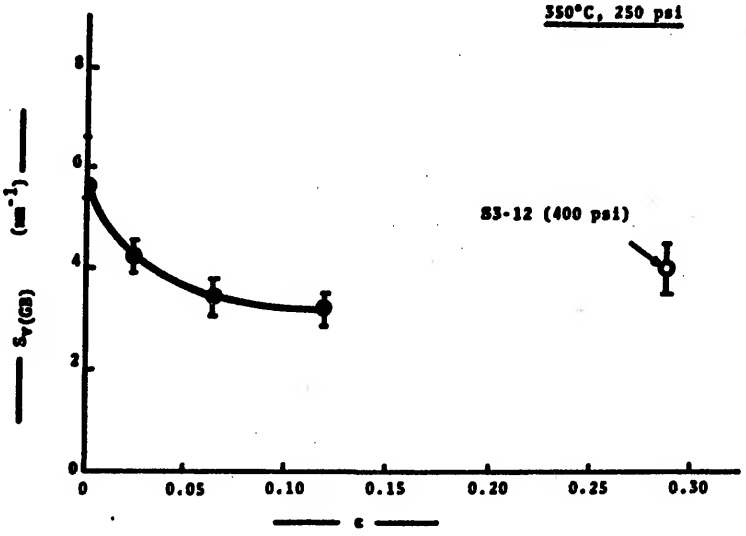

Figure 52. (continued)

(b) Specimens tested at 350°C under initial stresses of 250 and 400 psi.

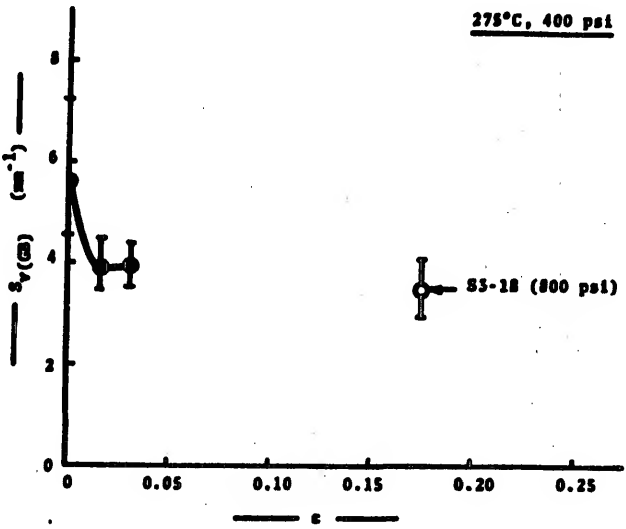

Figure 52. (continued)

(c) Specimens tested at 275°C under initial stresses of 400 and 800 psi.

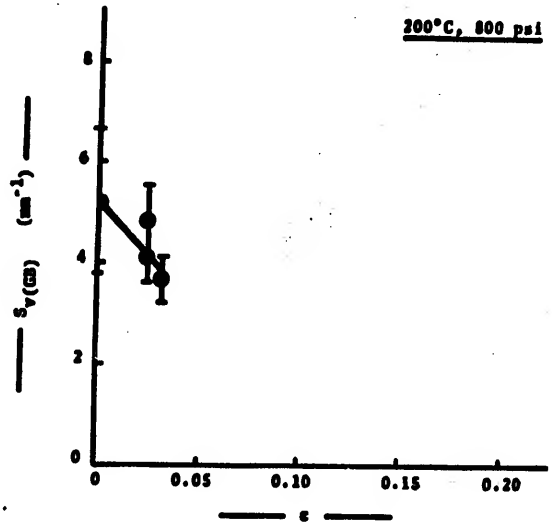

Figure 52. (continued)

(d) Specimens tested at 200°C under an initial stress of 800 psi.

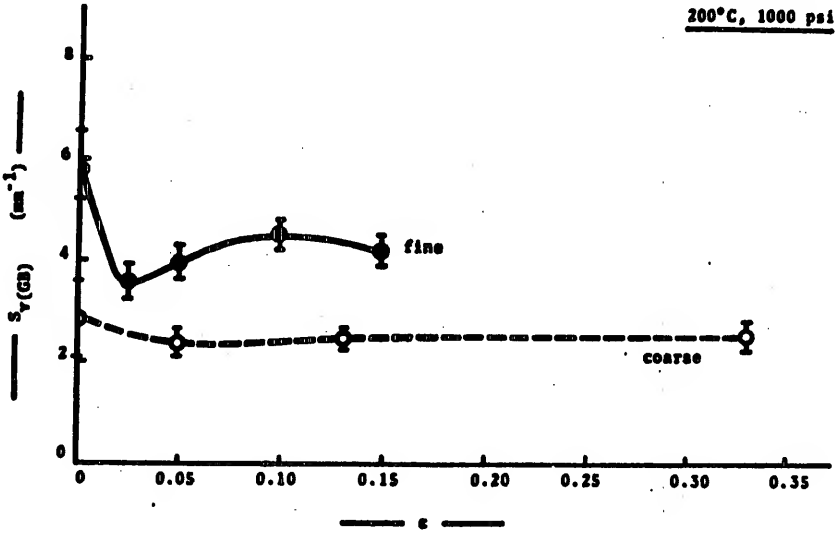

Figure 52. (continued)

(e) Specimens tested at 200°C under an initial stress of 1,000 psi. Dashed line is the curve for coarse-grained specimens; solid line is the curve for fine-grained specimens.

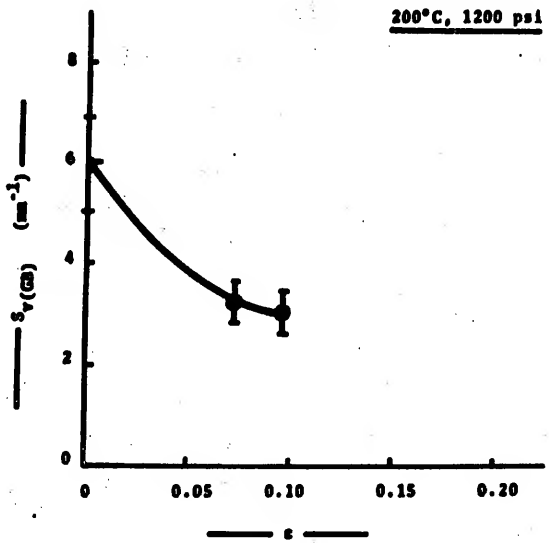

Figure 53. (continued)

(f) Specimens tested at 200°C under an initial stress of 1,200 psi.

conditions. In the fine-grained material tested at 200°C under a stress of 1,000 psi, Figure 52(e), the increase in grain boundary area following the initial decrease is not significant in view of the statistical tolerances on the data; however, the trend does seem to exist. The grain boundary area for the coarse-grained material, tested under the same conditions, does not significantly change with increasing strain, Figure 52(e).

Within the statistical tolerances, increasing the stress apparently has no effect on the ultimate grain size established after the initial grain growth. This is indicated by the points plotted for specimens tested at 350°C under a stress of 400 psi and at 275°C under a stress of 800 psi in Figures 52 (b and c), respectively.

3.7.2.3. Subgrain boundary area, $S_{V(SGB)}$, versus time

Polygonization, the result of which is subgrain formation, concurrent with creep deformation is widely held as the softening process which, operating in balance with work hardening, accounts for the secondary creep behavior of constant strain rate. The rate at which subgrain boundary area forms during the course of creep may be considered as a partial measure of the rate of softening by polygonization. Softening by polygonization removes dislocations from the crystal lattice by the in situ "precipitation" of lattice dislocations to form boundary surface. The amount of

boundary surface formed and the relative misorientation between the lattice on either side of the boundary is equal to the total length of dislocation line removed from the lattice. The length of dislocation line per unit area of boundary surface is to be connected with the degree of misorientation across the boundary; therefore, the subgrain boundary area is a measure of only a fraction of dislocation line length removed from the lattice. If, under any given set of creep conditions, the average misorientation across all subgrain boundaries is assumed to remain constant, the rate of deformation should be proportional to the rate at which subgrain boundary area forms.

Subgrain boundary surface area plotted versus time for each of the six sets of creep conditions is given in Figure 53 (a through f). Some of the curves shown are rather irregular; but, within the tolerances of the measurements, least squares straight lines fit the data well with two exceptions, these being the curves for creep tests at 350°C under a stress of 250 psi and tests at 200°C under a stress of 1,000 psi. However, it was believed that the increase in subgrain boundary area should be proportional to the strain, and since the strain during secondary creep increases linearly with time, then the subgrain boundary area should also increase linearly with time. For this reason, least squares straight lines are also shown in Figure 53 (b and e) for the tests at 350°C and 200°C, respectively. The slopes

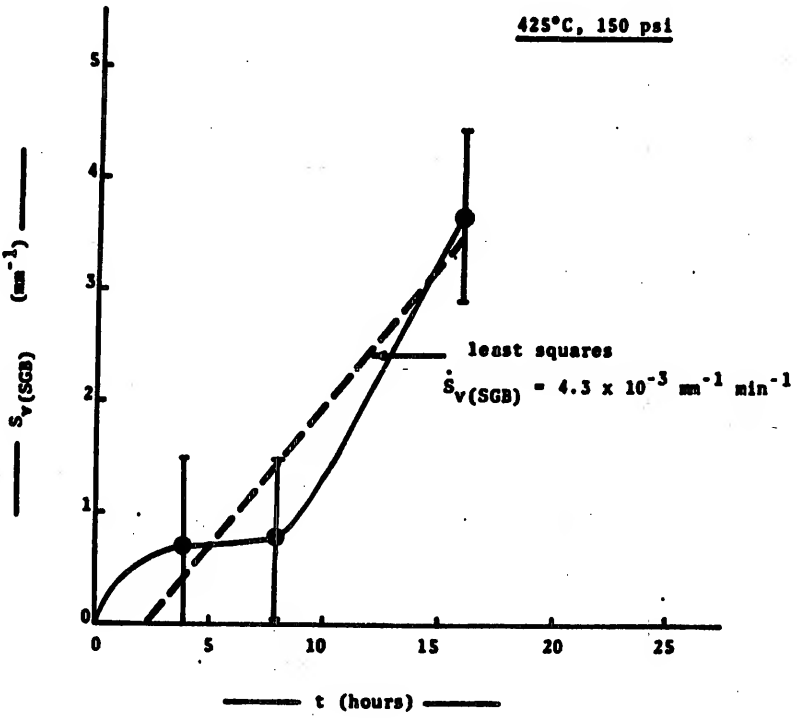

Figure 53. Subgrain boundary area, $S_{V(SGB)}$, versus time, t.

(a) Specimens tested at 425°C under an initial stress of 150 psi.

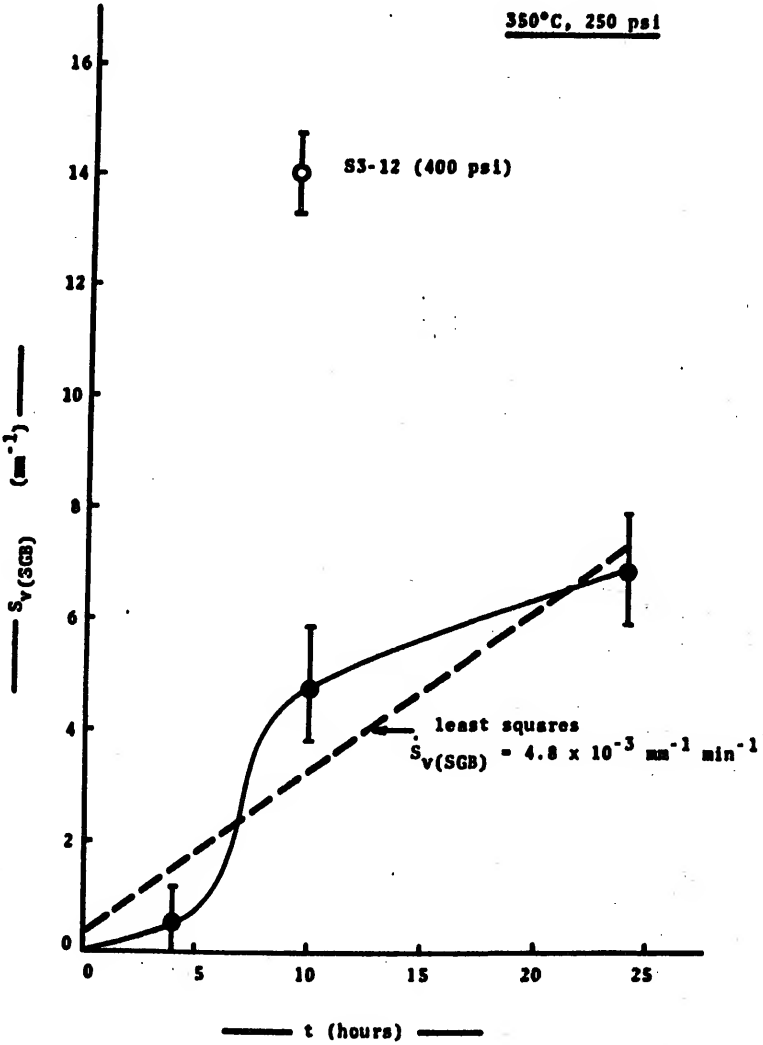

Figure 53. (continued)

(b) Specimens tested at 350 psi under initial stresses of 250 and 400 psi.

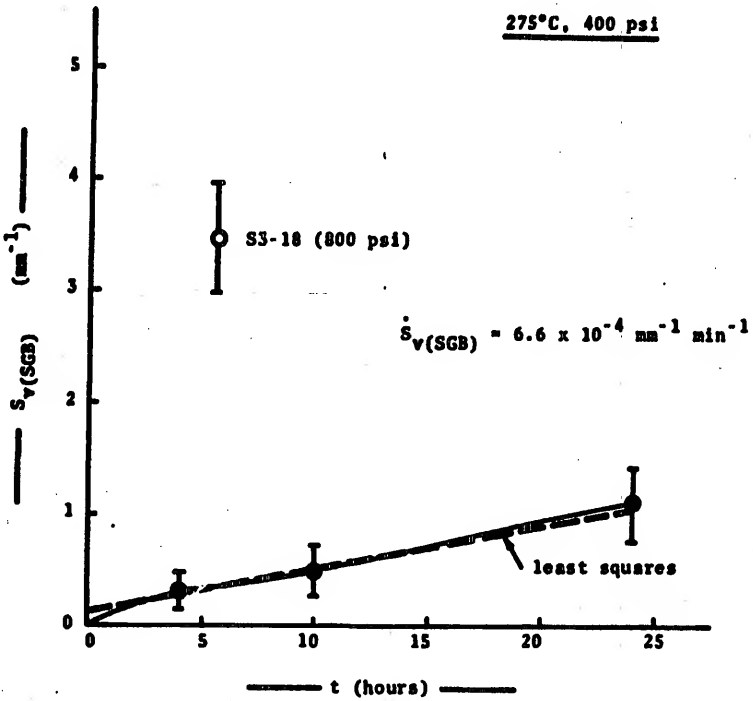

Figure 53. (continued)

(c) Specimens tested at 275°C under initial stresses of 400 and 800 psi.

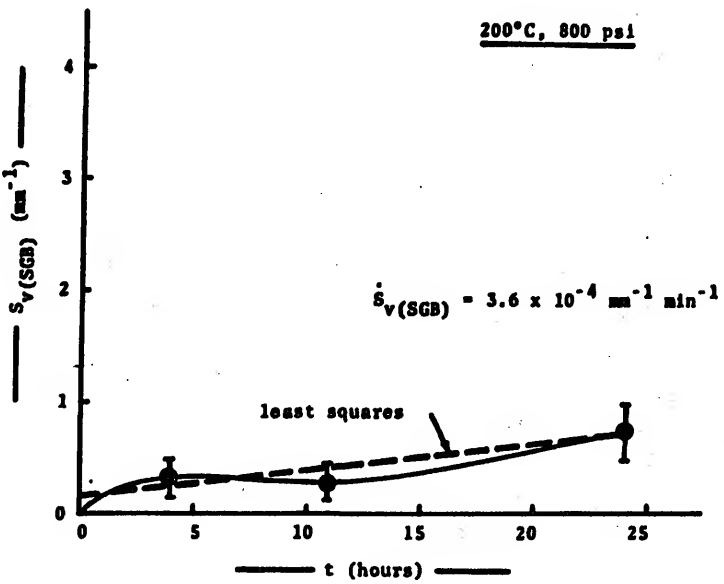

Figure 53. (continued)

(d) Specimens tested at 200°C under an initial stress of 800 psi.

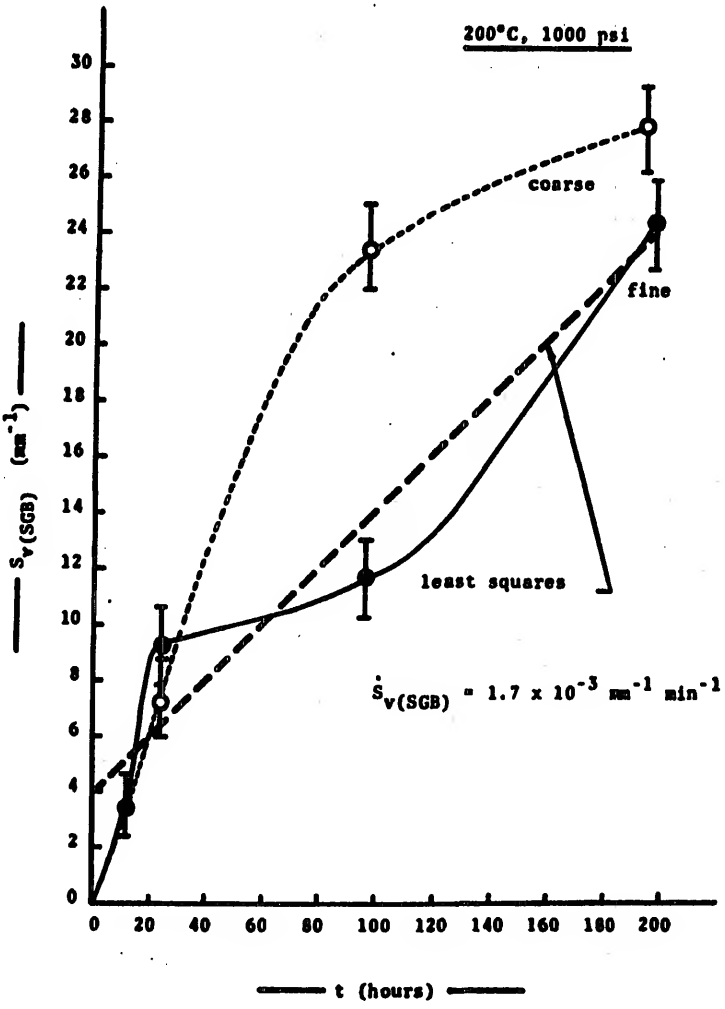

Figure 53. (continued)

(e) Specimens tested at 200°C under an initial stress of 1,000 psi. Dashed line is the curve for coarse-grained specimens; solid line is the curve for fine-grained specimens.

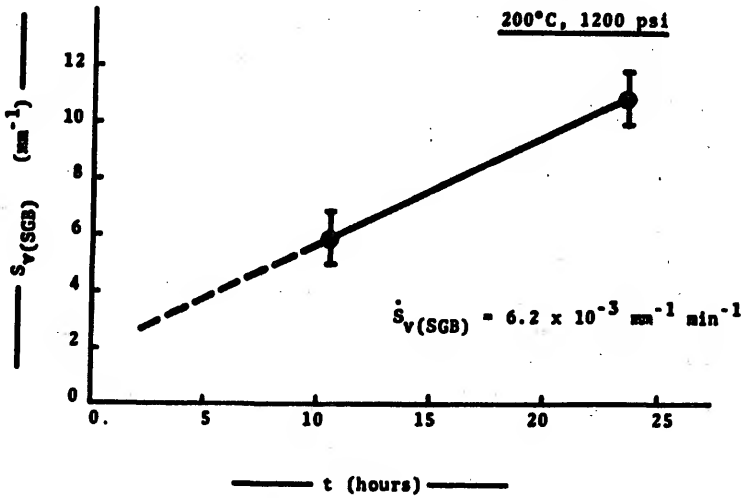

Figure 53. (continued)

(f) Specimens tested at 200°C under an initial stress of 1,200 psi.

of these straight lines were taken as an average rate of subgrain boundary formation. The rates of subgrain boundary formation determined in this way are given in Table XII. The data for the coarse-grained specimens tested at 200°C under a stress of 1,000 psi are neglected in the present evaluation, because two of the specimens in this series had formed necks and because no other coarse-grained specimens were tested under the other creep conditions.

Because of the assumed connection between the amount of strain and the subgrain boundary area, the rates of subgrain boundary area formation were subjected to an analysis similar to that for strain rates. As in the case of strain rates, a similar empirical equation was employed,

$$\dot{S}_{v(SGB)} = B\sigma^m e^{-\Delta H/RT} , \qquad (13)$$

where $\dot{S}_{v(SGB)}$ is the rate of formation of subgrain boundary area, B is a materials constant, m is a stress sensitivity constant, and the symbols ΔH, R and T have their usual meanings.

For the determination of the values for the constants in equation (13), the statistical scheme outlined previously for the determination of the constants in the strain rate equation (equation 10) was followed. Equation (13) was rewritten in the form

$$\log C = \log B + m \log \sigma , \qquad (14)$$

Table XII

The Rates of Subgrain Boundary Formation During the Creep of Aluminum

Creep Test Conditions		Rate of Subgrain Boundary Formation, $\dot{S}_{V(SG)}$
T (°C)	σ (psi)	($mm^2/mm^3/min$)
425	150	4.3×10^{-3}
350	250	4.8×10^{-3}
275	400	6.6×10^{-4}
200	800	3.6×10^{-4}
200	1,000	1.7×10^{-3}
200	1,200	6.2×10^{-3}

where $C = (\dot{S}_{v(SGB)} e^{\Delta H/RT})$, a term analogous to the Zener-Hollomon parameter. The symbols, B, m and σ have meanings as previously described. By plotting the log C versus log σ, m becomes the slope and log B the intercept of the straight line. In the present case, nine values of ΔH were assumed, ranging from 28 Kcal/mole to 34 Kcal/mole, inclusive. The assumed values for the activation energy, ΔH, the slopes of the log C versus log σ plots, m, the intercepts of the log C versus log σ plots, log B, and the values of the sums of the squares of the deviations between the calculated values of log C and the least squares values of log C, $\Sigma(\log C_i - \log \tilde{C}_i)^2$, are given in Table XIII. The assumed values of ΔH plotted versus the corresponding values of $\Sigma(\log C_i - \log \tilde{C}_i)^2$ are given in Figure 54. From the graph it can be seen that the assumed value of ΔH = 31 Kcal/mole represents the best fit to the rate of subgrain boundary area formation data. The graph of log C versus log σ for ΔH = 31 Kcal/mole is given in Figure 55.

From the analysis of the data concerning the rate of the formation of subgrain boundary area formation, it was concluded that the rate of subgrain boundary area formation during secondary creep could be expressed by

$$\dot{S}_{v(SGR)} = B\sigma^m e^{-\Delta H/RT} , \qquad (15)$$

where $B = 7.9450 \times 10^{-4}$, $m = 4.8418 \pm 0.8663$, and ΔH = 31 Kcal/mole.

Table XIII

Assumed Activation Energies, ΔH; Stress Sensitivity Constants, m; Intercepts, log B; and Sums of the Squares of the Deviations, $\Sigma(\log C_i - \log \tilde{C}_i)^2$

ΔH Kcal/mole	m	log B	$\Sigma(\log C_i - \log \tilde{C}_i)^2$
34.00	6.3342±1.1287	-5.8940	0.3863
33.00	6.1327±1.1187	-5.7603	0.3798
32.00	5.9349±1.1149	-5.6358	0.3772
31.25	5.7877±1.1153	-5.5454	0.3774
31.00	4.8418±0.8663	-3.0999	0.2277
30.75	5.6896±1.1168	-5.4850	0.3784
30.00	5.5398±1.1183	-5.3876	0.3795
29.00	5.3431±1.1233	-5.2659	0.3829
28.00	5.1450±1.1321	-5.1404	0.3890

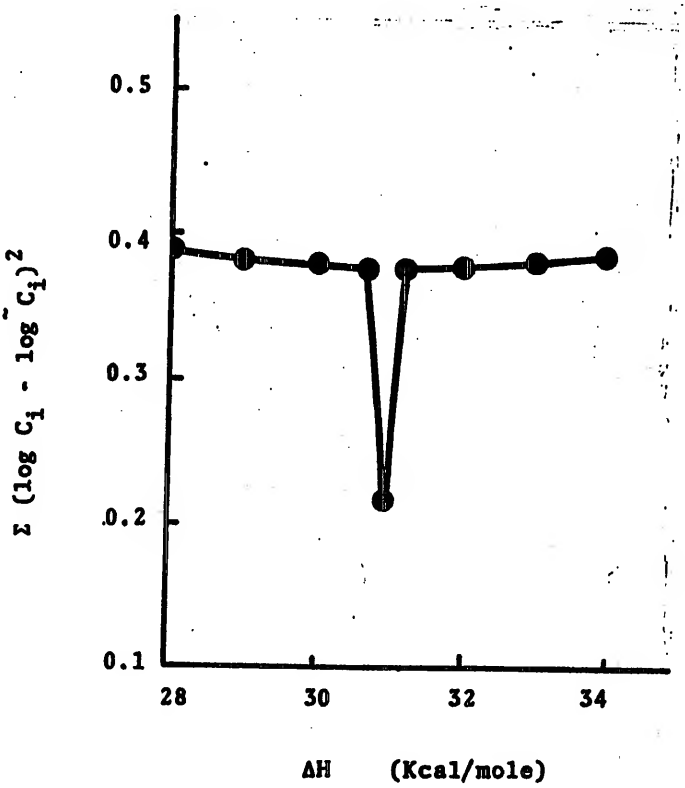

Figure 54. $\Sigma(\log C_i - \log \tilde{C}_i)^2$ versus ΔH. The parameter C_i is analogous to the Zener-Hollomon parameter and equals $S_{v(SGB)}e^{\Delta H/RT}$. Log C_i is the i^{th} value of log C for a given value of ΔH, and log C_i is the corresponding value of log C_i determined from the least squares straight line. The apparent activation is ΔH.

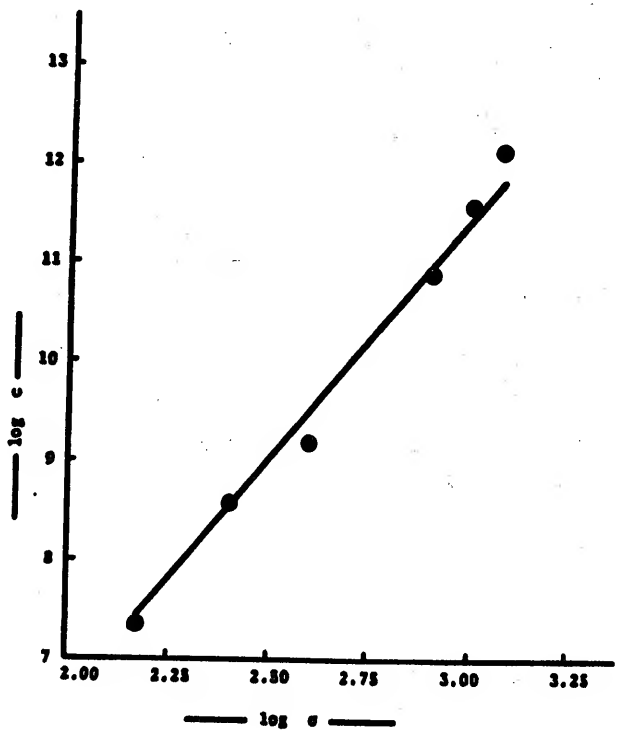

Figure 55. Log C ($C = \dot{S}_{v(SGB)}\, e^{\Delta H/RT}$) versus log σ (σ = stress (psi)).

3.7.2.4. Subgrain boundary area, $S_{v(SGB)}$, versus strain

It is easy to reason that the subgrain boundary area should increase with creep strain during the course of creep. The formation of subgrain boundary by polygonization concurrent with the creep process represents a softening process which balances work hardening and results in the constant strain rate associated with secondary creep. One would expect that the subgrain boundary area should increase with the amount of creep strain in a more or less linear manner during secondary creep, if recovery by polygonization is rate controlling. This effect can be observed from the graphs of subgrain boundary area, $S_{v(SGB)}$, plotted versus strain for the various sets of creep testing conditions in Figure 56 (a through f). Although the curves exhibit some undulations, it is not difficult to justify straight lines drawn through the data points when the statistical tolerances are taken into consideration. In contrast to the observation cited above, the curve for the coarse-grained material tested at 200°C under a stress of 1,000 psi, Figure 56(e), apparently levels out at large values of subgrain boundary area, attaining a value of 27.74 mm^2/mm^3 at a strain of 0.33. This observation seems to indicate that if creep proceeds far enough, further recovery associated with subgrain boundaries may be the result of continuously increasing misorientations across subgrain boundaries, rather than the result of forming new subgrain boundary. As the

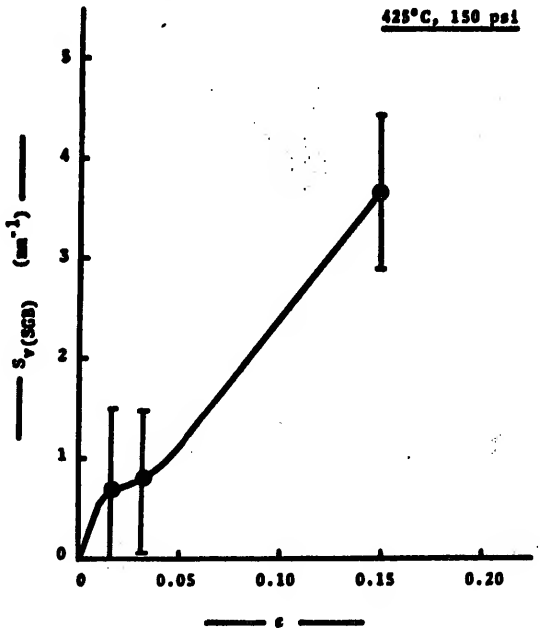

Figure 56. Subgrain boundary area, $S_{v(SGB)}$, versus strain, ε.

(a) Specimens tested at 425°C under an initial stress of 150 psi.

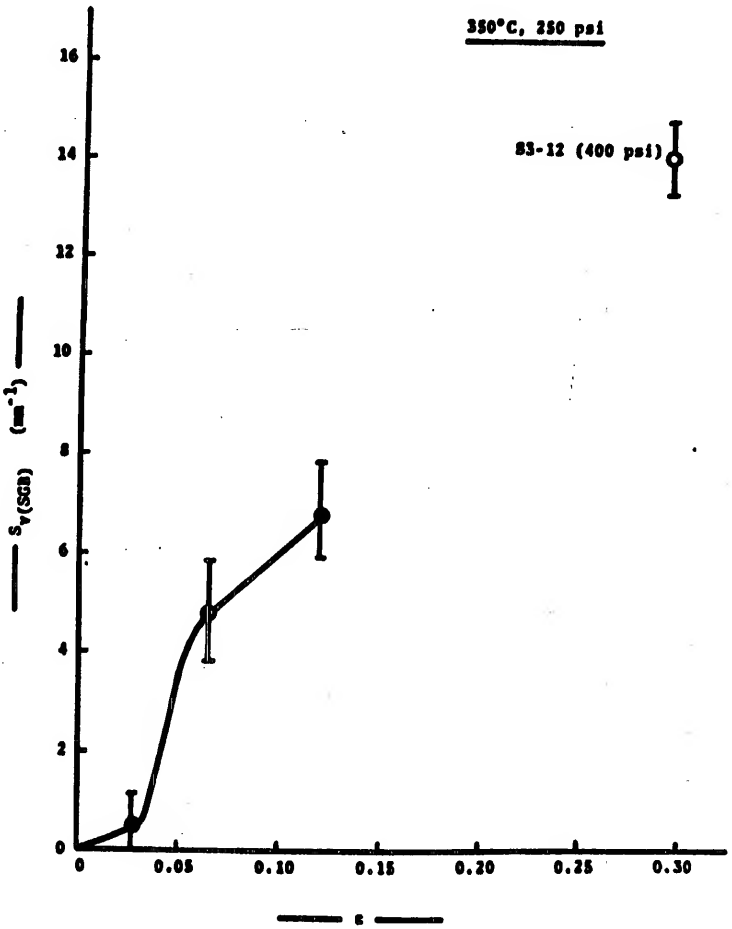

Figure 56. (continued)

(b) Specimens tested at 350°C under initial stresses of 250 and 400 psi.

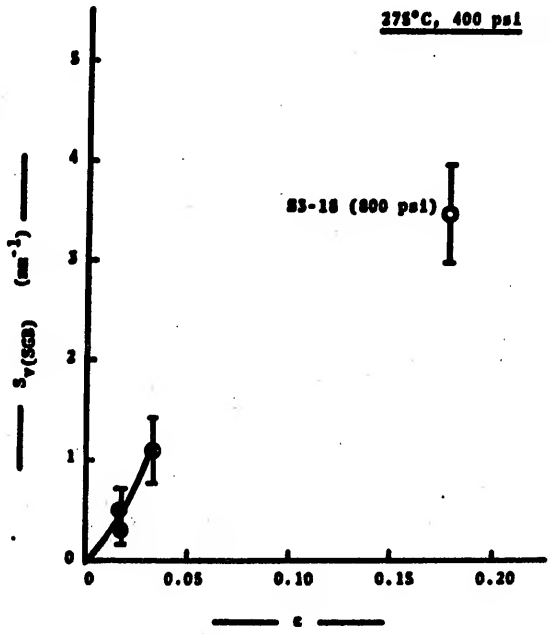

Figure 56. (continued)

(c) Specimens tested at 275°C under initial stresses of 400 and 800 psi.

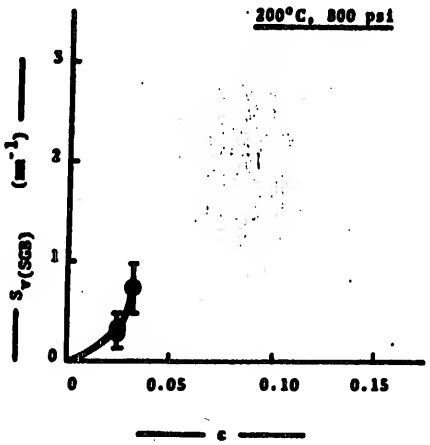

Figure 56. (continued)

(d) Specimens tested at 200°C under an initial stress of 800 psi.

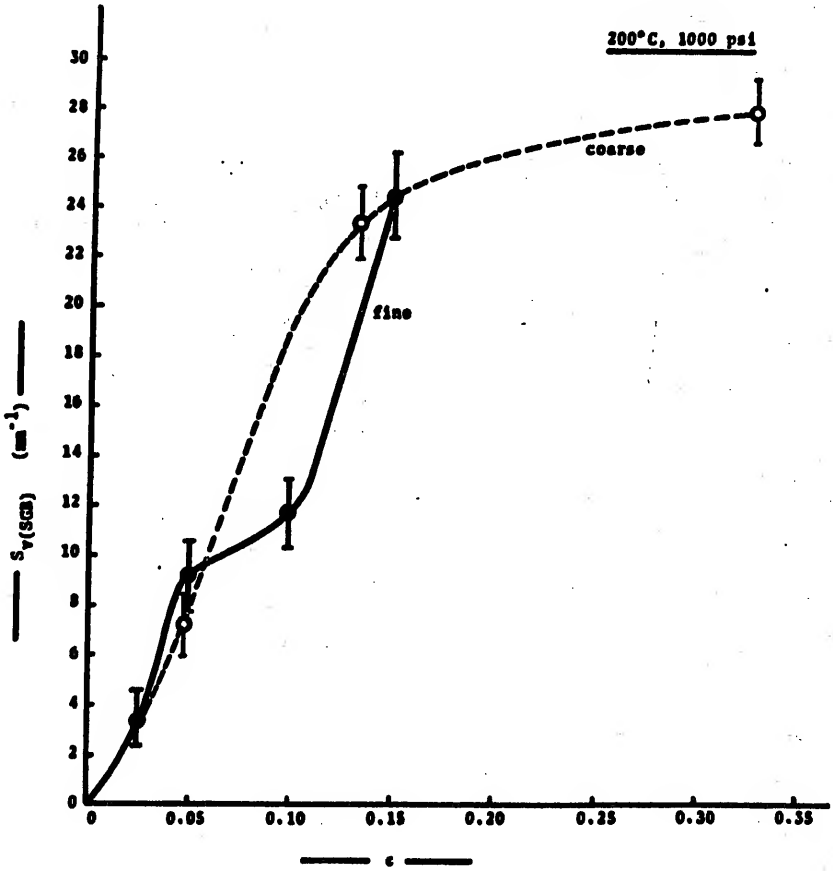

Figure 56. (continued)

(e) Specimens tested at 200°C under an initial stress of 1,000 psi. Dashed line is the curve for coarse-grained specimens; solid line is the curve for fine-grained specimens.

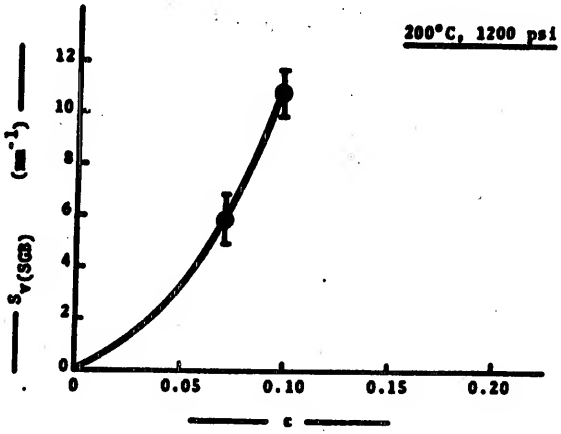

Figure 56. (continued)

(f) Specimens tested at 200°C under an initial stress of 1,200 psi.

stress increases due to necking in tertiary creep, it seems reasonable that again a part of the recovery might be related to the formation of new subgrain boundary.

It is entirely possible that a second process may account for reaching a maximum subgrain boundary area during creep. Past a certain amount of deformation, grain boundary migration, as a recovery process, may become activated. As grain boundaries sweep into sub-boundaries, the subgrain boundary area becomes decreased. The possibility exists that the rate of removal of subgrain boundary area by grain boundary migration might just balance the rate at which new subgrain boundary is formed.

From the data presented, it is evident that during secondary creep the formation of subgrain boundary area is favored by low temperatures and high stresses.

3.7.2.5. Fraction of grains containing subgrains and subgrain rows versus time and strain

Early in the course of this research, it was observed that a row-like pattern of subgrains appeared with great regularity in the microstructures of tested creep specimens. Their observation was particularly evident in specimens which had formed necks. In such specimens a great majority of the grains contained subgrain rows, and, for the most part, the rows appeared to be oriented at approximately 45° to the tensile axis. Up to this point in the research the usual subgrain structure appeared to be connected with

rather wavy serrations in the grain boundaries, but the newly observed subgrain rows gave the very distinct visual impression that they were aligned with dentate grain boundary serrations. The connection between subgrain rows and dentate forms of grain boundary serrations prompted an investigation aimed at characterizing the formation of subgrain rows from the beginning of creep. Since the formation of subgrain rows was thought to be concurrent with the development of the subgrain structure, it was important to investigate simultaneously the development of subgrains and subgrain rows.

In order to trace the evolution of subgrain rows during creep and to compare their formation to the formation of subgrains, one hundred neighboring grains were examined in each specimen, noting how many grains contained subgrains and how many contained subgrain rows. The fraction of grains which contain subgrains including subgrain rows, f_{SG}, and the fraction of grains which contain only subgrain rows, f_{SGR}, plotted versus time and strain for the several sets of creep conditions are given in Figures 57 (a through f) and 58 (a through f), respectively. It is to be noted that the curves for fractions of grains containing subgrains include the fraction of grains containing subgrain rows. The difference between the curves of f_{SG} and f_{SGR} reflects the fraction of grains containing subgrains but no subgrain rows.

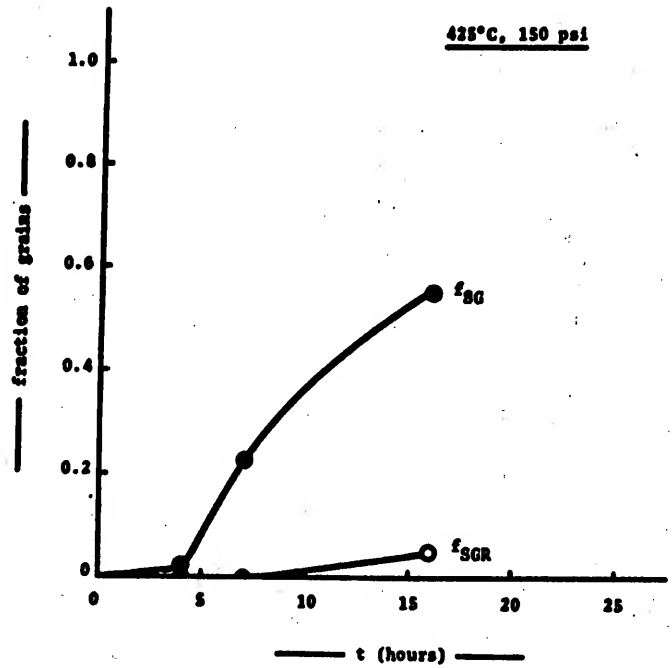

Figure 57. Fraction of grains containing subgrains, f_{SG}, and fraction of grains containing subgrain rows, f_{SGR}, versus time, t.

(a) Specimens tested at 425°C under an initial stress of 150 psi.

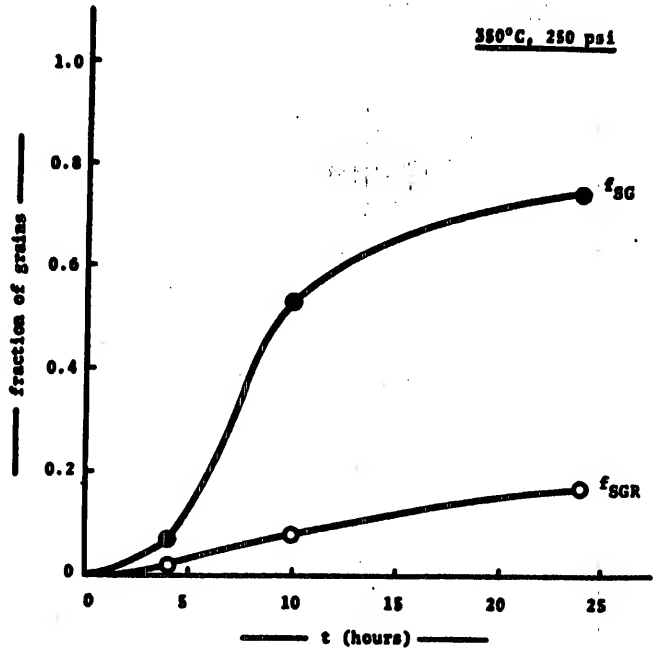

Figure 57. (continued)

(b) Specimens tested at 350°C under an initial stress of 250 psi.

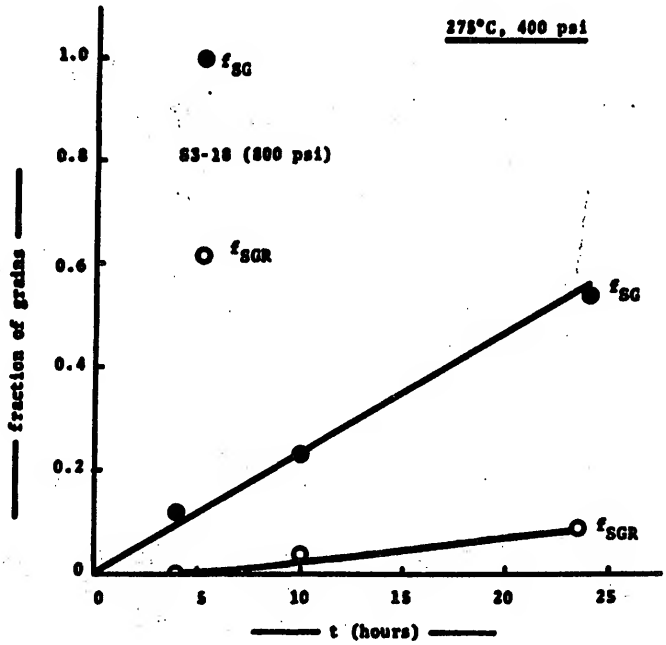

Figure 57. (continued)

(c) Specimens tested at 275°C under initial stresses of 400 and 800 psi.

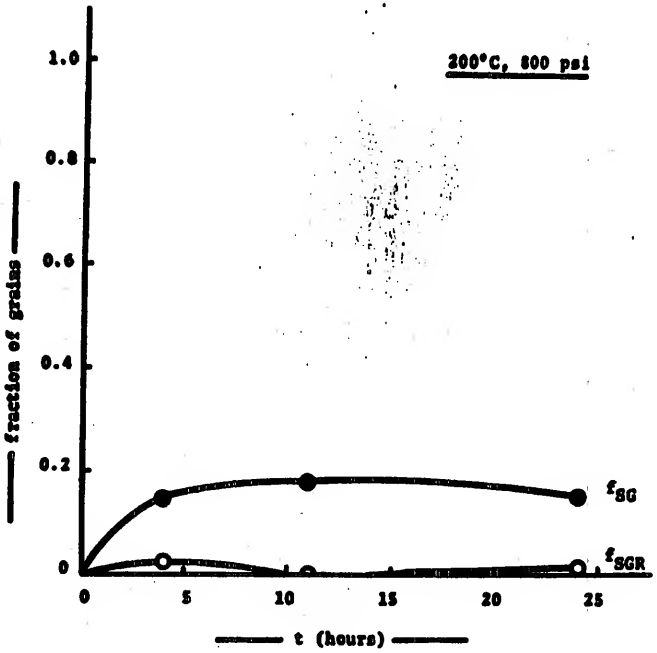

Figure 57. (continued)

(d) Specimens tested at 800°C under an initial stress of 800 psi.

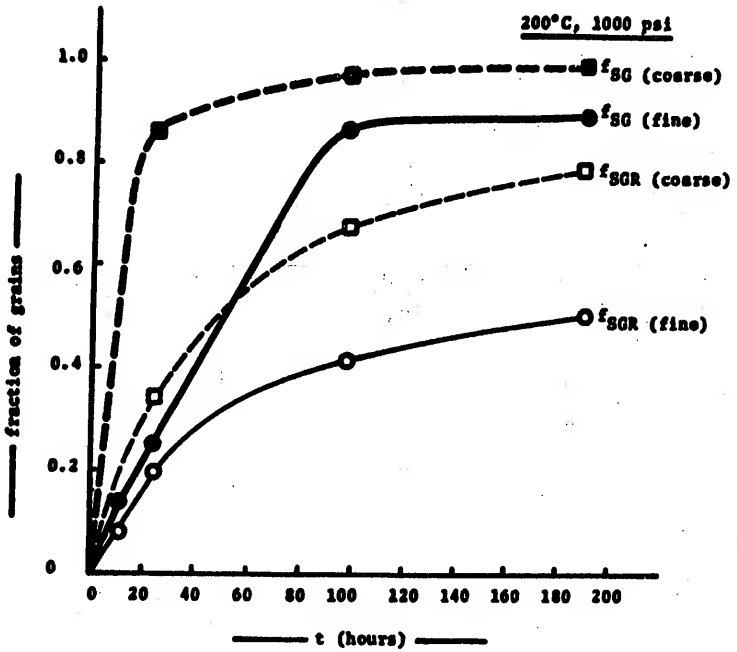

Figure 57. (continued)

(e) Specimens tested at 200°C under an initial stress of 1,000 psi. Dashed lines are curves for coarse-grained specimens; solid lines are curves for fine-grained specimens.

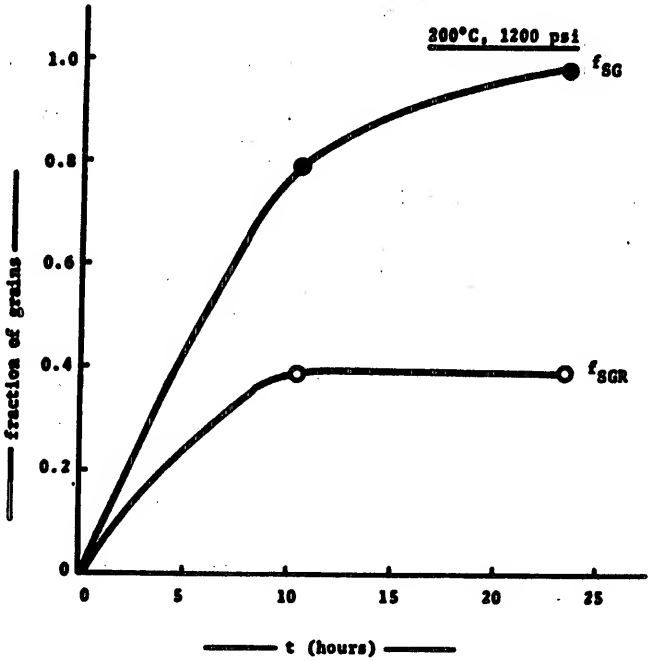

Figure 57. (continued)

(f) Specimens tested at 200°C under an initial stress of 1,200 psi.

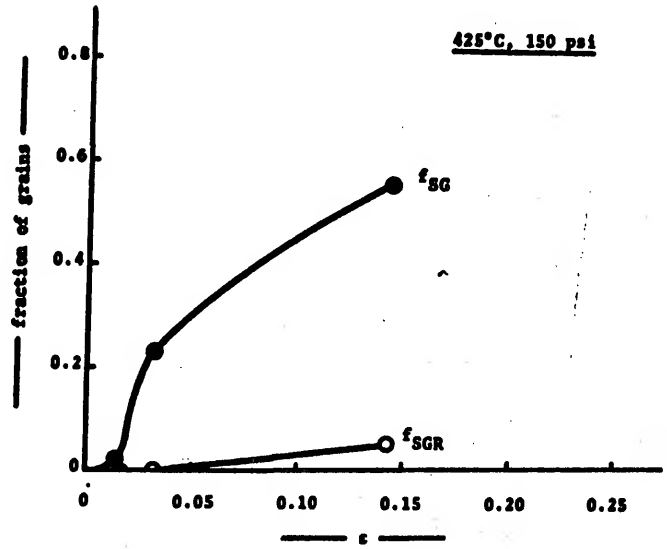

Figure 58. Fraction of grains containing subgrains, f_{SG}, and fraction of grains containing subgrain rows, f_{SGR}, versus strain, ε.

(a) Specimens tested at 425°C under an initial stress of 150 psi.

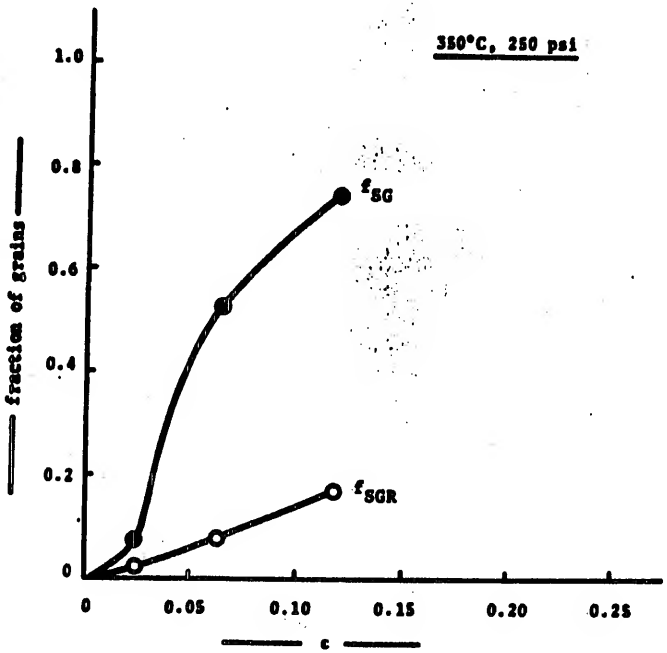

Figure 58. (continued)

(b) Specimens tested at 350°C under an initial stress of 250 psi.

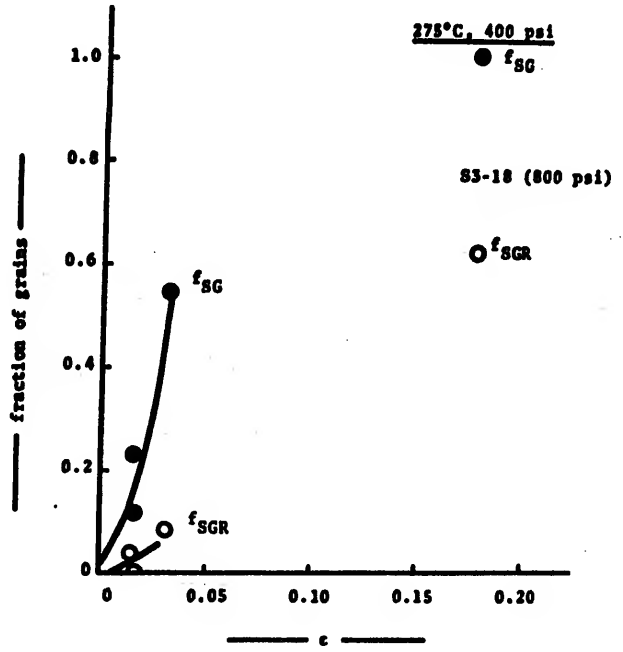

Figure 58. (continued)

(c) Specimens tested at 275°C under initial stresses of 400 and 800 psi.

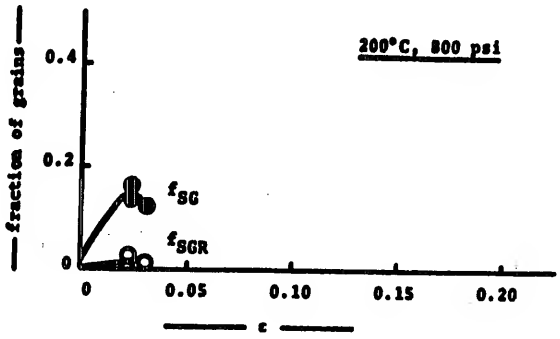

Figure 58. (continued)

(d) Specimens tested at 200°C under an initial stress of 800 psi.

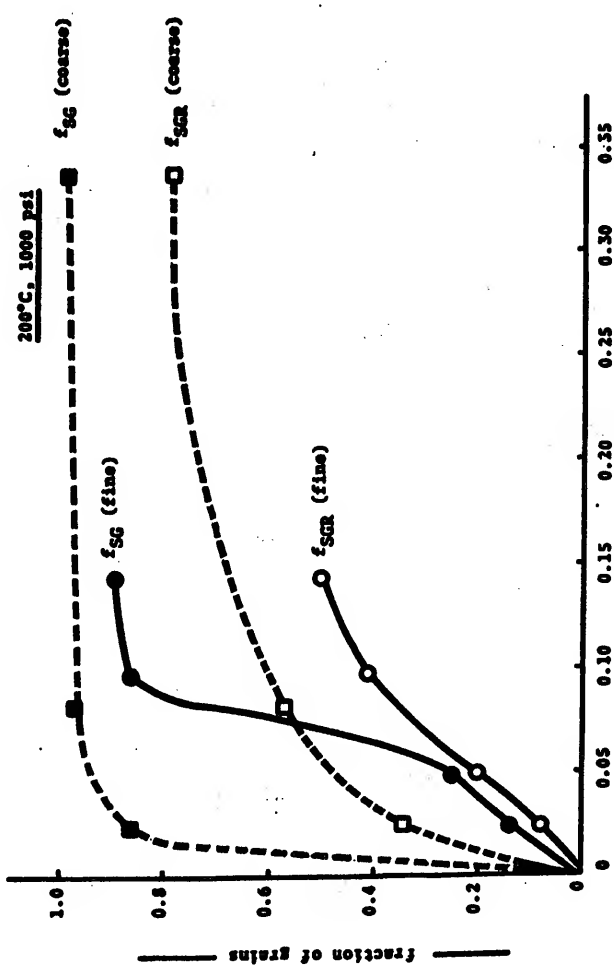

Figure 58. (continued)

(e) Specimens tested at 200°C under an initial stress of 1,000 psi. Dashed lines are curves for coarse-grained specimens; solid lines are curves for fine-grained specimens.

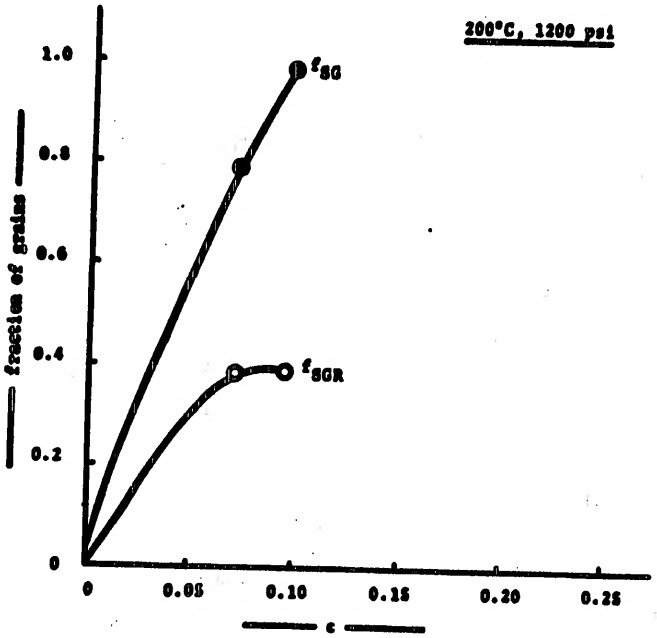

Figure 58. (continued)

(f) Specimens tested at 200°C under an initial stress of 1,200 psi.

Subgrains and subgrain rows begin to form early in the process of creep. The fraction of grains containing subgrains in most cases tends to level off after some amount of time or strain. By comparing the graphs for the various sets of creep testing conditions in Figure 57, it is apparent that the more severe the deformation, i.e., the greater the strain rate, the greater is the rate at which f_{SG} and f_{SGR} increase with time. The lower temperatures and higher stresses promote both subgrain and subgrain row formation.

It is important to emphasize that during the course of the high temperature creep of aluminum, subgrains do not form in all of the grains at the same time. The orientation of a given grain and the nature of the constraints to deformation are believed to play major roles in determining whether subgrains will form within the grain during creep. As the grains change in orientation, and as the constraints to deformation change with the progress of creep, it is reasonable to believe that more and more grains will become favorably oriented and/or constrained for the formation of subgrains.

With regard to the association between the formation of subgrain rows and the amount of strain, the creep conditions of low temperature and high stress are more efficient on a per unit strain basis in producing subgrain rows than the conditions of high temperature and low stress. The ratio of the fraction of grains containing subgrain rows

to the fraction of grains containing subgrains of the random morphology, $f_{SGR}/f_{SG}-f_{SGR}$, when considered in terms of the temperature, the stress and the strain, is an indicator of the way in which the substructure morphology is affected by the creep conditions. The higher the value for this ratio, the greater is the proportion of the number of grains with subgrain rows compared to the number of grains containing subgrains of the random morphology. Values for the ratio are given in Table XIV. These data generally indicate that high stresses and increasing strain favor the subgrain row morphology.

3.7.2.6. The orientation of subgrain rows with respect to the tensile axis

A set of data, not included in Table XI, concerning the distributions of the angles between subgrain rows and the tensile axis, is given in Figure 59 (a through f), in the form of histograms. Each histogram shows the angular distribution of the subgrain rows with respect to the tensile axis in terms of the number of grains containing subgrain rows whose angles with respect to the tensile axis fall within a specified angular range. A total of 100 neighboring grains were counted in each specimen. For instance, in Figure 59(b), specimen S3-12, out of 100 grains counted, 14 grains contained subgrain rows; their orientations with respect to the tensile axis distributed in the following way:

Table XIV

Specimens, Creep Conditions, Strain, and $f_{SGR}/f_{SG}-f_{SGR}$

Specimen Number	Temperature (°C)	Stress (psi)	Time (hours)	Strain (%)	$\frac{f_{SGR}}{f_{SG}-f_{SGR}}$
S3-6	425	150	4.00	1.6	0
S3-3	425	150	7.17	3.2	0
S3-5	425	150	16.17	14.4	0.10
S3-10	350	250	4.17	2.4	0.40
S3-9	350	250	10.00	6.4	0.18
S3-7	350	250	24.00	12.0	0.30
S3-12	350	400	8.83	28.8	0.16
S3-13	275	400	4.00	1.6	0
S3-16	275	400	10.00	1.6	0.21
S3-15	275	400	24.00	3.2	0.20
S3-18	275	800	5.37	17.6	1.63
S3-19	200	800	4.00	2.4	0.12
S3-24	200	800	10.92	2.4	0
S3-21	200	800	24.00	3.2	0.07
S1-1	200	1,000	11.85	2.5	1.80
S1-2	200	1,000	24.05	4.9	4.00
S1-4	200	1,000	95.78	9.8	0.91
S1-5	200	1,000	191.90	14.8	1.28
S1-7	200	1,000	24.00	4.9	0.65
S1-8	200	1,000	96.28	13.1	2.24
S1-9	200	1,000	192.37	33.0	2.54
S3-20	200	1,200	10.43	7.2	0.98
S3-22	200	1,200	23.47	9.6	0.80

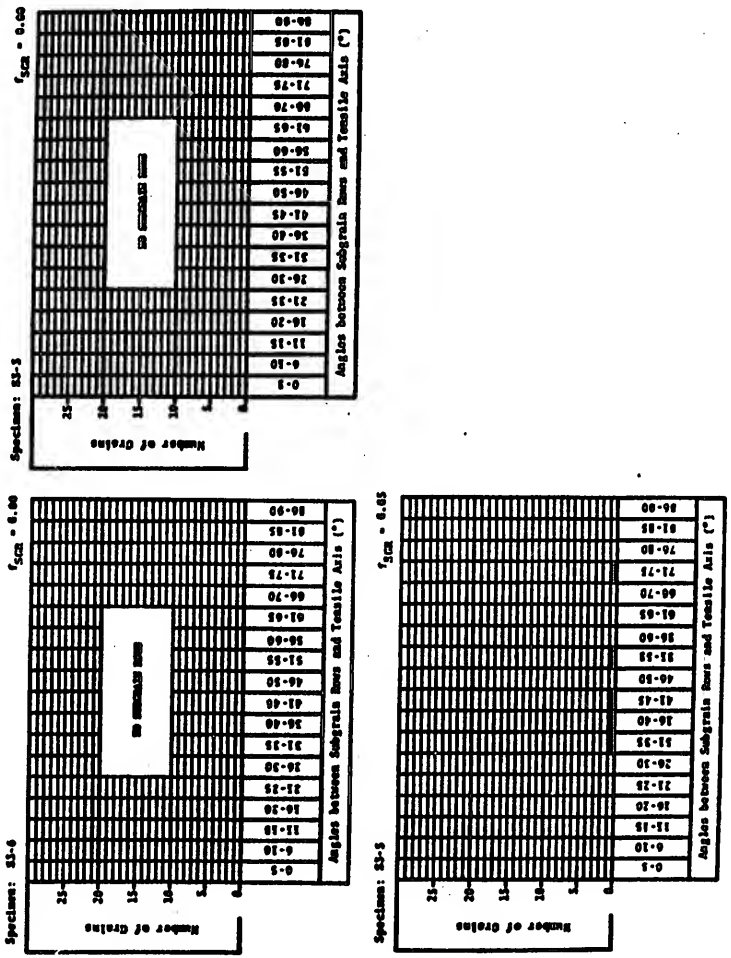

Figure 59. Histograms showing the distribution of the angles between subgrain rows and the tensile axis.

(a) Creep specimens tested at 425°C.

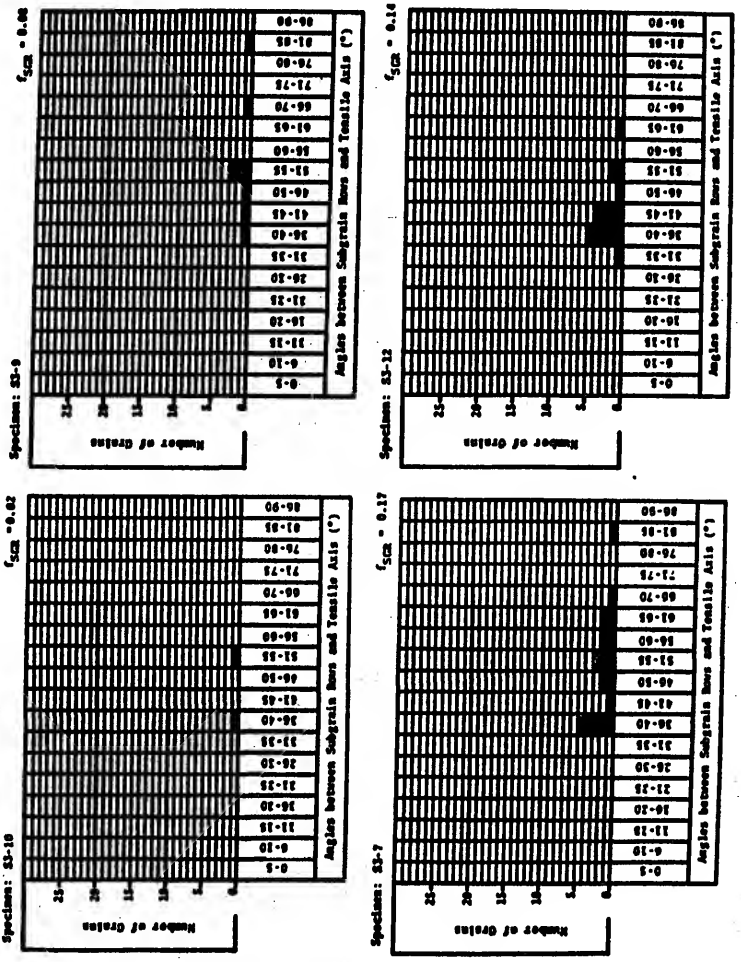

Figure 59. (continued)

(b) Creep specimens tested at 350°C.

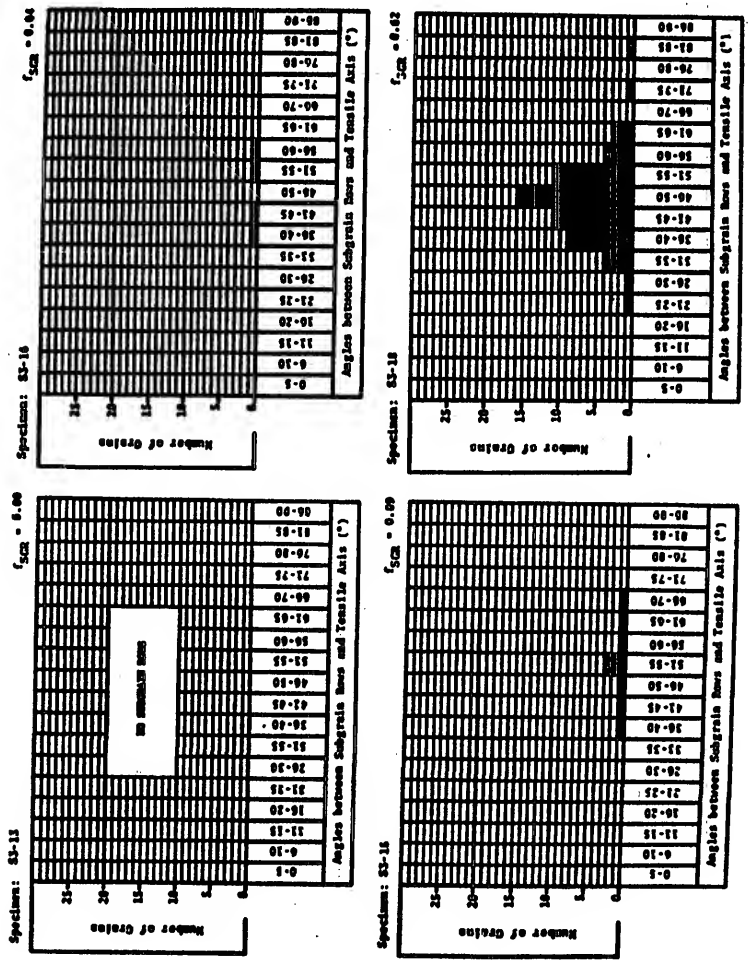

Figure 59. (continued)

(c) Creep specimens tested at 275°C.

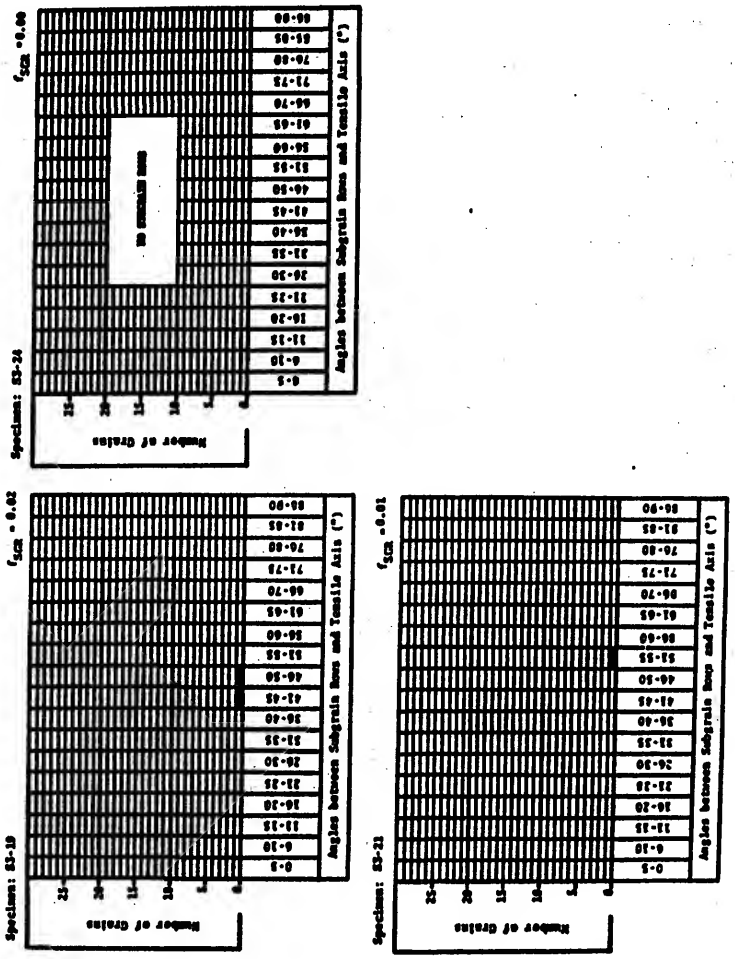

Figure 59. (continued)

(d) Creep specimens tested at 200°C under an initial stress of 800 psi.

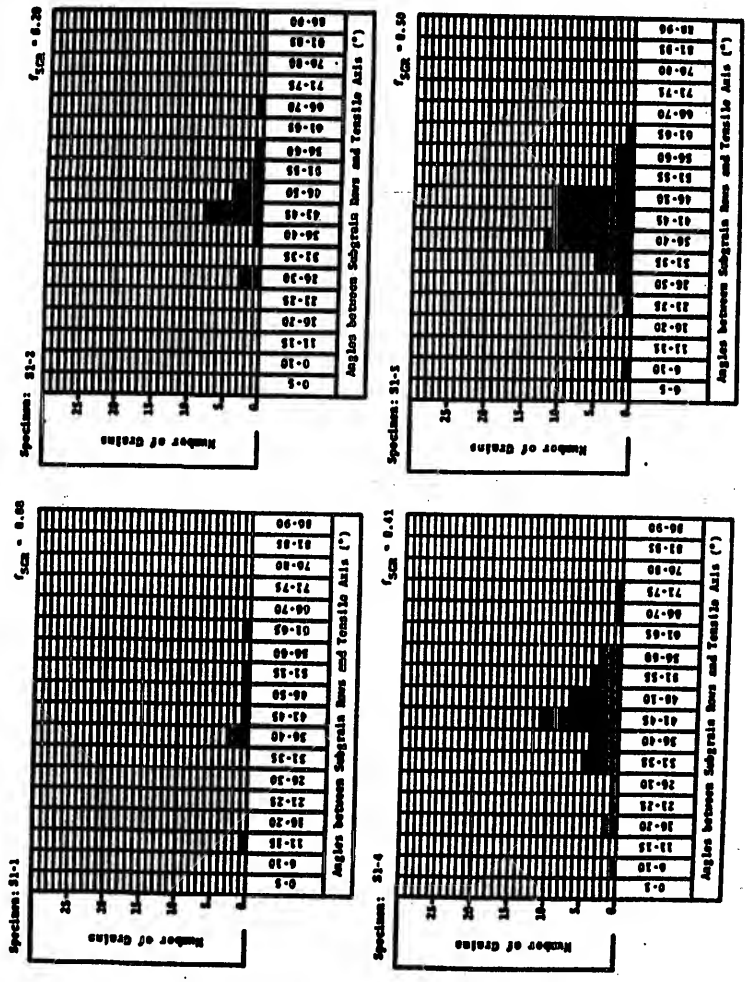

Figure 59. (continued)

(e1) Fine-grained creep specimens tested at 200°C under an initial stress of 1,000 psi.

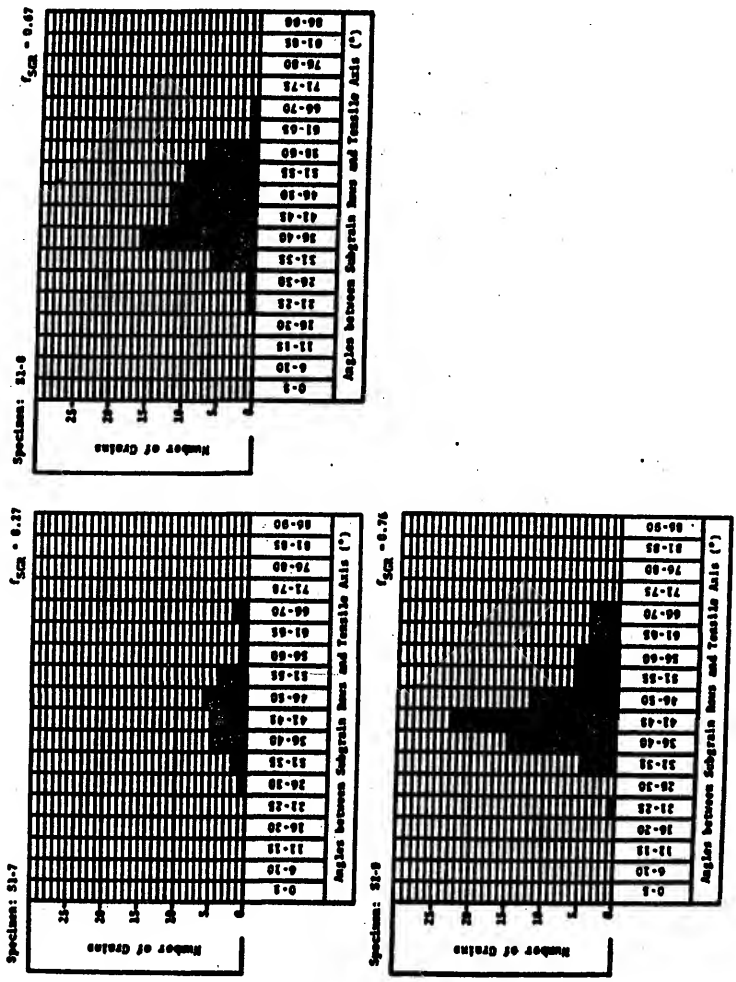

Figure 59. (continued)

(e2) Coarse-grained creep specimens tested at 200°C under an initial stress of 1,000 psi.

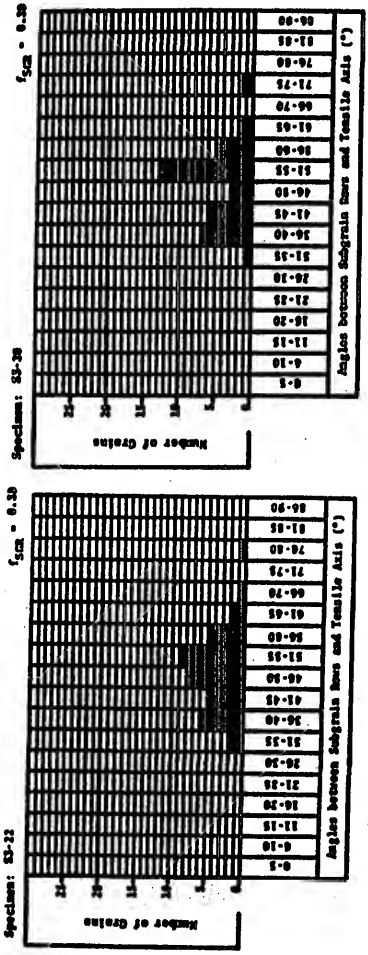

Figure 59. (continued)

(f) Creep specimens tested at 200°C under an initial stress of 1,200 psi.

1. One grain had subgrain rows making an angle of between 31° and 35° with the tensile axis.

2. Five grains had subgrain rows making angles between 36° and 40° with the tensile axis.

3. Four grains had subgrain rows making angles between 41° and 45° with the tensile axis.

4. One grain had subgrain rows making an angle between 46° and 50° with the tensile axis.

5. Two grains had subgrain rows making angles between 51° and 55° with the tensile axis.

6. One grain had subgrain rows making an angle between 61° and 65° with the tensile axis.

From the histograms given for each creep specimen in Figure 11, it is observed that the orientation of subgrain rows with respect to the tensile axis clusters strongly around 45°. Only a very small portion of the subgrain rows have angular orientations with respect to the tensile axis of less than 35° or greater than 55°. To illustrate this observation further, the fraction of grains containing subgrain rows within the angular range of 35° to 55°, inclusive, $f_{SGR(35-55)}$, is always high as shown in Table XI(c). The values for $f_{SGR(35-55)}$ range from 0.61 to 1.00, indicating quantitatively that of the grains containing subgrain rows, the great majority of the grains contain subgrain rows within the angular orientation range of 35° to 55° with respect to the tensile axis.

3.7.2.7. Some correlations between grain boundary serrations, subgrains and subgrain rows

It has previously been stated that the association between subgrains and grain boundary serrations is considered by a number of investigators to be a valid observation. Further, it has been observed during the course of this research that there is an apparent connection between subgrain rows and dentate grain boundary serrations. When no subgrain rows are present, no dentate grain boundary serrations are observed.

The converse of the statement regarding the association between subgrain rows and grain boundary serrations is not necessarily true. The existence of subgrain rows does not generally indicate that dentate grain boundary serrations will be observed. In fact, in a number of instances subgrain rows have been observed without the observation of dentate grain boundary serration. Even when subgrain rows were aligned across the span of several grains, the grain boundaries often remain remarkably smooth. The suggestion which stems from these observations is that dentate serrations are produced after the subgrain rows have been formed, although there is no direct experimental evidence which says conclusively that subgrain rows and dentate serrations cannot form more or less simultaneously.

These facts seem to indicate that wavy grain boundary serrations are to be related to the random subgrain morphology; while on the other hand, dentate grain boundary

serrations are to be related to the existence of subgrain rows. In assessing the associations between the forms of grain boundary serrations and the subgrain morphology, it must be first understood that serrations in grain boundaries "belong" to both grains conjoint upon the boundary. The nature of the serrations must be related to the substructures in both of the conjoint grains. For instance, it is generally observed that when a grain boundary is smooth, one of the conjoint grains has no substructure. When a boundary has wavy serrations, either both of the conjoint grains contain subgrains of the random morphology, or one of the pair contains subgrain rows and the other contains random subgrains. Dentate serrations have been observed only when both of the conjoint grains contain subgrain rows.

As part of the investigation of the microstructural evolution which takes place during the course of creep, the grain boundary surface area of serrated grain boundaries, $\tilde{S}_V$, was measured using the techniques of quantitative metallography. The ratio of the surface area of serrated grain boundaries to the total (serrated plus smooth) grain boundary area, $\tilde{S}_V/S_{V(GB)}$, plotted versus time and strain is used to trace quantitatively the formation of grain boundary serrations. Unfortunately, no quantitative method has been developed to separate wavy serrations from dentate serrations; therefore, the ratio, $\tilde{S}_V/S_{V(GB)}$, does not distinguish between wavy and dentate grain boundary serrations.

Graphs of $\tilde{S}_v/S_{v(GB)}$ versus time and strain are given in Figures 60 (a through f) and 61 (a through f), respectively. In comparing the graphs of $\tilde{S}_v/S_{v(GB)}$ versus time, Figure 60, to the graphs of f_{SG} and f_{SGR} versus time, Figure 53, a remarkable similarity can be seen in the shapes of the curves. The most striking similarities can be seen between $\tilde{S}_v/S_{v(GB)}$ versus time and f_{SGR} versus time. An immediate reaction to this observation was to associate grain boundary serrations with subgrain rows; however, it was recalled from visual observations of the microstructures that, during secondary creep, two forms of serrations usually coexist. The fraction, $\tilde{S}_v/S_{v(GB)}$, is a measure of the sum of both forms of serrations. Wavy serrations are associated primarily with the random subgrain morphology, while dentate serrations are always associated with subgrain rows. Wavy serrations may also exist at the ends of subgrain rows, particularly in early secondary creep. Dentate serrations do not become observable to any great degree until secondary creep has been in progress for some time. Therefore, it cannot be concluded that serrations are to be associated with only subgrain rows.

The effect of increasing the stress is to accelerate the formation of grain boundary serrations at a given temperature. Compare Figures 60(d) and (e) for tests at 200°C under stresses of 800 and 1,000 psi, respectively. The same effect is observed in Figures 58(b) and (c) for single

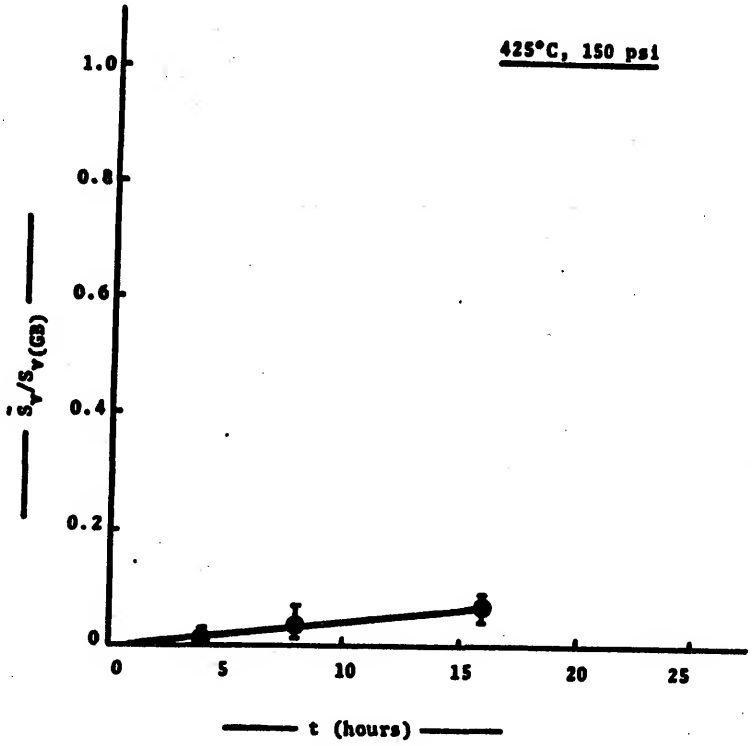

Figure 60. Fraction of the grain boundary area which is serrated, $\tilde{S}_V/S_{V(GB)}$, versus time, t.

(a) Specimens tested at 425°C under an initial stress of 150 psi.

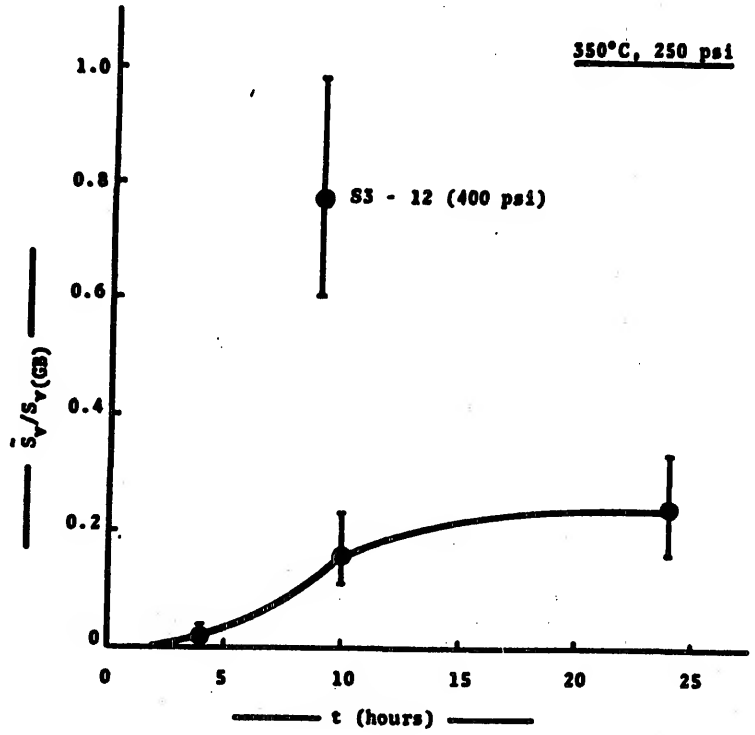

Figure 60. (continued)

(b) Specimens tested at 350°C under initial stresses of 250 and 400 psi.

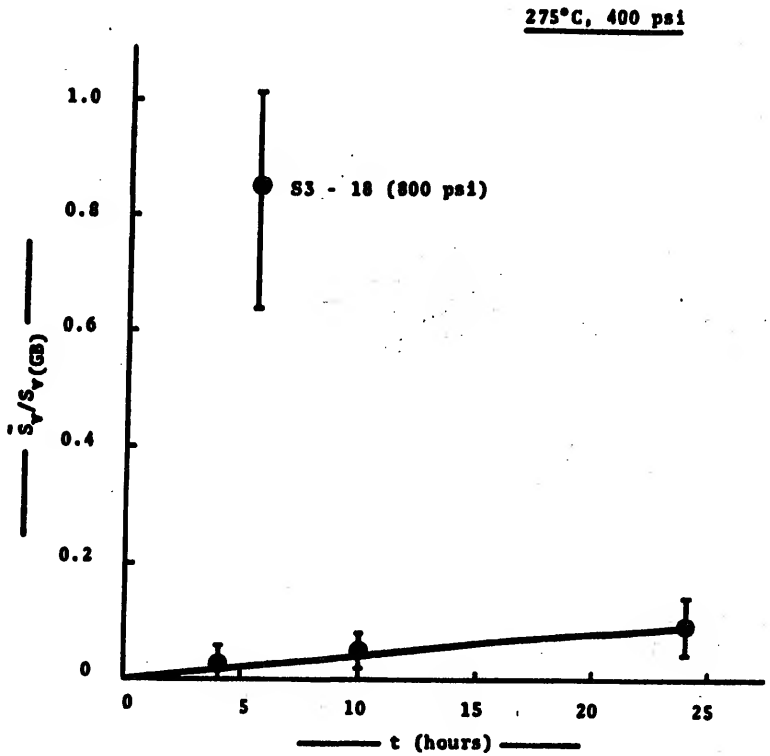

Figure 60. (continued)

(c) Specimens tested at 275°C under initial stresses of 400 and 800 psi.

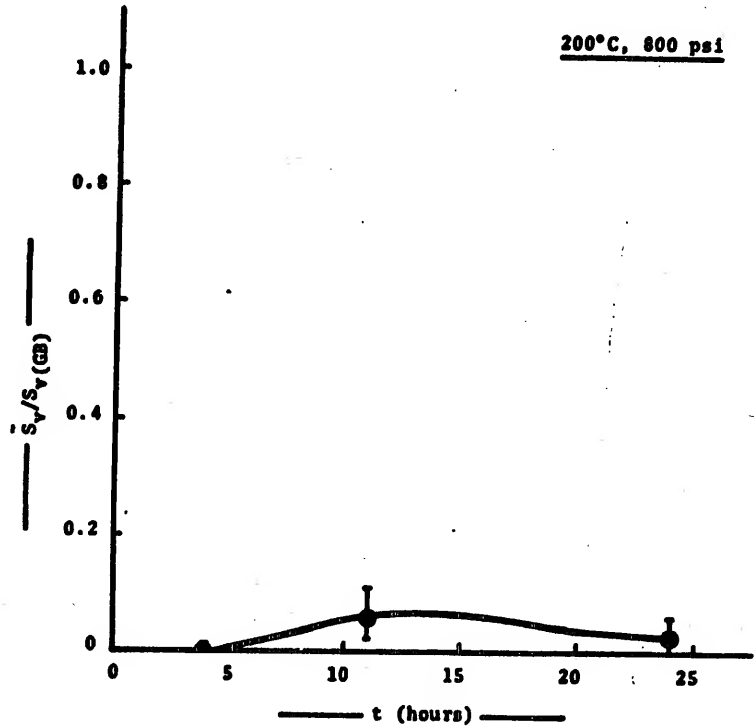

Figure 60. (continued)

(d) Specimens tested at 200°C under an initial stress of 800 psi.

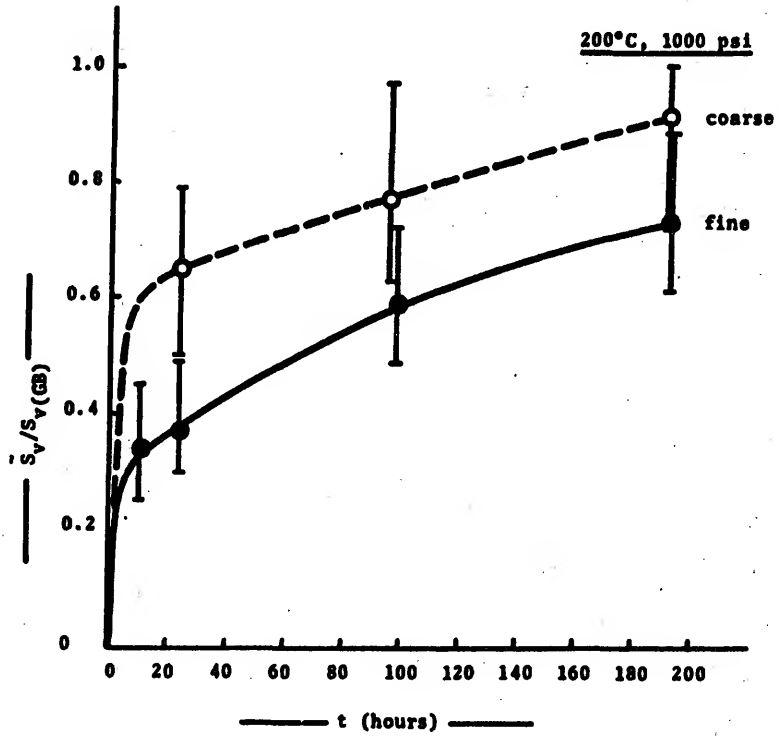

Figure 60. (continued)

(e) Specimens tested at 200°C under an initial stress of 1,000 psi.

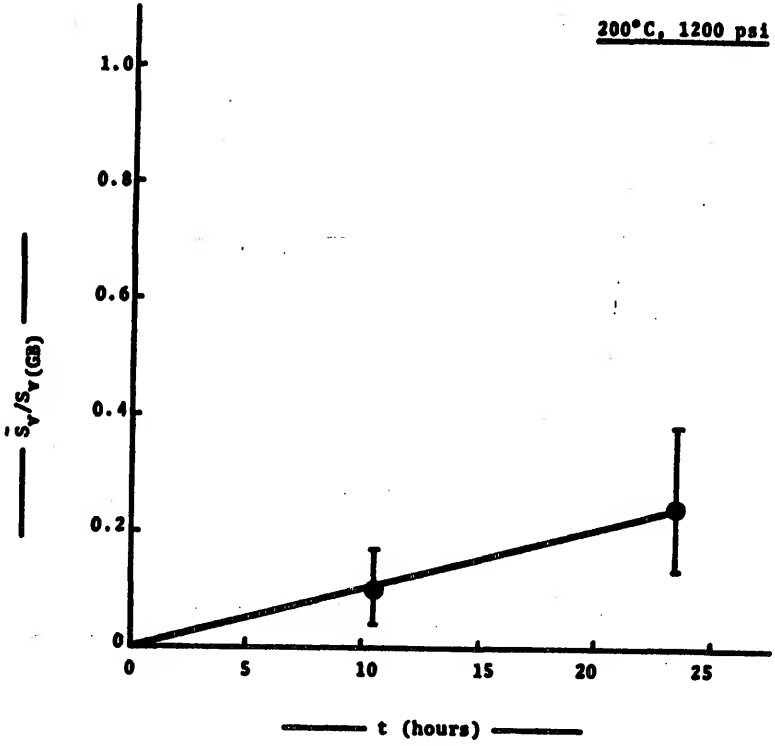

Figure 60. (continued)

(f) Specimens tested at 200°C under an initial stress of 1,200 psi.

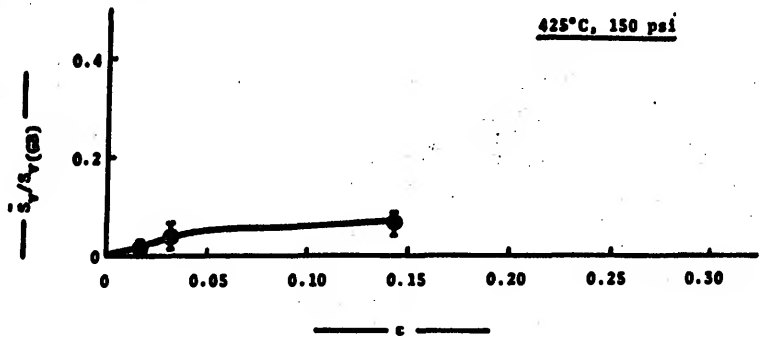

Figure 61. Fraction of the grain boundary area which is serrated, $S_v/S_{v(GB)}$, versus strain, ε.

(a) Specimens tested at 425°C under an initial stress of 150 psi.

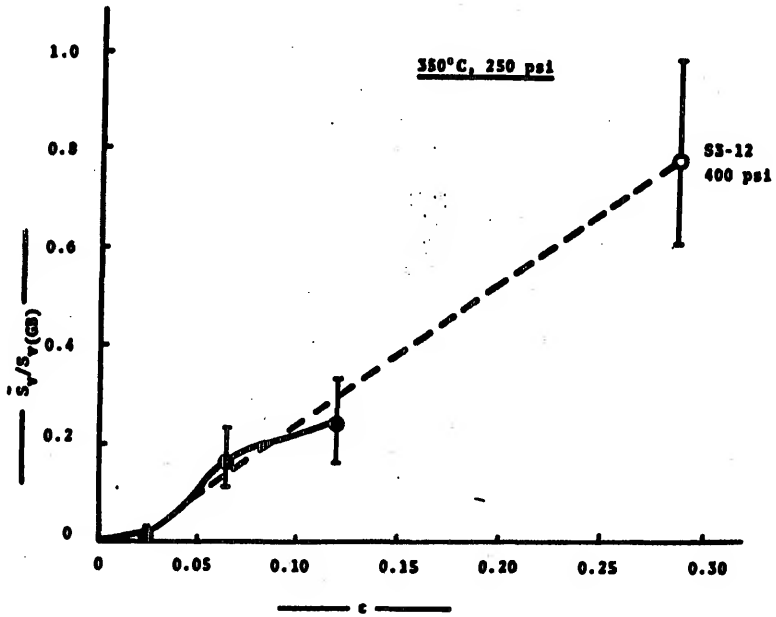

Figure 61. (continued)

(b) Specimens tested at 350°C under initial stresses of 250 and 400 psi.

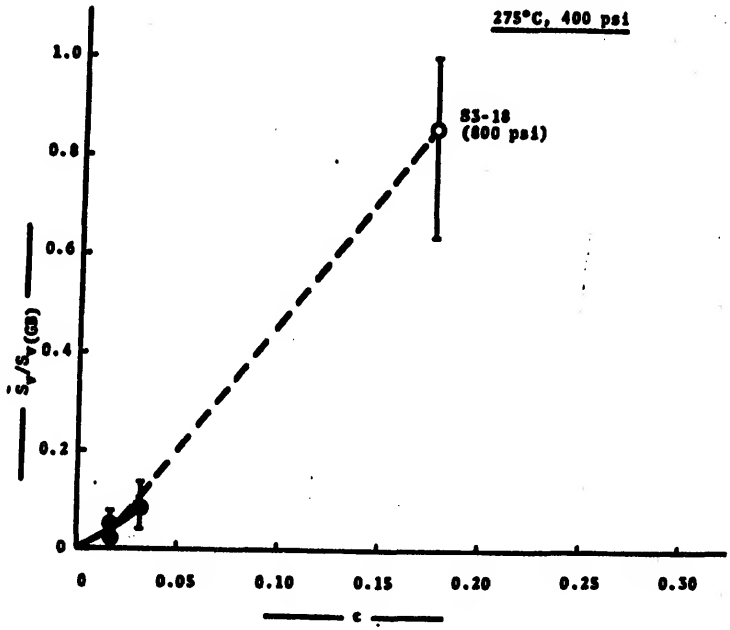

Figure 61. (continued)

(c) Specimens tested at 275°C under initial stresses of 400 and 800 psi.

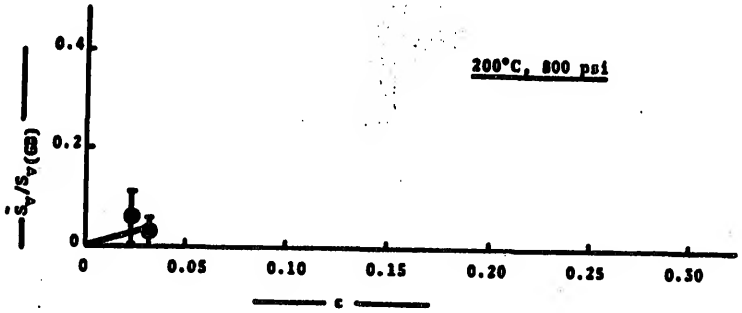

Figure 61. (continued)

(d) Specimens tested at 200°C under an initial stress of 800 psi.

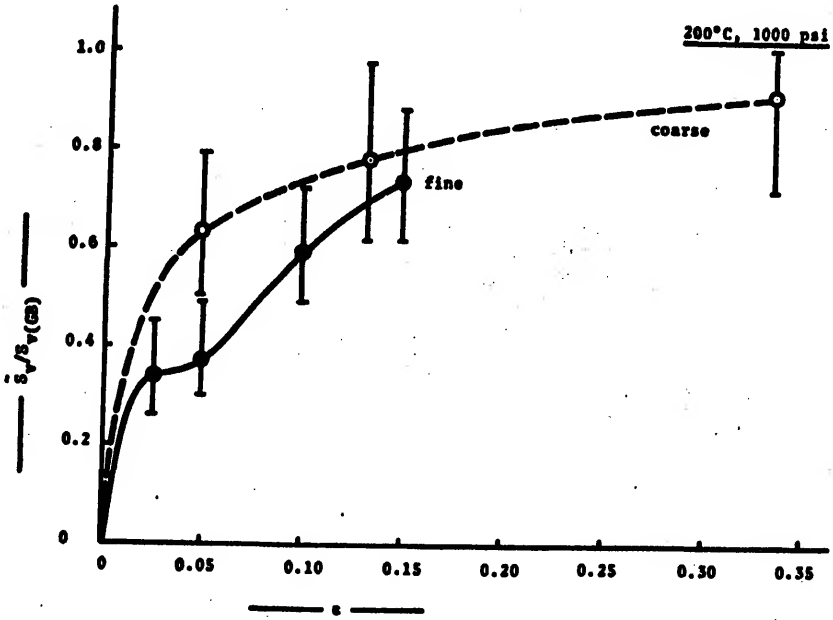

Figure 61. (continued)

(e) Specimens tested at 200°C under an initial stress of 1,000 psi.

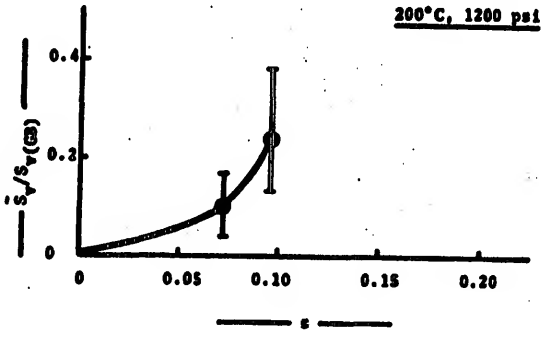

Figure 61. (continued)

(f) Specimens tested at 200°C under an initial stress of 1,200 psi.

specimens tested under higher stresses at 350°C and 275°C, respectively. An anomalous behavior in this respect seems to occur at 200°C. The formation of serrations under a stress of 1,200 psi proceeds more slowly than under a stress of 1,000 psi, Figures 60(e) and (f).

The graphs of $\tilde{S}_V/S_{V(GB)}$ versus strain, Figure 61 (a through f), show the same general trends as the graphs of f_{SGR} versus strain, Figure 58 (a through f), with the exception of the curve for the creep tests at 200°C under a stress of 1,200 psi. In comparing $\tilde{S}_V/S_{V(GB)}$ versus strain, Figure 61(f), with f_{SGR} versus strain, Figure 58(f), the latter curve levels off at the higher values of strain, while the curve for $\tilde{S}_V/S_{V(GB)}$ versus strain continues to increase at the higher strain values. Three possible explanations for this behavior are: (1) the increase in the serrated fraction of grain boundary area, $\tilde{S}_V/S_{V(GB)}$, is due to the formation of wavy serrations associated with subgrains of the random morphology; (2) the increase in $\tilde{S}_V/S_{V(GB)}$ is due to the formation of dentate serrations associated with subgrain rows; and (3) the increase in $\tilde{S}_V/S_{V(GB)}$ is due to the formation of both types of serrations. On the basis of visual examination of the microstructures, the third explanation seems to be the most reasonable. Along with the increase in the fraction of grains containing subgrains, f_{SG}, there seems to be a general increase in the amounts of both types of serrations.

Another interesting aspect of the graphs of Figure 61 is shown for the creep temperatures of 350°C and 275°C, Figures 61(b) and (c). The values plotted for the single specimens, S3-12 and S3-18, tested under higher initial stresses appear to indicate that the amount of grain boundary area containing serrations is strongly dependent upon the amount of strain, rather than upon the level of the stress. A straight line through the data points of both stress levels indicates that curves for the two stresses may be superimposed. If this is true, then within these limits of stress, the fraction of grain boundary area is primarily a function of the amount of strain rather than the applied stress.

With respect to strain, the creep condition of T = 200°C and σ = 1,000 psi is the most efficient in producing grain boundary serrations. This is particularly evident for small strains.

Additional information regarding the interrelations between grain boundary serrations, subgrains and subgrain rows has been obtained by plotting the fraction of the grain boundary area which is serrated, $\tilde{S}_V/S_{V(GB)}$, versus the fraction of grains with subgrains alone, f_{SG}-f_{SGR}, the fraction of grains with subgrain rows, f_{SGR}, and the fraction of grains with subgrains and subgrain rows, f_{SG}. The three curves are plotted for each temperature-stress set of creep conditions in Figure 62 (a through f). Because of the

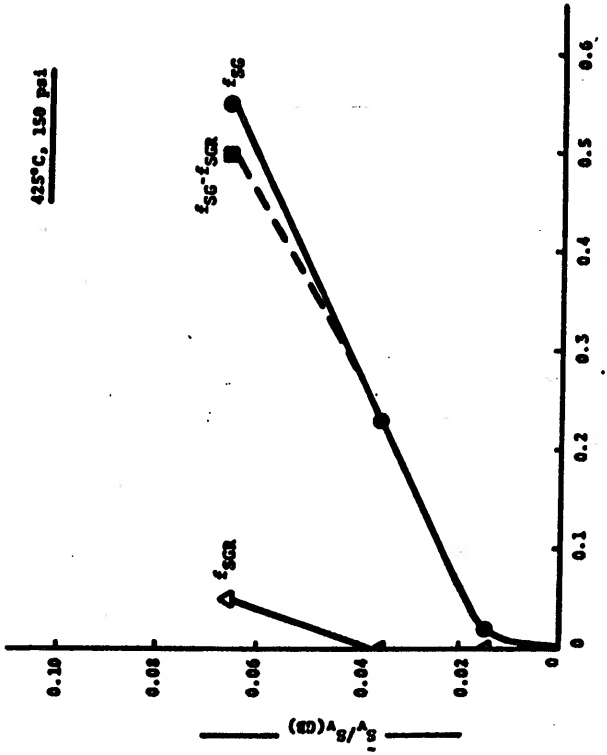

Figure 62. Fraction of grain boundary area which is serrated, $\tilde{S}_V/S_V(GB)$, versus fractions of grains which contain subgrains, f_{SG}, subgrain rows, f_{SGR}, and only subgrains of random morphology, $f_{SG}-f_{SGR}$.

(a) Specimens tested at 425°C under an initial stress of 150 psi.

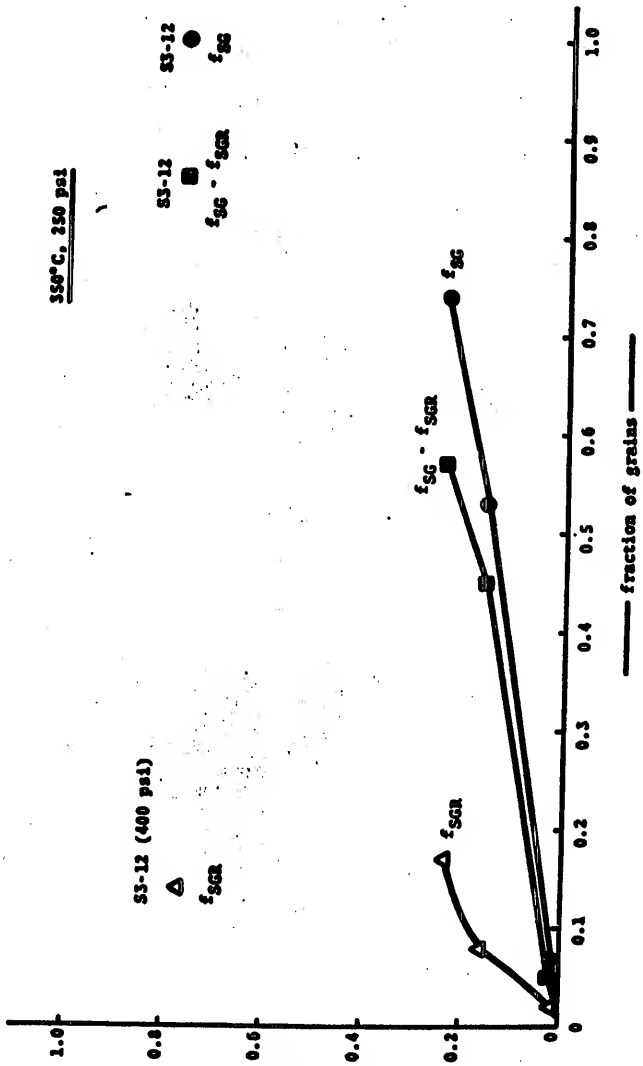

Figure 62. (continued)

(b) Specimens tested at 350°C under initial stresses of 250 and 400 psi.

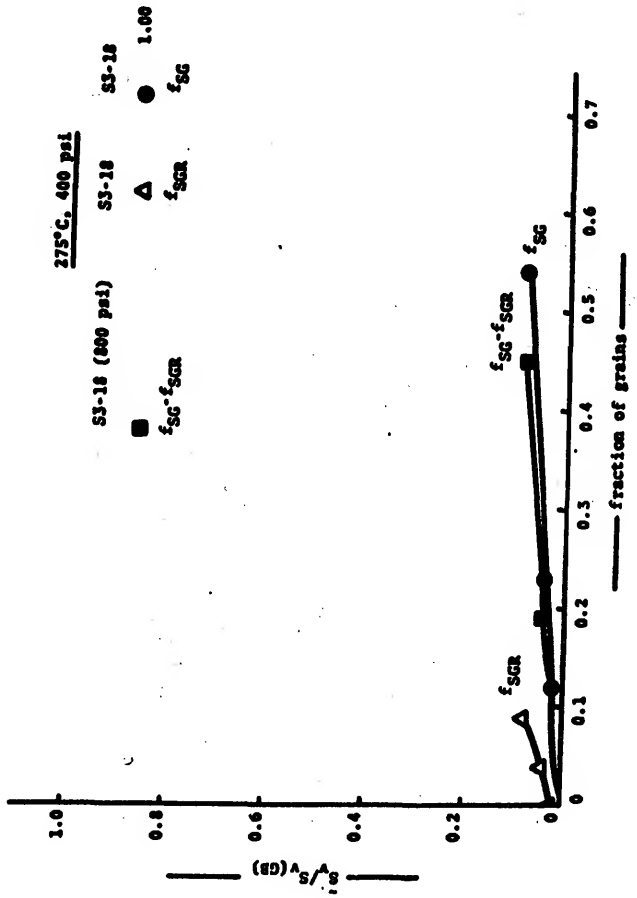

Figure 62. (continued)

(c) Specimens tested at 275°C under initial stresses of 400 and 800 psi.

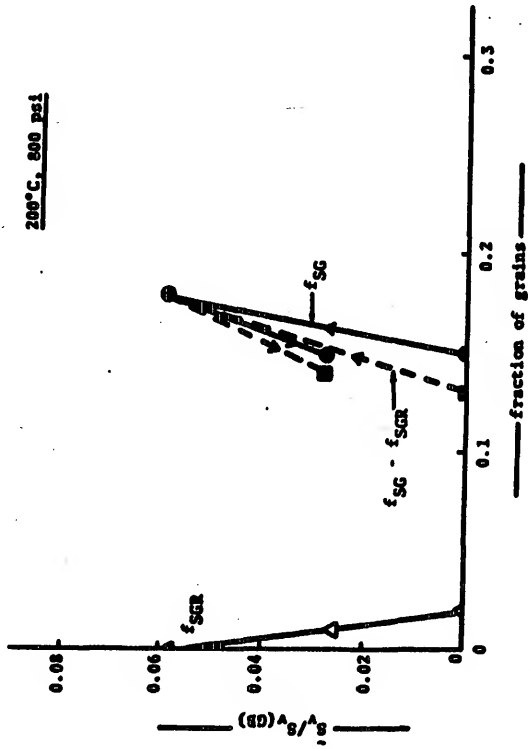

Figure 62. (continued)

(d) Specimens tested at 200°C under an initial stress of 800 psi.

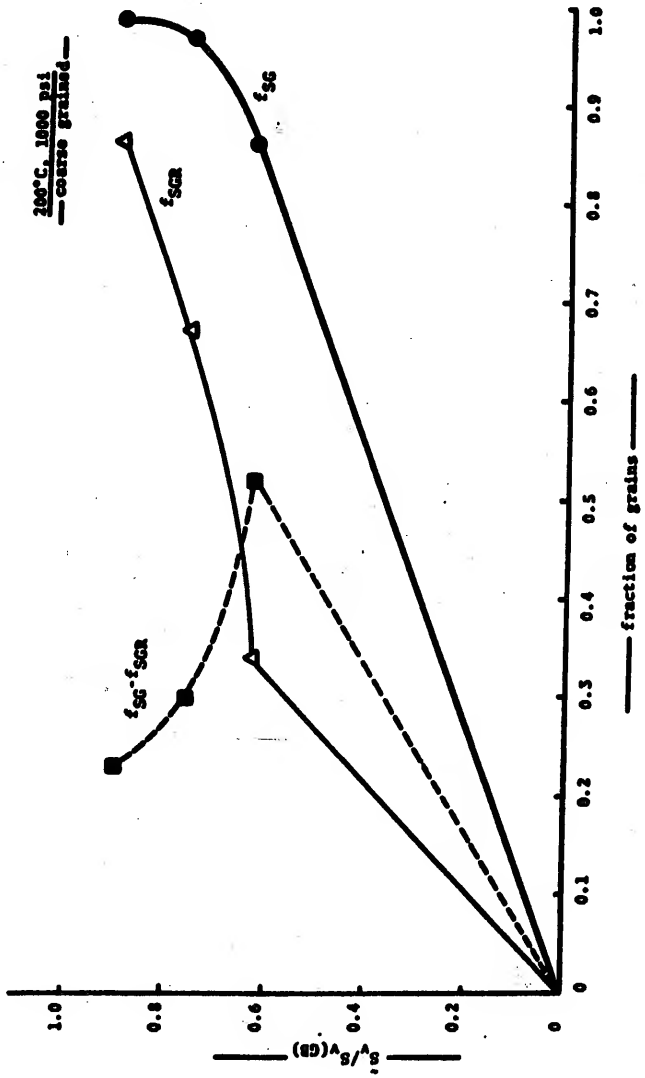

Figure 62. (continued)

(e1) Coarse-grained specimens tested at 200°C under an initial stress of 1,000 psi.

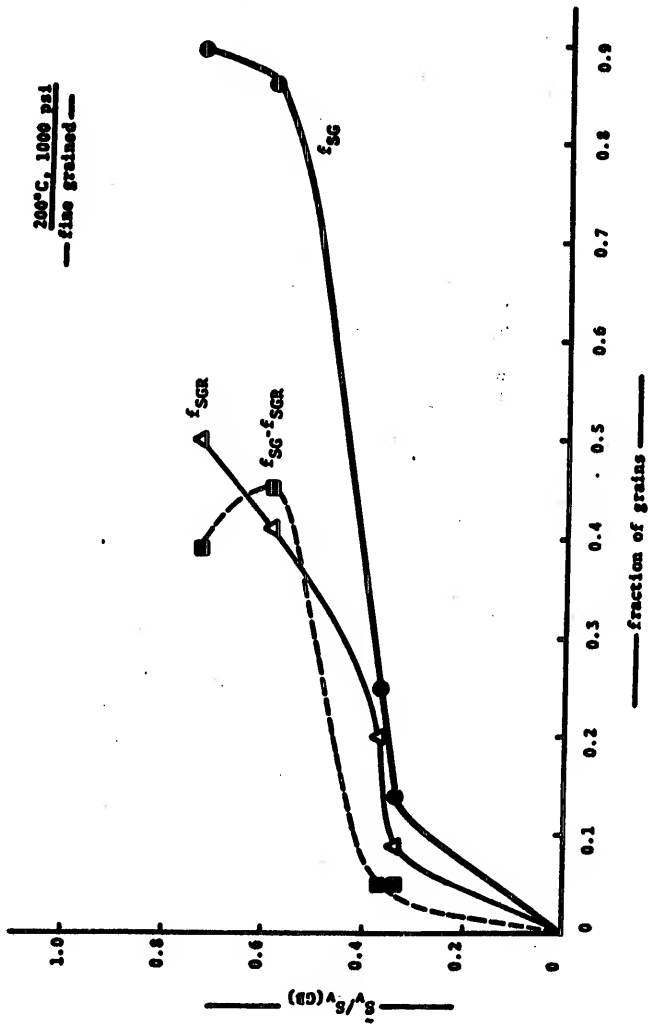

Figure 62. (continued)

(e2) Fine-grained specimens tested at 200°C under an initial stress of 1,200 psi.

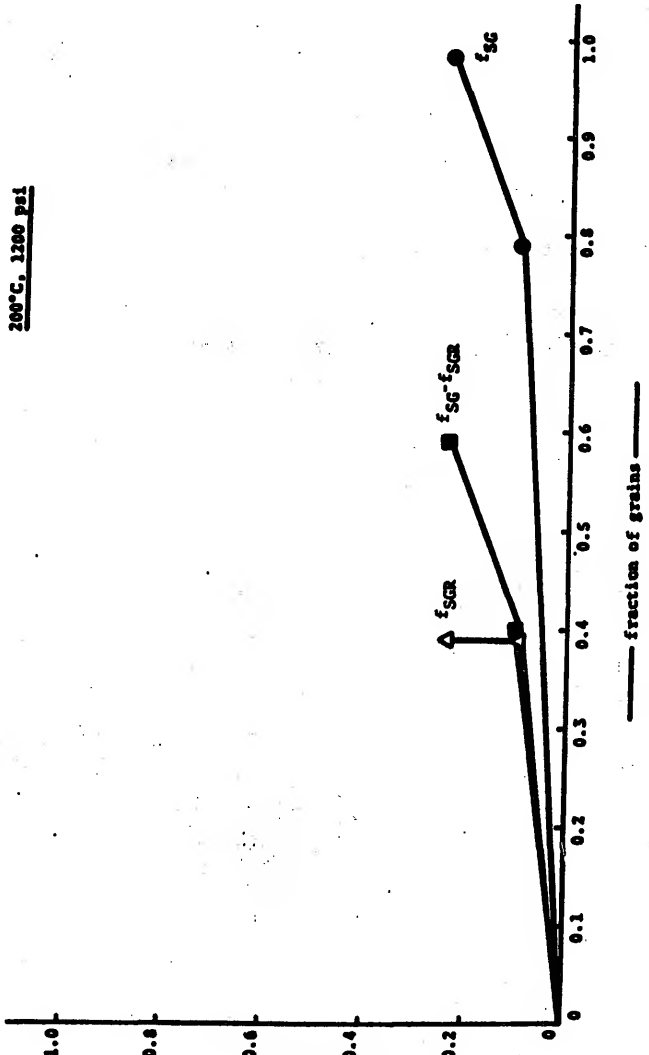

Figure 62. (continued)

(f) Specimens tested at 200°C under an initial stress of 1,200 psi.

detailed information in each of the several graphs, the results of each graph will be described individually in terms of the creep conditions of temperature and stress.

1. T = 425°c; σ = 150 psi, Figure 62(a).--Grain boundary serrations appear to be linked with the usual form of subgrains rather than with subgrain rows. Note that the increase in grain boundary serrations occurs with a large increase in the fraction of grains containing subgrains alone, f_{SG}-f_{SGR}, as compared to a very small increase in the fraction of grains containing subgrain rows.

2. T = 350°C; σ = 250 and 400 psi, Figure 62(b).--As under the previous set of creep conditions, the formation of grain boundary serrations is primarily related to subgrains rather than subgrain rows; however, the influence of subgrain rows is somewhat greater than under the former creep conditions. This observation appears to hold even at the higher stress of 400 psi as shown by the data points for a single specimen, S3-12. Further, it is important to note that the effect is presumed to persist well into secondary creep since the strain attained by this specimen was 0.288.

3. T = 275°C; σ = 400 and 800 psi, Figure 62(c).--For creep tests at 275°C under a stress of 400 psi, again the formation of grain boundary serrations is to be attributed to subgrains alone rather than subgrain rows. An increase in stress to 800 psi (specimen S3-18) has the reverse effect upon the relations between grain boundary serrations,

subgrains and subgrain rows. In the case of this single specimen, the grain boundary serrations exist in a microstructure of which the major portion of the grains contain subgrain rows. This specimen represents a substantial amount of strain: 0.176. It is quite possible in the evolution of the microstructure at this stress level that initially the grain boundary serrations are associated primarily with the random subgrain morphology. As deformation proceeds, more and more grains develop subgrain rows and the growing connection between serrations and subgrain rows becomes apparent. With further deformation, an alteration in the substructure of grains containing the random subgrain morphology gradually occurs, such that the substructure is transformed into that which is characterized by subgrain rows. The transformation of the random subgrain morphology into subgrain rows is viewed as a rather gradual evolution which comes about as a result of changes in the grain-to-grain constraints as deformation progresses. In effect, one may regard the transformation as the concurrent operation of two processes; polygonization to form subgrain rows, and the migration of pre-existing sub-boundaries into the walls separating subgrain rows. For the process to proceed with the least amount of difficulty, it is necessary that the sub-boundaries of the random subgrain morphology represent only small misorientations. The end point of this process is reached when all of the grains contain subgrain rows. It

seems evident that, under certain conditions of creep, some grains form subgrain rows at the outset of creep deformation.

4. T = 200°C; σ = 800 psi, Figure 62(d); σ = 1,000 psi, Figure 62(e); σ = 1,200 psi, Figure 62(f).--The plotted data appearing in Figure 62(d) give little information about the relations between grain boundary serrations and subgrain morphology for specimens tested under an 800 psi stress. It was felt that the measurements of fractions of grains containing subgrains and subgrain rows suffered from a too-small sample size, which resulted from the small portion of the grains containing subgrains. Nevertheless, there is an indication that the small fraction of serrated boundary is primarily related to the random subgrain morphology. Visual examination of the microstructures confirmed that the serrations were primarily of the wavy form and that the predominant subgrain morphology was that of random subgrains.

Both the fine- and coarse-grained material tested under a stress of 1,000 psi, Figure 62 (e1 and e2), exhibited a startling "turn-around" behavior in the relations between grain boundary serrations and subgrain morphology. During early secondary creep, serrations are related to both subgrain morphologies. In the coarse-grained material serrations are related more strongly to subgrain rows; whereas, the converse is true for the fine-grained material. With further deformation the fraction of grains containing

subgrains of the random morphology becomes smaller as the fraction of grains containing subgrain rows rapidly increases. Therefore, in the later stages of secondary creep, serrations are most strongly related to subgrain rows. Metallographic examinations of the specimens confirm that most of the serrations are dentate and that they are associated with subgrain rows. It is believed that this "turn-around" behavior is partly the result of the random subgrain morphology gradually transforming into the subgrain row morphology as described previously.

For specimens tested under a stress of 1,200 psi, Figure 62(f), the grain boundary serrations are initially related about equally to both subgrain morphologies. Later in creep, the serrations become more strongly related to the random subgrain morphology.

From the results presented in this section, it is apparent that the relations which exist between grain boundary serrations and the substructure vary rather widely, but a general tendency does seem to exist. The general tendency is that there exists intermediate creep conditions with respect to temperature and stress under which grain boundary serrations are rather strongly to be connected with existence subgrain rows. Under conditions of higher temperatures and lower stresses, and under conditions of lower temperatures and higher stresses, serrations are more strongly connected with the existence of the random form of subgrain morphology.

The intermediate conditions of creep under which the relation between serrations and subgrain rows is prominent are represented in this investigation by a temperature of 200°C and a stress of 1,000 psi. In all probability, a temperature of 275°C and a stress of 800 psi would give similar results.

3.7.2.8. The change in grain boundary anisotropy, $e_g(f)-e_g(i)$, versus time

The change in the grain boundary anisotropy as the result of creep deformation, $e_g(f)-e_g(i)$, plotted versus time for each of the six creep conditions is given in Figure 63 (a through f). Within the statistical tolerances of the measurements, there are no significant indications of grain elongation due to secondary creep under the following conditions:

1. $T = 425°C$; $\sigma = 150$ psi, Figure 63(a)
2. $T = 350°C$; $\sigma = 250$ psi, Figure 63(b)
3. $T = 275°C$, $\sigma = 400$ psi, Figure 63(c)
4. $T = 200°C$; $\sigma = 800$ psi, Figure 63(d).

When the creep is carried out at 200°C under initial stresses of 1,000 psi and 1,200 psi, there is a tendency for the grains to become elongated. For instance,in the fine-grained material tested at 200°C under a stress of 1,000 psi, the grains initially elongate and their shape remains unchanged throughout additional secondary creep, Figure 63(e). In the coarse-grained material tested under similar

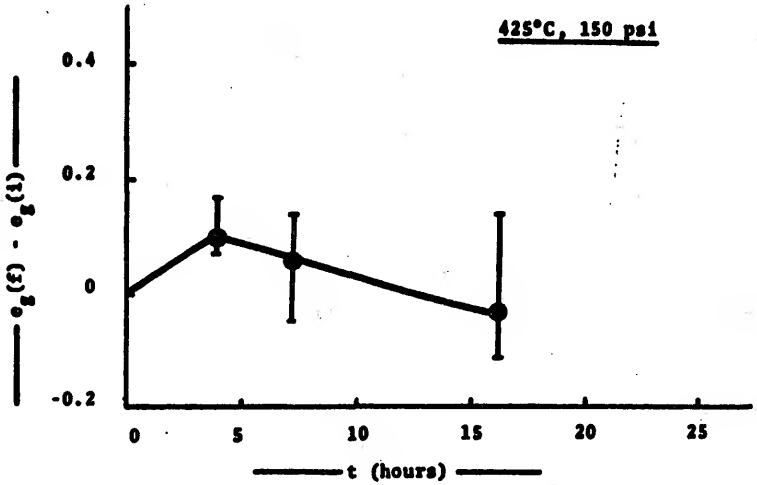

Figure 63. The change in grain boundary anisotropy, $e_g(f)-e_g(i)$, versus time, t.

(a) Specimens tested at 425°C under an initial stress of 150 psi.

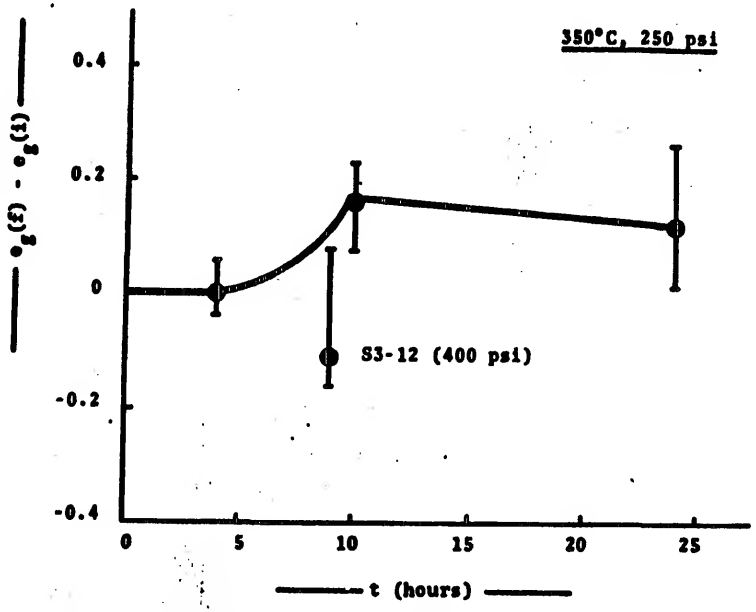

Figure 63. (continued)

(b) Specimens tested at 350°C under initial stresses of 250 and 400 psi.

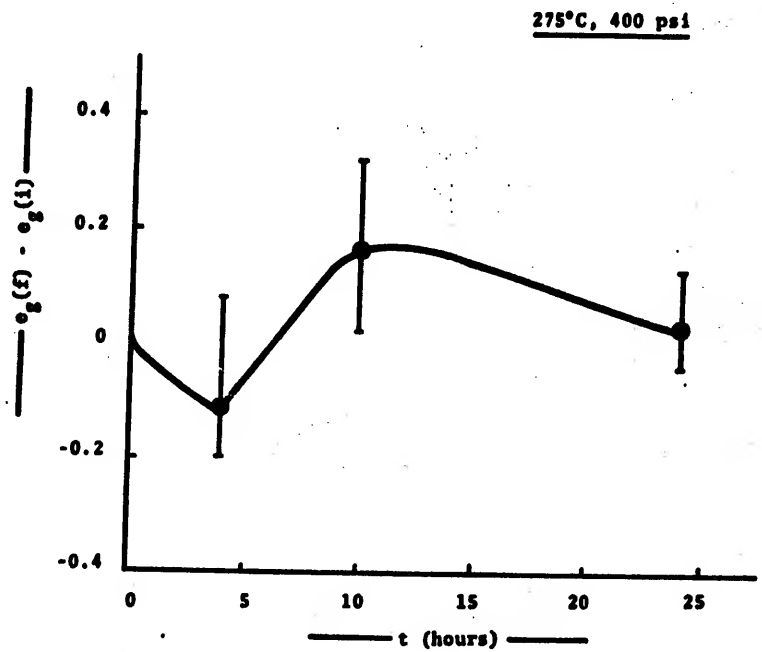

Figure 63. (continued)

(c) Specimens tested at 275°C under an initial stress of 400 psi.

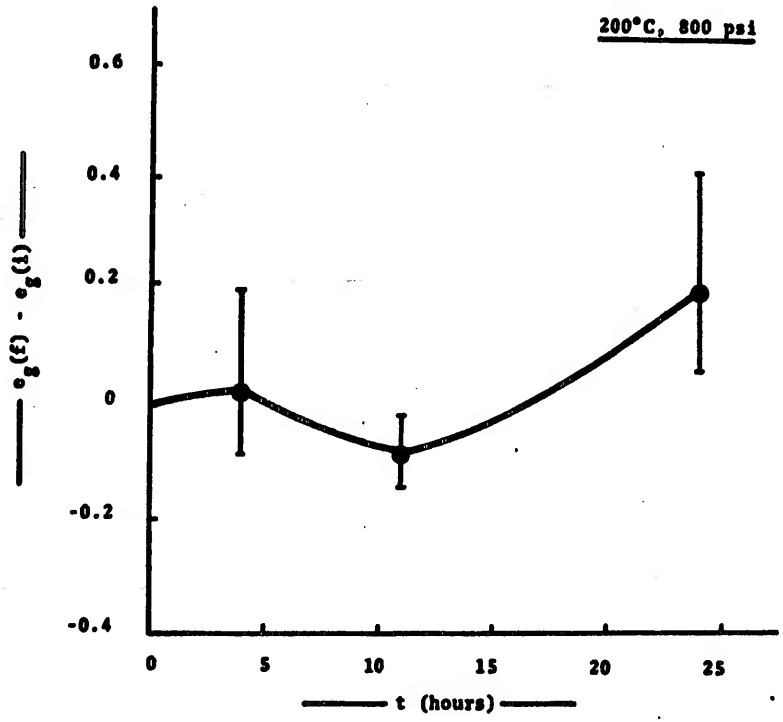

Figure 63. (continued)

(d) Specimens tested at 200°C under an initial stress of 800 psi.

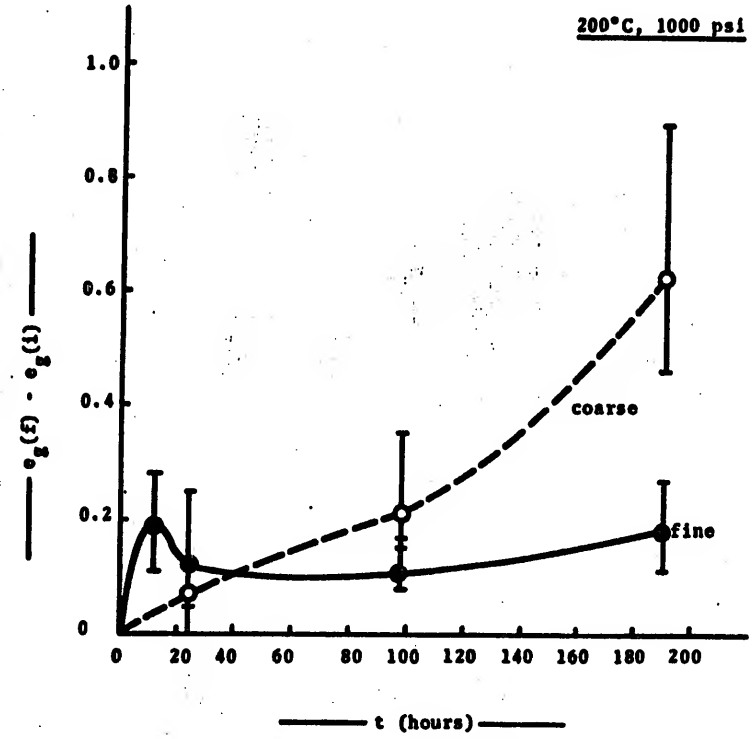

Figure 63. (continued)

(e) Specimens tested at 200°C under an initial stress of 1,000 psi. The coarse-grained specimen tested to 192.37 hours had entered third stage creep.

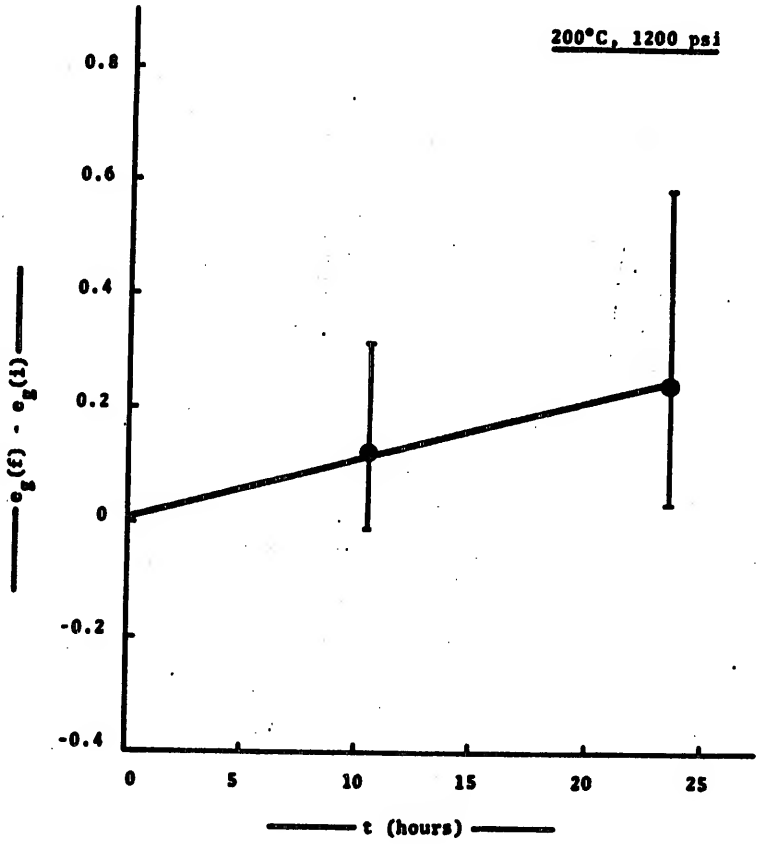

Figure 63. (continued)

(f) Specimens tested at 200°C under an initial stress of 1,200 psi.

conditions there is a significant elongation of the grains with creep. However, it must be pointed out that the last two of the coarse-grained specimens, S1-8 and S1-9, developed necks during creep, indicating the existence of tertiary creep behavior. Thus, the elongation of the grains cannot be attributed to secondary creep behavior for the coarse-grained specimens. The change in grain boundary anisotropy for specimens tested at 200°C under a stress of 1,200 psi is hardly significant when the statistical tolerances are considered; however, the trend is definitely upward, indicating that the grains tend to elongate during creep.

3.7.2.9. The change in grain boundary anisotropy, $e_g(f)-e_g(i)$, versus strain

It has been stated previously that the most meaningful way in which to consider the change in grain boundary anisotropy is to plot it against strain. If the slope of the resulting curve is greater than unity, the grains have elongated to a greater extent than has the specimen. Conversely, if the slope of the curve is less than unity, the grains have not elongated in the same proportion as the specimen. Thus, such plots indicate the existence of processes which tend to offset grain deformation, or enhance the grain elongation. Grain boundary sliding, according to the suggestion of Rachinger [127], will tend to maintain the equiaxed shape of the grains during deformation. Grain boundary migration may have the same effect upon grain elongation.

Graphs of the change in grain boundary anisotropy, $e_g(f)-e_g(i)$, plotted versus strain are given in Figure 64 (a through f). Within statistical tolerances, the grains, for the most part, remain essentially equiaxed during secondary creep. Evidence for significant grain elongation is observed only for coarse-grained material tested at 200°C under a stress of 1,000 psi, Figure 64(e).

Disregarding the statistical tolerances, there seems to be an increase in grain elongation for specimens tested at 200°C, Figure 64 (d, e and f). For specimens tested at higher temperatures (275°, 350° and 425°C), there is no clear-cut trend. There may exist a weak trend toward grain elongation followed by shortening; however, it is certain that at the three higher temperatures grains do not elongate to the extent they do at 200°C.

Rachinger [127] has attributed the lack of grain elongation during creep to grain boundary sliding. On the other hand, the grains can remain equiaxed during hot deformation if grain boundaries migrate during the course of deformation. This concept has previously been reported in regard to hot deformation studies on nickel [114] and uranium [117]. Of the two possible explanations, the latter is favored because it is difficult to accept the proposition that essentially all of the elongation is the result of grain boundary sliding.

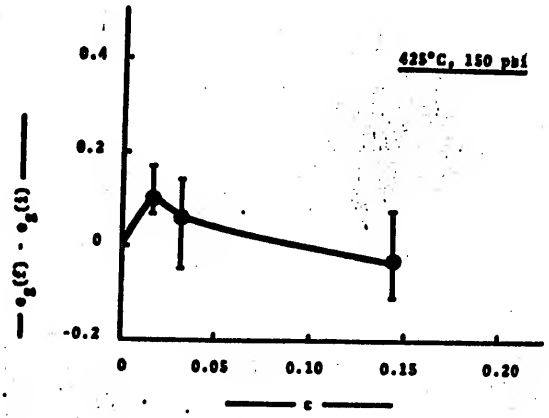

Figure 64. The change in grain boundary anisotropy, $e_g(f)-e_g(i)$, versus strain, ε.

(a) Specimens tested at 425°C under an initial stress of 150 psi.

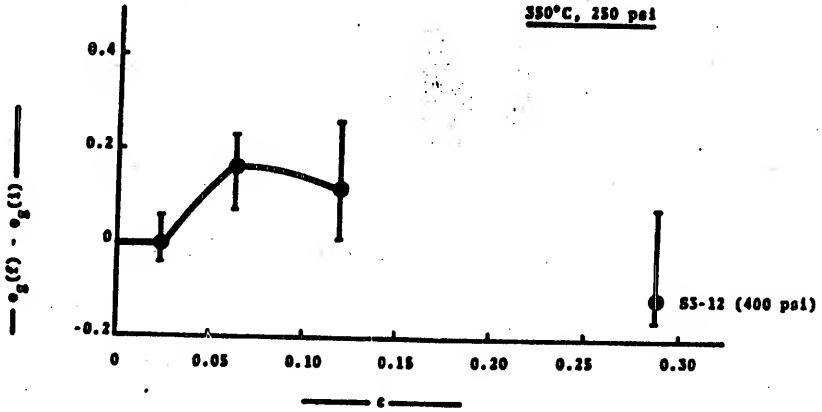

Figure 64. (continued)

(b) Specimens tested at 350°C under initial stresses of 250 and 400 psi.

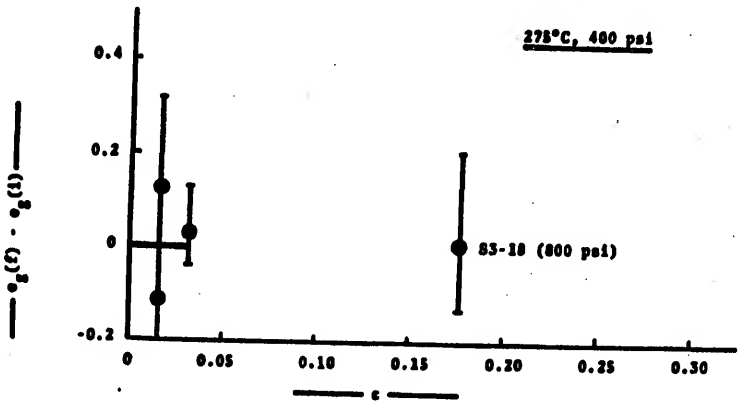

Figure 64. (continued)

(c) Specimens tested at 275°C under initial stresses of 400 and 800 psi.

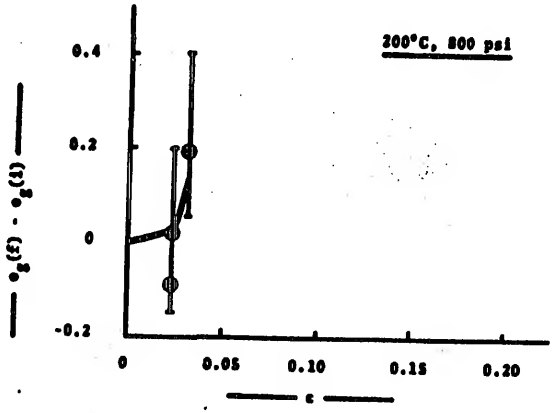

Figure 64. (continued)

(d) Specimens tested at 200°C under an initial stress of 800 psi.

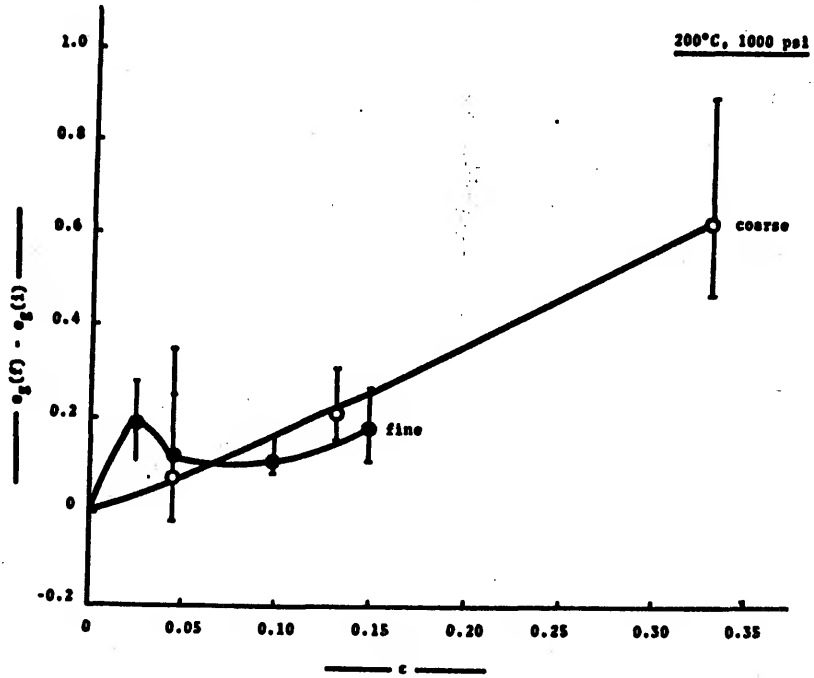

Figure 64. (continued)

(e) Specimens tested at 200°C under an initial stress of 1,000 psi. The coarse-grained specimen tested to a strain of 0.33 had entered third stage creep.

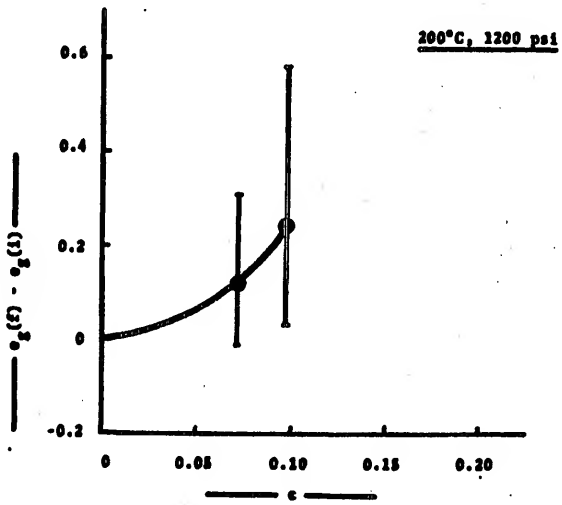

Figure 64. (continued)

(f) Specimens tested at 200°C under an initial stress of 1,200 psi.

3.8. The Microstructural Evolution During Creep II: Results from Variable Load and Temperature Creep Tests

The observations and results of this section are presented under two subsections. The first deals with qualitative observations from a set of preliminary experiments in which creep specimens tested under constant load were subjected to stepped increases in temperature, and the second is concerned with results based upon quantitative metallographic measurements obtained from the microstructures of creep specimens tested under similar conditions of stepped increases in temperature as well as under conditions of stepped decreases in load and stepped increases in temperature.

3.8.1. The Preliminary Experiments

In the previous section, it was pointed out that the tendency to form subgrain rows was enhanced at a given strain by lower creep temperatures and that a correlation between subgrain rows and grain boundary serrations appeared to be valid. It was thought that subgrain rows first developed with rather low angle boundaries separating the rows and, during the further progress of creep, the angular misorientation across these boundaries became increasingly larger. Late in the progress of secondary creep the boundaries between rows should then represent misorientations large enough so that they would respond rather like grain boundaries to further deformation. Since, as previously documented, a

great majority of the rows were oriented at angles of nearly 45° with respect to the tensile axis, high values of resolved shear stress would be directed along the boundaries separating the subgrain rows. This situation would be particularly conducive to shear along subgrain row boundaries, very much like in kind to the shear that occurs along grain boundaries during high temperature creep.

There is no question that dentate grain boundary serrations represent an energy state above that attained upon annealing. Therefore, dentate teeth in grain boundaries must be a consequence of deformation. They certainly cannot be formed during an annealing process subsequent to cold deformation. Shearing along subgrain rows during deformation appeared to be an attractive way in which dentate teeth might be formed.

On the basis of this reasoning it was decided to perform several creep tests in which creep specimens were tested at low temperatures for some period of time followed by a period of testing at a higher temperature. It was thought that subgrain rows would form during the period of testing at the lower temperature, and that their boundaries would become stable features of the microstructure. Upon raising the testing temperature, the angles of misorientation among the rows would rapidly increase and shear along the subgrain row boundaries would ensue. Because it had been observed that subgrain rows were often aligned across several neighboring

grains, it was reasoned that shearing along subgrain rows should form dentate serrations in grain boundaries at sites where subgrain rows were aligned in neighboring grains. It must again be emphasized that dentate serrations have been observed only when grains on both sides of the boundary possess subgrain rows. Dentate serrations belong to both grains, just as the boundary itself belongs to both grains. Such a mechanism would then provide for the transmission of shear across grain boundaries without reliance upon traditional dislocation concepts and near coincidence of crystallographic orientations across conjugate boundaries.

The methods employed for creep testing specimens under conditions of varying temperature have been described previously in Chapter II. It is important to recall that the step-wise temperature changes were made by changing the set point of the temperature controller and allowing the furnace to heat or cool at its maximum rate. These heating and cooling rates proved to be about 10°C per minute as measured at the specimen surface. Elongation of the specimens was monitored by a photographic technique also described in Chapter II. A list of the specimens tested in this portion of the research and the various creep testing conditions are given in Table XV. Note that each specimen was tested under constant load. Graphs showing the variation in temperature and specimen strain with time are given for the seven specimens in Figures 65 through 71. In each graph, the upper

Table XV

Creep Testing Conditions for the Preliminary Experiments

Specimen Number	Stress (psi)	Temperature (°C) [Time] (hours)
S5-5	1,000	100 [29], 205 [19], 354* (R)**
S5-6	500	105 [27], 207 [21], 316 [6]
S5-7	650	103 [10], 217 [10], 102 [10], 216 [10], 360* (R)**
S5-9 (SA)***	500	105 [23], 214 [26], 340 [9]
S5-11	450	280 [24]
S5-12	450	198 [24]
S5-13	450	204 [24], 25 [96]****, 205 [12], 329 [24]

*The temperature did not reach equilibrium following the temperature change prior to the end of the test.

**(R) indicates that the specimen ruptured.

***(SA) indicates that the specimen was strain annealed prior to testing to produce a very large grain size.

****The test was interrupted because of a malfunction of the photographic measuring camera. The specimen remained loaded for 96 hours at room temperature.

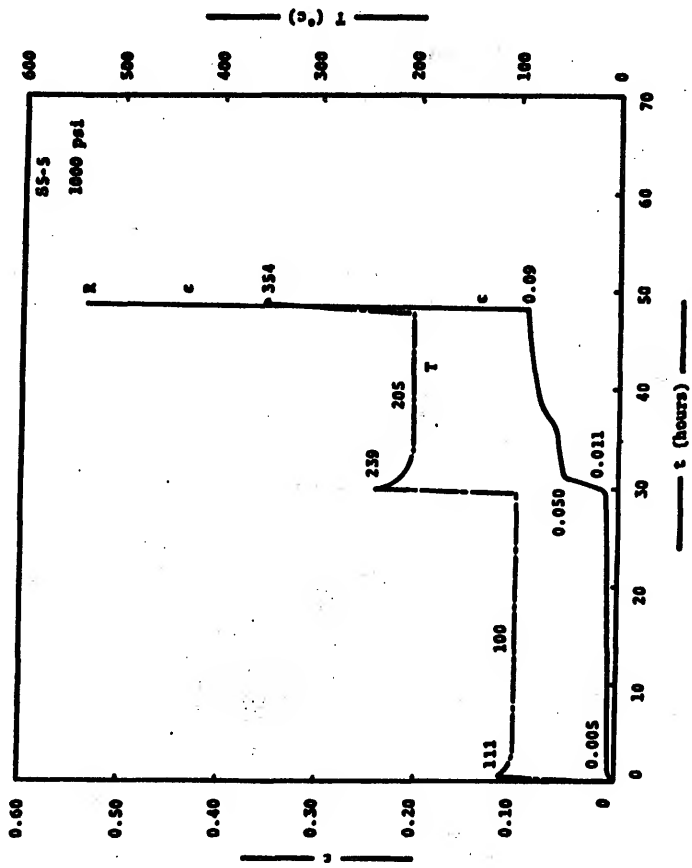

Figure 65. Strain, ε (solid line), and temperature, T (broken line), versus time, t, for specimen S5-5.

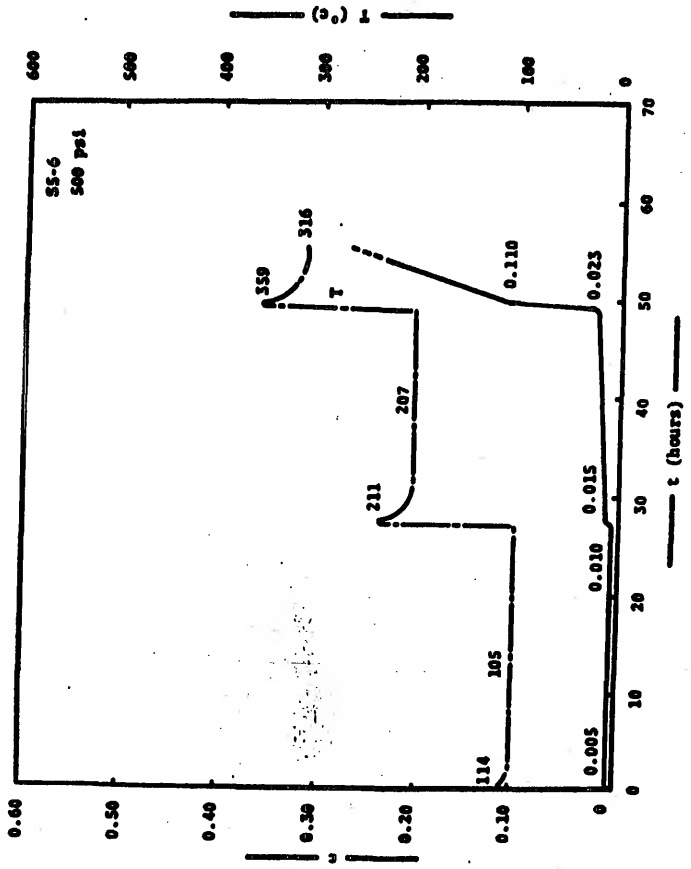

Figure 66. Strain, ε (solid line), and temperature, T (broken line), versus time, t, for specimen S5-6.

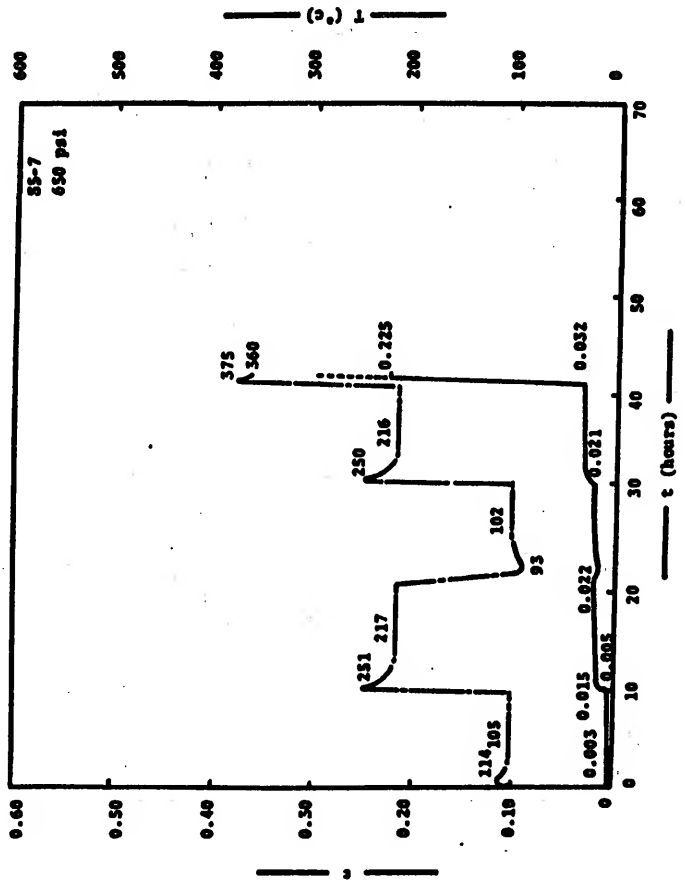

Figure 67. Strain, ε (solid line), and temperature, T (broken line), versus time, t, for specimen S5-7.

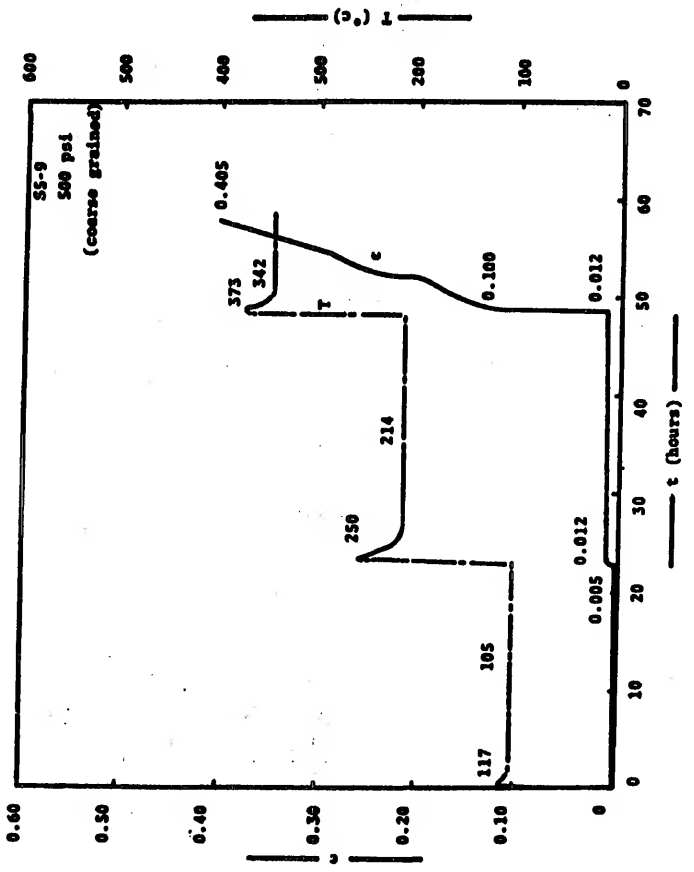

Figure 68. Strain, ε (solid line), and temperature, T (broken line), versus time, t, for specimen S5-9.

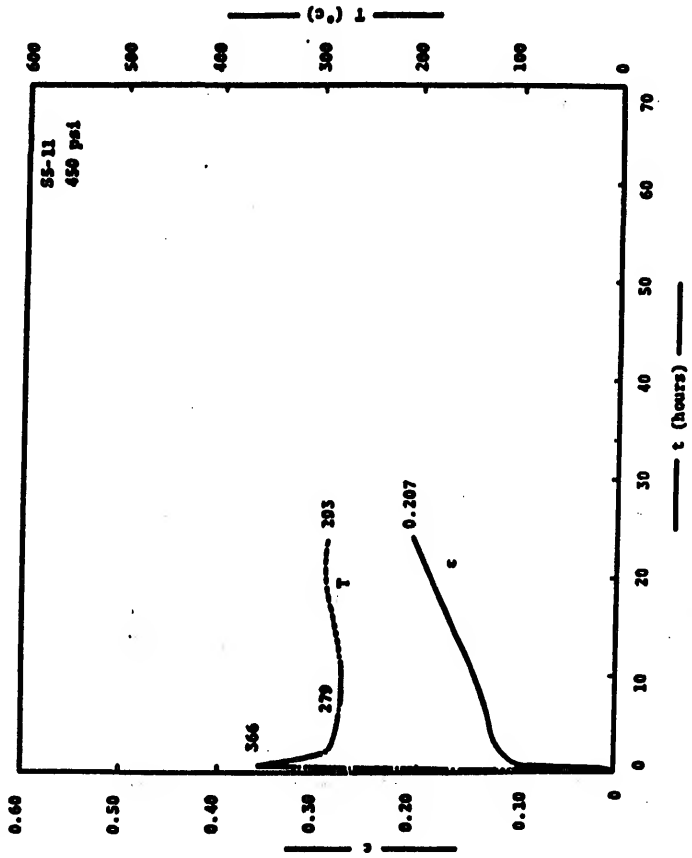

Figure 69. Strain, ε (solid line), and temperature, T (broken line), versus time, t, for specimen S5-11.

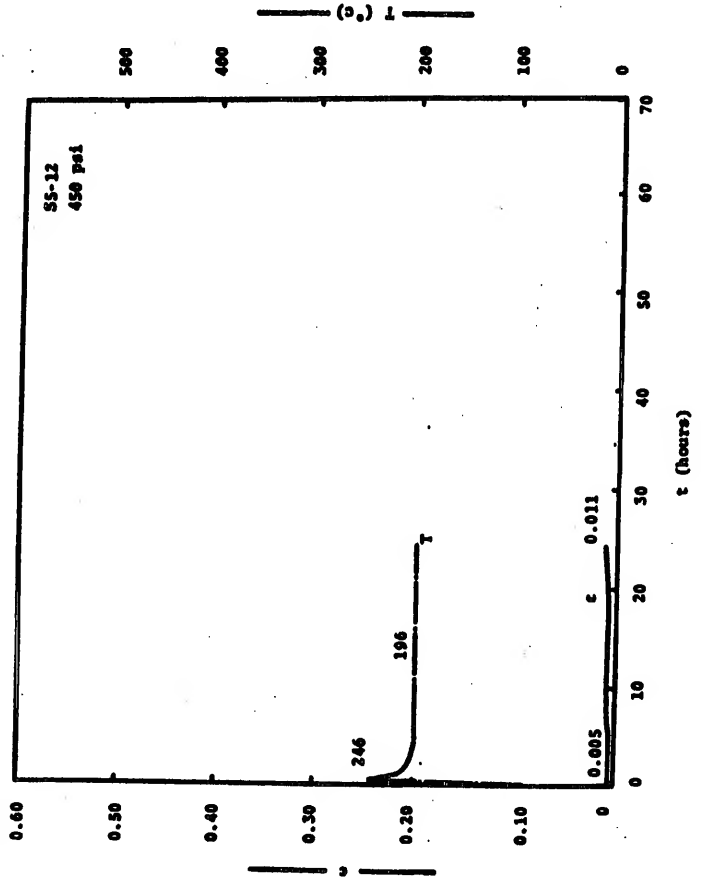

Figure 70. Strain, ε (solid line), and temperature, T (broken line), versus time, t, for specimen S5-12.

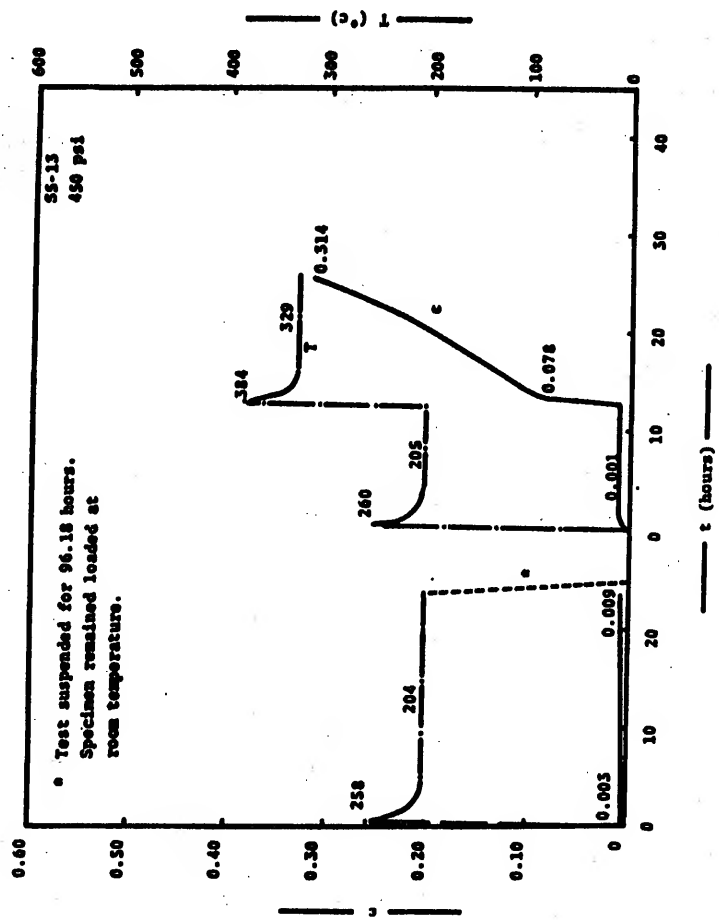

Figure 71. Strain, ε (solid line), and temperature, T (broken line), versus time, t, for specimen S5-13.

curve indicates the temperature change, and the lower curve indicates the change in strain. Also indicated in these graphs are the values of strain at various times during each creep test. The information sought from these experiments was qualitative in nature; therefore, no quantitative metallographic measurements were made. Visual observations of the microstructures and comparisons between the creep curves constitute the results of the experiments. In cases where a creep specimen ruptured, the lower half of the specimen was quenched in water. This portion of the specimen was used for metallographic evaluation. When the creep test was terminated prior to specimen rupture, the specimen was water quenched under load from the creep testing temperature, and a metallographic specimen was cut from the center of the gage length for evaluation of the microstructure.

The microstructure produced in specimen S5-5 by creep at 100°, 200° and 300°C under a stress of 1,000 psi was very much as expected. Most of the grains had very well developed subgrain rows and the grain boundaries exhibited large numbers of very dentate serrations. For the most part, the serrations were coincident with subgrain rows at sites where the rows intercepted the grain boundaries. At positions on the metallographic specimen near the fracture, the rows were more fully developed. The terminology "more fully developed" means that the contrast under polarized light among the rows was higher than when the subgrain rows were less well

developed. The high contrast under polarized light indicated that the boundaries between subgrain rows represented rather large crystallographic misorientations between adjacent rows. The subgrain rows alternated in shading, indicating the existence of alternating crystallographic orientation. In some grains, there appeared to be two superimposed sets of subgrain rows at right angles to one another. It was reasoned that this sort of subgrain morphology was the result of double bending and concurrent polygonization. The several microstructural features described above are shown in the photomicrographs of Figure 72 (a through c). All three photomicrographs show subgrain rows and serrated grain boundaries. Two superimposed sets of subgrain rows are shown most clearly in the photomicrograph of Figure 72(c). The photomicrograph of Figure 72(b) was taken at a position much closer to the fracture than were the photomicrographs in Figure 72 (a and c). Note the greater contrast in shading among the subgrain rows in Figure 72(b) as compared to the other two photomicrographs.

Specimen S5-6, tested under a stress of 500 psi according to a stepped temperature sequence much the same as that of specimen S5-5, did not proceed immediately to rupture upon increasing the temperature from 207°C to 316°C, as did specimen S5-5. Compare the creep curve of Figure 66 with that of Figure 65. Upon increasing the temperature, the transient response of the strain was superseded by a

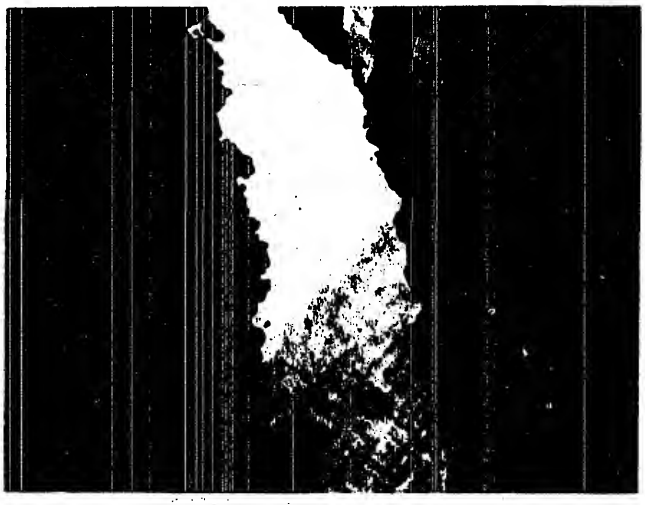

(a) 110X

Figure 72. Microstructure of specimen S5-5 illustrating subgrain rows and dentate grain boundary serrations.

(b) 60X

Figure 72. (continued)

(c) 50X

Figure 72. (continued)

secondary creep behavior. The test was terminated by quenching the specimen six hours following the temperature change from 207°C to 316°C.

The subgrain structure developed during creep at the lower stress was somewhat coarser than that observed after creep rupture of the specimen tested at the higher stress (S5-5). Subgrain rows were observed, but their boundaries were not as regular as those in the specimen tested at the higher stress. Grain boundary serrations were also present, but they were rather less dentate than in the former specimen. Since the specimen was not tested to rupture, it is reasonable to expect that the greater deformation of the former specimen might have played a significant role in the sharpening of subgrain rows and the development of dentate grain boundary serrations. The microstructure was inhomogeneous with respect to the subgrain morphology. Some areas displayed rather rough and ragged subgrain rows, while others exhibited the random subgrain morphology. Photomicrographs given in Figure 73 (a and b) show the general features of the microstructure of specimen S5-6. A subgrain structure with little evidence of subgrain rows or dentate grain boundary serrations is shown in the photomicrograph of Figure 73(a). The grain boundaries are wavy rather than dentate. In the upper center part of the field there is evidence of poorly defined subgrain rows. The photomicrograph of Figure 73(b) shows the rather rough subgrain rows

(a) 25X

Figure 73. Microstructure of specimen S5-6 illustrating wavy grain boundary serrations and the random morphology of subgrains.

(b) 25X

Figure 73. (continued)

that were observed in many areas of the specimen. Note that there is some alignment of subgrain rows in adjacent grains, but the boundaries are wavy rather than dentate.

By increasing the stress and cycling the temperature twice between nominal temperatures of 100°C and 200°C prior to increasing the temperature to above 300°C (specimen S5-7, Figure 67), the prominence of subgrain rows was greatly enhanced. The specimen ruptured shortly following the final temperature increase. Photomicrographs were taken in the region of the neck. Photomicrographs in Figure 74 (a and b) show the prominence of the subgrain rows formed during creep, dentate serrations in grain boundaries and the alternate shading of the subgrain rows.

In order to ascertain whether subgrain row formation would be enhanced or retarded by a very large grain size, specimen S5-9 was strain annealed (strained 1 percent at room temperature and annealed at 600°C for 53 hours) to produce very large grains. Most of the grains extended through the thickness of the specimen. The specimen was creep tested under a stress of 500 psi according to a stepped temperature sequence similar to that used in testing specimen S5-6. The creep strain and temperature curves are given in Figure 68. The creep test was terminated after 58 hours by water quenching the specimen under load. Metallographic examination after testing revealed that subgrain rows had formed in most of the grains and that the rows were very

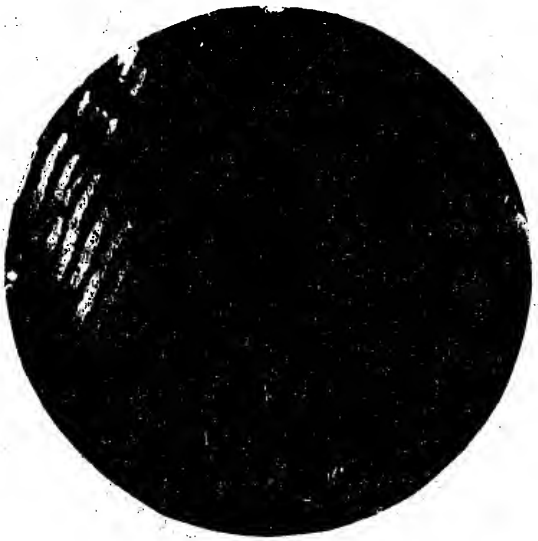

(a) 25X

Figure 74. Microstructure of specimen S5-7 illustrating subgrain rows and dentate grain boundary serrations. Note the alignment of subgrain rows across the grain boundaries.

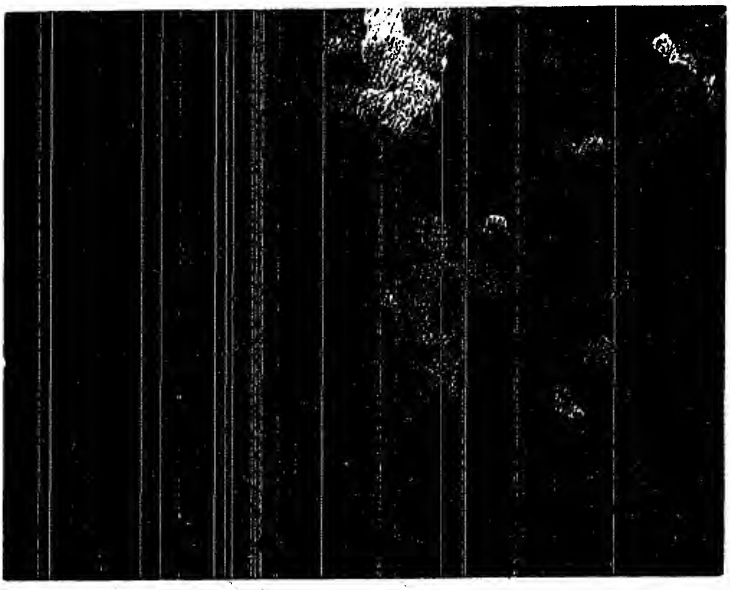

(b) 100X

Figure 74. (continued)

much more prominent than the rows formed in the finer-grained specimen, S5-6. Photomicrographs showing the subgrain rows are given in Figure 75 (a and b). In the photomicrograph of Figure 75(b), a grain boundary has been all but obliterated by subgrain rows and dentate serrations. Note the nearly perfect alignment of the subgrain rows across the grain boundary. Apparently, when grain boundaries are anchored by surface effects, subgrain row formation is enhanced. Compare the microstructures of Figure 75 with those of Figure 73.

The final three specimens (S5-11, S5-12 and S5-13) in this experiment are to be considered primarily in terms of their creep curves, Figures 69, 70 and 71. All three specimens were tested under a stress of 450 psi at nominal temperatures of 300°C (S5-11), 200°C (S5-12) and under a stepped temperature sequence of 200°C followed by 300°C (S5-13). The important feature to observe is that the creep rate for specimen S5-13 at 329°C (Figure 71) is very much greater than the creep rate of Specimen S5-11 (Figure 69). Specimen S5-13 had been tested for 36 hours at 205°C prior to raising the temperature. Admittedly the temperatures were somewhat different, but it is believed that the difference was not great enough to affect the very great increase in strain rate at the higher temperature, about 300°C. In the case of specimen S5-13, creep at the lower temperature was interrupted for 96 hours due to an equipment malfunction, but it

(a) 25X

Figure 75. Microstructure of specimen S5-9 illustrating subgrain rows and grain boundary serrations.

(b) 30X

Figure 75. (continued)

was believed that the interruption had no major effect on the outcome of the experiment. Metallographic examination of the microstructures showed that the specimen tested only at 300°C (S5-11) had developed some subgrain rows and wavy grain boundary serrations, whereas the specimen tested at 200°C (S5-12) showed no evidence of subgrains, subgrain rows or grain boundary serrations. Because specimen S5-12 had attained a strain of approximately the same magnitude as specimen S5-13 prior to the temperature change, it is presumed that their microstructures were equivalent. The microstructure of specimen S5-13,compared to that of specimen S5-11, showed that considerably more subgrain formation had taken place, probably because the strain attained during creep was greater. Photomicrographs showing the differences in the microstructures among specimens S5-11, S5-12 and S5-13 are given in Figures 76, 77 and 78, respectively.

The dentate grain boundary serrations shown in the photomicrographs of this section are some of the sharpest observed during the course of the research. In this regard see Figures 74 and 75.

The observations of the preliminary experiments may be summarized by the following statements.

1. When creep testing is performed by step-wise increasing the temperature during the course of the test, increasing the initial stress enhances the tendency to form subgrains and subgrain rows. This observation is consistent with those under conditions of constant temperature testing.

Figure 76. Microstructure of specimen S5-11 illustrating the subgrain structure and grain boundary serrations developed during 24 hours of creep at 300°C under an initial stress of 450 psi.

25X

Figure 77. Microstructure of specimen S5-12 showing that no observable subgrain structure was developed during 24 hours of creep at 200°C under an initial stress of 450 psi.

25X

Figure 78. Microstructure of specimen S5-13 illustrating the subgrain structure and grain boundary serrations developed in a stepped temperature creep test (200°C and 330°C) under an initial stress of 450 psi.

2. Very large grain sizes apparently enhance subgrain row formation during the course of high temperature creep subsequent to low temperature "precreep."*

3. Creep testing first at low temperatures, followed by testing at higher temperatures, accelerates the creep rates at higher temperatures.

4. If the initial stress is large enough, precreep testing at low temperatures results in the circumvention of secondary creep behavior during subsequent testing at higher temperatures.

3.8.2. Creep Experiments with Stepped Variations in Temperature and Stress

Of the several observations listed for the preliminary tests, the acceleration of creep rates during creep testing at a high temperature subsequent to low temperature precreep was thought to be the most significant. It was hoped that similar tests would produce useful information regarding the establishment of subgrain rows, their relationships to dentate grain boundary serrations and correlation of the microstructure to creep behavior. Therefore, a series of creep specimens were tested under more closely controlled conditions of temperature in order to monitor with quantitative metallographic measurements the microstructural evolution which occurs as the result of low temperature precreep treatments. Supplementary results were obtained from visual observations of microstructure and Laue x-ray diffraction photographs.

---

*The term "precreep" refers to all creep testing at the lower temperatures (100° and 200°C) that takes place prior to the final period of testing at the higher temperature (300°C).

Previous experience indicated that visible changes in the microstructure could not be produced by creep testing at 100°C. For this reason, tests were conducted using only nominal temperatures of 200° and 300°C. Initial stress levels were selected so that premature rupture of the specimens would not occur within ten hours of testing at temperatures in the range 300°C. This was done to ensure that the acceleration of creep rates following precreep at 200°C could be directly related to the effects of precreep. An initial stress of 417 psi was arrived at by trial and error testing of specimens at temperatures in the range of 300°C. All tests at the elevated temperature were performed at this stress level.

The creep testing conditions listed were chosen to facilitate the characterization of the microstructural evolution which occurred during the course of two creep experiments. The first creep experiment consisted of precreep at 210°C under a stress of 417 psi for 168 hours, followed by creep at 332°C under the same stress. Tracing of the microstructural evolution through the course of this experiment was accomplished by characterizing the microstructures of specimens S5-43, S5-45 and S5-40 using the techniques of quantitative metallography. The second experiment consisted of precreep at 212°C under a stress of 834 psi for 24 hours, followed by creep at 330°C under a stress of 417 psi. Metallographic characterization of the microstructures of specimens

S5-41, S5-42, S5-44 and S5-39 was used to trace the microstructural evolution which occurred during the course of the second experiment. The metallographic results obtained from these two experiments were compared with the results obtained from the control specimen, S5-38, and with those obtained from the microstructure of specimen S5-31. Specimen S5-38 received no precreep treatment prior to high temperature creep at 330°C, whereas specimen S5-31 received a short precreep treatment at 217°C under a stress of 417 psi for 24 hours prior to being tested at 338°C under the same stress for a period of ten hours.

Table XVI lists the specimens, their creep testing conditions and the values of the microstructural parameters computed from the quantitative metallographic measurements. As in the creep experiments under constant load and temperature, the parameters monitored were:

1. Grain boundary surface area, $S_{V(GB)}$.
2. Subgrain boundary surface areas, $S_{V(SGB)}$.
3. The change in grain boundary anisotropy, $e_g(f)-e_g(i)$.
4. The ratio of serrated grain boundary area to the grain boundary area, $\tilde{S}_V/S_{V(GB)}$.
5. The fraction of grains containing subgrains, f_{SG}.
6. The fraction of grains containing subgrain rows, f_{SGR}.
7. The fraction of grains containing only subgrains, $f_{SG}-f_{SGR}$.

Table XVI

Creep Testing Conditions, Strain Rates and Microstructural Parameters for Specimens Tested Under Conditions of Stepped Variations in Stress and Temperature

(a) Specimens and Creep Testing Conditions

	Specimen Number	Temperature (T_1) °C	Stress (σ_1) psi	Time (t_1) hours	Strain (ε_1) %	Temperature (T_2) °C	Stress (σ_2) psi	Time (t_2) hours	Strain (ε_2) %
	S5-38	--	--	--	--	330	417	10	16.00
	S5-31	217	417	24	1.44	338	417	10	16.60
	S5-43	210	417	168	2.35	--	--	--	--
I	S5-45	210	417	168	2.43	332	417	2	8.46
	S5-40	212	417	169	2.60	332	417	∿6	R*
	S5-41	214	834	24	5.87	--	--	--	--
II	S5-42	208	834	24	6.22	342**	417	1	7.19
	S5-44	211	834	24	5.06	312	417	2	9.40
	S5-39	212	834	24	4.70	330	417	∿5	R*

*R indicates that the specimen ruptured.

**Temperature did not reach equilibrium following temperature change before the test was terminated.

Table XVI (continued)

(b) Specimens and Creep Rates

Specimen Number	(Precreep) Low Temperature Strain Rate ($\dot{\varepsilon}_1$) (min^{-1})	High Temperature Strain Rate ($\dot{\varepsilon}_2$) (min^{-1})
S5-38	--	1.50×10^{-4}
S5-31	1.70×10^{-6}	2.00×10^{-4}
S5-43	1.36×10^{-6}	--
S5-45	1.37×10^{-6}	--
S5-40	1.29×10^{-6}	1.09×10^{-3}
S5-41	1.21×10^{-5}	--
S5-42	6.56×10^{-6}	--
S5-44	8.98×10^{-6}	--
S5-39	9.20×10^{-6}	8.84×10^{-4}

Table XVI (continued)

(c) Initial Values of Grain Boundary Area, $S_{V(GB)}(i)$ and Grain Boundary Anisotropy, $e_g(i)$

Specimen Number	$S_{V(GB)}(i)$ (mm^2/mm^3)	$e_g(i)$
S5-38	7.16±0.40	0.01+0.09-0.03
S5-31	7.00±0.40	0.01+0.09-0.13
S5-43	6.62±0.40	0.01+0.09-0.14
S5-45	6.72±0.36	0.00+0.08-0.12
S5-40	6.70±0.38	0.01+0.09-0.13
S5-41	6.62±0.38	0.02+0.08-0.14
S5-42	6.76±0.34	-0.04+0.11-0.10
S5-44	6.80±0.38	-0.06+0.13-0.09
S5-39	6.88±0.38	-0.12+0.16-0.05

Table XVI (continued)

(d) Specimens, Fractions of Grains Containing Subgrains, f_{SG}, Subgrain Rows, f_{SGR}, Subgrains of the Random Morphology, f_{SG}-f_{SGR}, and Fraction of Grains with Subgrain Rows Whose Angles Fall Between 35° and 55° with Respect to the Tensile Axis, $f_{SGR(35-55)}$

Specimen Number	f_{SG}	f_{SGR}	$f_{SG}-f_{SGR}$	$f_{SGR(35-55)}$
S5-38	0.82	0.07	0.75	0.72
S5-31	1.00	0.07	0.93	0.72
S5-43	0.02	0.00	0.02	0.00
S5-45	0.85	0.13	0.72	0.77
S5-40	0.97	0.24	0.73	0.79
S5-41	0.94	0.22	0.72	0.64
S5-42	0.91	0.18	0.73	0.78
S5-44	0.99	0.16	0.83	0.87
S5-39	1.00	0.29	0.71	0.80

Table XVI (continued)

(e) Specimens, Total Boundary Area, $S_{V(TOT)}$, Smooth Grain Boundary Area, $\bar{S}_V$, Serrated Grain Boundary Area, $\tilde{S}_V$, and Grain Boundary Area, $S_{V(GB)}$

Specimen Number	$S_{V(TOT)}$ mm^{-1}	$\bar{S}_V$ mm^{-1}	$\tilde{S}_V$ mm^{-1}	$S_{V(GB)}$ mm^{-1}
S5-38	11.88±0.84	2.44±0.50	1.46±0.30	3.88±0.52
S5-31	15.82±0.88	2.68±0.41	1.43±0.32	4.16±0.42
S5-43	5.22±0.48	5.14±0.46	0.18±0.12	5.32±0.46
S5-45	9.98±0.84	2.46±0.44	1.44±0.32	3.88±0.46
S5-40	22.64±0.88	0.66±0.30	3.02±0.48	3.76±0.54
S5-41	11.42±0.84	3.24±0.38	0.96±0.24	4.18±0.44
S5-42	11.40±0.68	3.98±0.44	0.56±0.20	4.46±0.44
S5-44	14.62±0.68	4.14±0.42	1.16±0.30	5.32±0.46
S5-39	28.36±0.94	1.68±0.48	3.62±0.54	5.24±0.62

Table XVI (continued)

(f) Specimens, Fraction of Serrated Grain Boundary Area, $\tilde{S}_V/S_{V(GB)}$, Subgrain Boundary Area, $S_{V(SGB)}$, and Change in Grain Boundary Anisotropy, $e_g(f)-e_g(i)$

Specimen Number	$\tilde{S}_V/S_{V(GB)}$	$S_{V(SGB)}$ mm^{-1}	$e_g(f)-e_g(i)$
S5-38	0.376+0.148-0.122	7.98±0.72	-0.09±0.18
S5-31	0.344+0.124-0.102	11.64±0.90	-0.13+0.10-0.02
S5-43	0.034+0.028-0.024	0.22±0.16	-0.04+0.08-0.01
S5-45	0.371+0.144-0.113	6.06±0.70	-0.05+0.08-0.02
S5-40	0.803+0.197-0.212	18.88±0.92	0.26±0.34
S5-41	0.230+0.091-0.074	7.18±0.76	0.06+0.13-0.11
S5-42	0.126+0.063-0.053	6.98±0.66	0.00+0.09-0.15
S5-44	0.218+0.082-0.069	9.30±0.80	0.01+0.02-0.05
S5-39	0.690+0.210-0.164	23.12±1.02	0.12+0.10-0.14

The effect of low temperature precreep upon secondary creep rates attained during subsequent creep testing at a higher temperature, and the details of the microstructural evolution which takes place during the two creep experiments are described in the several paragraphs which follow.

3.8.2.1. The effect of precreep upon the secondary creep rate at a higher temperature

The graphs in Figures 79 through 87 show the creep curves and the temperature versus time curves for each of the nine creep specimens tested in this portion of the research. Results from the preliminary tests indicated that one of the effects of low temperature precreep was the acceleration of secondary creep rates obtained when precreep was followed by creep at a higher temperature. The present experiments verify that the earlier observation was a real effect. Comparison among the creep curves given in Figures 79, 80, 83 and 87 and the strain rate data given in Table XVI(b) illustrate the effect of precreep upon accelerating the steady state strain rate during subsequent creep at a higher temperature. Precreep treatments of 168 hours at 210°C under a stress of 417 psi and 24 hours at 212°C under a stress of 834 psi had similar effects upon accelerating the steady state creep rate at the higher creep temperature. Compare strain rates for specimens S5-40 and S5-39 with the strain rate for specimen S5-38 in Table XVI(b). Precreep at 217°C under a stress of 417 psi for the shorter time of 24

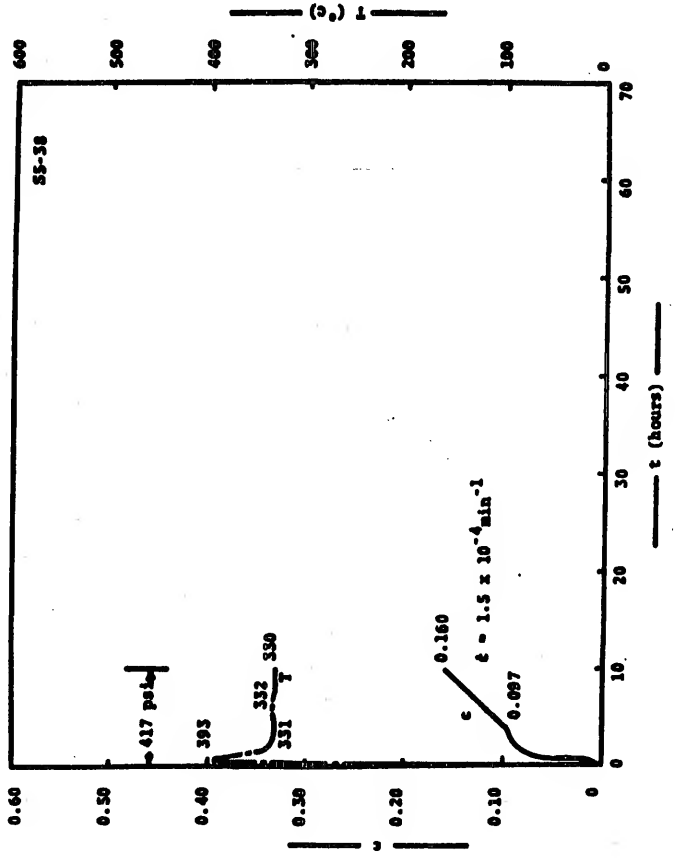

Figure 79. Strain, ε (solid line), and temperature, T (broken line), versus time, t, for specimen S5-38.

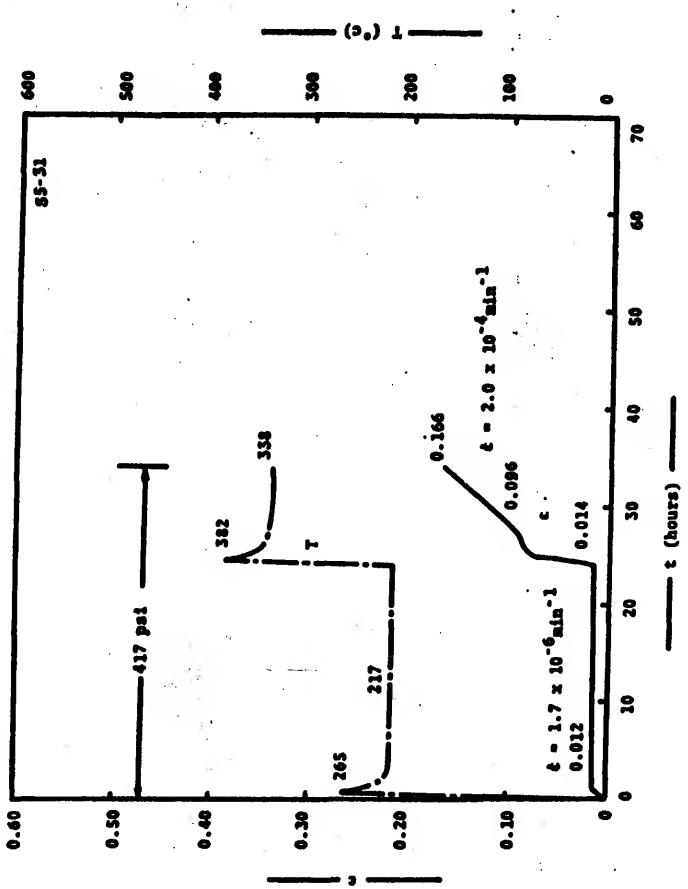

Figure 80. Strain, ε (solid line), and temperature, T (broken line), versus time, t, for specimen S5-31.

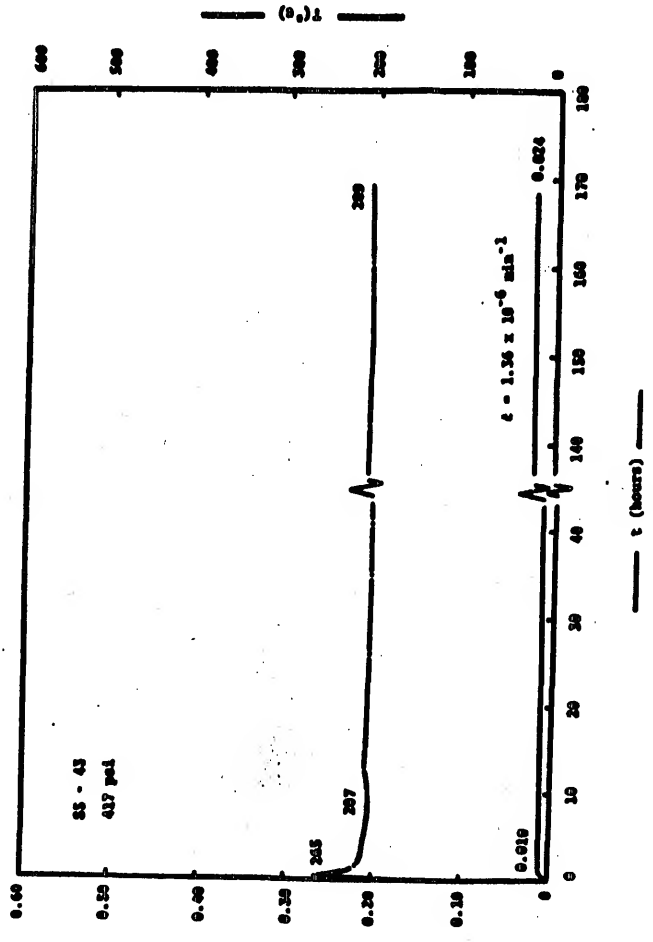

Figure 81. Strain, ε (solid line), and temperature, T (broken line), versus time, t, for specimen S5-43.

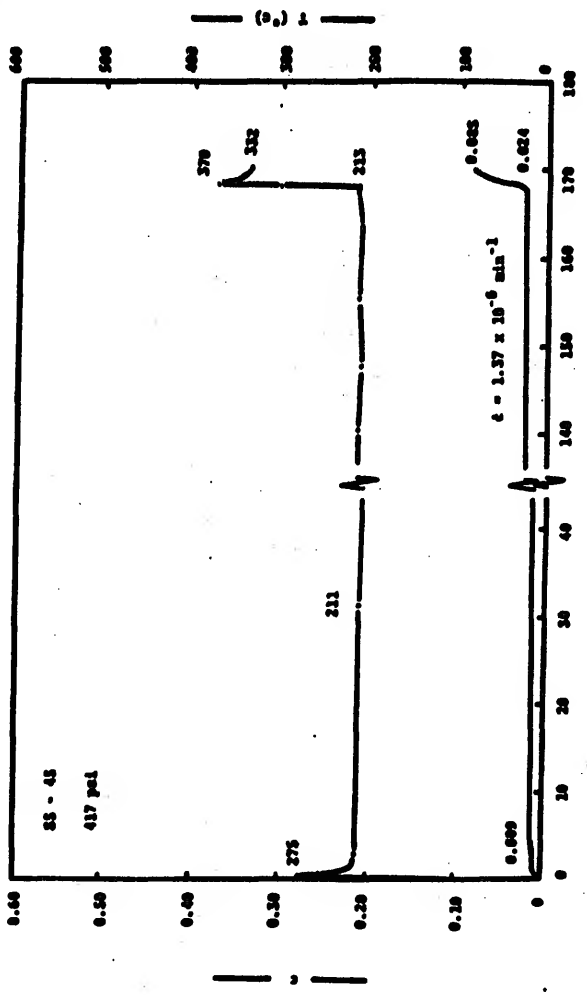

Figure 82. Strain, ε (solid line), and temperature, T (broken line), versus time, t, for specimen S5-45.

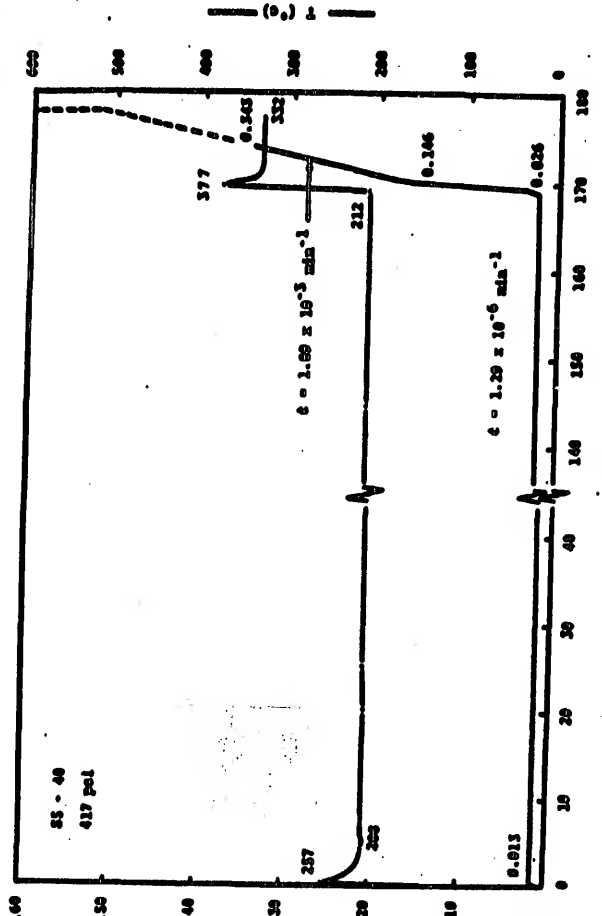

Figure 83. Strain, ε (solid line), and temperature, T (broken line), versus time, t, for specimen S5-40.

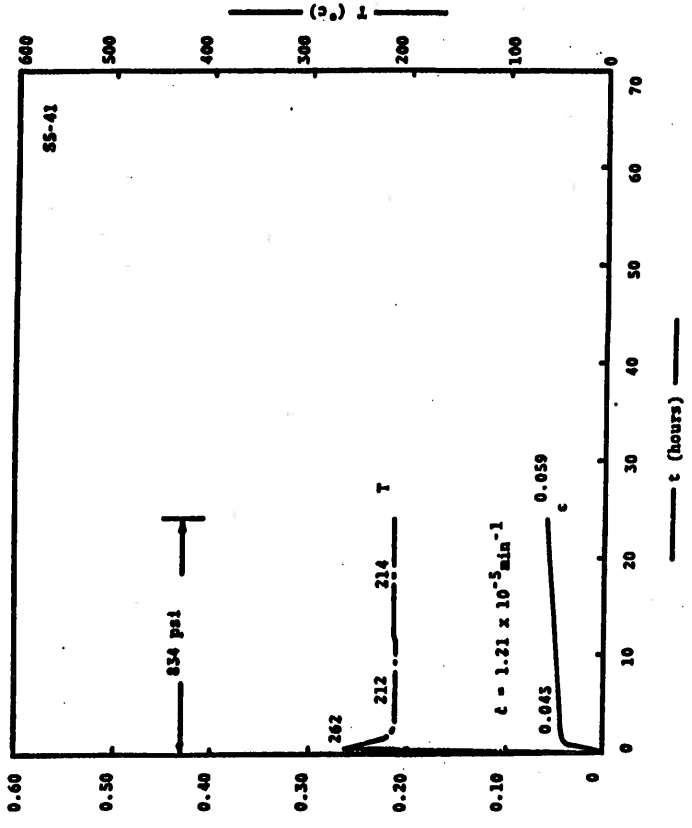

Figure 84. Strain, ε (solid line), and temperature, T (broken line), versus time, t, for specimen S5-41.

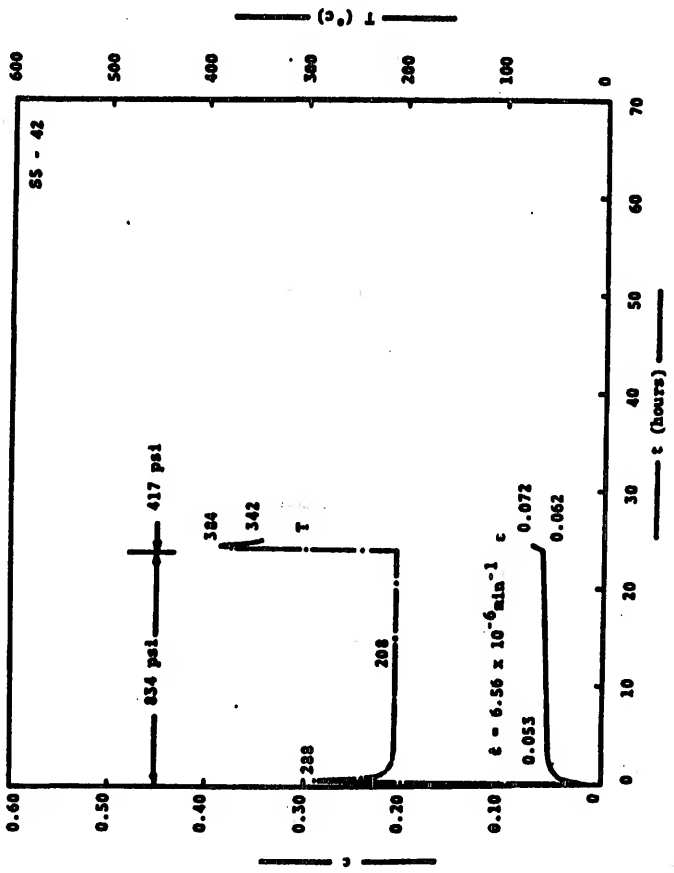

Figure 85. Strain, ε (solid line), and temperature, T (broken line), versus time, t, for specimen S5-42.

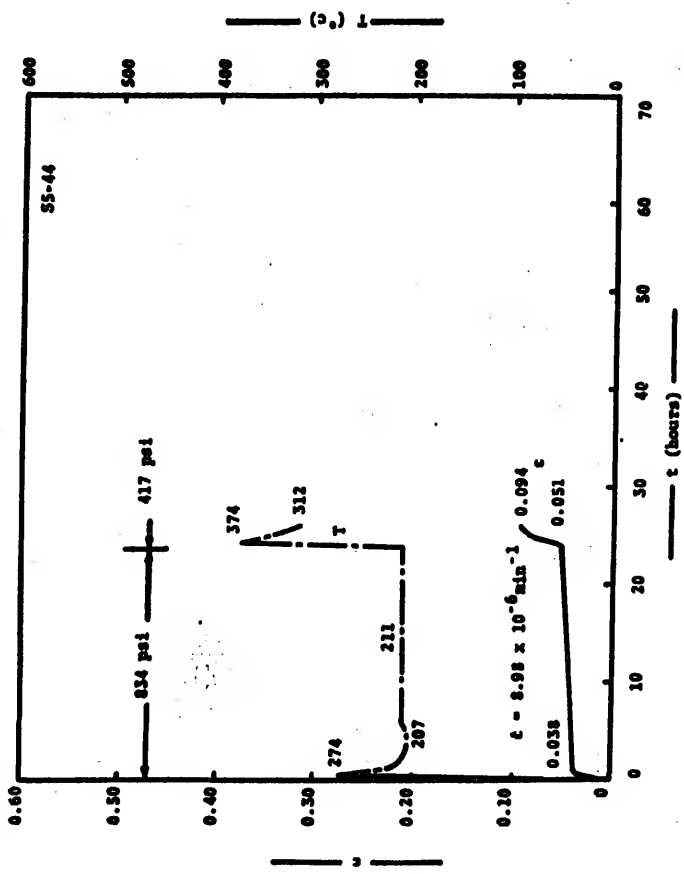

Figure 86. Strain, ε (solid line), and temperature, T (broken line), versus time, t, for specimen S5-44.

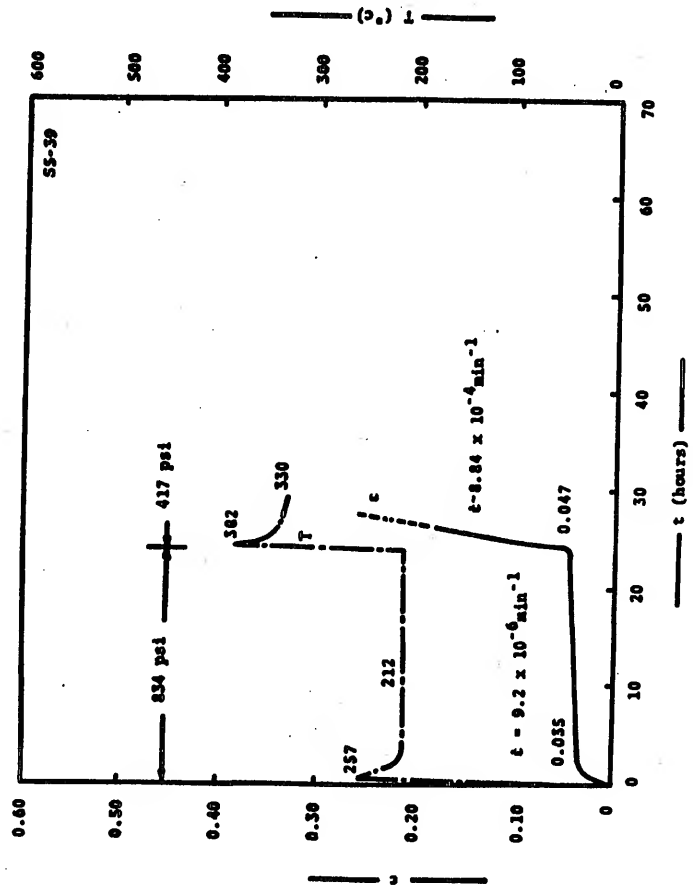

Figure 87. Strain, ε (solid line), and temperature, T (broken line), versus time, t, for specimen S5-39.

hours had practically no effect upon accelerating the steady state creep rate at the higher temperature, 338°C. Compare the strain rates given in Table XVI(b) for specimens S5-31 and S5-38. Under low stresses it apparently requires a considerable amount of time in precreep to greatly increase the secondary creep rate at the higher temperature.

3.8.2.2. Grain boundary area, $S_{V(GB)}$, versus time

Grain boundary area, $S_{V(GB)}$, versus time graphs are given in Figure 88 (a and b) for the first and second creep experiments, respectively. Both graphs show the expected decrease in grain boundary area during the precreep portion of the experiment. The portion of the curves connecting the initial values of grain boundary area with the values at the end of precreep are dashed, because no measurements were made during the course of precreep. The decrease in grain boundary area during precreep is to be associated with grain growth. It is to be noted that the grain growth during precreep in the first experiment, Figure 88(a), is rather smaller than that encountered in previous creep tests under constant load. The magnitude of the decrease in grain boundary area in the precreep portion of the second experiment, Figure 88(b), coincides with the observations from previous creep tests. Upon increasing the temperature following the precreep portion of the experiments, the grain boundary area decreases significantly in the first experiment,

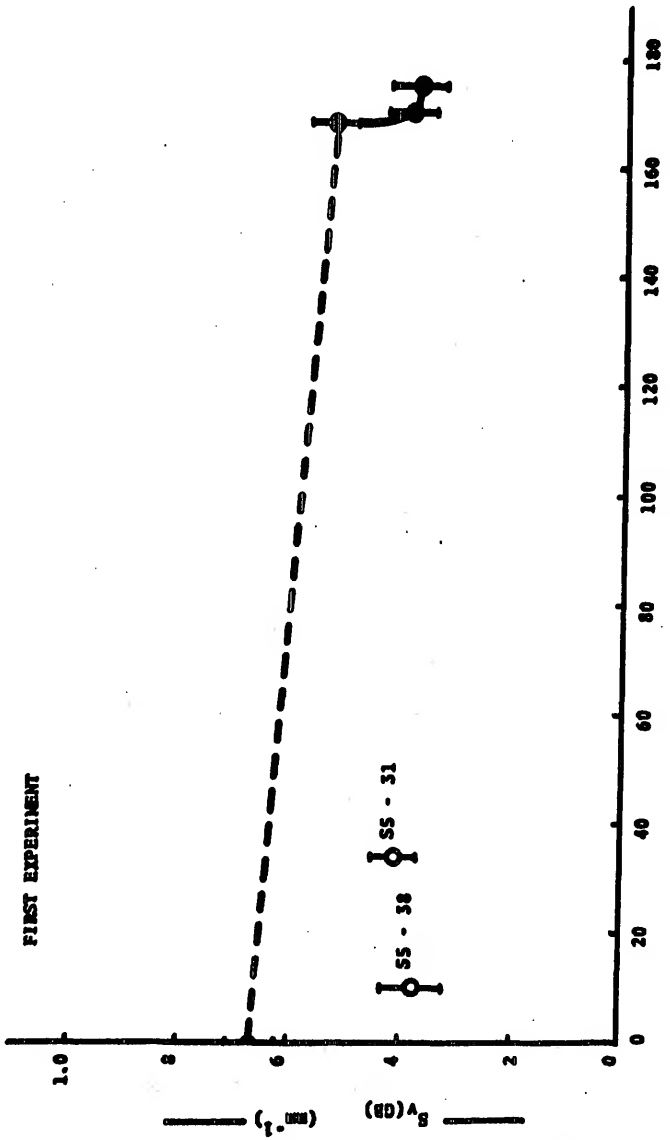

Figure 88. Grain boundary area, $S_{V(GB)}$, versus time, t.
(a) Specimens of the first experiment.

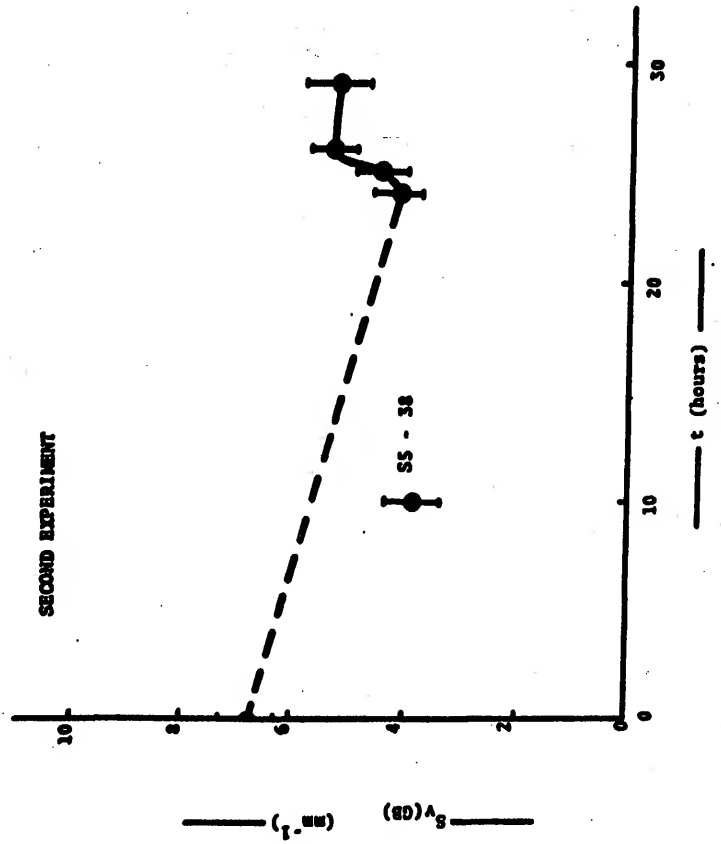

Figure 88. (continued)

(b) Specimens of the second experiment.

indicating grain growth (Figure 88(a)), while in the second experiment (Figure 88(b)), it increases. When the tolerances on the plotted points are considered the increase in the second experiment is, for practical purposes, insignificant. An increase in grain boundary area may arise from the formation of new grains or from the formation of grain boundary serrations. It is entirely possible that some subgrain boundaries may have been interpreted as grain boundaries and/or grain boundary serrations may have contributed to the increase in grain boundary area. The microstructure of specimen S5-39 displayed heavily serrated grain boundaries and well-outlined subgrains, while the microstructure of specimen S5-44 showed well-outlined subgrains and few dentate grain boundary serrations.

The grain boundary area attained at the end of the first experiment, Figure 88(a), has a value very close to that attained by the control specimen, S5-38, and by specimen S5-31. The conclusion is that precreep at 210°C under a stress of 417 psi for 168 hours or at 217°C under a stress of 417 psi for 24 hours has little effect upon the grain boundary area ultimately attained during creep at the higher temperature.

As described previously, the grain boundary area increases during the final portion of the second experiment, Figure 88(b). The result is that the grain boundary area attained at the end of the second experiment is significantly

larger than that attained by the control specimen, S5-38. It is apparent that the precreep at 211°C under a stress of 834 psi for 24 hours has an effect upon the ultimate grain boundary area attained during creep at the higher temperature. It is believed that the increase in the grain boundary area subsequent to the temperature change results from the formation of new grains by partial recrystallization. If the amount of deformation is great enough during precreep, it would be reasonable to expect the occurrence of partial recrystallization when the stress is reduced and the temperature increased.

3.8.2.3. Subgrain boundary area, $S_{V(SGB)}$, versus time

Subgrain boundary area, $S_{V(SGB)}$, plotted versus time for the first and second experiments are given in the graphs of Figure 89 (a and b), respectively. In both creep experiments, the formation of subgrain boundary during precreep occurs at a much slower rate than during subsequent creep at the higher temperature. The average rates of formation of subgrain boundary area, $S_{V(SGB)}$, are given in Figure 89 (a and b). Subgrain boundary forms at a much slower rate during the low-stress precreep (first experiment, Figure 89(a)) than during the high-stress precreep (second experiment, Figure 89(b)). Neither the amount of subgrain boundary formed nor the rate at which it forms during precreep has a large effect upon the rates of subgrain formation during creep at the higher temperatures. Compare the

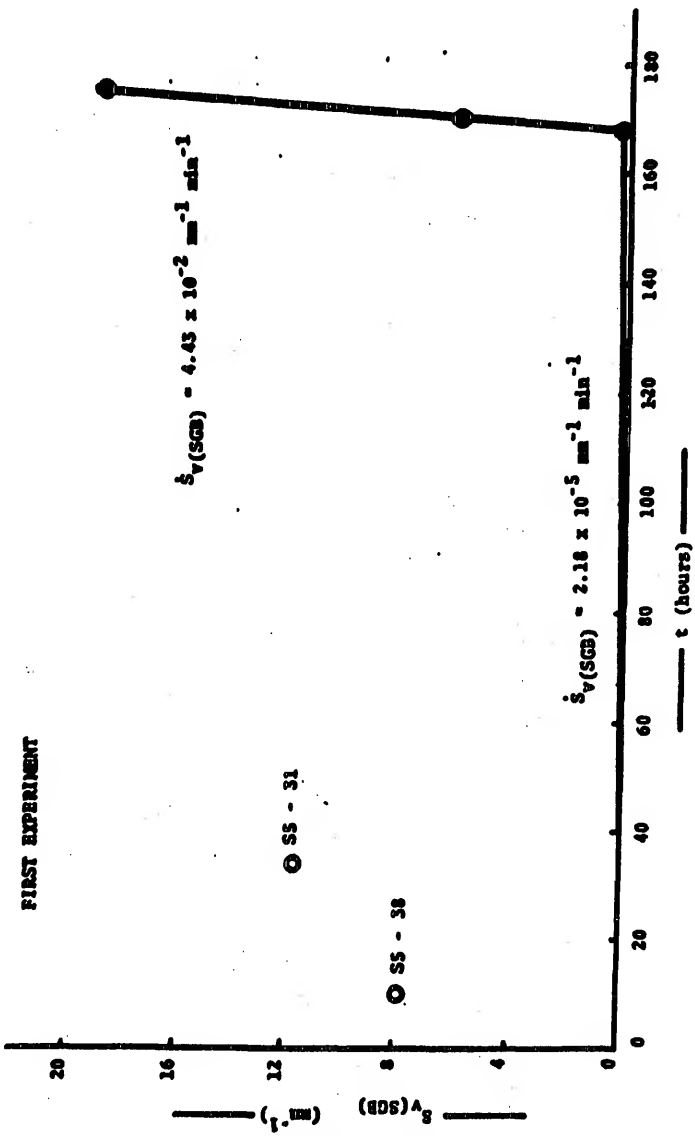

Figure 89. Subgrain boundary area, $S_{V(SGB)}$, versus time, t.
(a) Specimens of the first experiment.

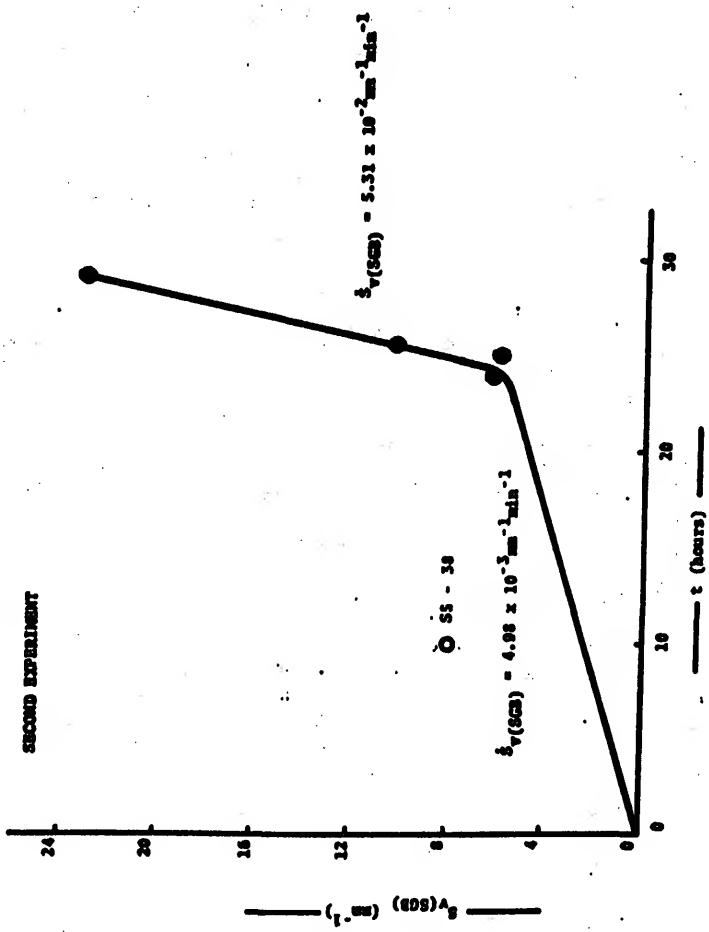

Figure 89. (continued)

(b) Specimens of the second experiment.

average rates of subgrain boundary area shown in the graphs of Figure 89 (a and b).

By comparing the amount of subgrain boundary area formed during high temperature creep following precreep with the amount formed in the control specimen, S5-38, it is obvious that low temperature precreep treatments greatly enhance the formation of subgrain boundary. In both experiments the amount of subgrain boundary area formed during the high temperature creep is greater than twice the amount of subgrain boundary area formed in the control specimen, S5-38. The conclusion to be drawn here is that low temperature precreep treatments enhance the rate of polygonization, and the observed faster strain rates at the high temperature may be a direct consequence of this more rapid polygonization.

3.8.2.4. Fraction of grains containing subgrains, f_{SG}, versus time

The fraction of grains containing subgrains, f_{SG}, plotted versus time are shown for the first and second experiments in the graphs of Figure 90 (a and b), respectively. In the first experiment, Figure 90(a), the fraction of the grains which contain subgrains at the end of precreep is small. Upon increasing the temperature, this fraction rapidly increases until nearly all of the grains contain subgrains. The fraction of grains containing subgrains plotted versus time for the second experiment, Figure 90(b),

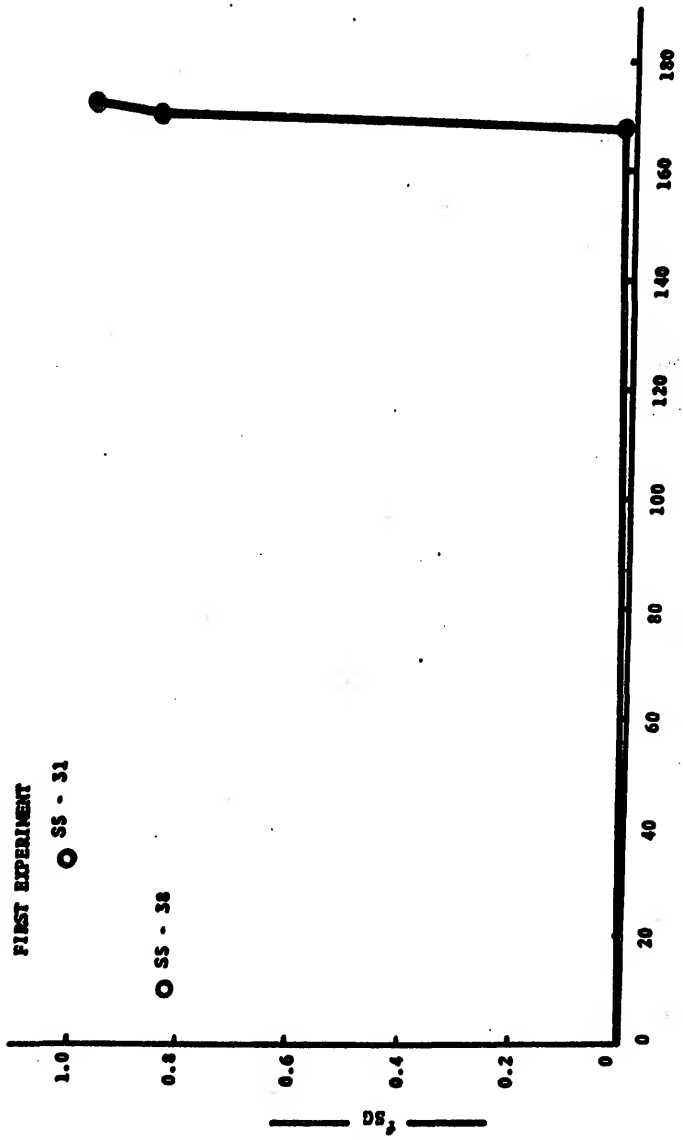

Figure 90. Fraction of grains containing subgrains, f_{SG}, versus time, t.
(a) Specimens of the first experiment.

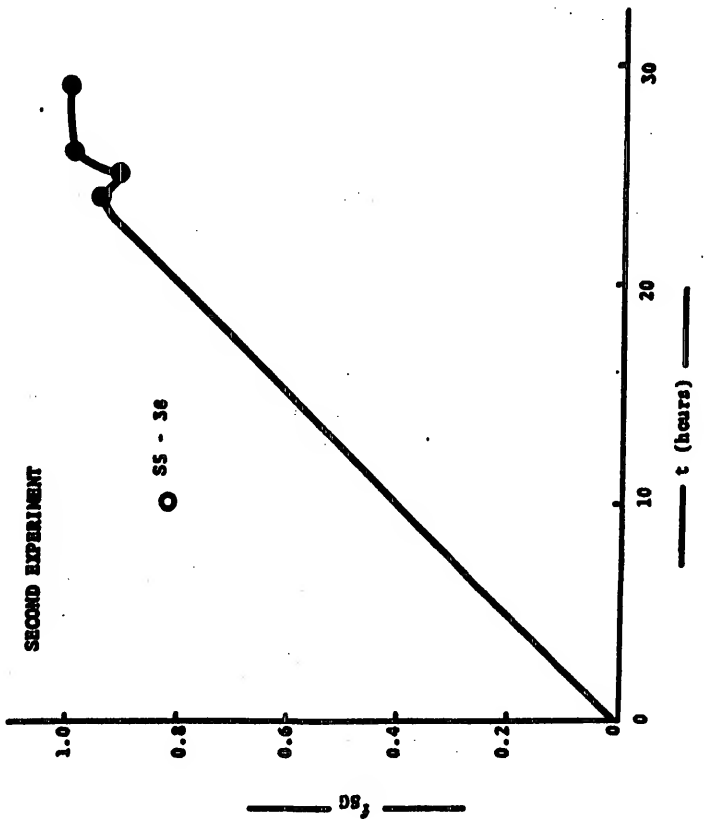

Figure 90. (continued)

(b) Specimens of the second experiment.

exhibits a rather different behavior. During the precreep treatment, subgrains form in almost all of the grains; and, upon increasing the temperature, the fraction of grains containing subgrains decreases slightly then again increases until all of the grains contain subgrains. Further comment on this behavior is reserved the for next section dealing with the fraction of grains containing subgrain rows.

An important observation is made when the fraction of grains containing subgrains developed in the two creep experiments is compared to the fraction in the control specimen, S5-38. It can be seen from Figure 90 (a and b) that most of the grains in the control specimen contain subgrains. Precreep at low temperatures seems to have only a small effect upon the fraction of grains which ultimately contain subgrains. Yet, in the preceding section, it was discovered that precreep enhances the formation of subgrain boundary. These observations indicate that precreep treatments possibly result in a finer subgrain size. Visual observations of the microstructure substantiate this conclusion. Photomicrographs in Figure 91 (a, b and c) of the microstructures of specimens S5-38, S5-40 and S5-39, respectively, show that specimens which have undergone low temperature precreep have smaller subgrains than the control specimen. Compare the photomicrographs of Figure 91 (b and c) with that of Figure 91(a). The smaller subgrain size is no doubt related to the faster rates of polygonization at the higher temperature which are enhanced by low temperature precreep.

(a) S5-38 (control specimen) 25X

Figure 91. Microstructures illustrating the effects of precreep upon subgrain structure.

(a) Specimen S5-38, creep tested at 330°C under an initial stress of 417 psi for 10 hours.

(b) S5-40 25X

Figure 91. (continued)

(b) Specimen S5-40, creep tested at 330°C under an initial stress of 417 psi for 6 hours subsequent to precreep at 212°C for 169 hours under the same stress.

(c) S5-39 30X

Figure 91. (continued)

(c) Specimen S5-39, creep tested at 330°C under an initial stress of 417 psi for 5 hours subsequent to precreep at 212°C under a stress of 834 psi for 24 hours.

3.8.2.5. Fraction of grains containing subgrain rows, f_{SGR}, versus time

The fraction of grains containing subgrain rows plotted versus time is shown in the graphs of Figure 92 (a and b) for the two creep experiments. In the first creep experiment, Figure 92(a), no grains contain subgrain rows at the end of the precreep treatment; but upon increasing the temperature the fraction of grains containing subgrain rows increases markedly. It appears that the low temperature precreep enhances the formation of subgrain rows. Compare the curve of f_{SGR} versus time for the first experiment with the fraction of grains containing subgrain rows for the control specimen, Figure 92(a).

In the case of the second creep experiment, Figure 92(b), the fraction of grains containing subgrain rows is greater at the termination of precreep than in the control specimen. The conclusion to be drawn from this observation is that creep at 211°C under a stress of 834 psi for 24 hours results in more subgrain row formation than does creep at 330°C under a stress of 417 psi for 10 hours. Upon increasing the temperature following precreep, the fraction of grains containing subgrain rows decreases then increases with further creep at the higher temperature. A similar behavior was shown in Figure 90(b) for the fraction of grains containing subgrains plotted versus time. Because the values of the fraction of grains containing subgrains, f_{SG}, include the values of the fraction of grains containing subgrain rows, the difference

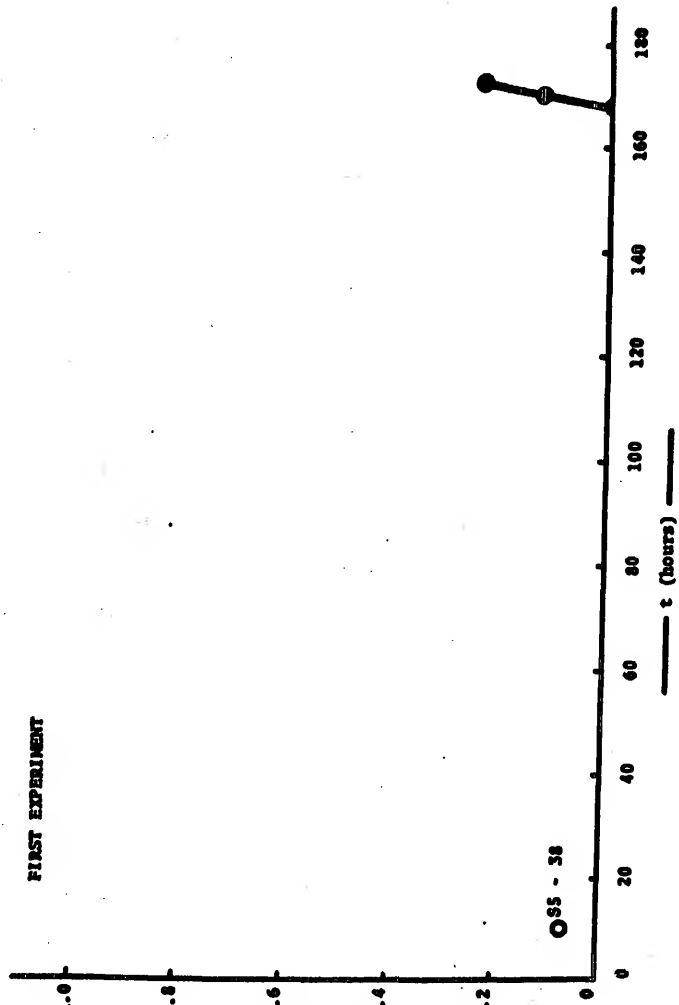

Figure 92(a). Fraction of grains containing subgrain rows, f_{SGR}, versus time, t, for specimens of the first experiment.

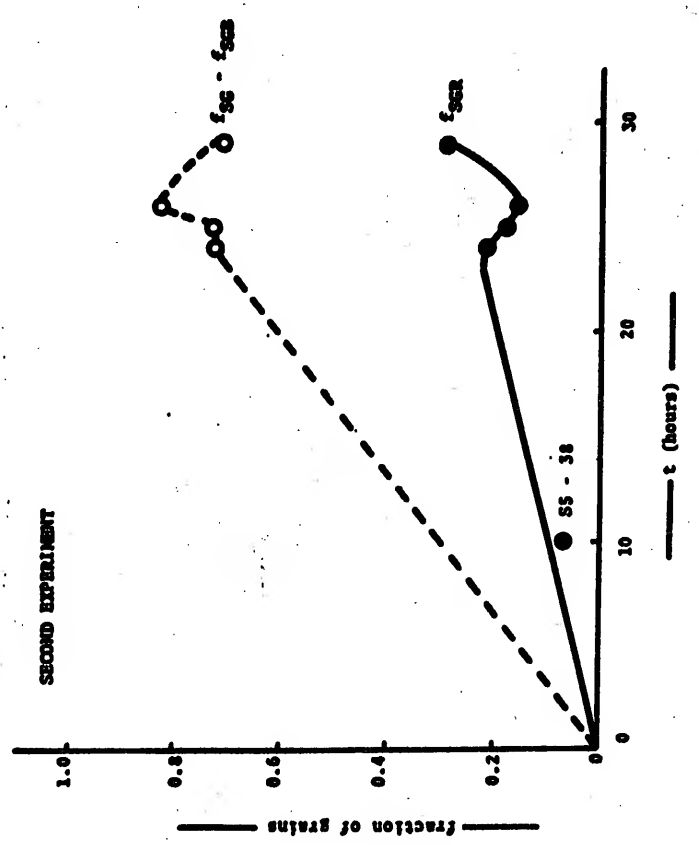

Figure 92(b). Fractions of grains containing subgrain rows, f_{SGR}, and the random morphology of subgrains, f_{SG}-f_{SGR}, versus time, t, for specimens of the second experiment.

between the values, f_{SG}-f_{SGR}, was plotted versus time. This curve is shown also in Figure 92(b) and is represented by the open circles and dashed line. The curve represents the fraction of grains containing subgrains of the random morphology. The decrease in the f_{SG} curve and increase in f_{SG}-f_{SGR} curves represent a "trade off" between subgrain rows and subgrains. Initially, as the temperature increases the subgrain row morphology gives way to the random form of subgrains. With further creep at the higher temperature, the increase in f_{SGR} and a decrease in (f_{SG}-f_{SGR}) represents a "reverse trade off" of the random subgrain morphology for that of subgrain rows.

The above-described behavior of the subgrain morphology upon increasing the temperature and decreasing the stress subsequent to low temperature precreep, is thought to be the result of partial recrystallization as described in section 3.8.2.2. It seems reasonable that the most "imperfect" grains, those containing subgrain rows, might be preferentially recrystallized. Following such an event it might require a considerable amount of deformation to reform subgrain rows.

In all of the measurements of fractions of grains, the measurements were made in an un-necked portion of the gage length; therefore, these measurements do not give any information regarding the subgrain morphology in the necked portions of the specimen.

3.8.2.6. Some correlations between grain boundary serrations, subgrains and subgrain rows

The ratio of the grain boundary area which is serrated to grain boundary area which is both smooth and serrated, $\tilde{S}_v/S_{v(GB)}$, has been used previously as a measure of the degree to which grain boundaries have become serrated during during the course of hot deformation. The graphs of this ratio plotted versus time are given in Figure 93 (a and b) for the first and second creep experiments, respectively. During the precreep portion of the first experiment, Figure 93(a), the ratio $\tilde{S}_v/S_{v(GB)}$ increased only slightly; however, upon increasing the temperature and during creep at the higher temperature, the ratio increased markedly. The value of the ratio which is ultimately attained is much larger than that attained by the control specimen, S5-38, or for specimen S5-31. It would appear that the long (168 hours) precreep treatment enhances the formation of grain boundary serrations during subsequent high temperature creep. The short precreep treatment (24 hours), specimen S5-31, apparently has no effect upon enhancing the formation of grain boundary serrations. In the second experiment, Figure 93(b), grain boundary serrations are rather more readily formed during the precreep treatment than in the case of the first experiment. Again, as the temperature is increased and during further creep at the high temperature, the ratio $\tilde{S}_v/S_{v(GB)}$ increased rapidly with time. The rates at which

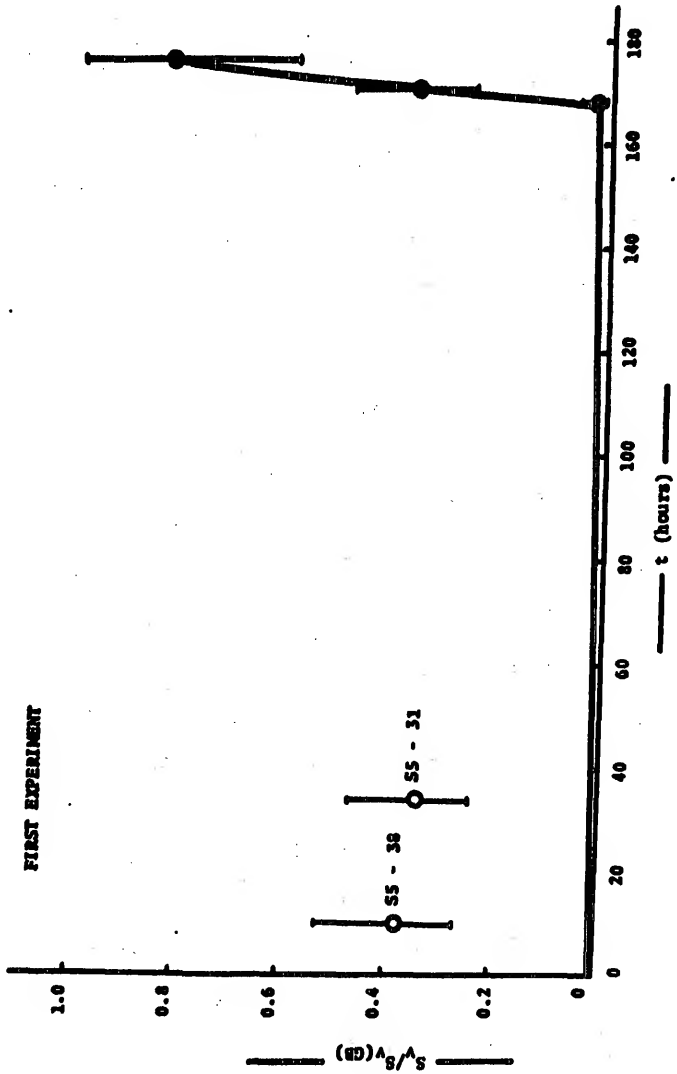

Figure 93. Fraction of the grain boundary area which is serrated, $\tilde{S}_V/S_{V(GB)}$, versus time, t.

(a) Specimens of the first experiment.

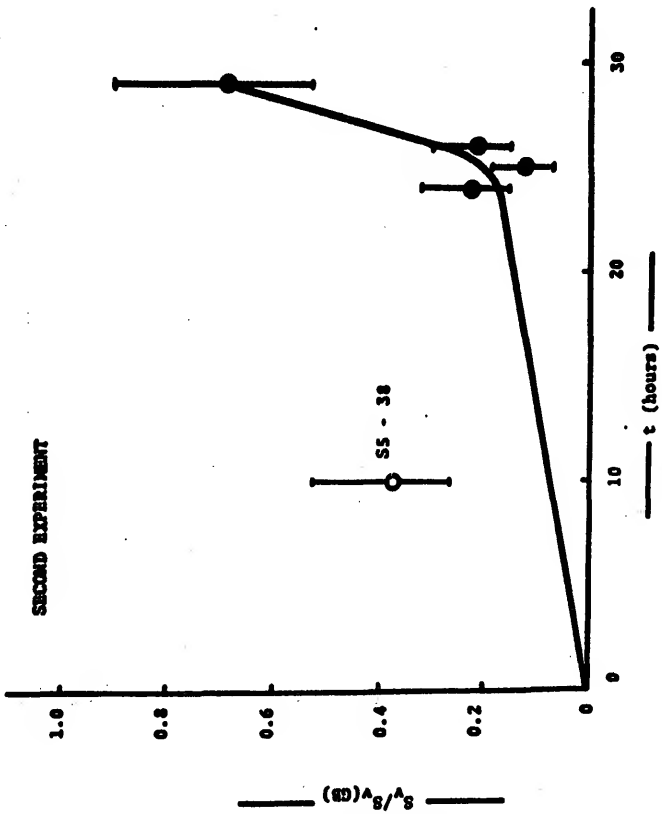

Figure 93. (continued)

(b) Specimens of the second experiment.

the ratio increases are about the same for the two experiments. As in the first experiment, the precreep treatment enhances the formation of grain boundary serrations.

The degree to which a precreep treatment enhances the formation of grain boundary serrations appears to be strongly sensitive to the stress level of the precreep treatment. For example, a 24-hour precreep treatment at 217°C under a stress of 417 psi has no effect upon enhancing the formation of grain boundary serrations; while a similar precreep treatment, but under a stress of 834 psi, has a very great influence upon enhancing the formation of grain boundary serrations during subsequent creep at the higher temperature. In this regard, the effect of the precreep for 24 hours at the higher stress (834 psi) is nearly equivalent to a precreep treatment at the lower stress (417 psi) of 168 hours in enhancing the formation of serrations.

In order to more completely describe the correlations between grain boundary serrations, subgrains and subgrain rows, the ratio $\tilde{S}_v/S_{v(GB)}$ plotted against the fraction of grains containing subgrains, f_{SG}, and the fraction of grains containing subgrains alone, f_{SG}-f_{SGR}, are given for consideration in Figure 94 (a and b). In Figure 94(a), it can be seen that, during the precreep portion of the first experiment, few boundaries became serrated. With the increase in temperature and further creep at the higher temperature, increases in grain boundary serrations were primarily

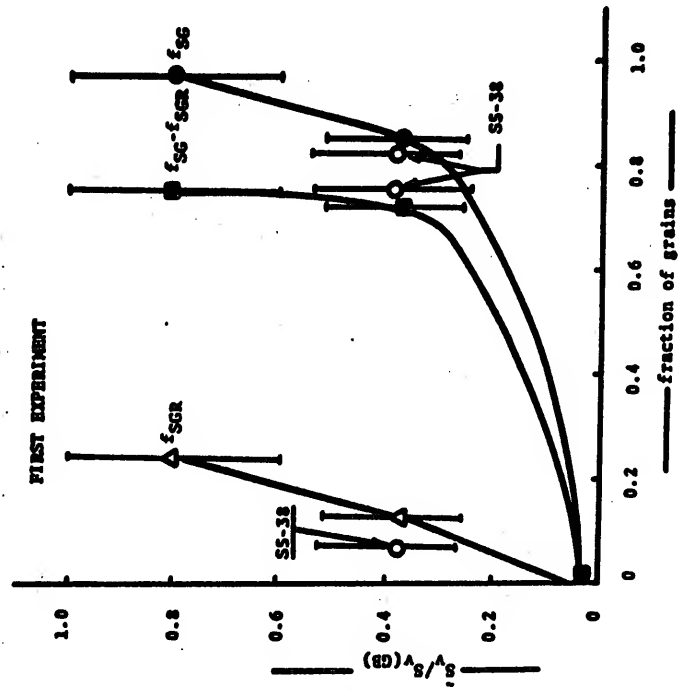

Figure 94. Fraction of the grain boundary area which is serrated, $\tilde{S}_V/S_V(GB)$, versus fractions of grains containing subgrains, f_{SG}, subgrain rows, f_{SGR}, and the random morphology of subgrains, $f_{SG}-f_{SGR}$.

(a) Specimens of the first experiment.

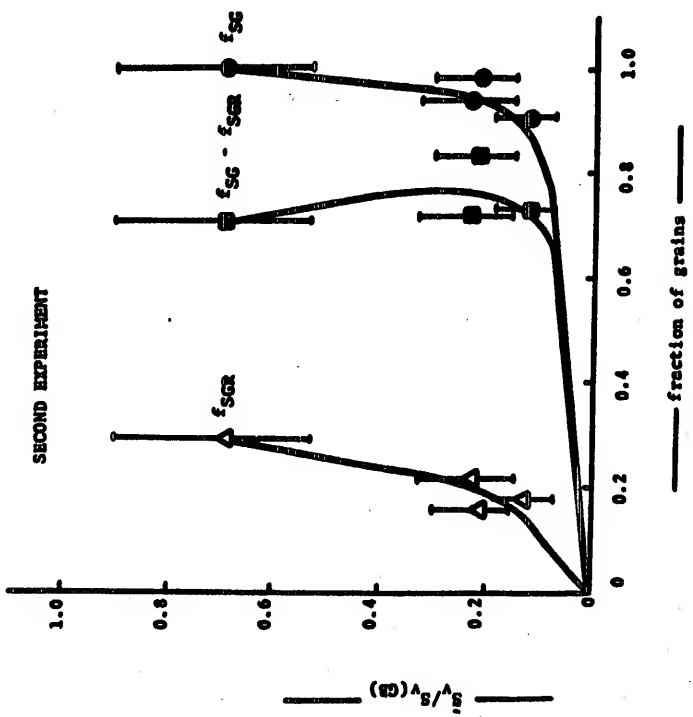

Figure 94. (continued)

(b) Specimens of the second experiment.

correlated to the random morphology of subgrains. Evidence for this can be seen by the fact that the curve for $\tilde{S}_v/S_{v(GB)}$ versus f_{SG}-f_{SGR} lies to the right of the curve for $\tilde{S}_v/S_{v(GB)}$ versus f_{SGR}. The correlation between grain boundary serrations and subgrain rows increases during creep at the higher temperature. Beyond the second points on the graph, those for specimen S5-45, the value of f_{SG}-f_{SGR} increases very little in comparison to the value of f_{SGR}. Grain boundary serrations tend to continue forming with the trade-off of the random subgrain morphology for the subgrain row morphology. This observation is more striking in the second experiment, Figure 94(b). During the course of the temperature increase, grain boundary serrations are more strongly related to the usual form of subgrains, but with further creep at the higher temperature the trend is reversed. The curve representing the usual morphology of subgrains swings back to the left, while the curve representing subgrain rows continues to increase to the right as the ratio $\tilde{S}_v/S_{v(GB)}$ increases. Similar correlations have been made between grain boundary serrations, subgrains and subgrain rows based upon the results of creep tests under constant stress and temperature. Although the correlations described above do not distinguish between wavy and dentate forms of grain boundary serrations, they do seem rather tenable in light of several other previously described qualitative observations. These observations relate dentate serrations to subgrain rows. Subgrain

rows predominate under conditions of high stress, lower creep temperatures and the onset of tertiary creep. Dentate grain boundary serrations likewise appear to predominate under conditions of high stress, lower temperatures and the onset of tertiary creep.

3.8.2.7. The orientation of subgrain rows

In the presentation of the results obtained from creep tests under conditions of constant load and constant temperature, it was pointed out that a majority of the subgrain rows were oriented with their long axes at an angle of approximately 45° to the tensile axis. Histograms were given to show the distribution of the orientations of subgrain rows with respect to the tensile axis. In a similar manner the subgrain row orientation histograms are given in Figure 95 (a through j) for each of the nine creep specimens of this investigation. Again, the indications are that, in most of the grains which contain subgrain rows, the row orientations tend to cluster about an angle of 45° with respect to the tensile axis.

3.8.2.8. The change in grain boundary anisotropy, $e_g(f)-e_g(i)$, versus time

The change in grain boundary anisotropy plotted as a function of time is given in the graphs of Figure 96 (a and b) for the first and second creep experiments, respectively. Within the statistical tolerances, the change in grain boundary anisotropy with time is insignificant for both

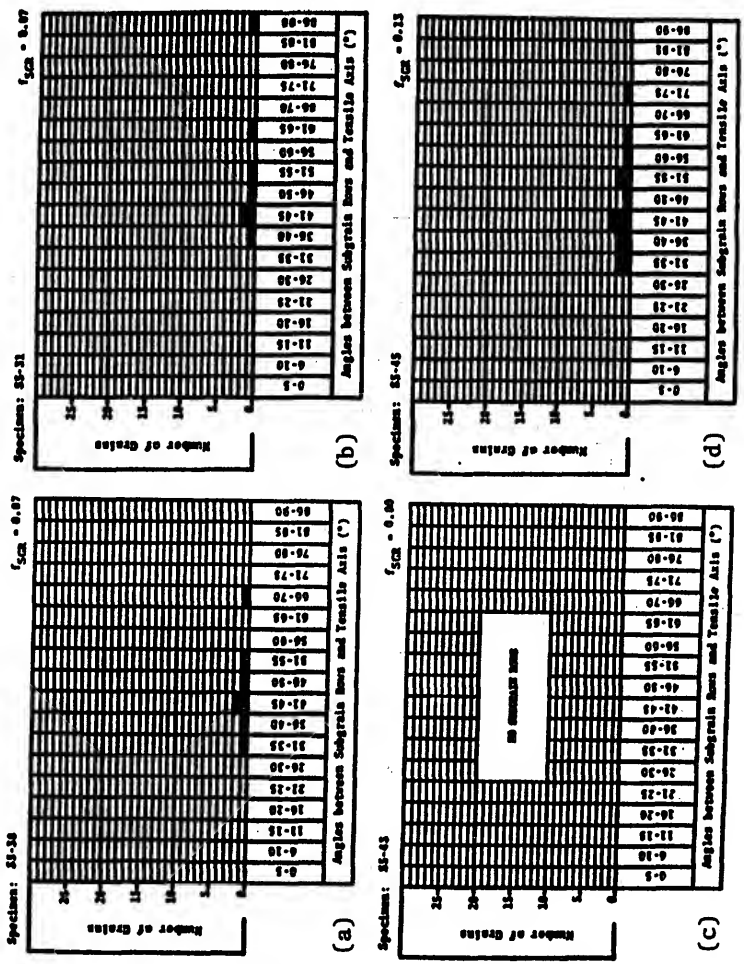

Figure 95. Histograms showing the distribution of angles between subgrain rows and the tensile axis.

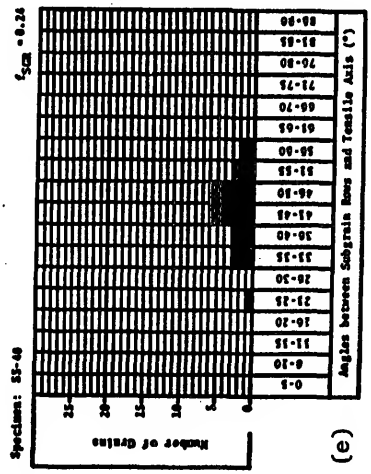

(e)

Figure 95. (continued)

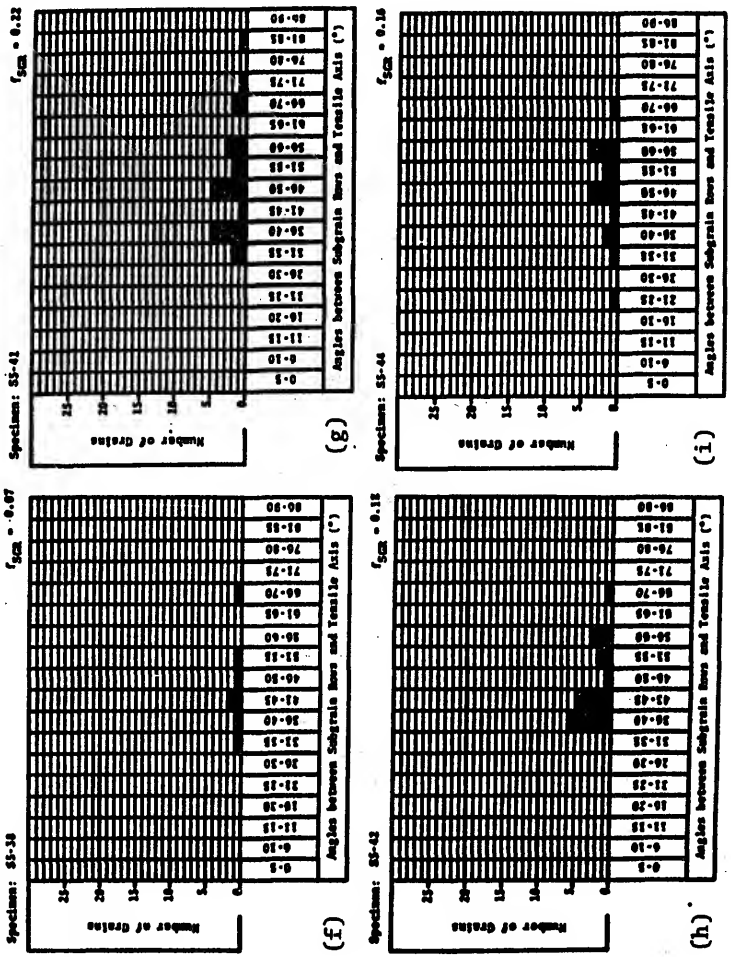

Figure 95. (continued)

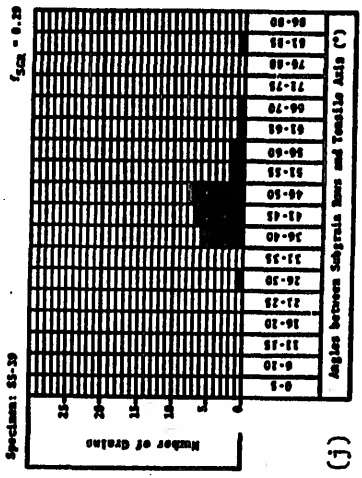

(j)

Figure 95. (continued)

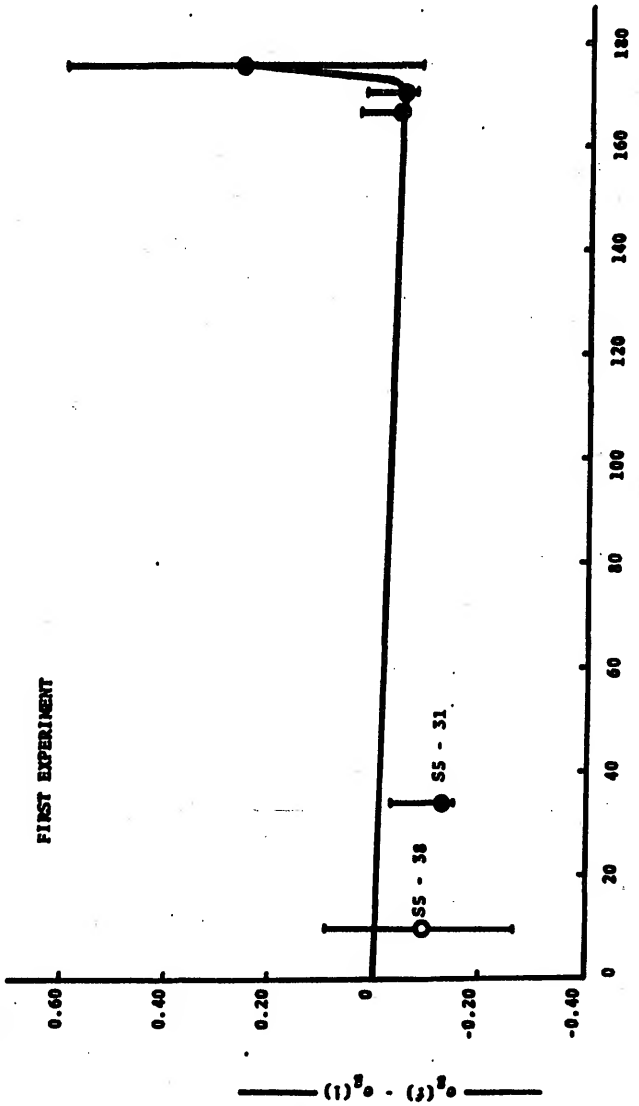

Figure 96. Change in grain boundary anisotropy, $e_g(f)-e_g(i)$, versus time, t.
(a) Specimens of the first experiment.

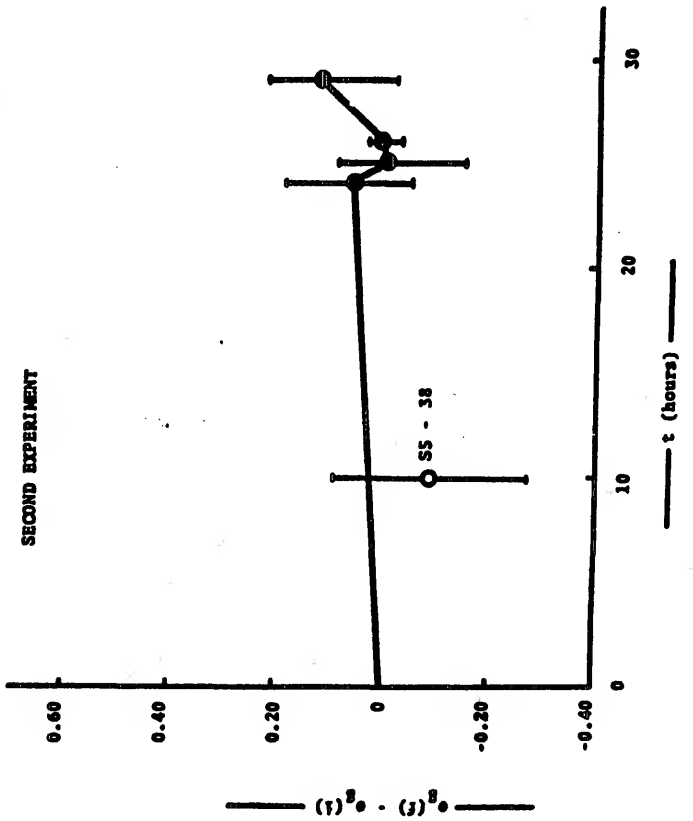

Figure 96. (continued)

(b) Specimens of the second experiment.

experiments. However, there appears to exist a tendency for grains to elongate toward the termination of the first experiment. Because quantitative metallographic measurements were not made in the necked portions of creep specimens, it is believed that the plotted values of the change in the anisotropy factor underestimate the average behavior of the entire creep specimen at the end of the two creep experiments. If any significant grain elongation occurs, it is no doubt confined to the necked portions of the creep specimen. Visual observations of the microstructure support this statement. The maintenance of equiaxed grains during creep is an indication that boundary migration is an active process.

3.8.2.9. Observations from Laue x-ray diffraction photographs

Laue x-ray diffraction photographs were made at several positions on each of the metallographic specimens in order to obtain additional qualitative information about the subgrain structure. Unfiltered molybdenum radiation was used and the x-ray tube was operated at 35 kilovolts and 15 milliamperes. Prints of representative Laue photographs of each specimen are given in Figures 97 through 105.

Varying degrees of subgrain development are shown in the several Laue photographs. In general, there was no asterism of the Laue spots; therefore, the subgrains in all specimens were free of lattice bending. In many of the

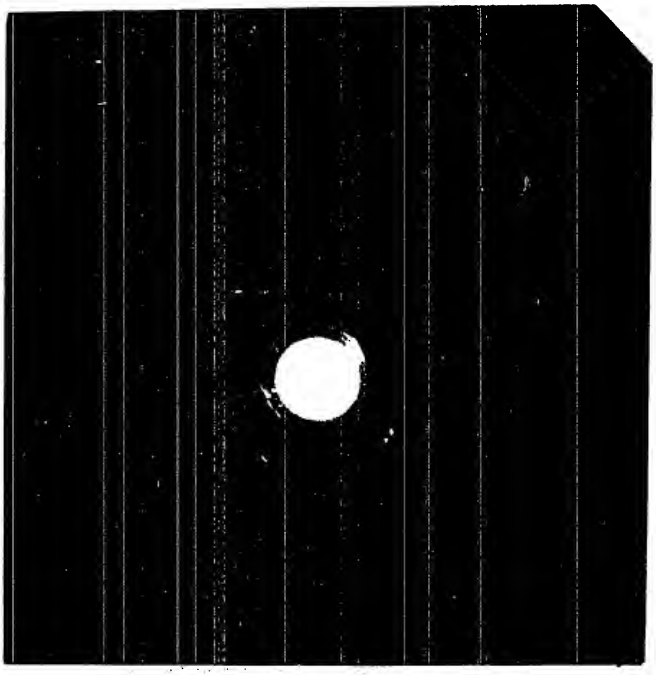

Figure 97. Laue x-ray diffraction photograph from specimen S5-38.

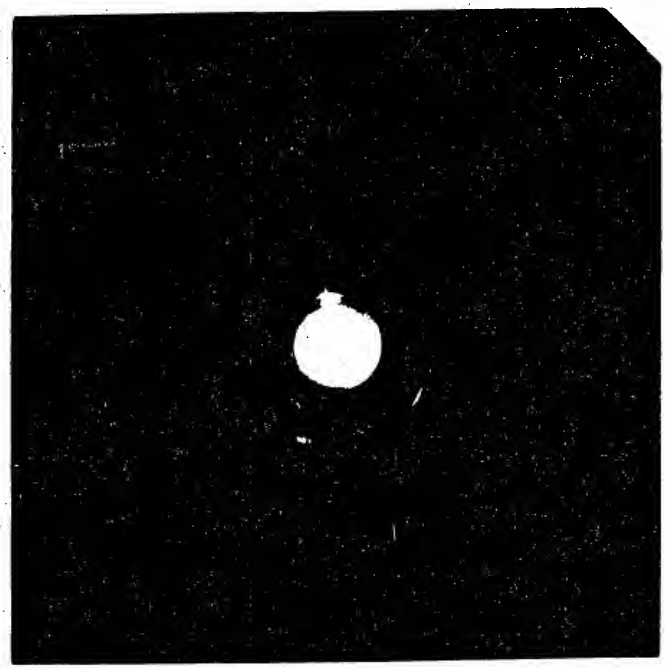

Figure 98. Laue x-ray diffraction photograph from specimen S5-31.

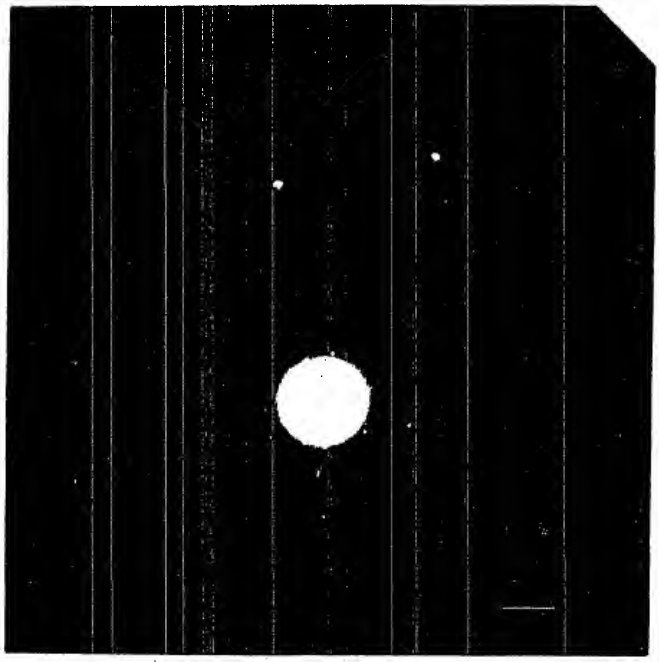

Figure 99. Laue x-ray diffraction photograph from specimen S5-43.

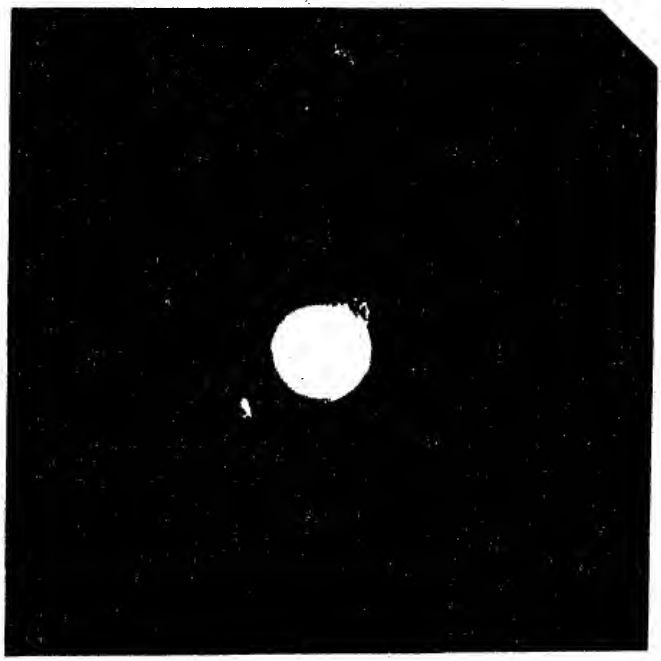

Figure 100. Laue x-ray diffraction photograph from specimen S5-45.

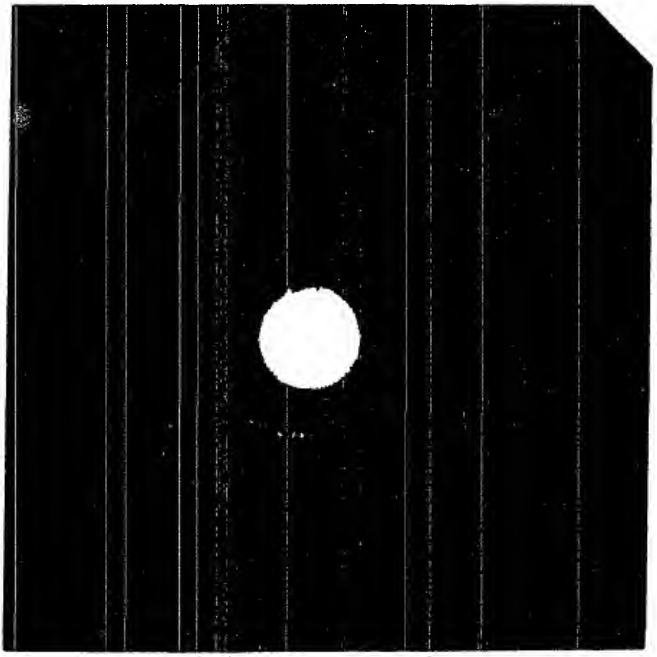

Figure 101. Laue x-ray diffraction photographs from specimen S5-40.

(a) Center of gage length.

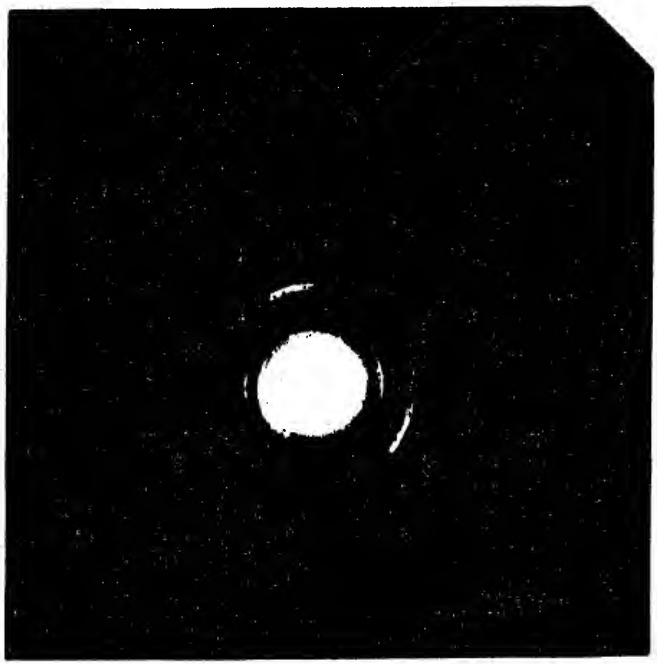

Figure 101. (continued)

(b) Necked region.

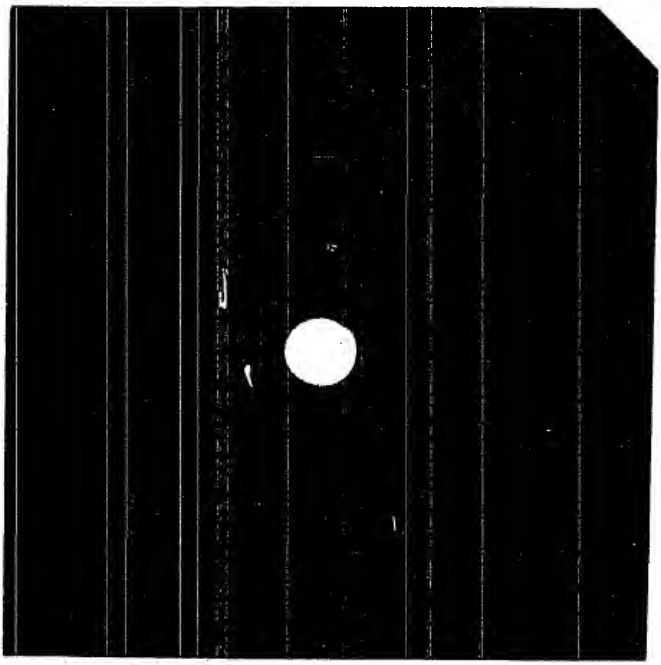

Figure 102. Laue x-ray diffraction photograph from specimen S5-41.

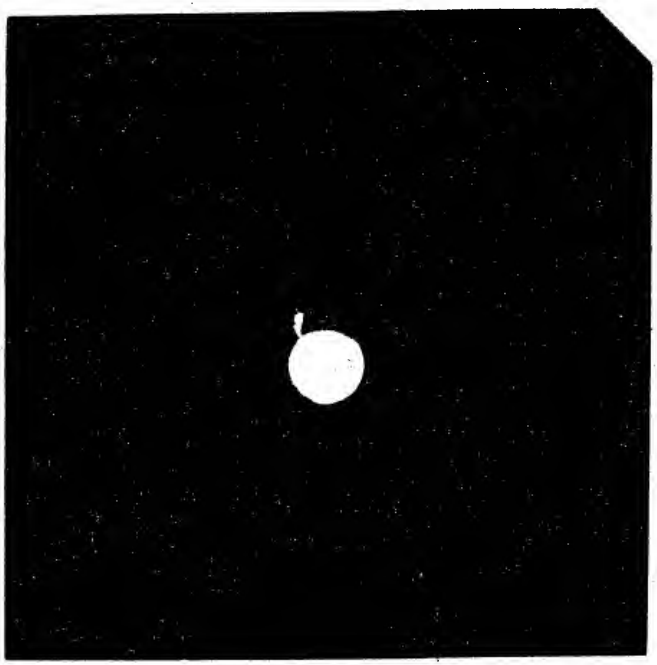

Figure 103. Laue x-ray diffraction photograph from specimen S5-42.

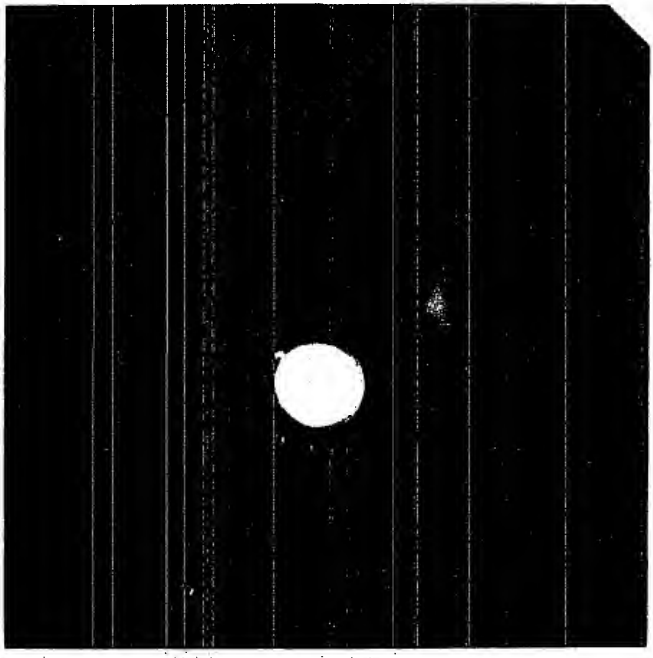

Figure 104. Laue x-ray diffraction photograph from specimen S5-44.

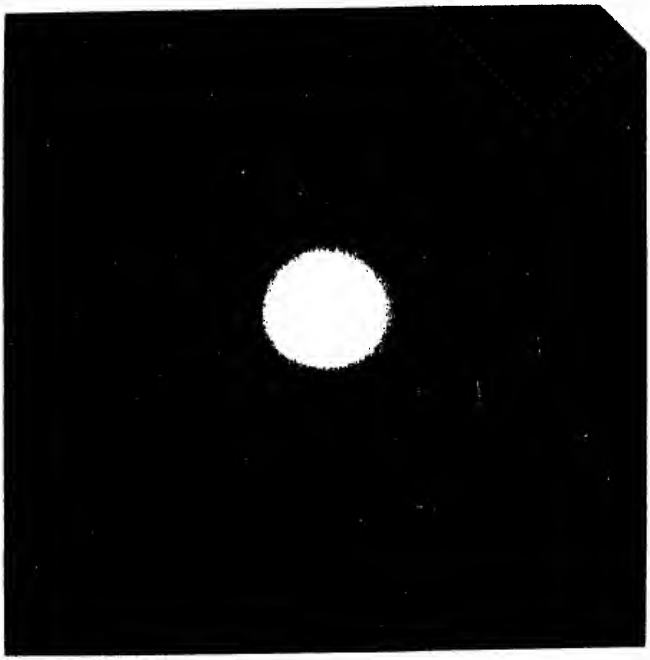

Figure 105. Laue x-ray diffraction photograph of specimen S5-39.

photographs the Laue spots were smeared circumferentially into segments of Debye rings. At a magnification of 70X the Debye ring segments were resolvable as small, closely spaced spots. Because each spot represents diffraction from a particular plane of a single crystalline element, the segments of Debye rings indicate the presence of a large number of fine subgrains with a range of crystallographic orientations proportional to the arc length of the Debye ring segment.

In the control specimen, S5-38, creep testing for 10 hours at 330°C under a stress of 417 psi, subgrains were produced with an angular range of crystallographic orientations up to about 15°, Figure 97. By preceding the high temperature creep with a precreep treatment of 24 hours at 217°C under a stress of 417 psi, specimen S5-31, the angular spread of the subgrain orientations was increased. The Laue photograph of Figure 98 indicates that the angular spread of subgrain orientations is as great as 25°. Since the ultimate strains obtained by both specimens is approximately the same, the increase in angular orientations of the subgrains may be attributed to the effects of the low temperature precreep treatment.

The evolution of the substructure throughout the course of the first creep experiment may be followed by comparing the Laue photographs given in Figures 99, 100 and 101 for specimens S5-43, S5-45 and S5-40, respectively. The Laue

photograph of Figure 99 corresponds to the microstructure at the end of the low temperature precreep treatment. The pattern of Laue spots is apparently the result of the superposition of the diffraction spots from only a few crystalline elements or subgrains. Quantitative metallographic measurements of the corresponding creep specimen, S5-43, have shown that at the end of precreep the subgrain boundary area is small, Figure 89(a), and the fraction of grains containing subgrains is also small, Figure 90(a). Two hours after the beginning of the temperature increase, the Laue photograph of Figure 100 shows that the pattern observed at the end of precreep has begun to disappear and that short segments of Debye rings have formed. The faint spots corresponding to a single crystal exhibit asterism; therefore some lattice bending does exist. This corresponds to an increase in the subgrain boundary area and an increase in the fraction of grains containing subgrains shown previously in Figures 89(a) and 90(a), respectively. With continued creep at the higher temperature, the Laue photograph of Figure 101(a) shows an increase in the length of Debye ring segments and the complete disappearance of the superimposed single crystal patterns observed in Figure 99. A further increase in subgrain boundary area and the fraction of grains containing subgrains has been previously shown in Figures 89(a) and 90(a), respectively. It is interesting to note that the spread of angular orientations in the necked portion of the specimen is rather larger than elsewhere in the

gage length. Compare the Laue photographs of Figures 101 (a and b). The Laue photograph of Figure 101(b) was taken in the region of the neck, whereas that of Figure 101(a) was taken in the center of the gage length where no neck existed. The greater continuity of the Debye rings exhibited in the Laue photograph of Figure 101(b) indicates that a greater number of subgrains are present in the necked portion of the specimen, and that their range of crystallographic orientations is also greater than in other parts of the creep specimen.

By comparing the Laue x-ray photographs of the second experiment specimens, the evolution of the subgrain structure may be followed throughout the course of precreep and subsequent creep at the higher temperature. At the end of precreep in the second experiment, the Laue photograph of Figure 102 shows by its short segments of Debye rings that subgrains have formed with a rather narrow range of crystallographic orientations. Correspondingly, Figures 89(b) and 90(b), respectively, indicate a substantial amount of subgrain boundary has formed and that most of the grains contain subgrains. One hour after the temperature was increased the Laue photograph of Figure 103 displayed a weak pattern of superimposed Laue spots from several crystalline elements in addition to several very short segments of Debyr rings. The Laue spots exhibit some degree of asterism, which indicates the presence of lattice bending. The graph of Figure 89(b)

indicates that no significant change in the subgrain boundary area had occurred, while the graph of Figure 90(b) shows a slight decrease in the fraction of grains containing subgrain rows.

Two hours after the temperature increase, the subgrain boundary area had increased markedly, Figure 89(b), and the fraction of grains containing subgrains had again increased, Figure 90(b). The corresponding Laue photograph, Figure 104, shows short segments of Debye rings and the complete absence of single crystal patterns. At the termination of the test, the subgrain boundary area had drastically increased, Figure 89(b), and all of the grains contained subgrain rows. The Laue photograph of Figure 105 is a pattern of many very weak spots. No one single crystal Laue pattern can be detected. It is thought that the pattern obtained represents a second generation of subgrains whose crystallographic orientations are not easily related to that of the parent grain.

The sequence of changes observed in the Laue photographs of the second experiment is thought to be a consequence of recrystallization which occurred when the temperature was raised and the stress decreased. The complete sequence of events cannot be traced in the available photographs, because of the rather large time interval between each successive observation.

3.9. The Evidence for Shear Along Subgrain Boundaries

The observations and results obtained in this research have led the author to believe that shear occurs along subgrain boundaries, the phenomenum being much like grain boundary shear. That subgrain rows form during the course of creep provides families of boundaries which are rather more straight than the boundaries separating the subgrains in the random subgrain morphology. It is reasonable to expect that the straighter boundaries are more favorable for boundary shear than those which are less straight. There are several pieces of evidence which further support the idea that boundary shear occurs along subgrain boundaries. In enumerating these evidences, there are similarities between the usual grain boundary shear and subgrain boundary shear that must also be stated. The following statements present evidence for subgrain boundary shear and supporting similarities between grain and subgrain boundary shear.

1. The angles of misorientation between subgrain rows can be rather large. This is particularly evident in specimens which have suffered rather large amounts of deformation. Boundaries between subgrain rows, then, should behave much as do ordinary grain boundaries. The larger the misorientation associated with a grain boundary, the more the boundary is favored for grain boundary shear.

2. Subgrain rows are oriented with respect to the tensile axis such that the boundaries separating the rows are subjected to high values of resolved shear stress. High values of shear stress directed parallel to boundaries are a requisite for grain boundary shear.

3. Subgrain rows have been observed to align with ledges at the edges of a creep specimen. These ledges have much the same appearance as ledges produced by grain boundary shear. Photomicrographs illustrating these ledges and the alignment of subgrain rows are shown in Figure 106. A ledge produced by grain boundary shear is shown in the photomicrograph of Figure 107.

4. Surface bands produced during creep are aligned with the boundaries between underlying subgrain rows. Grain boundary shear also produces a band or trace on the surface as seen in Figure 107; therefore, it is believed the surface bands are produced by shear along the boundaries of subgrain rows.

5. Surface bands have been observed to be in alignment with shears through photoengraved grids on the photomicrograph of Figure 108. Grain boundary shear also produces shear steps in reference marks on surfaces.

6. Subgrain rows are aligned with dentate grain boundary serrations.

7. A three-dimensional model constructed from photomicrographs of serial sections has shown that grain boundary serrations correspond to the shapes of subgrain rows rather than being planar. Photographs of the three-dimensional model, constructed from the photomicrographs of previously described serial sections, are shown in Figure 109. Section by section comparisons of the microstructure with the model have shown good alignment between dentate serrations and the subgrain rows.

Grain boundary shear has been observed in progress by the author and by several other investigators. Therefore, it was thought that if subgrain boundary shear could be observed while in progress, there would be no doubt that the phenomenum does in fact exist. In a number of attempts to observe the surface of specimens during creep testing, it was found that surface rumpling invariably masked the

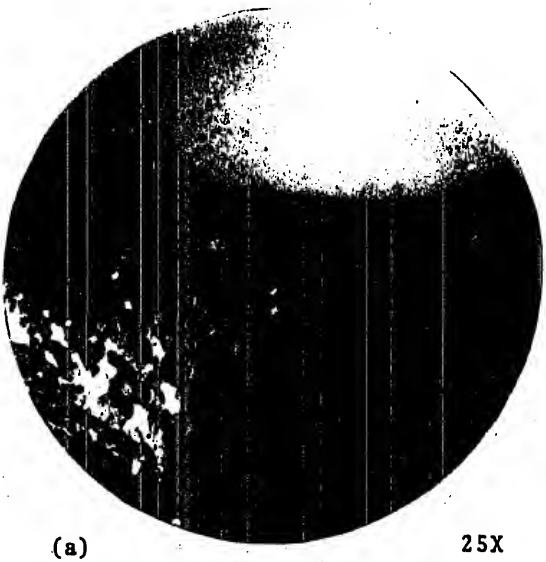

(a) 25X

Figure 106. Photomicrographs showing the alignment of subgrain rows and ledges in the edge of a creep specimen.

(b) 70X

Figure 106. (continued)

(c) 30X

Figure 106. (continued)

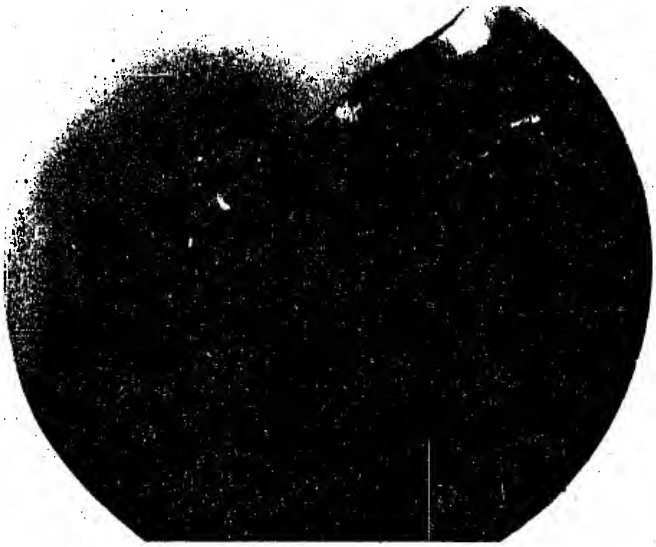

30X

Figure 107. Photomicrograph showing the ledge in the edge of a creep specimen produced by grain boundary shear. Note the trace of the shear on the surface of the specimen.

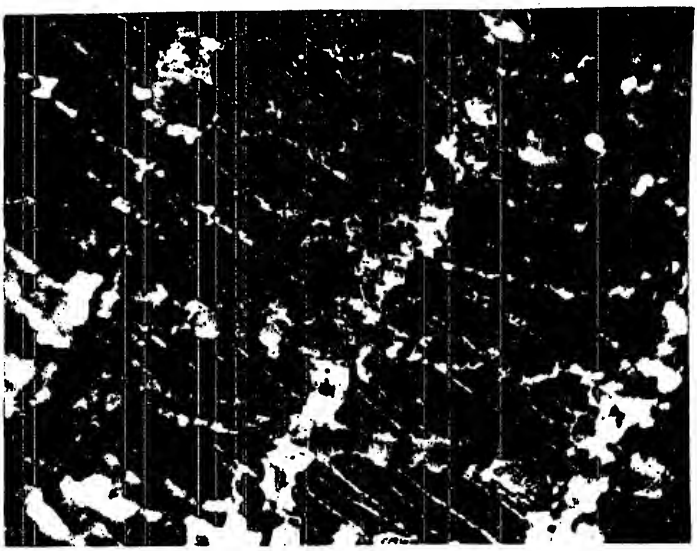

100X

Figure 108. Photomicrograph showing surface bands aligned with shear steps in a photoengraved grid.

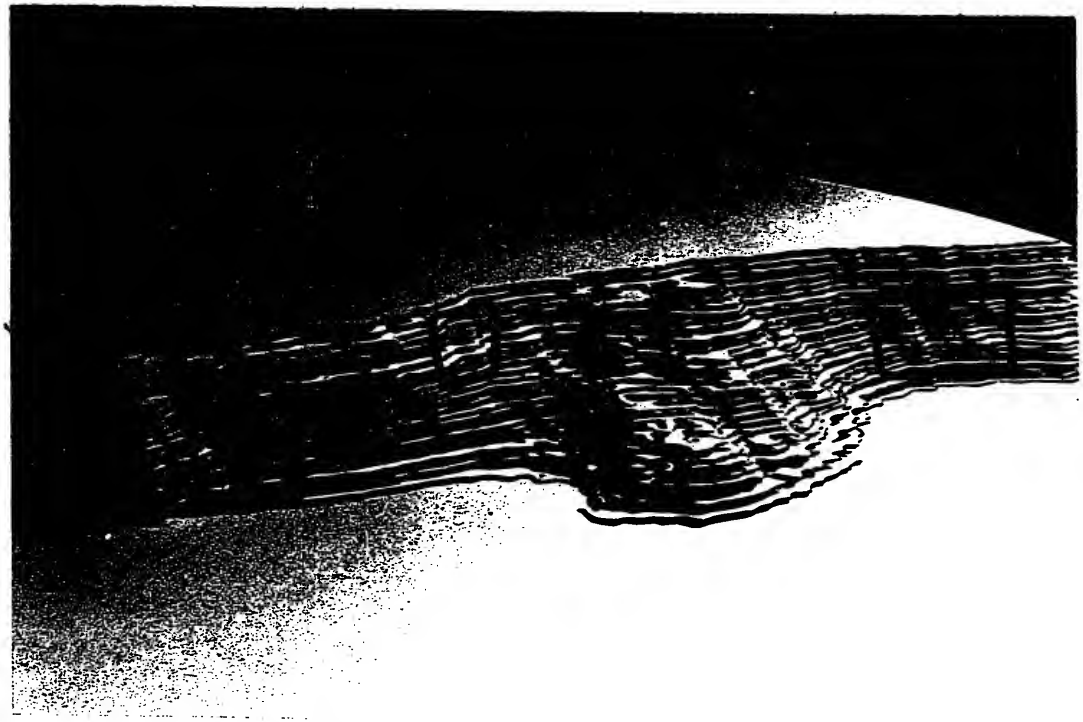

Figure 109(a). Photographs of a three-dimensional model of a serrated grain boundary. The more prominent dentate serrations are marked.

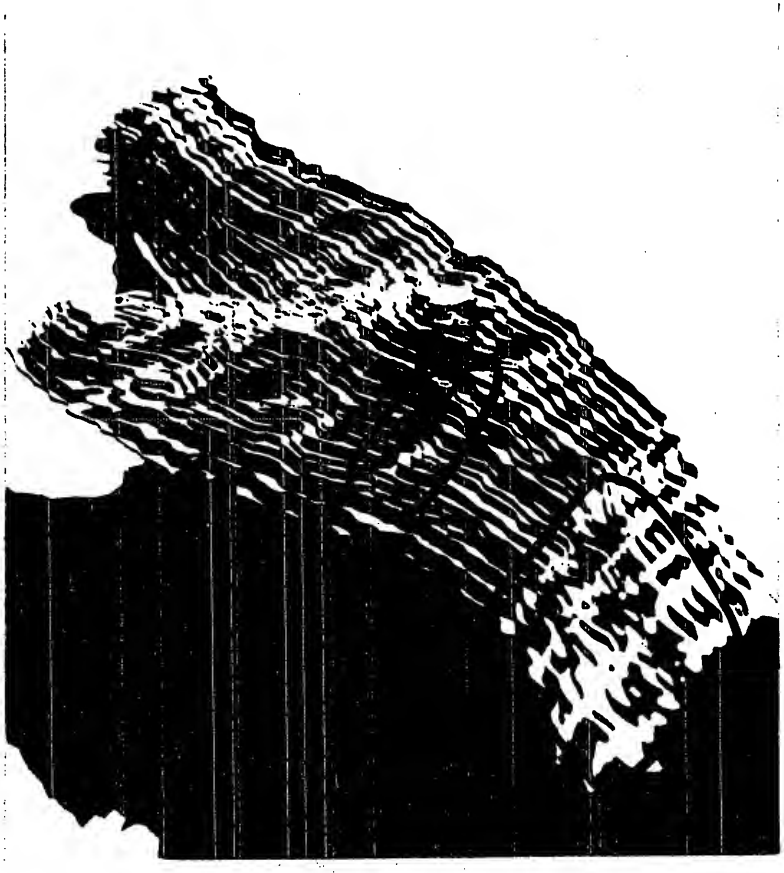

Figure 109(b). (continued).

observations of fine details such as the small displacements that would result from shear along subgrain boundaries. In order to overcome the masking effects of surface rumpling an experiment was planned in which a specimen was to be creep tested to develop subgrain rows, then the surfaces repolished and the specimen again creep tested. During the second test the surface was to be visually observed through a microscope continuously to observe shear along subgrain row boundaries. Several attempts were made to carry out such an experiment, but surface rumpling was a persistent problem and the shear too small to be observed at low magnifications. However, after the conclusion of creep testing evidence was found that irregular shear had occurred within grains. To give a comprehensive view of the overall experiment and to present its results, the details of the experiment and metallographic observations are hereby described.

A specimen, S5-30, was creep tested four times and examined metallographically after each test in order to observe the possible existence of shear along subgrain rows and/or the development of the subgrain row structure. In each test the specimen was heated to the test temperature under load and quenched under load at the end of the test. After metallographic examination the specimen was repolished and fine vertical scratch marks were made on the surface with 600 grit SiC AB Microcut paper to serve as reference marks for shear displacements in the next creep test.

Table XVII lists the conditions of each of the creep test and comments concerning metallographic observations after each test.

Reference to Table XVII indicates that no evidence of subgrain row shear was observed until after rupture of the specimen at the end of the fourth creep test. Microscopic examination of the specimen surface both with the scanning electron microscope and the metallograph showed that displacements in the scratched reference marks had occurred within grains. The displacements observed had taken place along paths which were entirely too irregular to be the results of slip. In addition, the shears which produced displacements in the reference marks resulted in surface bands which were aligned with grain boundary serrations, on steps in the edge of the creep specimen. The scanning electron micrograph and the photomicrographs shown in Figure 110 illustrate the nature of the shears and the displacements of the surface reference scratches.

The scanning electron micrograph of Figure 110(a) shows the displacement of a reference scratch. In this case, the shear occurred within a grain and did not follow a straight path as would be expected of slip. The displacement was about 1.07×10^{-5} inches. The photomicrographs of Figure 110 (b and c) show similar but larger shear displacements. Note that in the photomicrograph of Figure 110(c) the surface band makes a rather sharp bend as if conforming to the

Table XVII

Creep Tests of Specimen S5-30

Creep Test	Stress (psi)	Temperature (°C)	Time (hours)	Metallographic Observations
1	360	320	15.53	Poorly formed subgrain rows were developed during testing.
2	450	320	50.12	There was no observable evidence of subgrain boundary shear. The subgrain rows were more fully developed.
3	450	320	22.97	There was no observable evidence of subgrain boundary shear. The subgrain rows were well developed.
4	650 1,000*	240 240	8.05 2.05	Displacements of reference marks on the surface were observed and these displacements can be related to the underlying subgrain structures.

*The stress was increased during test and the specimen ruptured 2.05 hours after the stress increase. Upon rupture, the lower portion of the specimen was water quenched.

(a) 2,000X

Scanning electron micrograph

Figure 110. Displacement of surface reference scratches in specimen S5-30.

(b) 800X

Figure 110. (continued)

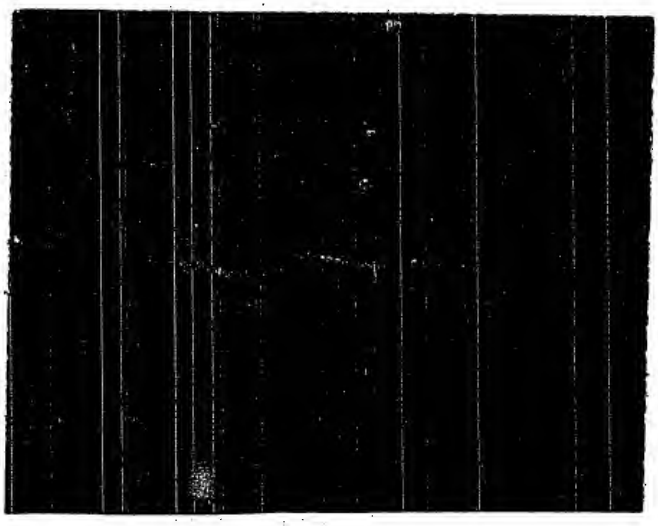

(c) 800X

Figure 110. (continued)

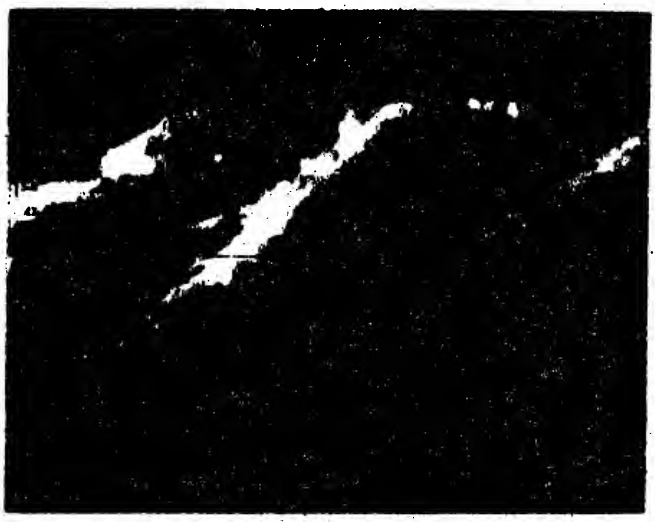

(d) 400X

Figure 110. (continued)

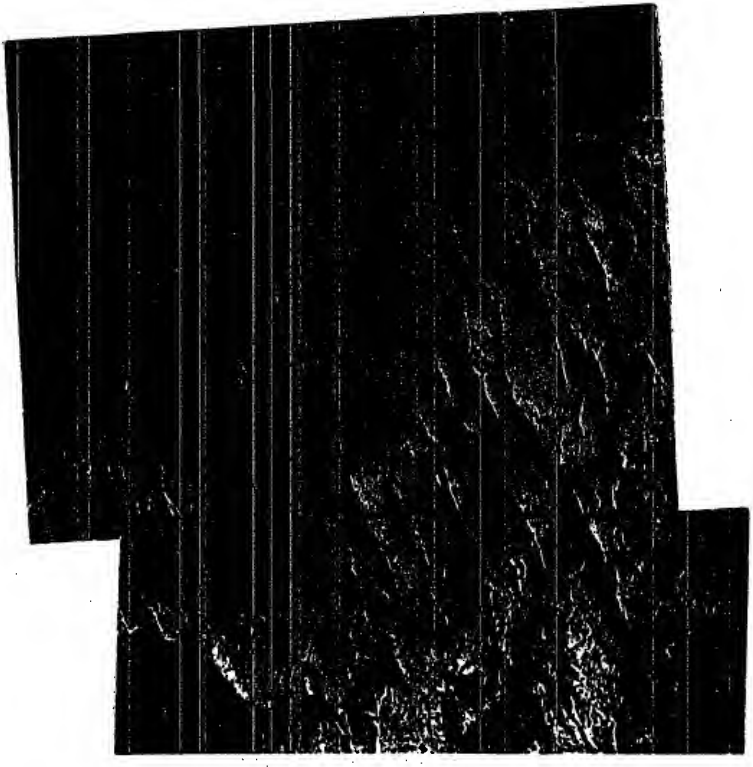

(e) 100X

Figure 110. (continued)

boundary of a subgrain. Shear displacements and ledges in the edge of the creep specimen are shown in Figure 110(d). The shear appears to occur in a thickness of metal which is analogous to a like characteristic of grain boundary shear. The shears which produce displacements in a reference scratch are aligned with offsets in a grain boundary as shown in the composite photomicrograph of Figure 110(e). It is important to point out the irregular form of the surface bands in this photomicrograph. Such an irregular path would not be expected if the shear were produced by slip.

The surface bands which produced offsets in reference scratches were found to correspond to boundaries between subgrain rows. This fact was observed by lightly anodizing the deformed surface to render the subgrains sensitive to polarized light. Unfortunately, the contrast between subgrains was too low to obtain satisfactory photomicrographs; however, the observed effect was no doubt real.

Another point of interest concerning the above described experiment is that, during the third creep test, a neck was formed in the creep specimen. In preparation for the fourth creep test, the neck was removed by careful filing and grinding the specimen to a uniform and smaller cross-section. When the specimen ruptured, terminating the fourth creep test, the neck that formed was in the same position as the neck formed in the previous creep test. This observation suggests the possibility that some form of local microstructural change had occurred during the course of the third

creep test which rendered a local region of the specimen more susceptible to deformation than other portions of the specimen.

The microstructure developed in the necked region of the specimen during the four creep tests displayed rather well-formed subgrain rows and dentate grain boundary serrations as shown in the photomicrograph of Figure 111.

3.10. A Summary of the Observations and Results

The observations and results presented in the several previous sections of this chapter are many and varied; therefore, a summary of the major points given by the following statements is in order.

1. The secondary creep rates obey the relation $\dot{\varepsilon} = A\sigma^n e^{-\Delta H/RT}$, where $\dot{\varepsilon}$ is the strain rate, σ is the stress, ΔH is an apparent activation energy, R is the gas constant, T is the absolute temperature and A and n are constants. Values for A, ΔH, and n were found to be: $A = 5.81 \times 10^{-8}$, $\Delta H = 33$ Kcal/mole, $n = 6.05$.

2. Subgrain boundary area usually forms at a constant rate during secondary creep and its rate of formation obeys the relation $\dot{S}_{V(SGB)} = B\sigma^m e^{-\Delta H/RT}$, where $\dot{S}_{V(SG)}$ is the rate of formation of subgrain boundary area, σ is the stress, ΔH is the apparent activation energy, R is the gas constant, T is the absolute temperature and B and m are constants. Values for B, ΔH and m were found to be: $B = 7.95 \times 10^{-4}$, $\Delta H = 31$ Kcal/mole, $m = 4.84$.

3. Grain growth occurs early in creep and thereafter the grain size remains constant throughout secondary creep.

25X

Figure 111. Microstructure of specimen S5-30 after test.

4. Two forms of grain boundary serrations have been observed; wavy and dentate. The formation of wavy serrations is favored by high temperature, low stress, and small amounts of strain. Dentate serrations are favored by low temperature, high stress and large amounts of strain.

5. Two morphologies of subgrain structure form during creep depending upon the temperature, the stress and the amount of strain. The random morphology of subgrains is favored by high temperature, low stress and small amounts of strain; whereas the subgrain row morphology is favored by low temperatures, high stress and large amounts of strain. Subgrain rows are often aligned across several grains.

6. In three dimensions, subgrain rows were found to lie in planar arrays, the planes being spatially oriented such that their poles make angles in the range of 40° to 60° with respect to the tensile axis. Subgrain rows as observed on metallographically prepared surfaces are primarily oriented at nearly 45° to the tensile axis. Therefore, the boundaries separating subgrain rows are subjected to high values of resolved shear stress.

7. The boundaries between subgrain rows are often complex in terms of dislocation content, but in many cases they approach simple tilt boundaries. These boundaries may represent rather large angular misorientations, and there is evidence to suggest that the misorientation increases with increasing creep strain. Subgrain rows have been found to alternate in crystallographic orientation.

8. The fraction of grains containing subgrains, f_{SG}, and the fraction of grains containing subgrain rows, f_{SGR}, both increase with time and strain. Low temperatures and high stresses favor increases in both fractions.

9. The fraction of the grain boundary area which is serrated, $S_V/S_{V(GB)}$, increases with time and strain. Creep at 200°C under a stress of 1,000 psi favors the formation of serrated grain boundaries more than do the other creep testing conditions investigated.

10. Microstructural examination has shown that an association exists between the wavy form of grain boundary serrations and the random morphology of subgrains, and between dentate grain boundary serrations and the subgrain row morphology.

11. Relationships between the amount of serrated grain boundary and the subgrain structure have been obtained from graphs of the fraction of the grain boundary area which is serrated, $S_V/S_{V(GB)}$, versus the fraction of grains which contain subgrains, f_{SG}, the fraction of grains which contain subgrain rows, f_{SGR}, and the fraction of grains which contain only subgrains of the random morphology, f_{SG}-f_{SGR}. When most of the grain boundary area has become serrated, the fraction of grains which contain subgrain rows, f_{SGR}, has a high value.

12. Regardless of the temperature or stress of creep testing, when creep has progressed into the third stage, almost all of the grains contain subgrain rows, and a majority of the grain boundaries exhibit dentate serrations.

13. Surface bands are developed during secondary creep which do not bear resemblance to slip lines. They have been observed to cross grain boundaries without an apparent change in direction. In general, the bands are wavy in appearance and often branched. When they intersect a grain boundary they coincide with a noticeable perturbation of the boundary.

14. Boundaries between subgrain rows have been observed to coincide with surface bands, with ledges in the edges of creep specimens and with displacements in grain boundaries.

15. Creep at a low temperature increases the steady state creep rate during subsequent creep testing at a higher temperature. Increasing the amount of creep strain attained during the low temperature creep, either by increasing the stress or by testing for longer times, increases the steady state creep rate during subsequent creep testing at a higher temperature.

16. Evidence from Laue x-ray diffraction patterns shows that there exists a change in the nature of the subgrain structure during creep at a high temperature after previous creep at a lower temperature. The rate and the amount of deformation at the lower temperature appears to have an effect upon the way in which the subgrain structure changes during subsequent creep at the higher temperature.

17. The small changes in grain boundary anisotropy during secondary creep indicate that boundary migration is an active process.

18. The effects of grain boundary influence upon deformation have been observed microstructurally in the "blocky" appearance of the substructure within individual grains and in a variation in the appearance of grain boundary serrations among grain boundaries.

3.10.1. An Overview of the Microstructural Evolution

At the outset of the high temperature creep of polycrystalline aluminum, the individual grains begin to fragment as subgrain boundaries begin to form. Not all of the grains begin to form sub-boundaries at the same time or at the same macroscopic strain. Presumably, each grain deforms in response to the applied stress according to its orientation and the constraints to deformation offered by its grain boundaries with adjacent grains. As the grains initially become subdivided by the formation of sub-boundaries, the subgrains appear to be more or less equiaxed (random subgrain morphology) with small misorientations across their boundaries. It is significant that the whole of each grain does not become subgrained all at one time; rather, the subgrains appear to develop in response to an interaction with

neighboring grains. Thus, it is rather common that each grain develops patches of subgrains, the subgrains within each patch having similar crystallographic orientations. This effect is believed to be the consequence of grain-to-grain constraints to deformation.

With continued deformation, subgrains are observed to evolve as rows. Metallographic examination has shown that, under certain conditions of temperature and stress, subgrain rows form very early in creep. Subgrain rows develop in more and more grains as the deformation progresses. Like the formation of equiaxed subgrains, subgrain rows as a general rule do not develop in the whole of individual grains all at one time. The subgrain rows often appear in several patches within one grain. By the time tertiary creep begins, most of the grains contain subgrain rows and, in the region of the specimen which necks, all of the grains contain subgrain rows.

The subgrain rows as they first appear have relatively small angles of misorientation across their boundaries. With the progress of deformation, the angular misorientations of the boundaries separating the subgrain rows increase continuously.

One of the more striking features of subgrain rows is their alignment from one grain to another across grain boundaries. This alignment has been observed in two dimensions to extend across several grains without large changes in the

directions of the subgrain rows as they meet at grain boundaries. It is more common, however, for subgrain rows not to be aligned across more than one or two grains. The rows often have been observed to change directions within grains, the change of direction seeming to be coincident with the patchy structure of the rows within single grains.

Concurrent with the evolution of the subgrain structure during the course of high temperature creep, an evolution in the development of grain boundary serrations also takes place. During the early part of creep, wavy grain boundary serrations begin to develop. It has been difficult to detect the exact time or strain at which grain boundary waviness first appears, but it is clear that all of the grain boundaries do not become perceptably wavy at the same time. In order for the grain boundary to exhibit waviness, it seems that grains on both sides of the boundary must contain subgrains. The wavy serrations are presumably the result of small local adjustments of the grain boundary in response to the presence of sub-boundaries in the deforming microstructure. As deformation progresses more and more of the grain boundary area becomes perceptably serrated, and the serrations gradually increase in amplitude. When subgrain rows first appear in the microstructure they have apparently no effect upon the form of the grain boundary serrations. Only late in secondary or at the beginning of tertiary creep, when a majority of the grains contain

subgrain rows, do the grain boundary serrations take on a predominately dentate form. Dentate serrations exist only when subgrain rows are present on both sides of the grain boundary, and only when these rows are well aligned across the boundary. As the angular misorientation across the subgrain row boundaries increases with increasing deformation, they behave more and more as do ordinary grain boundaries. Therefore, they become subject to boundary shear, a phenomenum which is like in kind to that of grain boundary shearing.

Dentate grain boundary serrations become observable during secondary creep, but their occurrence in the microstructure is rather scattered until very late in secondary creep. At the outset of tertiary creep, almost all of the grain boundaries exhibit dentate serrations. As tertiary creep progresses to fracture, the grain boundaries become more and more serrated until their identity is lost and the microstructure takes on the appearance of a fine-grained structure in which the grains are aligned in rows. The general configurations of the original grains can be observed only as patches of fine grains, each patch having grains which are generally related to one another by their crystallographic orientations.

CHAPTER IV
DISCUSSION

In the creep of polycrystalline aluminum, the individual grains respond to the applied load, not only according to their crystallographic orientations with respect to the directions of the macroscopic shear stresses, but also according to the deformation imposed upon them by their surrounding neighbors. Because each individual grain is surrounded by a different set of grains, the response of any given grain to the applied stresses is uniquely different from that of the others; yet each grain contributes to the overall macroscopic shape change by deforming in concert with the other members of the aggregate. The deformation suffered by a grain is rather complex, because the grain must respond to as many different "deformation commands" as there are conjoint neighboring grains. A deformation command is the result of shear being passed from one grain to its conjoint neighbor through their common boundary interface.

As each grain responds to its various deformation commands, its lattice becomes bent in a rather complex and inhomogeneous way. Within a single grain, the lattice tends to deform according to each of its deformation commands

simultaneously. Because the deformation commands differ, response of the lattice to any one command would conflict with the others. These conflicts in response to the various deformation commands cause complex bending or rumpling of the lattice. In effect, the deformation of a grain is confined by the presence of its neighboring grains.

Once the lattice has become rumpled, if the temperature is above that required for recovery, intersecting planes of sub-boundaries form to reduce the strain energy of the lattice bending. The observed formation of subgrain rows is believed to be the result of this sort of process. With the further progress of deformation, the misorientation across the boundaries separating subgrain rows increases continuously until, upon the basis of misorientation, no distinction can be made between the sub-boundaries and ordinary grain boundaries. From this point on, sub-boundaries behave as do ordinary grain boundaries in that they are subject to boundary shearing.

It is the primary thesis of this dissertation that simultaneous shearing along the sub-boundary planes in conjoint grains occurs in response to local shear stresses. In order for this sort of shearing to occur, cooperative shearing across the grain boundary must also occur along the boundaries separating subgrain rows. The result of these cooperative shears is that the boundary interface separating the conjoint grains becomes roughly stepped.

When a metallographic section is prepared by obliquely cutting through the subgrain rows and the roughened grain boundary interface, the resultant appearance of the boundary in the two-dimensional surface is that of dentate grain boundary serrations.

The preceding proposition has been developed out of the observations and results presented in the previous chapter. The following is a list of the major new observations.

1. The blocky pattern of the subgrain structure developed within the grains reflects the effects of the surrounding conjoint grains upon the passage of shear from one grain to its neighbors.

2. Subgrain rows are oriented at approximately 45° to the tensile axis.

3. In three dimensions, subgrain rows are separated by planes of sub-boundaries which are oriented so that they coincide with directions of high resolved shear stresses.

4. Subgrain rows, as first formed, are separated by boundaries of rather small misorientations; and, as deformation progresses, the misorientation increases.

5. Subgrain rows exist prior to the formation of dentate grain boundary serrations.

6. Dentate grain boundary serrations exist only when subgrain rows are well aligned across the boundary, and these serrations are associated with the intersections of subgrain rows and the boundary.

7. Banding upon the surfaces of creep specimens is aligned with underlying subgrain rows. Surface banding is aligned with steps in grain boundaries and with steps in the edges of creep specimens.

8. In three dimensions, grain boundaries are rather roughly stepped, or "lumpy," and these steps coincide with the intersections of subgrain rows and grain boundaries.

The defense of the proposition is based primarily upon the constraints to deformation offered by the presence of grain boundaries. These constraints to deformation are discussed in following sections of this chapter.

Having established that cooperative shearing across grain boundaries along the boundaries separating subgrain rows is an additional mechanism of high temperature creep, it became necessary to discover how it fits into the overall deformation process. Through the use of a schematic representation of high temperature creep, described in a later section of this chapter, it is evident that shearing along the boundaries of subgrain rows is a recovery process which becomes active late in secondary creep. It is proposed that the additional recovery provided by the shearing along the boundaries of subgrain rows contributes to accelerating creep rates and the onset of tertiary creep without requiring the prior formation of a necked region in the specimen. The microstructural evolution which occurs during the course of the high temperature creep is also discussed in terms of the schematic representation of the overall process of high temperature creep.

4.1. Grain Boundaries and Deformation

The way in which the individual grains of a polycrystalline metal deform under the action of applied deforming stresses to a large degree depends upon the way in which shear is transmitted across grain boundaries and upon the way in which grain boundaries act to restrict the passage of shear. On the basis of the orientations of the various grains with respect to the applied shear stress, it is easy to understand why a difference in the crystallographic orientation between adjacent grains might make it difficult to transmit shear from one grain to its neighbor. Such considerations, however, lead to an incomplete understanding of the deformation in polycrystalline metals. When the geometric characteristics of grain boundaries are taken into account, additional constraints to deformation become apparent.

For the purposes of this discussion, a grain boundary may be defined as an interface, the two sides of which are distinguishable by differences in crystallographic orientation. In more detail, a grain boundary interface is considered in terms of the mating surfaces of the conjoint grains. It is an essential feature of the geometry of grain boundaries that the grain boundary interface be contiguous. That is, the areas and the shapes of the mating surfaces of two conjoint grains must be identical. The mating surfaces of conjoint grains must maintain overall contact. The way

in which shear is passed across a grain boundary and the constraints that grain boundaries offer to the passage of shear arise out of the condition of contiguity. A change in the area or shape of a grain boundary interface which occurs as the result of the passage of shear, such a change being governed by the condition of contiguity, gives rise to constraints to deformation.

For a more complete description of the geometric aspect of grain boundaries, the reader's attention is directed to Appendix VIII.

4.1.1. Grain Boundary Constraints to Deformation in a Polycrystalline Metal

Grain boundaries offer at least three constraints to deformation. One constraint arises from the condition that a grain boundary must change its surface area if the relative tilts between conjoint grains are changed by deformation. Consequently, for the boundary between two grains to change its area, the dimensions of the grain boundary network must also be altered. A second constraint arises out of the condition of contiguity. If the contiguity of a grain boundary is violated by the deformation in the conjoint grains, an adjustment, such as grain boundary shearing, must be made in order to maintain contiguity of the grain boundary network. Grain boundary shearing, as it occurs within one of the conjoint grains and parallel to the boundary interface, requires a local adjustment of the grain

boundary network. The third constraint to deformation arises from the physical confinement of each individual grain by its surrounding neighbors. A given grain deforms according to the commands it receives from all of its conjoint neighbors. Due to the presence of its common boundaries with each of the several conjoint grains, a given grain rarely, if ever, receives deformation commands which would result in an overall homogeneous deformation. Therefore, each grain boundary interface surrounding a grain acts to constrain the deformation commanded by each of the other surrounding grains.

The concepts of the geometry of grain boundary interfaces described in terms of the relative tilts of the conjoint grains applies equally to subgrain boundaries. Neither the magnitude of the misorientation across a boundary nor the origin of a boundary has any fundamental significance to the foregoing concepts of the geometry of grain boundary interfaces. In the following sections of this chapter, the term "boundary" will be used generally to refer to both grain and subgrain boundaries.

4.1.1.1. Changes in grain boundary area

When a polycrystalline metal is deformed, shear must be passed through the interfaces of grain boundaries. In principle, the shearing of one grain causes the area of its surface mating with a conjoint neighbor to be increased or decreased and its shape to be altered. In response, the

conjoint grain would tend to shear in such a way that its mating surface would likewise be altered in area and in shape by an amount required to preserve the contiguity of the boundary interface. The resulting change in the area and/or shape of the boundary interface represents a constraint to deformation, because it requires a dimensional adjustment of the grain boundary network.

In practice, the deformation of a polycrystalline metal specimen should result in a monotonic increase in grain boundary area with continuous deformation, provided that neither recrystallization nor grain growth occurs. It is the author's view that it would be impossible to devise a deformation process which would simultaneously reduce the relative tilts across all of the grain boundaries and thereby reduce the total boundary area. Even in a bicrystal it would be impossible to reduce the area of the boundary, because the boundary is physically "tied" to the external surfaces. Further, it seems unreasonable that the relative tilts between the two halves could be reduced by deformation, because of the improbability of causing each crystal half to shear on exactly those slip planes upon which shear would be required for the untilting of the crystals. In reality, new shears would be introduced and the boundary would become rumpled.

4.1.1.2. Violations of boundary contiguity and grain boundary shearing

It is a basic hypothesis of the geometry of grain boundaries that the contiguity of the boundary interface must not be violated by the passage of shear through the boundary, Appendix VIII. But, what if it is? If, under the action of an applied stress, one grain of a conjoint pair should change the area of its mating surface more than its neighbor, then adjustments along the plane of the boundary would be required to maintain contiguity. A reasonable adjustment would be a shear along one side of the boundary. Since the boundary surface is bounded by triple lines, then the adjustment by shear may in turn require adjustments of one of the conjugate boundary surfaces along one or more of the triple lines. If the contiguity of a grain boundary is violated only locally by inhomogeneities in the deformation, the adjustment along the boundary by grain boundary shearing may not extend to the triple lines bounding the boundary interface. It is the belief of the author that such violations of the condition of contiguity supply the driving force for grain boundary shearing. This concept explains the often observed alteration of a conjugate grain boundary and the existence of a shear zone opposite the sheared boundary, Figure 112.

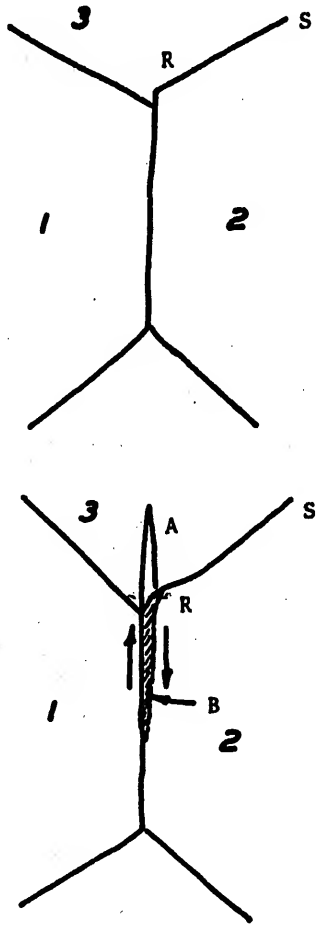

Figure 112. Grain boundary shearing as an adjustment required by a violation of the condition of contiguity. (a) Violation of the condition of contiguity. The area of the mating surface of grain 2 is greater than that of grain 1. (b) Adjustment by grain boundary shearing in the shear zone "B" produces a change in the shape of boundary RS separating grains 2 and 3 and a shear band "A" in grain 3.

4.1.1.3. The confinement of grains and the formation of subgrain rows

During deformation each grain in a polycrystalline metal specimen deforms in response to deformation commands it receives by the passage of shear through the grain boundary interfaces of each of its conjoint neighbors. Each grain receives as many different commands to deform as it has boundary interfaces with conjoint neighbors. The deformation commands differ from one another both in the directions and in the magnitudes of the shears they command. In response to these commands the grain cannot respond to just one command and shear accordingly without deforming against one or more of the other commands.

According to the geometric concept of grain boundaries, the passage of shear through a grain boundary requires that each of the conjoint grains concurrently alters its tilts with respect to one another and with respect to the grain boundary interface, Appendix VIII. If a pair of grains is free to deform according to the command of its conjoint boundary interface, then each grain must tilt or physically "rotate" with respect to another as shear is passed through the common boundary. In a polycrystalline specimen this free rotation could not occur without deforming against the deformation commands of other grain boundary interfaces. Hence, each grain is in effect physically confined by its surrounding neighbors.

Consider, in two dimensions, the restriction to rotation of a grain imposed by its neighbors, Figure 113. Assume that, under the action of a deformation command, grain 1 has a tendency to rotate upward into grain 2, as shown in Figure 113(a). Initially, the lattice planes (indicated by parallel lines within each grain) are unperturbed. This rotation is counter to the deformation command of the boundary between grains 1 and 2. Therefore, grain 2 restricts the rotation of grain 1. As the two grains are forced together along their common boundary by the rotation of grain 1, the lattices of both grains become "rumpled" by alternate lattice bending. The alternate lattice bending has a repetitive pattern much like that associated with a series of deformation or kink bands. Lattice bending in grains 1 and 2 imposes similar lattice bending in grain 3 and imparts a waviness to the boundaries separating grains 1 and 3 and grains 2 and 3, Figure 113(b). If the temperature is above that required for polygonization, then the elastic strain associated with the alternate lattice bending may be relieved by the formation of sub-boundaries perpendicular to the bends, Figure 113(c). The directions of the sub-boundaries should vary from grain to grain depending upon the differences in the crystallographic orientations among the grains. In the preceding two-dimensional development, the sub-boundaries separate two-dimensional rows or subgrains. These rows alternate in crystallographic orientation with respect to each other.

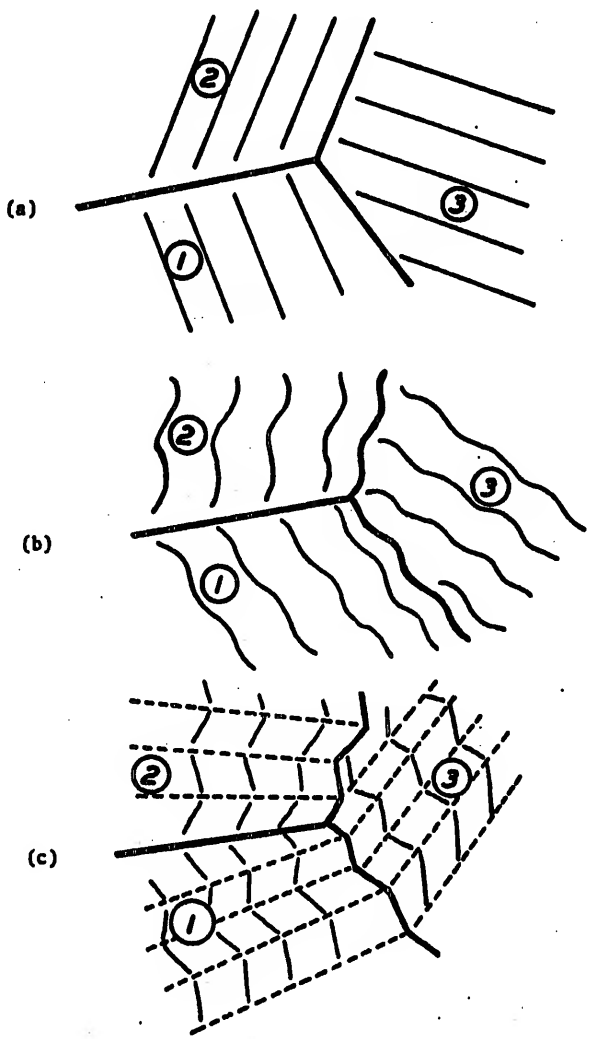

Figure 113. The development of subgrain rows. (a) Grain 1 has a tendency to rotate into grain 2 because of deformation commands from other neighboring grains. (b) Grain 2 restricts the rotation of grain 1 and the lattices of grains 1, 2 and 3 become alternately bent. (c) As the result of polygonization, sub-boundaries form perpendicular to the bent lattice planes.

In extending the above development to three dimensions, it is necessary to consider that, in response to deformation, grains 1 and 2 may rotate into or out of the plane of the sketches in Figure 113. Neighboring grains above and below the plane of the sketches would restrain these rotations. Restraint to the rotations of grains 1 and 2 by these neighboring grains would produce alternate lattice bending in a second direction in each of the rotating grains (1 and 2). The sketch of Figure 114(a) shows schematically how a lattice plane alternately bent in two directions might appear. If the temperature is sufficiently high and polygonization occurs to relieve the elastic strains of the bending, the lattice plane would take on the contour of a doubly folded accordion surface, and three-dimensional subgrain rows would be formed, Figure 114(b). Note that the crystallographic orientation among the subgrain rows alternates in two directions. It is expected that in three dimensions grain boundaries might also take on the appearance of a doubly folded accordion surface. Metallographic observations of this research have shown that the subgrain rows alternate in crystallographic orientation and that the grain boundary surface between grains containing subgrain rows has a rather lumpy appearance somewhat like a rough doubly folded accordion surface.

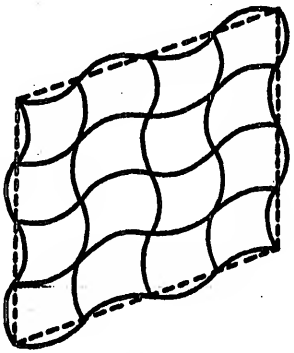

(a)

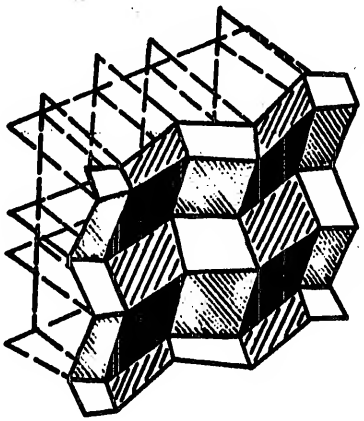

(b)

Figure 114. Three-dimensional lattice bending and the formation of sub-boundaries. (a) Doubly bent lattice plane. (b) Lattice plane and sub-boundaries after polygonization.

4.1.2. Shearing Along the Boundaries Separating Subgrain Rows and the Formation of Dentate Grain Boundary Serrations

There is no doubt that the evidence presented in Chapter III conclusively indicates that shearing occurs along the boundaries separating subgrain rows. A main point of the observations is that the shearing as it occurs along subgrain row boundaries must be cooperative across grain boundaries in order to account for the appearance of the observed dentate grain boundary serrations.

In preceding sections of this chapter, discussions of the constraints to deformation imposed by the presence of grain boundaries have led to a tenable mechanism for the formation of subgrain rows and provide a basis for the occurrence of grain boundary shear. Planes of sub-boundaries, provided for in the mechanism for the formation of subgrain rows, are believed to act as macroscopic shear planes within grains. Shearing along these planes under the action of an applied shear stress serves as a basis for proposing a mechanism for the formation of dentate grain boundary serrations.

Once subgrain rows have formed, continued hot deformation causes the misorientation across the boundaries separating the rows to increase to a degree where the sub-boundaries become indistinguishable from ordinary grain boundaries. From this point on, the sub-boundaries presumably behave as do ordinary grain boundaries in that they

are subject to boundary shearing. Accepting that shearing does occur along the boundaries, that dentate serrations are always associated with subgrain rows in both grains conjoint upon a common boundary, and that dentate serrations appear to form rather later in deformation than do subgrain rows, all of which have been indicated by the results of this research, it is now necessary to investigate how shearing along the boundaries of subgrain rows might lead to the formation of dentate grain boundary serrations.

It is apparent that by whatever process dentate grain boundary serrations form, cooperation across the grain boundaries is required in order that the serrations be aligned with subgrain rows on both sides of the grain boundary. Consider in two dimensions that subgrain rows in adjacent grains impinge upon a common boundary, and that they are not well aligned across the boundary as shown in Figure 115(a). Under the action of the local deformating stresses it may become necessary for shearing to occur in a direction roughly perpendicular to the length dimension of the subgrain rows and in a plane parallel to a sub-boundary plane separating subgrain rows (plane of the sketch). It is reasonable that such a shear might occur, since observations of the microstructures containing subgrain rows have shown that the planes of sub-boundaries are most often aligned with a direction of high resolved shear stress (45° to the

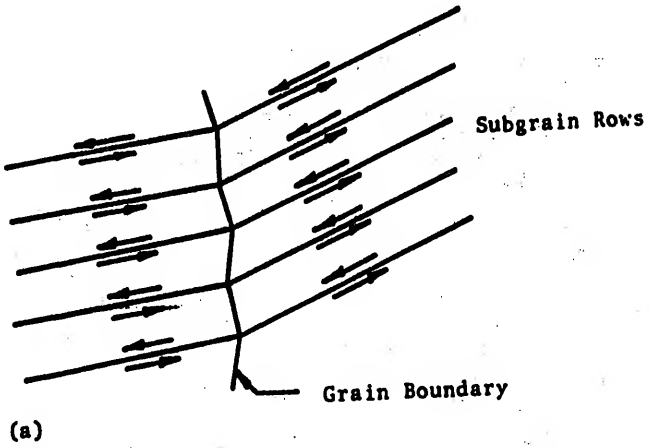

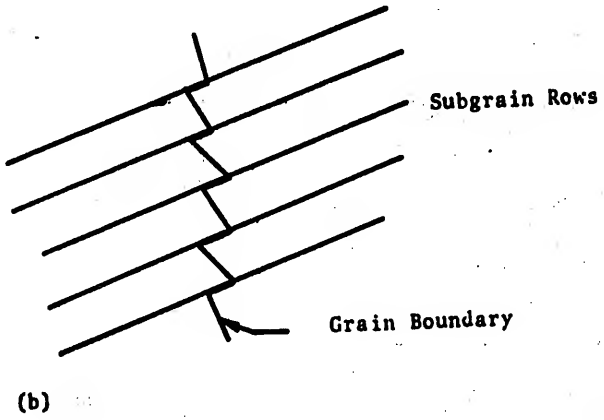

Figure 115. Shearing along the boundaries separating subgrain rows. (a) Shear stresses along the boundaries separating subgrain rows. (b) After shear has occurred along the subgrain rows, the grain boundary has become "sawtoothed" and the rows exhibit better alignment across the grain boundary.

tensile axis). If shearing should occur along sub-boundary planes of this sort in both grains, cooperative shearing would also be called for along the boundaries separating the subgrain rows as indicated in the sketch of Figure 115(a). The shearing along the boundaries separating subgrain rows must also be cooperative across the grain boundary. This shearing process would improve the two-dimensional alignment of the subgrain rows across the boundary and leave the grain boundary "saw-toothed" as shown in the sketch of Figure 115(b). The improved subgrain row alignment is the result of the "rotations" of the conjoint grains.

If one now considers the three-dimensional case, where concurrent shearing is called for in two directions in the conjoint grains, the resulting grain boundary is stepped in two directions. The sequence of sketches in Figure 16 (a-c) showsthe shears in one of a conjoint pair of grains and the configuration of the grain boundary surface after each shear has occurred. A section taken so as to cut obliquely the subgrain rows and the grain boundary showsthe presence of dentate teeth in the boundary, Figure 116(d). This sort of section is of the type one might expect to obtain by preparing a surface for metallographic examination.

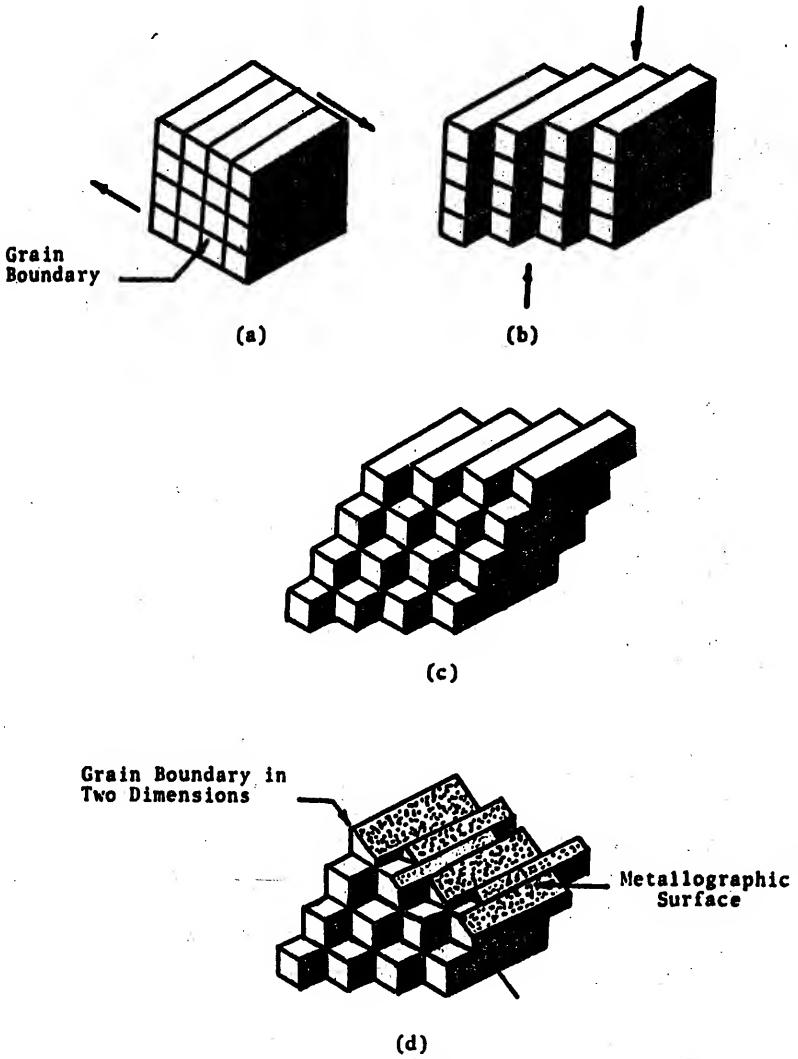

Figure 116. Three-dimensional view of bi-directional shearing to produce dentate grain boundary serrations. (a) Crystal before shear. (b) Crystal after shear in one direction. (c) Crystal after shear in a second direction. (d) Oblique section through doubly sheared crystal exhibits dentate serrations in boundary.

4.2. A Schematic Representation of High Temperature Creep

As a device for cataloging the processes which take place during the course of high temperature creep, a schematic representation of the overall process in terms of dislocation line length has been developed. In addition to its catalog function, the schematic representation has proven to be useful in systematically examining the interactions among the deformation and recovery mechanisms of high temperature creep. A block diagram of the schematic representation, Figure 117, indicates how dislocations are introduced into a specimen, and how they may be stored within or removed from the specimen during the course of hot deformation.

Dislocations are introduced into the lattice as lattice bending, and as long as they remain in the lattice they are potential contributors to work hardening. Work hardening results from the elastic interactions among the dislocations in the lattice. In order that creep deformation not be stifled by work hardening, recovery processes must occur. Two types of recovery processes occur during hot deformation: (1) those which remove dislocations from the specimen, and (2) those which remove dislocations from the lattice by causing them to precipitate into boundaries. Recovery processes which are of the first type are (1) annihilation (Rec. 4), (2) recrystallization (Rec. 6), and (3) grain

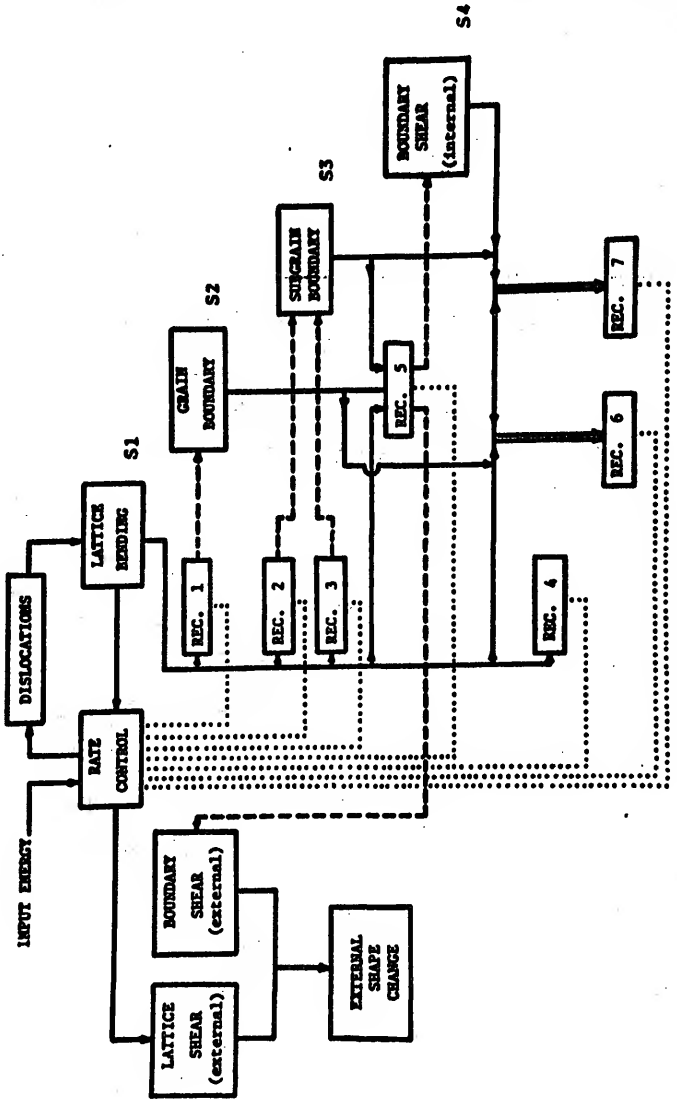

Figure 117. Block diagram of the schematic representation of high temperature creep.

growth (Rec. 7). For the purposes of this discussion, both recrystallization and grain growth, as they occur concurrently with high temperature creep, are considered as recovery processes, because they tend to return the metal specimen to its initial undeformed state. Recovery processes which are of the second type are (1) that recovery in which dislocations are precipitated into pre-existing grain boundaries (Rec. 1), (2) dynamic recovery (Rec. 2), (3) polygonization (Rec. 3), and (4) that recovery associated with grain and subgrain boundary shearing (Rec. 5).

Dislocations, during the course of high temperature creep, may be stored in the lattice as lattice bending (S1), in grain boundaries (S2), in subgrain boundaries (S3), and in grain and subgrain boundaries as the result of boundary shear (S4). The length of dislocation line stored within a grain or subgrain boundary not only depends upon the area of the boundary, but also upon the misorientation of the conjoint grains. Therefore, the boundary area alone does not give a complete measure of the dislocation line length stored in the boundaries. The specific misorientation across each unit area of boundary, or the dislocation line length per unit area of boundary, must also be measured.

To follow the processes of hot deformation in terms of the schematic representation, consider that the applied stress generates dislocations within the lattice. For the purposes of discussion, any unit length of dislocation line

in the lattice represents lattice bending; admittedly, even on an atomic scale, the bending is small. Lattice dislocations may shear through the lattice and interact with grain boundaries so as to transmit shear completely through the entire specimen to the external surfaces. At any time during deformation, the instantaneous rate at which dislocations shear through the lattice under the action of the applied stress depends upon the level of the work hardening.

To overcome work hardening, recovery processes operate to remove dislocations from the lattice by either annihilation or precipitation into boundaries. Some of the dislocations may, through a recovery process (Rec. 1), be precipitated into pre-existing grain boundaries (S2). Other dislocations surmount obstacles by cross-slip, and if during the process screw components of opposite senses are annihilated (Rec. 4), walls of edge dislocations may be left behind according to the concepts of Seeger [157]. This process of forming sub-boundaries is "dynamic recovery" (Rec. 2). It requires no thermal activation and leaves dislocations stored as subgrain boundaries (S4). The subgrain row structure developed in aluminum specimens tensile tested at room temperature, Figure 29, is taken as evidence for the operation of dynamic recovery.

In response to lattice bending, a portion of the dislocations generated may, by climb and glide, form additional subgrain boundary. This recovery process, polygonization

(Rec. 3), requires thermal activation for climb, and liberates heat in proportion to the reduction in the strain energy of the lattice. The tendency for both dynamic recovery and polygonization to occur are related to the stacking-fault energy of the metal. Metals, such as aluminum, with high stacking-fault energies, tend to recovery readily by both dynamic recovery and polygonization.

Still another fraction of the generated dislocations never form boundaries or precipitate in pre-existing boundaries. These dislocations are removed from the lattice by annihilation (Rec. 4).

During deformation, should the shearing of grain or subgrain boundaries be called for as described in the discussion of Section 4.1.2, additional dislocations from the lattice are precipitated in boundaries. The boundary shearing itself results in recovery (Rec. 5) because it reduces the strain energy of the lattice by absorbing dislocations into boundaries or by allowing for the annihilation of opposite dislocation segments. The net microstructural effect is a greater misorientation across that portion of the boundary which has sheared as observed by Rhines et al. [156]. If the boundary shearing is confined to the interior of the specimen, dislocations become stored (S4); however, if shearing produces surface steps, dislocations report out as external shape change and are removed from the system.

Recrystallization (Rec. 6) and grain growth (Rec. 7) eliminate boundary from the system; thus, dislocations stored in grain boundaries (S2), in subgrain boundaries (S3) and in grain and subgrain boundaries as the result of boundary shear (S4) are removed from the system. In both of these recovery processes, boundary surface sweeps through the lattice, leaving behind essentially undistorted crystal; therefore, dislocations in the lattice ahead of the sweeping boundary are assumed to be "absorbed" by the boundary. When a length of dislocation line is absorbed by a boundary, the boundary becomes altered by a change in position, a change in misorientation or a change in area, or by a combination of the three altering effects.

The rate at which the metal specimen deforms depends upon the rate at which dislocations move through the lattice and the rate at which dislocations are generated. As work hardening increases, dislocation generation becomes slowed as does the movement of dislocations. Recovery, offsetting the work hardening, has the tendency of increasing the rates of dislocation motion and generation. Dotted lines from the recovery block to the rate control block in Figure 117 indicate that it is the efficiency with which the recovery processes operate that controls the rates of lattice shear and dislocation generation.

One of the more significant aspects of the schematic representation concerns an increasing capability of the

specimen to recover as creep deformation proceeds into late second-stage and early third-stage creep. As subgrain boundaries increase in misorientation so that they may act as do ordinary grain boundaries with respect to boundary shearing, there is an increased capacity of the metal to recover by boundary shearing along the boundaries separating the rows of subgrains. The author believes that the rather long straight boundaries separating subgrain rows are more favored for shear than the boundaries separating the subgrains of the random morphology. Thus, the subgrain rows represent a greater recovery capability than does the random subgrain morphology. In turn, those creep conditions which favor the formation of subgrain rows favor an increased recovery capability.

4.3. The Microstructural Evolution with Respect to the Schematic Representation of Hot Deformation

The schematic representation of hot deformation has provided a framework within which the microstructural evolution of aluminum during high temperature creep may be discussed. It is important to realize from the outset that the quantitative metallographic results of Chapter III do not describe quantitatively the relative activities of the hot deformation processes, because the measurement of microstructural features cannot be readily interpreted in terms

of dislocation line lengths. For example, one may measure the area of subgrain boundary surface in a specimen, but it is not a measure of the dislocation line length associated with the subgrain boundary surface. The microstructural evolution as measured by quantitative metallographic techniques does, however, provide rather qualitatively some information about the relative importance of the several recovery processes. This information indicates how dislocation line length is stored within an aluminum specimen during creep.

4.3.1. The Strain Rate Versus the Rate of Formation of Subgrain Boundary Area

The analyses of strain rate and the rate at which subgrain boundary area forms during secondary creep, as given in Chapter III, have indicated that the two rates depend upon temperature and stress to a rather strikingly similar degree. This observation suggests that, during creep, the dislocation line length stored in sub-boundaries may be approximately the same as that which results in strain by forming shear steps at the external surface of the specimen.

A comparison between the length of dislocation line stored in subgrain boundaries after a given amount of creep and the length of dislocation line which produces shear steps at the surface can be made by using the rate equations to obtain the strain and the amount of subgrain boundary area after a given amount of secondary creep. These

calculations have been made in Appendix IX, for a specimen strained 24 hours in secondary creep at 200°C under an initial stress of 1,000 psi. Because the steady state rate equations for the strain and the formation of subgrain boundary area have been used for this calculation, the strain attained and the subgrain boundary area developed during primary creep are not given by the results of the calculations. In the calculations, several assumptions have been made regarding the external shear steps and the misorientation of the subgrain boundaries. These assumptions are:

1. Shear steps at the external surfaces are inclined at 45° to the tensile axis and are the result of pure edge dislocations only.
2. Sub-boundaries are composed of edge dislocations only.
3. The average misorientation across sub-boundaries is 5° of tilt.

While the above assumptions are not representative of the actual metallographic state of creep deformed specimens, they do allow "order of magnitude" calculations of dislocation line lengths to be made.

For a specimen strained in secondary creep for 24 hours at 200°C under an initial stress of 1,000 psi, the lengths of dislocation line which result in the strain, l_S, and which are "stored" in sub-boundaries, l_B, are

$l_s = 2.09 \times 10^6$ mm, and

$l_B = 1.648 \times 10^6$ mm, respectively.

A similar calculation was made, Appendix IX, using the measured values of strain and subgrain boundary area per unit area from specimen S1-4 strained in creep at 200°C under an initial stress of 1,000 psi for 95.78 hours. This calculation, because it is based upon the actual strain attained and the measured subgrain boundary area developed in creep, does reflect the effects of primary creep. The lengths of dislocation line which result in the strain, l_s, and which are stored in sub-boundaries, l_B, are

$l_s = 3.08 \times 10^6$ mm, and

$l_B = 1.08 \times 10^8$ mm, respectively.

The values given above indicate that the length of dislocation line stored in sub-boundaries is as great or greater than the length of dislocation line which results in strain. Then, in the creep of aluminum, the processes of dynamic recovery and polygonization are quite active. When other recovery processes such as dislocation annihilation, boundary shear, recrystallization and grain growth are considered, it is conceivable that only a minor fraction of the dislocation line length generated during deformation actually reports out of the specimen as strain.

4.3.2. Subgrain Boundary Behavior During Hot Creep

That the subgrain boundary area increases monotonically with time and strain indicates that the mean subgrain intercept continuously decreases during the course of secondary creep. It does not give any information about the real size of subgrains. On the other hand, the subgrain size based upon measurements made in scattered regions of the specimen where subgrains exist have shown the subgrain size to be constant during secondary creep. This sort of statement is misleading, because to say that the subgrain size is constant throughout secondary creep implies that the subgrain boundary area is also constant. It has been observed that not all of the grains form subgrains at the same time during secondary creep. For any given grain, it is not only the temperature and the stress under which creep occurs that determines when subgrains begin to form or their size. The additional effects of lattice bending which is dependent upon grain-to-grain constraints must also be taken into account. Within a given grain, the sharper the lattice bending the smaller should be the size of the subgrains formed and the greater the grain boundary area.

As more and more grains develop subgrains during secondary creep, the subgrain boundary area increases accordingly. If, at some point during secondary creep all of the grains have developed subgrains, then the subgrain

boundary area may remain constant or increase with further deformation, provided widespread recrystallization and grain growth do not occur. Results obtained from coarse-grained specimens tested at 200°C under an initial stress of 1,000 psi, Figures 53(e) and 56(e), indicate that the subgrain boundary area tends to become constant late in secondary creep. The last specimen in the series formed a neck, which suggests that the constancy of grain boundary area may be in some way linked to higher deformation rates through higher recovery rates. These higher recovery rates are presumed to be associated with shearing along subgrain row boundaries.

The subgrain boundary area may remain constant if dislocations continue to be "stored" within the subgrain boundaries. That is to say that the subgrain boundary area remains constant, but the misorientation across the sub-boundary continues to increase. Once the sub-boundaries have attained a sufficiently large misorientation, shear occurs along them under certain favorable conditions. As pointed out previously, shearing along boundaries is to be associated with the "storage" of additional dislocations within the boundary. Therefore, as long as the boundaries continue to "store" dislocations, recovery and deformation proceed.

It is believed that the onset of shearing along sub-boundaries, particularly along those separating subgrain

rows, represents an increase in the recovery rate which is sufficiently large to trigger the onset of tertiary creep. Consider, for example, that in a region of the gage length in a creep specimen the microstructure which has evolved during secondary creep, by virtue of the grain-to-grain constraints and the orientations of individual grains, is more favored for shear along the boundaries of subgrain rows than other regions of the gage length. Should shearing commence, the rate of recovery would increase, and, in turn, the rate of deformation would increase. Thus, the increased rate of deformation confined to a small region would tend to produce a neck. The neck, once formed, would result in an increase in the effective stress, and tertiary creep behavior would be established.

During the course of creep, it seems inconceivable that boundaries could indefinitely "store" dislocations and, in doing so, affect recovery. If a boundary had reached its "storage limit" (maximum misorientation), then dislocation pile-ups in the lattice could be removed in at least three ways. Namely, these are (1) the formation of new boundary surface, (2) shearing along the boundary through a layer of recovering material in which dislocation segments of opposite sign are annihilated and new subgrain boundary area is formed, and (3) migration of the boundaries through adjacent lattice.

The formation of new sub-boundary area has already been ruled out by the previous discussion, at least for late secondary and early tertiary creep where the subgrain boundary area is constant. However, if creep is carried far enough into the third stage, there is qualitative evidence that new subgrain boundary area is formed. Compare the photomicrographs of Figure 23(d) and (e), and note that the microstructure of the specimen extended to rupture, (e), has much smaller subgrains than that of the specimen extended to a strain of 0.176, (d).

The author considers that grain boundary shearing is capable of removing dislocation pile-ups from the lattice. Consistent with the concepts of Rhines et al. [156], and with the observations of this research, grain boundary shearing through a layer of recovering material adjacent to the boundary interface is believed to allow for the annihilation of dislocation segments of opposite signs and for the formation of new sub-boundary area. The presence of fine subgrains adjacent to grain and subgrain row boundaries is taken to be a manifestation of the shearing process. In effect, boundary shearing is a recovery process.

The migration of boundaries through the lattice, a process which is like in kind to recrystallization and grain growth, provides for the absorption of dislocations by the boundaries. The observation that grains do not elongate in the same proportion as does the boundary as a whole is

evidence that boundaries do migrate during creep. Additional comments concerning the migration of boundaries are given in Section 4.3.5.

The author is convinced that, in the case of aluminum, the development of subgrain rows constitutes the microstructural manifestation of "creep damage." It is the shearing along the boundaries separating the rows which triggers the onset of tertiary creep. Whether shearing occurs in such a way as to increase the misorientation of the boundary or by the process proposed by Rhines et al. [156] is of no consequence to the general behavior. The important aspect of the boundary shearing is that it represents recovery. And, it is an increased recovery rate which allows the more rapid deformation required to initiate tertiary creep. The significance of the subgrain rows is that their boundaries provide places for rapid recovery associated with boundary shearing.

4.3.2.1. The amount of boundary shear as related to subgrain morphology

In Section 4.2.2, it was pointed out that boundary shearing may favor the more or less straight boundaries separating subgrain rows rather than the boundaries separating the equiaxed subgrains of the random subgrain morphology. It seems more tenable that shearing could be more easily transmitted along a straight boundary than along a boundary which, at closely spaced intervals, sharply changes direction

through significant angles. This concept agrees with observations that dentate grain boundary serrations coincide with the boundaries separating subgrain rows rather than with the boundaries of equiaxed subgrains. If shear occurred to the same degree along the boundaries of equiaxed subgrains as it does along subgrain row boundaries, the question arises: Why are not dentate grain boundary serrations associated with equiaxed subgrains? The only tenable answer lies in the assumption that significant amounts of shear do not occur along the boundaries of equiaxed subgrains. It is believed that shearing may occur along these boundaries, but not to the extent that it does along the boundaries separating subgrain rows.

4.3.2.2. Grain boundary serrations in relation to subgrain morphology

Metallographic examinations of microstructures produced in aluminum by high temperature creep have shown that dentate grain boundary serrations are to be associated with subgrain rows. An indirect indicator of this association was found in the graphs of the fraction of grain boundary area which is serrated, $\tilde{S}_v/S_{v(GB)}$, plotted versus the fraction of grains containing subgrains, f_{SG}, subgrain rows, f_{SGR}, and the random morphology of subgrains, f_{SG}-f_{SGR} (Section 3.7.2.7 and Figure 63). Those conditions of creep which favor subgrain row formation also favor dentate grain boundary serrations. Corresponding graphs of fractions of grain boundary

areas which are serrated versus fractions of grains, Figure 63 (e1 and e2), show a reduction in the fraction of grains containing the random morphology of subgrains with increasing fractions of serrated grain boundary areas while the fraction of grains containing subgrain rows continues to increase. This observation is taken to mean that subgrain rows form in grains which were previously unsubgrained. Moreover, the possibility that the random subgrain morphology may transform to that of subgrain rows should not be ruled out. During the course of creep, should the grain-to-grain constraints become altered, grains containing equiaxed subgrains may have a tendency to form subgrain rows. "Grain growth" of subgrains to form subgrain rows in response to lattice bending is viewed as being a possible mechanism for this transformation. Should this "grain growth" occur, it would undoubtedly be a process in which the sweeping boundaries are strongly directed into the planes corresponding to those separating subgrain rows. The "rest positions" of the sweeping boundaries would depend primarily upon the nature of lattice bending. In their new positions, it is believed that these boundaries may be rather more complex in terms of dislocation composition than boundaries of subgrain rows formed in situ.

"Noncrystallographic" shear through the grains prior to the formation of subgrain rows is ruled out, because it is a general observation that subgrain rows exist prior to the formation of dentate grain boundary serrations.

4.3.3. The Change in Grain Boundary Area During Creep

Within the ranges of temperature and stress investigated in this research, aluminum, during the course of creep, exhibits a decrease in grain boundary area which is confined to the first few percent of strain. (Refer to Sections 3.7.2.2 and 3.7.2.3 and to Figures 52 and 53.) This decrease in grain boundary area is to be associated with grain growth. After the initial grain growth, the grain boundary area does not change significantly with further creep.

A series of coarse-grained specimens tested at 200°C under an initial stress of 1,000 psi did not exhibit the initial grain growth behavior. Surface effects are presumed to have "pinned" a large enough portion of the grain boundary network so that grain growth could not occur. Surface effects upon grain boundaries are also believed to be the underlying reason why the stable grain boundary area attained after the initial grain growth appears to be independent of the stress and temperature of creep testing. If the initial grain size had been very much smaller or the size of the creep specimens had been larger, it is expected that the grain boundary area would have decreased continuously during the course of secondary creep. Without the influence of surface effects upon the grain boundary network, it would be reasonable to believe that high temperatures and low stresses would favor grain growth.

The more rapid the deformation at any temperature, the more rapidly the subgrain boundary network develops. Once the subgrain boundary network becomes joined to the grain boundary network, the sweeping of grain boundary surfaces should be retarded. Therefore, high stresses should favor a more stable grain size. That such an effect was not observed in this research is attributable to surface effects upon the grain boundary network.

While the results of this research are not conclusive regarding the role of grain growth during secondary creep, the evidence suggests that, in aluminum, it may contribute significantly to recovery during hot creep. Certainly during the first few percent of strain, where the grain boundary area is diminished, on the average, by one-third, grain growth must be considered as an important recovery process.

4.3.4. Recrystallization During Creep

Microstructurally, newly formed grains in hot deformed metals are those which are free of lattice bending and subgrains. In the case of metallographic specimens of aluminum which have been prepared by anodizing, lattice bending is manifested by a continuous change in shading as viewed under polarized light rather than the sharp changes associated with subgrain boundaries. Early in creep a significant fraction of the grains are free of lattice bending and subgrains. These grains, however, are not considered as

recrystallized grains, rather, they are grains which have not yet become sufficiently deformed for lattice bending to be microscopically observable.

In some specimens which were creep tested to rupture, small new grains were found just adjacent to the fracture. It is concluded, therefore, that recrystallization can be neglected as a recovery process in aluminum during primary and secondary creep. Only when the rate of deformation is very great, as in the neck of a creep specimen just prior to fracture, should recrystallization even be considered as a significant recovery process.

Because creep specimens tested to rupture were not quenched under load, it is entirely possible that the observed new grains might have formed within a very short time just following the rupture event. The time allotted for recrystallization in ruptured specimens corresponds to the time interval between rupture and quenching which in all cases was less than 0.5 seconds.

4.3.5. The Elongation of Grains During Creep

The grain boundary anisotropy factor, e_g, derived by Rachinger [127], was used in this research as a measure of the elongation due to creep of the interior grains of creep specimens. When the anisotropy factor is plotted versus the strain, a slope of unity indicates that the grains on the average changed shape in the same manner as did the overall specimen during deformation. A slope of less than unity

indicates that the grains did not elongate as much as did the specimen as a whole. Conversely, a slope greater than unity indicates that the grains elongated more than the specimen as a whole. Rachinger [127] found in the creep of aluminum that for interior grains the slope of the anisotropy factor versus strain was much less than unity and attributed the difference to a contribution of grain boundary sliding to the total elongation.

From a statistical point of view, the results of this research regarding the elongation of grains during creep are unclear as to their meaning, Sections 3.7.2.8 and 3.7.2.9. However, it appears that, at the higher temperatures and lower stresses, Figure 64 (a, b and c), the grains elongate to a smaller extent than at 200°C, Figure 64 (d, e and f). If it is correct that deformation at high temperatures occurs only as the results of grain elongation and grain boundary shearing, then, according to the above observation, the contribution of grain boundary shearing to the total deformation is greater for the higher temperatures and the lower stresses. Such a conclusion means that the recovery process associated with grain boundary shearing is greater the higher the temperature and the lower the stress, at least during secondary creep. This statement is consistent with the general results reported in the literature, Section 1.2.7.

The author wishes to point out that the grain boundary anisotropy factor gives no direct information about the shearing along subgrain boundaries. However, it is interesting to note in Figure 63(e), where the change in grain boundary anisotropy is plotted versus time for creep tests at 200°C under a stress of 1,000 psi, that for the coarse-grained material there is a significant upswing in the curve between 100 and 200 hours. This upswing coincides with the onset of tertiary creep and the appearance of dentate grain boundary serrations, Figure 26(c). It is, therefore, tempting to connect the elongation of grains with subgrain rows and to shearing along the boundaries separating the rows. Wood et al. [67] have already suggested grains may change shape by shearing along subgrain boundaries; however, the connections among subgrain rows, shearing along their boundaries, dentate grain boundary serrations and the onset of tertiary creep are new concepts which have developed out of this research.

It has been pointed out [117] that, during the course of hot deformation, the grains may remain equiaxed if there is a sufficient amount of grain boundary migration concurrent with the deformation. The author finds it difficult to believe that either process, grain boundary shearing or boundary migration, alone could maintain equiaxedness of the grains during creep, since any alteration of the grain boundary network by boundary shearing would require some boundary migration in order to maintain contiguity of the network.

4.3.6. Low Temperature Precreep in Relation to the Processes of Hot Deformation

Low temperature precreep, as described in Section 3.8, causes an increase in the steady state creep rate during subsequent creep testing at a higher temperature. By increasing the amount of deformation in the precreep treatment, either by longer treatment or by increasing the stress, the effect of the low temperature precreep upon the secondary creep rate at the higher temperature is enhanced. There is an indication in the grain boundary area data which suggests that new grains appear when the temperature is raised following precreep, provided the precreep deformation has been sufficiently severe. That is to say, new grains appear at the higher temperature when the stored energy due to precreep is great enough.

These microstructural parameters which are indicators of recovery processes are all affected in such a way by low temperature precreep as to indicate that low temperature precreep speeds up recovery during subsequent creep testing at a higher temperature. For example, the rates of formation of subgrain boundary area and of grain boundary serrations at the high temperature are both increased by low temperature precreep. Changes in the fractions of grains containing subgrains, f_{SG}, and subgrain rows, f_{SGR}, are also enhanced by precreep.

From the evidence given in Chapter III, it is clear that low temperature precreep treatments enhance at least

those recovery processes which are associated with substructure. While the results of the precreep experiments do not give any specific answers as to why the precreep treatments should enhance recovery, it seems as though a "pattern" is laid down during precreep which determines the rates of recovery during subsequent testing at a higher temperature. If such a proposal is valid, it again brings to mind the concept of creep damage [44,45]. From the metallographic examinations of precreep specimens, it is evident that creep damage or the "pattern" of recovery established during precreep may be essentially unobservable by the conventional techniques of optical metallography. The results of the first precreep experiment in which there was little microstructural change during precreep, Section 3.8.2, support this statement.

The grain boundary serrations produced in the precreep experiments were some of the most sharply dentate ones observed in the entire course of the research; hence, it is tempting to connect creep damage to dentate serrations and subgrain rows. It is particularly tempting, upon the basis of the microstructures developed during precreep, to connect creep damage to a metallographically unobservable structural feature which has the ability to enhance the formation of subgrain rows. Intuitively, it seems unreasonable that such a structural feature could be described in terms of a dislocation structure within one grain, or even within a number

of separate grains. Certainly, grain boundaries must play a role in creep damage; therefore, the deformation of a polycrystalline metal leading to creep damage must be considered in terms of an aggregate of grains with a contiguous grain boundary network.

The precreep experiments make abundantly clear that the microstructural changes which occur within the first few percent of strain during creep may have a pronounced effect upon the further progress of creep.

CHAPTER V

CONCLUSIONS

At the outset, the objectives of this research were primarily concerned with ascertaining what relations exist between the formation of dentate grain boundary serrations and the mechanisms involved in the high temperature creep of aluminum. A detailed study of the microstructural evolution during the course of hot creep has yielded evidence which connects the formation of dentate serrations to "non-crystallographic" shear across grain boundaries. The shear is non-crystallographic in that it follows sub-boundaries rather than definite crystallographic slip systems. The major conclusions reached as a result of this research are listed in the following statements.

1. During the high temperature creep of polycrystalline aluminum, the individual grains deform inhomogeneously. The inhomogeneity of deformation, observed by the patchy appearance of the substructure developed during creep, results from the several deformation responses of each grain to several different deformation commands. Each deformation command received by a grain is the result of the passage of shear across a common boundary interface with a conjoint neighbor. The differences among the deformation commands require a grain to respond simultaneously in several different ways.

2. In the response of a grain to several different deformation commands, its lattice becomes rumpled by alternate bends in two or more directions. Polygonization concurrent with deformation results in the formation of intersecting planes of sub-boundaries. These sub-boundary planes are most often spatially oriented coincident with directions of high resolved shear stress, and they separate subgrain rows. Because the sub-boundaries form in response to alternate lattice bending, the resulting subgrain rows alternate in crystallographic orientation.

3. As initially formed, the boundaries separating subgrain rows represent rather small angles of misorientation between adjacent subgrain rows. With the progress of deformation, this misorientation increases until the sub-boundaries are no longer distinguishable from ordinary grain boundaries; therefore, they become subject to boundary shearing.

4. Macroscopic shearing occurs along the boundaries separating subgrain rows. The shearing is cooperative across grain boundaries, and as a consequence, leaves the boundary in a rather roughly stepped configuration. In a two-dimensional metallographic surface prepared by cutting obliquely through subgrain rows and roughly stepped grain boundary surfaces, the grain boundaries exhibit a dentate form.

5. Shearing along the boundaries separating subgrain rows is viewed as a recovery process. Because shearing and the formation of dentate grain boundary serrations commence concurrently with the onset of tertiary creep, it is proposed that the additional recovery associated with sub-boundary shearing contributes to an accelerating creep rate and the onset of third-stage creep.

6. Calculations based upon the rate at which subgrain boundary area increases with time indicate that the length of dislocation line which is stored in sub-boundaries is as great or greater than the length of dislocation line which reports out of the specimen as an external shape change. Considering that recovery processes other than polygonization are operative

during creep, the length of dislocation line which is responsible for external shape changes is believed to be only a minor portion of total length of dislocation line generated.

CHAPTER VI

FUTURE WORK

The observed relations among the formation of dentate grain boundary serrations, sub-boundary shear and the onset of tertiary creep, together with the concept that boundary shearing is, in effect, a high temperature recovery process, provide a basis for further research related to the microstructures developed during the course of high temperature creep. Aside from the obvious extensions of this research to other pure metals, there are several subject areas open for investigation which the author believes might be most fruitful in terms of practical importance. Suggestions for research in some of these areas are given briefly in the following sections.

6.1. The Kinetics of Shearing Along Subgrain Boundaries

Rhines et al. [156] have observed that grain boundary shearing occurs spasmodically, that the overall rate of shearing at constant temperature and stress is related to the difference in the orientation between conjoint grains and that the overall rate of shearing diminishes with the

amount of shear. It is suggested that a similar study related to the shearing behavior of sub-boundaries be made. Measurements of the shear displacements of the sub-boundaries on the surfaces of deforming specimens might be best carried out in a specially designed deformation apparatus fitted into the specimen chamber of a scanning electron microscope. The kinetic information from such a study is prerequisite to the other suggested studies.

6.2. A Correlation Between the Onset of Tertiary Creep and Microstructure

Previous investigations [44,45] and the observations of this research have suggested that there exists more than a casual correlation between the microstructure developed during the course of secondary creep and the onset of third-stage creep. A very careful investigation needs to be made to establish the coincidence between the beginning of sub-boundary shearing and the onset of third-stage creep. For the establishment of this correlation, exceptionally accurate and continuous measurements of the strain as a function of time would be required in order to determine the beginning of an accelerating creep rate. Further, it would be necessary to evaluate microstructures just prior to, at the initiation of and just after the initiation of the accelerating creep rate. Creep specimens should be quenched under load to preserve the microstructures for metallographic evaluation.

6.3. The Effects of Minor Alloying Additions to Aluminum Upon the Kinetics of Sub-boundary Shearing

If the overall rate of shearing along sub-boundaries could be controlled in aluminum by minor alloying additions, the practical implications may be of significance in (1) the development of alloys with superior creep resistance and (2) the development of alloys which may be hot deformed to very large strains.

By reducing the overall rate of sub-boundary shearing, the onset of tertiary creep may be significantly delayed. In order to produce an alloy which exhibits a delay in the beginning of third-stage creep, alloying additions should be capable of attenuating the rate of sub-boundary shearing. The work of Nemy and Rhines [45] on the creep of aluminum 5052 alloy suggests that solution hardening leads to the formation of internal cavities during creep. This is particularly the case when the applied stress is small. In selecting alloying additions large solution hardening effects should be avoided, lest the creep resistance be lowered by the formation of internal cavities. Whether an alloying addition can be found which will retard sub-boundary shearing without promoting cavity formation is a critical question.

By increasing the overall rate of sub-boundary shearing, and hence the rate of recovery, it may be possible to obtain larger than ordinary amounts of deformation at elevated

temperatures. In this case, the promotion of both the overall rate of sub-boundary shearing and polygonization would be a desirable result. The objective of this investigation would be to discover an alloying addition which would not retard polygonization significantly but would increase the overall rate of sub-boundary shearing.

It is suggested that, once the kinetics of sub-boundary shearing in high purity aluminum have been established, additional studies be initiated to discover the effects of small alloying additions upon (1) the degree of polygonization during the hot deformation of aluminum and (2) the overall rate of sub-boundary shearing. As previously suggested, employment of the scanning electron microscope would be essential to the second part of this investigation.

As a first approach, the effects of additions of the common alloying elements -- copper, magnesium, manganese, silicon and zinc -- should be investigated. It is suspected that small additions of these elements, on the order of a few hundredths of a percent, might be most effective in producing the desired effects.

Because nickel and its alloys are of general applicability in high temperature environments, the above investigations should be extended to include a study of the effects of minor alloying additions upon microstructural evolution during the hot creep of nickel. Nickel, like aluminum, has a high stacking-fault energy; thus, results similar to those obtained for aluminum may be expected.

6.4. The Effects of Subgrain Structures Produced by Creep Upon the Mechanical Properties at Ordinary Temperatures

The fine-grained microstructures produced in aluminum by large amounts of creep strain may impart useful mechanical properties to the metal for application at and below ordinary temperatures. It is presumed that the high angle sub-boundaries produced by creep might have a strength increasing effect similar to that of refining the grain size. A preliminary study should be undertaken to determine whether the microstructures produced by high temperature creep result in significantly improved mechanical properties at ordinary temperatures. Should higher low temperature strengths be obtained by deformation under creep conditions, the forming of metals such as aluminum and nickel by similar techniques may be of importance to specialized applications where the high purity of the metal is a primary consideration.

APPENDICES

APPENDIX I

EQUATIONS FOR THE TIME DEPENDENCE OF STRAIN DURING PRIMARY CREEP

1. de Lacombe [28]

$$\varepsilon = a + bt^m + ct^n \tag{I-1}$$

2. Andrade [25]

$$\ell = \ell_o(1 + \beta t^{1/3})e^{kt} \tag{I-2}$$

3. Garofalo [27]

$$\varepsilon = \varepsilon_o + \varepsilon_t(1 - e^{-rt}) + \dot{\varepsilon}_s t \tag{I-3}$$

4. Cottrell and Aytekin [26]

$$\varepsilon = a + bt^{1/3} + ct \tag{I-4}$$

Definition of terms:

ε = strain

ε_o = strain after instantaneous creep

$\dot{\varepsilon}_s$ = steady state creep rate

ε_t = strain at time t

t = time

ℓ = length of specimen at time t

ℓ = initial length of specimen

m = a constant between zero and unity

n = a constant slightly greater than unity

a, b, c, β, k and r = constants.

APPENDIX II

SOLUTIONS FOR ELECTROPOLISHING AND ANODIZING

1. Anodizing Solution

Hydrofluoric acid	34.6 ml
Boric acid (crystals)	13.6 gms
Water (distilled)	to make 1 liter

Cathode: graphite (Cl^- free)
Voltage (open circuit): 20 volts
Temperature: 25°C
Time: 30 seconds to 1 minute
Agitation: solution should be stirred gently

2. Electropolishing Solution #1

Phosphoric acid (ortho)	136 ml
Sulfuric acid	22 ml
Chromium trioxide (crystals)	26 gms
Water (distilled)	7 ml

Cathode: Type A.I.S.I. 304 stainless steel
Voltage (open circuit): 10-15 volts
Temperature: 85°-95°C
Agitation: solution should be stirred rapidly

3. Electropolishing Solution #2

Phosphoric acid (ortho)	70 ml
Water (distilled)	10 ml
Ethylene glycol	15 ml
Methoxyethanol	5 ml

Cathode: Type A.I.S.I. 304 stainless steel
Current Density: 0.75-1.00 amps/in^2
Temperature: 25°C (solution becomes heated with use and should not be used if temperature exceeds 60°C)
Agitation: solution should be stirred rapidly

APPENDIX III

THE PHOTOENGRAVING PROCESS

1. Electropolish the specimen by either of the two methods given in Appendix II. Wash the specimen thoroughly in cold tap water and dry in cold air blast.

2. Immediately after electropolishing, apply Kodak KMER Photoresist which has been thinned with three parts of Kodak KMER Thinner to one part KMER Photoresist. Apply Photoresist by pouring thinned solution on surfaces of specimen and handing the specimen in a vertical position so that excess solution may run off.

3. Allow Photoresist to dry in still air for 30 minutes.

4. Prebake Photoresist coating at 100°C for 10 minutes.

5. Expose the film grid for 12 seconds using a 650 watt quartz iodide lamp placed 14 inches from specimen.

6. Develop Photoresist in Kodak KMER Developer for 2 minutes.

7. Rinse in running tap water for 1 minute.

8. Dry specimen in cold air blast, then in still air for 3-5 minutes.

9. Postbake Photoresist at 100°C for 10 minutes.

10. Etch grid either electropolishing solution #1 at 4 volts for 2 minutes or in electropolishing solution #2 at 6 volts for 30 seconds to 1 minute.

APPENDIX IV

LIST OF SPECIMENS AND DEFORMATION CONDITIONS

Table IV-1

Specimens Creep Tested Under Conditions of Constant Load and Constant Temperature

Specimen Number	Stress (psi)	Temperature (°C)	Time (hrs.)	Strain
53-4	750	425	∿0.07	R*
53-2	400	425	∿3.00	R
53-1	250	425	∿0.60	R
53-6	150	425	4.00	0.016
53-3	150	425	7.17	0.032
53-5	150	425	16.17	0.128
53-8	500	350	∿2.00	0.500 R
53-12	400	350	8.83	0.288
53-10	250	350	4.17	0.024
53-9	250	350	10.00	0.064
53-7	250	350	24.00	0.120
53-17	800	275	∿8.00	R
53-18	800	275	5.37	0.176
53-13	400	275	4.00	0.016
53-16	400	275	10.02	0.016
53-15	400	275	24.02	0.032
53-19	800	200	4.03	0.024
53-24	800	200	10.92	0.024
53-21	800	200	24.05	0.032
S1-1	1,000	200	11.85	0.025
S1-2	1,000	200	24.05	0.049
S1-4	1,000	200	95.78	0.098
S1-5	1,000	200	191.90	0.148
S1-7	1,000	200	24.00	0.049
S1-8	1,000	200	96.28	0.131
S1-9	1,000	200	192.37	0.330

Table IV-1 (continued)

Specimen Number	Stress (psi)	Temperature (°C)	Time (hrs.)	Strain
S3-22	1,200	200	10.43	0.072
S3-20	1,200	200	23.47	0.096
S3-23	2,407	200	0.80	0.48 R
S3-30	4,311	132	1.00 min.	R
S3-25	4,330	136	2.00 min.	R
S3-28	4,790	141	0.33 min.	R
S3-29	4,792	128	1.75 min.	R

*R indicates rupture of specimen.

Table IV-2

Specimens Tested at Constant Strain Rate

Specimen Number	Strain Rate ($min.^{-1}$)	Temperature (°C)	Elongation to Fracture, ε_F (%)
S4-1	1.33×10^{-3}	32	54.67
S4-4	1.33×10^{-2}	32	42.67
S4-5	5.33×10^{-2}	32	49.67
S4-6	1.33×10^{-1}	32	54.00
S4-3	1.33	32	41.33
S4-2	3.33	32	30.67
S4-7	2.66×10^{-2}	24	44.67
S4-13	5.33×10^{-2}	24	42.00
S4-11	8.33×10^{-2}	24	47.34
S4-8	8.33×10^{-2}	24	44.67
S4-9	1.33×10^{-1}	24	--
S4-12	1.33×10^{-1}	24	44.67
S4-18	5.33×10^{-3}	0	45.33
S4-21	1.33×10^{-2}	0	36.00
S4-15	3.33×10^{-2}	0	42.67
S4-20	5.33×10^{-2}	0	46.00
S4-22	1.33×10^{-1}	0	42.00
S4-23	3.33×10^{-1}	0	35.33
S4-17	8.33×10^{-1}	0	38.66
S4-14	1.33	0	34.67
S4-16	1.67	0	41.33
S4-24	3.33	0	42.00

Table IV-3

Specimens Creep Tested Under Conditions of Variable Load and Variable Temperature

Specimen Number	Stress (psi)	Temperature (°C) [Time] (hrs.)
S5-5	1,000	100 [24], 205 [19], 354* [R]**
S5-6	500	105 [27], 207 [21], 316 [6]
S5-7	650	103 [10], 217 [10], 102 [10], 216 [10], 360* [R]*
S5-8(SA)***	500	116 [24], 228 [25], 348* [R]**
S5-9(SA)***	500	105 [23], 214 [26], 340 [9]
S5-10	350	227 [12], 355 [6], 224 [9], 342 [9], 221 [10], 341 [18], Cycle 3 times between 225 and 330 at 45 minute intervals.
S5-11	450	280 [24]
S5-12	450	198 [24]
S5-13	450	204 [24], 25 [96]****, 205 [12], 329 [24]
S5-31	417	217 [24], 338 [10]
S5-32	500	214 [48], 336 [10]
S5-34	500	219 [24]
S5-36	500	217 [24], 335 [3R]**
S5-37	500	338* [R]**
S5-38	417	330 [10]
S5-39	834 417	217 [24] 330 [4R]**
S5-40	417	212 [169], 332 [8R]**
S5-41	834	214 [24]

Table IV-3 (continued)

Specimen Number	Stress (psi)	Temperature (°C) [Time] (hrs.)
S5-42	834	208 [24] 342* [1]
S5-43	417	210 [168]
S5-44	834 417	211 [24] 312 [2]
S5-45	417	210 [168], 332* [2]

*The temperature did not reach equilibrium following the temperature change prior to the end of the test.

**R indicates that the specimen ruptured.

***[SA] indicates that the specimen was strain annealed prior to testing to produce a very large grain size.

****The test was interrupted because of a malfunction of the photographic measuring camera. The specimen remained loaded for 96 hours at room temperature.

APPENDIX V

WORK SHEET FOR THE CALCULATION OF STATISTICAL TOLERANCE LIMITS ON THE MEAN OF N_L

Area	Number of Intercepts	Intercepts per unit length of test line	
(i)	$N_{(i)}$	$N_{L(i)} = N_{(i)}/L$	$(N_{L(i)} - \hat{N}_L)^2$
1	$N_{(1)}$	$N_{L(1)}$	$(N_{L(1)} - \hat{N}_L)^2$
2	$N_{(2)}$	$N_{L(2)}$	$(N_{L(2)} - \hat{N}_L)^2$
3	$N_{(3)}$	$N_{L(3)}$	$(N_{L(3)} - \hat{N}_L)^2$
.	.	.	.
.	.	.	.
.	.	.	.
n	$N_{(n)}$	$N_{L(n)}$	$(N_{L(n)} - \hat{N}_L)^2$

$\hat{N}_L$ = mean value of $N_L = \sum_{i=1}^{n} N_{L(i)}/n$

s = sample standard deviation $= \left(\frac{\sum_{i=1}^{n} (N_{L(i)} - \hat{N}_L)^2}{n - 1} \right)^{1/2}$

tolerance limit $= \frac{s}{\sqrt{n}} \frac{t\alpha}{2}, \nu$

$\frac{t\alpha}{2}, \nu$ = the percentage point of the t-distribution at $\frac{\alpha}{2} = 0.025$ and $\nu = n-1$.

APPENDIX VI

FORTRAN IV PROGRAM FOR CALCULATING THE MEAN VALUES OF N_L AND THE TOLERANCE LIMITS

```
      DIMENSION F(200),X(200),SUM(200),DIFF(200),SUM2(200),
     1S(5),TCAL(5)
   10 READ(5,11) NOMORE,SERIES,SPEC,TEST,COUNT
   11 FORMAT(2X,I1,2X,I2,2X,I2,2X,I1,2X,I1)
      IF (NOMORE.EQ.1) GO TO 200
      READ(5,20) N,Y,T
   20 FORMAT(I5,F6.3,F6.3)
      READ(S,22) (F(I),I=1,N)
   22 FORMAT(40F2.0)
      DO 30 I=1,N
      X(I)=F(I)/Y
   30 CONTINUE
      SUM(1)=X(1)
      DO 40 K=2,N
      SUM(K)=SUM(K-1)+X(K)
   40 CONTINUE
      XBAR=SUM(N)/N
      DO 50 IJ=1,N
      DIFF(IJ)=(X(IJ)-XBAR)**2
   50 CONTINUE
      SUM2(1)=DIFF(1)
      DO 60 IK=2,N
      SUM2(IK)=SUM2(IK-1)+DIFF(IK)
   60 CONTINUE
      S(1)=SQRT(SUM2(N)/(N-1))
      XX=N
      TCAL(1)=T*S(1)/SQRT(XX)
      WRITE(6,70) NOMORE,SERIES,SPEC,TEST,COUNT
   70 FORMAT(2X,I1,2X,'SERIES   ',I1,'-SPEC   ',
     12X,'TEST=  ',I1,2X,'COUNT=  ',I1//)
      WRITE(6,75) N,Y,T
   75 FORMAT(2X,'N= ',I5,2X,'Y= ',F5.3,2X,'T= ',F5.3//)
      WRITE(6,80)
   80 FORMAT(5X,'XBAR= ',F8.3)
      WRITE(6,90) S(i)
   90 FORMAT(5X,'S= ',F8.3)
      WRITE(6,100) TCAL(i)
  100 FORMAT(5X,'TCAL= ',F8.3///)
      GO TO 10
  200 STOP
      END
```

NOTE: N = number of areas

Y = length of test line

$T = t_{\frac{\alpha}{2}}$,

XBAR = $\hat{N}_L$ = mean of N_L

S = standard deviation

TCAL = tolerance limit = $\frac{s}{\sqrt{n}} t_{\frac{\alpha}{2}}$, ν

APPENDIX VII

QUANTITATIVE METALLOGRAPHIC DATA FOR SPECIMEN S3-12

Table VII-1

Lineal Intercept Counts

Longitudinal Area	$N_{(TOT)}$	$\bar{N}$	$\tilde{N}$	$N_{(GB)}$	$N_{(SGB)}$
1	7	0	2	2	5
2	8	1	2	3	5
3	9	1	2	4	5
4	11	0	2	2	9
5	16	0	1	1	15
6	10	0	3	3	7
7	8	0	1	1	7
8	10	1	1	2	8
9	7	2	1	3	4
10	15	1	3	4	11
11	12	3	0	3	9
12	12	2	0	2	10
13	9	3	0	3	6
14	14	0	4	4	10
15	10	1	1	2	8
16	8	0	0	0	8
17	8	1	1	2	6
18	11	1	1	2	9
19	10	0	2	2	8
20	10	0	0	0	10
21	12	0	1	1	11
22	13	0	2	2	11
23	12	1	1	2	10
24	7	1	0	1	6
25	10	3	5	8	2
26	12	1	1	2	10
27	11	0	2	2	9
28	9	3	2	5	4
29	7	5	0	5	2
30	14	0	2	2	12
31	10	1	0	1	9
32	11	2	0	2	9
33	11	0	1	1	10

Table VII-1 (continued)

Longitudinal

Area	$N_{(TOT)}$	$\bar{N}$	$\tilde{N}$	$N_{(GB)}$	$N_{(SGB)}$
34	10	1	0	1	9
35	12	1	2	3	9
36	11	3	3	6	5
37	12	1	1	2	10
38	12	0	2	2	10
39	11	1	0	1	10
40	10	1	1	2	8
41	6	0	1	1	5
42	8	0	0	0	8
43	8	1	2	3	5
44	9	1	2	3	6
45	9	2	1	3	6
46	15	1	2	3	12
47	12	0	4	4	8
48	9	2	0	2	7
49	9	2	1	3	6
50	7	0	0	0	7

Transverse

Area	$N_{(TOT)}$	$\bar{N}$	$\tilde{N}$	$N_{(GB)}$	$N_{(SGB)}$
1	7	0	1	1	6
2	10	0	1	1	9
3	11	2	1	3	8
4	14	0	4	4	10
5	11	1	0	1	10
6	12	0	3	3	9
7	12	1	0	1	11
8	11	1	1	2	9
9	12	0	2	2	10
10	6	1	0	1	5
11	8	2	0	2	6
12	10	2	2	4	6
13	13	1	2	3	10
14	7	2	0	2	5
15	10	2	1	3	7
16	11	1	0	1	10
17	10	2	1	3	7
18	11	0	2	2	9
19	10	0	1	1	9
20	12	0	1	1	11
21	10	0	2	2	8
22	6	1	0	1	5

Table VII-1 (continued)

Transverse Area	$N_{(TOT)}$	$\bar{N}$	$\tilde{N}$	$N_{(GB)}$	$N_{(SGB)}$
23	11	3	1	4	7
24	10	0	2	2	8
25	12	1	2	3	9
26	11	1	0	1	10
27	11	2	0	2	9
28	11	2	0	2	9
29	13	0	3	3	10
30	10	1	0	1	9
31	11	1	0	1	10
32	10	1	1	2	8
33	11	2	1	3	8
34	11	3	2	5	6
35	10	2	0	2	8
36	11	0	1	1	10
37	14	1	5	6	8
38	11	0	3	3	8
39	12	1	3	4	8
40	12	1	3	4	8
41	11	1	1	2	9
42	9	0	3	3	6
43	7	0	1	1	6
44	11	1	1	2	9
45	9	1	1	2	7
46	10	0	2	2	8
47	15	0	2	2	13
48	10	1	3	4	6
49	13	0	2	2	11
50	14	3	0	3	11

Table VII-2

Counts of Grains Containing Subgrains and Subgrain Rows, and the Angles Between Subgrain Rows and the Tensile Axis

Grain	Count	Grain	Count	Grain	Count
1	X	35	X	68	X
2	X	36	X	69	X
3	X	37	X	70	X
4	X	38	X	71	38
5	X	39	X	72	X
6	X	40	X	73	X
7	X	41	X	74	X
8	X	42	X	75	X
9	X	43	X	76	X
10	X	44	X	77	35
11	X	45	X	78	X
12	X	46	X	79	X
13	51	47	X	80	X
14	X	48	X	81	36
15	X	49	52	82	X
16	39	50	X	83	X
17	X	51	X	84	X
18	X	52	43	85	X
19	X	53	X	86	62
20	X	54	X	87	44
21	X	55	X	88	X
22	X	56	X	89	X
23	X	57	X	90	X
24	38	58	X	91	X
25	X	59	X	92	X
26	X	60	X	93	X
27	X	61	X	94	X
28	44	62	X	95	X
29	40	63	X	96	42
30	X	64	X	97	X
31	X	65	X	98	X
32	X	66	X	99	X
33	X	67	X	100	49
34	X				

NOTE: X indicates subgrains. An integer indicates subgrain rows and the angle (°) the rows make with the tensile axis.

Table VII-2 (continued)

Totals: 0 grains without subgrains
86 grains with subgrains
14 grains with subgrain rows

$f_{SG} = \frac{100}{100} = 1.00$

$f_{SGR} = \frac{14}{100} = 0.14$

$f_{SG}-f_{SGR} = 1.00-0.14 = 0.86.$

Distribution of angles between subgrain rows and tensile axis:

Angles (°)	Number of Grains
0-5	0
6-10	0
11-15	0
16-20	0
21-25	0
26-30	0
31-35	1
36-40	5
41-45	4
46-50	1
51-55	2
56-60	0
61-65	1
66-70	0
71-75	0
76-80	0
81-85	0
86-90	0

APPENDIX VIII

A GEOMETRIC CONCEPT OF GRAIN BOUNDARIES

A quite satisfactory concept of grain boundaries which provides the details of grain boundary surface geometry can be based upon the coincidence of the mating surfaces of two conjoint grains. For the purposes of this discussion, a grain boundary may be defined as a surface, the two sides of which are distinguishable by differences in the crystallographic orientations between the conjoint grains and between each grain and the boundary interface.

A grain boundary can be formed, in principle, in a single crystal by twisting and/or bending the crystal at a sufficiently high temperature to form only a single boundary. For a boundary to be formed by twisting alone, the boundary interface must be coincident with a slip plane. Schematically, this form of boundary is shown in Figure VIII-1, in which one portion of a crystal is rotated through an angle, ρ, about an axis normal to a slip plane. The other forms of grain boundaries involve single or multiple shearing of the conjugate grains to form their mating surfaces. These boundaries are best described by first considering only one of a conjoint pair of grains and its orientation relation

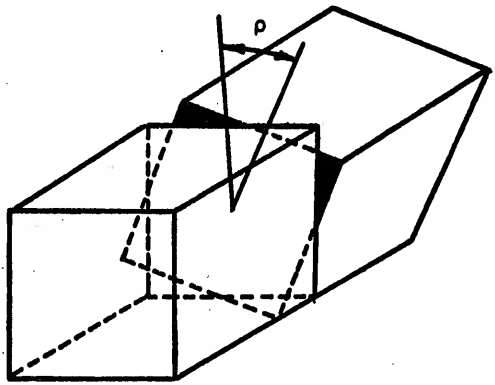

Figure VIII-1. Twist boundary formed by rotating one-half of a crystal with respect to the other through an angle, ρ. The plane of the boundary interface is coincident with a slip plane which is common to both crystal halves.

to the boundary interface. In Figure VIII-2, a tilt of a two-dimensional grain is formed by first shearing the grain to produce a tilt angle, θ, between the line G-G and the boundary B-B, then by rotating the grain through an angle, θ, to bring the line G-G into coincidence with the boundary. When two such grains go through a similar process in opposite senses, the result is a simple symmetrical tilt boundary as shown in Figure VIII-3.

In three dimensions the orientation of each conjoint grain with respect to the boundary interface may be represented by a single tilt, by a combination of two tilts or by a combination of two tilts and a skew. The possible single tilts of one grain of a conjoint pair with respect to the boundary interface are shown schematically in Figure VIII-4. If the plane of the boundary interface corresponds to the xz-plane in Figure VIII-4, then the sketches (a) and (b) correspond to angular tilts of θ and ϕ with respect to the boundary. The sketch (c) represents a skew through an angle, δ, about the y-axis which is normal to the boundary interface. This letter case can occur only if the boundary coincides with a slip plane.

Both twist boundaries and skew boundaries require that the boundary plane be coincident with a slip plane. It is necessary, therefore, to make a distinction between the two. A twist boundary can be produced by two orthogonal shears of equal magnitude in the plane of the boundary, Figure

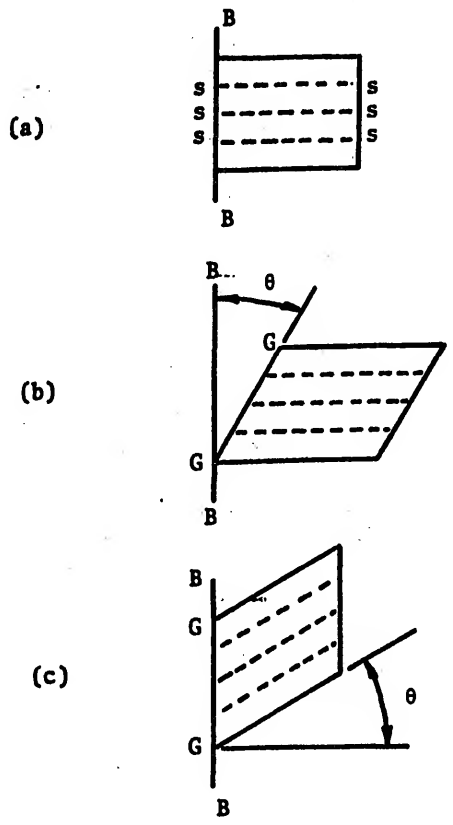

Figure VIII-2. Two-dimensional grain sheared to form a tilt orientation with respect to the plane of the boundary interface. An unsheared grain (a) is sheared along the slip directions, S-S, producing a tilt and increasing the length of its mating line, G-G, (b). The grain is then rotated counter-clockwise through an angle, θ, to bring the mating line, G-G, in to coincidence with the boundary interface, B-B, (c).

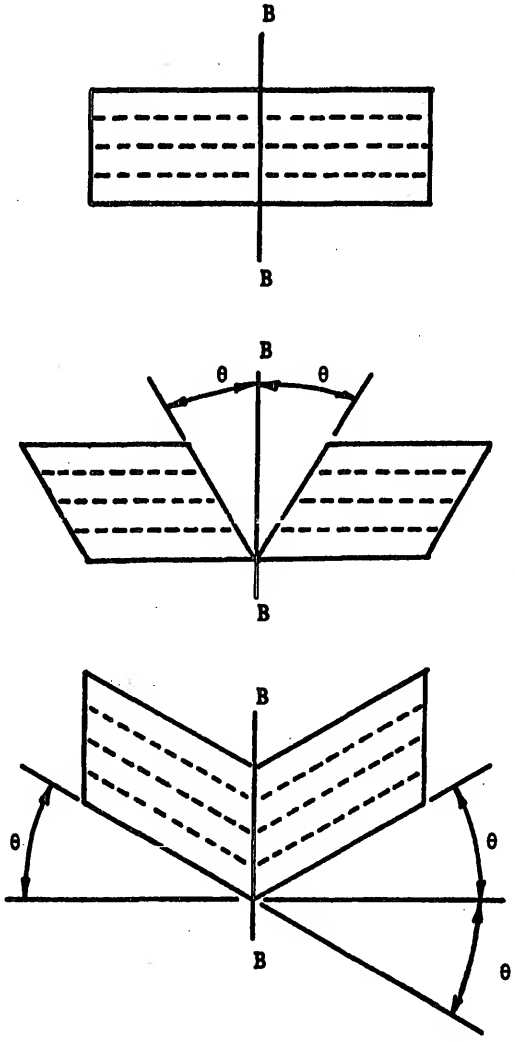

Figure VIII-3. The formation of a simple tilt boundary by joining two grains which have been sheared oppositely. Opposing but equal tilts with respect to the boundary interface are produced.

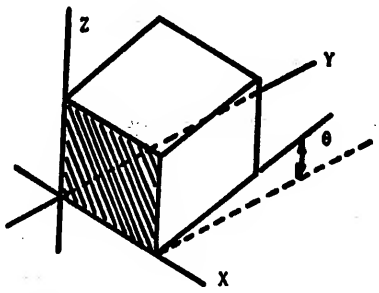

(a) Tilt

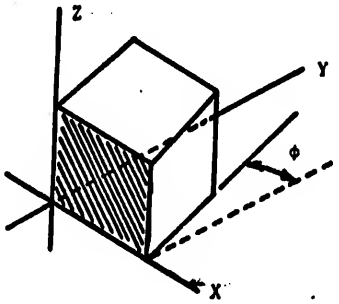

(b) Tilt

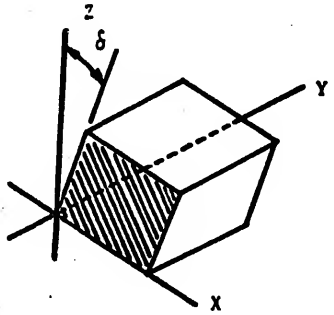

(c) Skew

Figure VIII-4. Single tilts (a) and (b), and a skew (c) of a crystal with respect to the plane of the boundary interface.

VIII-5(a); whereas, a skew boundary requires only one shear in the boundary plane, Figure VIII-5(b). Only the twist boundary represents a rotation of one crystal with respect to its conjoint neighbor.

Combinations of single tilts and a skew produce more complex boundary surfaces as shown in Figure VIII-6. If the plane of the boundary interface is coincident with the xz-plane, the sketch (a) represents a crystal doubly tilted through the angles θ and ϕ about the x- and z-axes, respectively. The sketches (b) and (c) each represent a tilt and a skew, and the sketch (d) represents a double tilt and a skew. The latter three cases, all involving a skew component, require that the boundary coincide with a slip plane. Therefore, forming boundaries in which the mating surface of one of the conjoint grains contains a skew component demands that the boundary plane coincide with a slip plane common to both of the conjoint grains.

Boundaries involving only tilts of the conjoint grains with respect to one another may be classified, as shown by the two-dimensional sketches of Figure VIII-7, in terms of the directions of the shears acting on the conjoint crystals in producing their mating surfaces. In the present discussion, the formation of a boundary in a single crystal is considered in terms of the tilts (shears) that must be produced in the two halves of the crystal. Therefore, it is convenient to separate the crystal along an imaginary

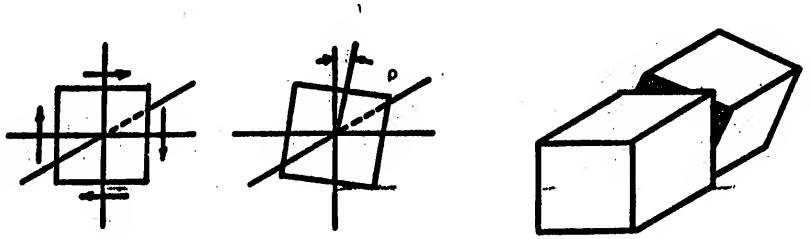

(a) Twist Boundary

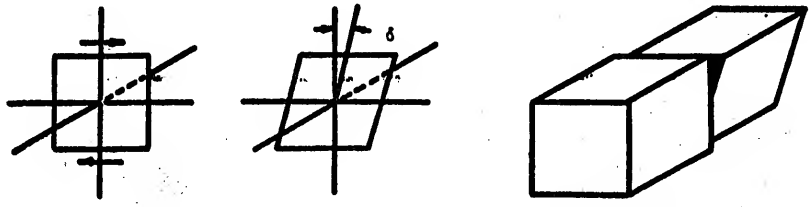

(b) Skew Boundary

Figure VIII-5. Geometric difference between a twist boundary (a) and a skew boundary (b).

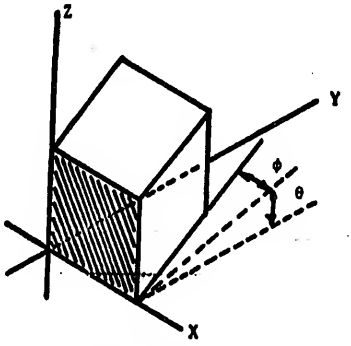

(a) Double Tilt

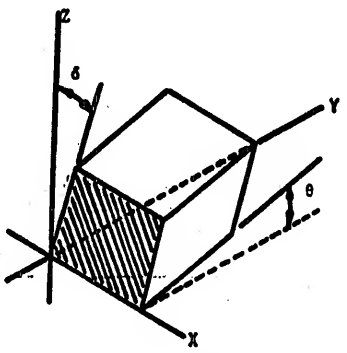

(b) Single Tilt and Skew

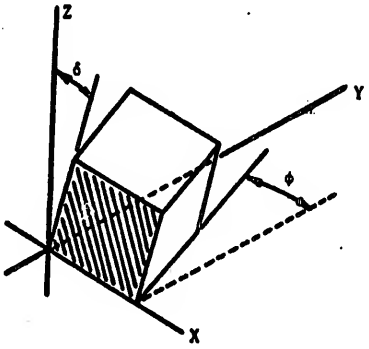

(c) Single Tilt and Skew

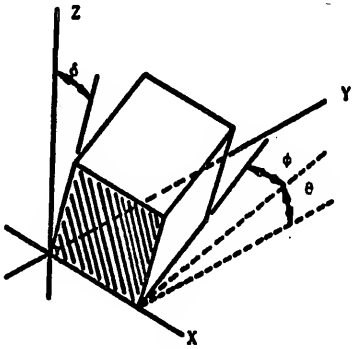

(d) Double Tilt and Skew

Figure VIII-6. Combinations of tilts and a skew of a crystal with respect to the plane of the boundary interface. (a) Doubly tilted through angles θ and φ. (b) Tilted through an angle, θ, and skewed through an angle, δ. (c) Tilted through an angle, φ, and skewed through an angle, δ. (d) Doubly tilted through angles θ and φ, and skewed through an angle, δ.

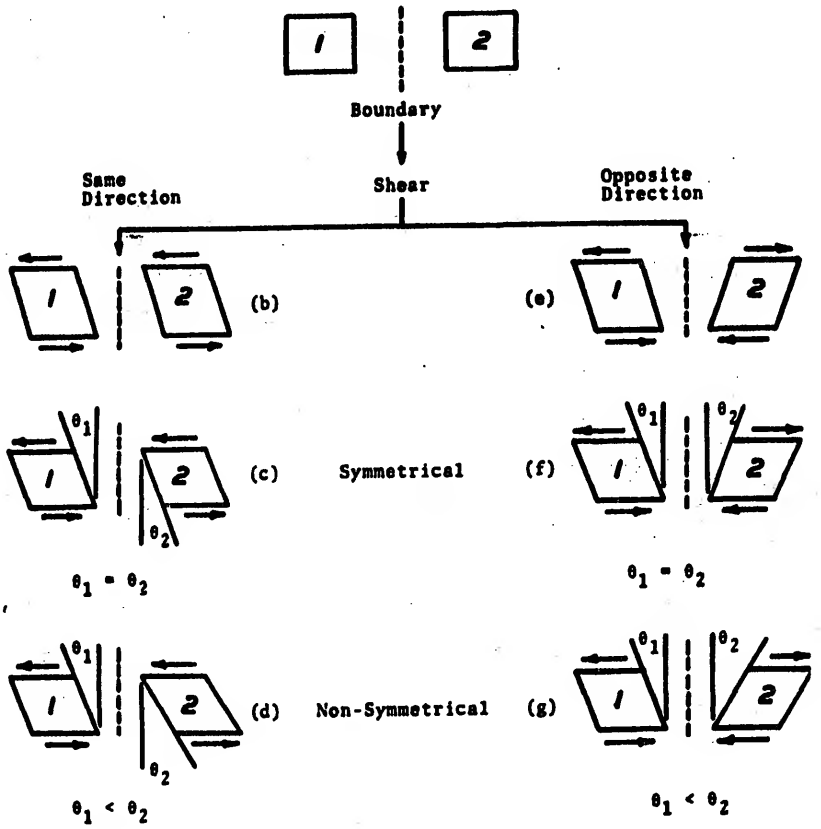

Figure VIII-7. Classification of tilt boundaries.

boundary interface, Figure VIII-7(a), then shear and tilt each half separately. Two major classes of boundaries result, depending upon whether the shears in the crystal halves are in the same, Figure VIII-7(b), or opposite, Figure VIII-7(c), directions. Under each of these classes, the boundaries may be symmetrical or non-symmetrical, depending upon the relative magnitudes of the tilts (shears) between each crystal half and the boundary interface.

When the shears in two crystal halves are in the same direction, and the tilt angles between each mating surface and the boundary interface are equal, Figure VIII-7(c) (symmetrical boundary), the two halves possess identical crystallographic orientations with respect to the boundary interface. Hence at the boundary surface the two crystals have coincident crystal lattices and no boundary exists. If, however, the tilt angles are unequal, Figure VIII-7(d), a non-symmetrical boundary exists. If, in the formation of a non-symmetrical boundary, only one slip system is allowed to operate, then that crystal half which tilted to the greatest degree with respect to the plane of the boundary interface will have the greater area of its mating face. In order that the contiguity of the boundary be maintained, some adjustment in the dimensions of the two crystal halves is called for. The necessary adjustment would be realized if additional slip systems were allowed to operate. The only requirement upon these additional slip systems is that any

changes which they effect in the mating surfaces of the two crystal halves must be such that the mating surfaces are continuously maintained contiguous.

When the shears in the two crystal halves are in opposite directions, Figure VIII-7(e), and the tilt angles between each crystal half and the plane of the boundary interface are equal, Figure VIII-7(f), the two crystal halves are symmetrically tilted with respect to the boundary interface. A boundary of this type corresponds to tilt boundaries formed by heating a single crystal which has been deformed by pure bending.

A non-symmetrical tilt boundary, Figure VIII-7(g), is formed when the shears in the two crystal halves are in opposite directions, and the tilt angles with respect to the plane of the boundary interface are unequal. For the reasons cited previously, additional slip systems must be allowed to operate in the formation of this type of boundary in order for the contiguity of the boundary to be maintained.

The classification of tilt boundaries given in the preceding paragraphs may be extended to three dimensions for singly and doubly tilted crystals. Some specific examples of boundaries based upon this classification are shown in the sketches of Figure VIII-8.

A more convenient way to illustrate the various types of grain boundaries is in terms of stereographic projection. Consider an element of cubic single crystal which is to be doubly tilted to form a boundary. Let the crystal element

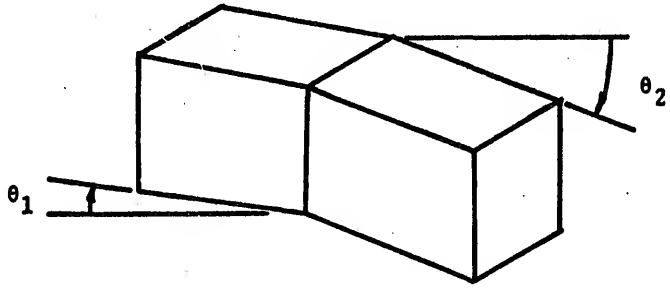

(a1) Single Tilt (Non-Symmetrical)

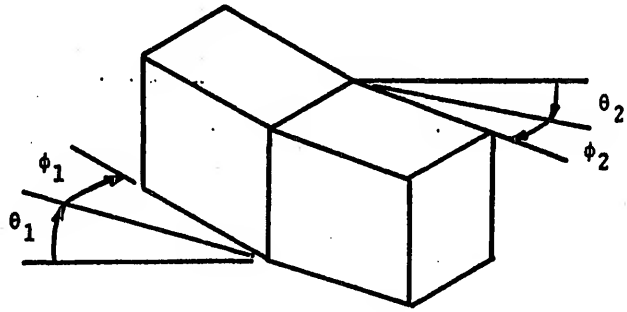

(a2) Double Tilt (Both Tilts are Non-Symmetrical)

(a) The shears producing tilts with respect to the boundary interface are in the same directions

Figure VIII-8. Combinations of symmetrical and non-symmetrical tilts in forming a grain boundary.

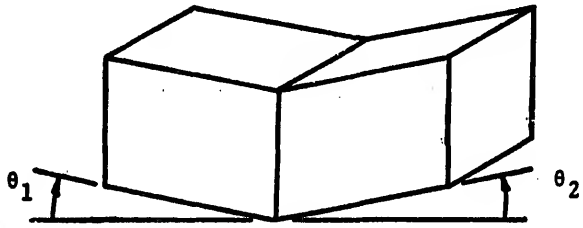

(b1) Single Tilt (Symmetrical)

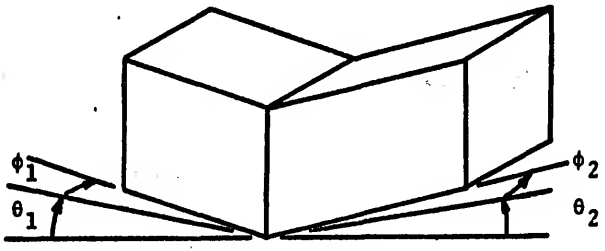

(b2) Double Tilt (Both Tilts are Symmetrical)

(b) The shears producing tilts with respect to the boundary interface are in opposite directions

Figure VIII-8. (continued)

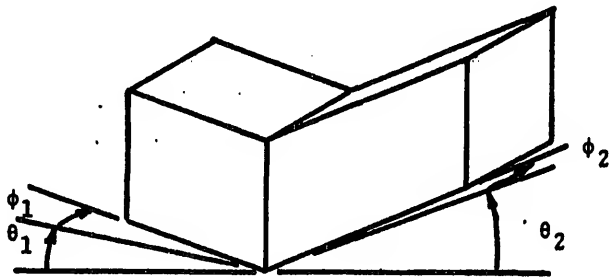

(b3) Double tilts (one tilt is non-symmetrical)

Figure VIII-8. (continued)

be placed upon a rectangular coordinate system as shown in Figure VIII-9(a), such that the plane of the boundary interface to be formed is coincident with the xz-plane. Plotting stereographically, Figure VIII-9(b), the undeformed element has its xy-poles at the north and south poles, its yz-poles at the east and west extremes of the equatorial great circle and its xz-poles at the center of the projection. Consider that the crystalline element is divided into two halves by the plane of the boundary interface which is coincident with the xz-plane.

To form a symmetrical single tilt boundary in the xz-plane, oppositely rotate each crystal half upward through an angle, θ, as shown in Figure VIII-9(c). The results of this operation are shown stereographically in Figure VIII-9(d). The pole of the boundary interface, P, is at the center, the pole of the xz-face of the left-hand crystal half is positioned at an angle, θ, north of P, and the pole of the xy-face is positioned at an angle, θ, north of the south pole. Similarly, the corresponding poles of the right-hand crystal half have been moved symmetrically in a direction opposite to that of the left-hand crystal half. The positions of the yz-poles remain unchanged.

To produce a doubly tilted boundary, tilt each crystal half through an angle, ϕ, about the z-axis as shown in Figure VIII-9(e). The results of this operation are shown stereographically in Figure VIII-9(f). Again the pole of

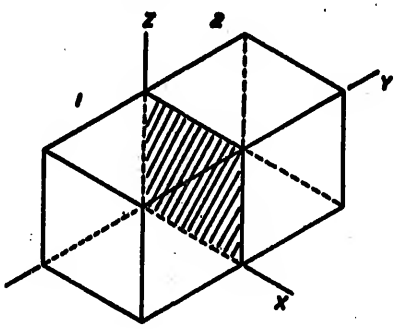

(a)

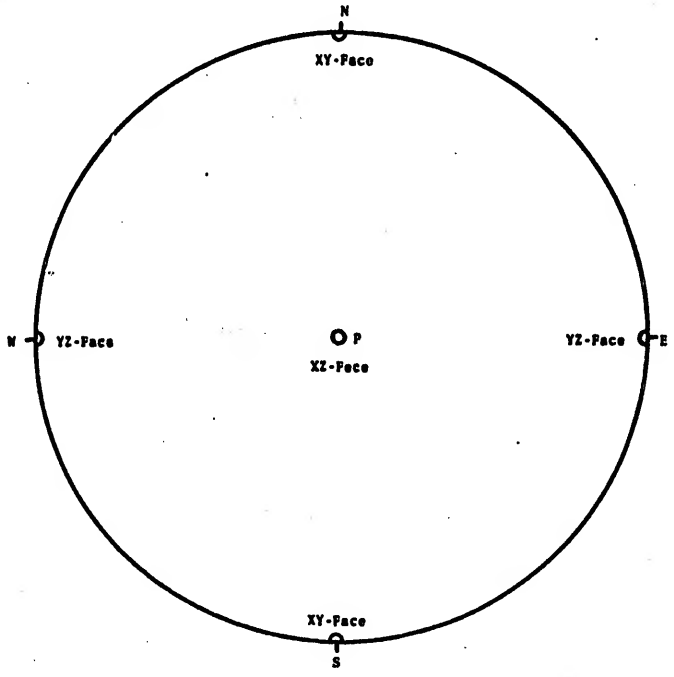

(b)

Figure VIII-9. Stereographic projections showing the differences in the orientations of the conjoint crystals with respect to the plane of the boundary interface.

(a and b) Before tilting.

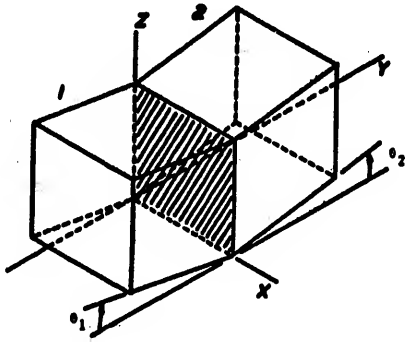

(c)

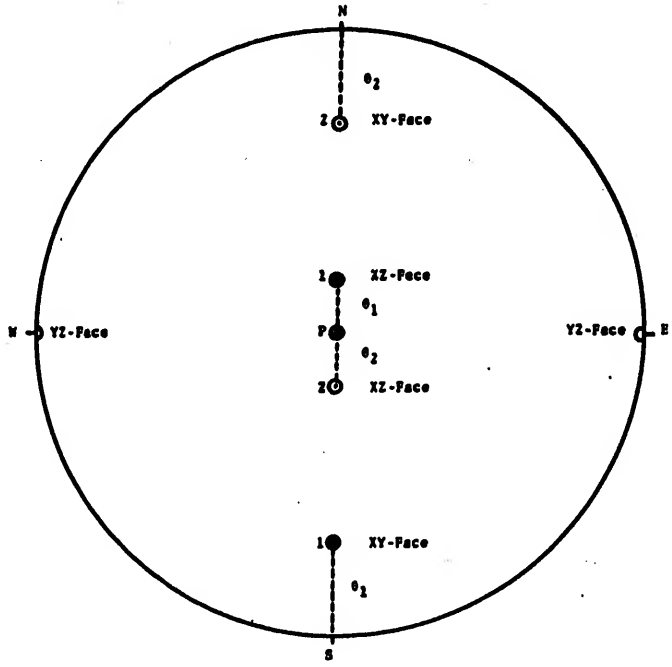

(d)

Figure VIII-9. (continued)

(c and d) Single tilt.

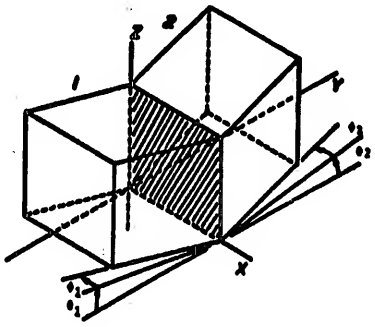

(e)

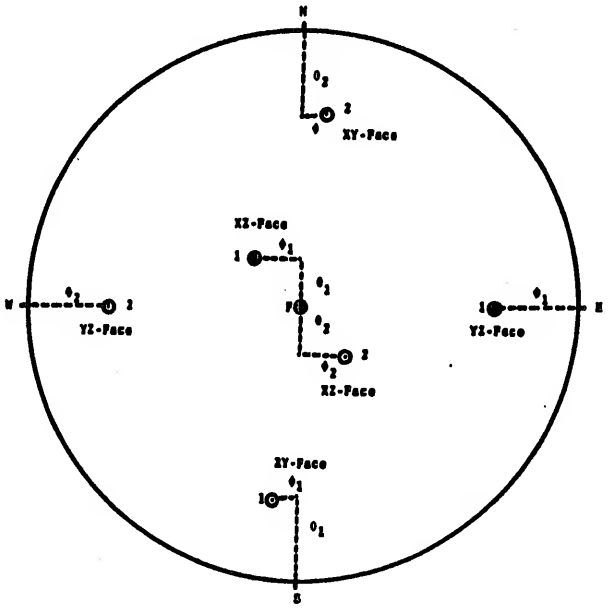

(f)

Figure VIII-9. (continued)

(e and f) Doubly tilted.

the boundary interface is at the center of the projection. Note that the poles of the yz-faces of both crystal halves have been moved inward by an angle, ϕ. A stereographic plot such as that shown in Figure VIII-9(f) represents the symmetrical double tilt boundary shown in Figure VIII-8(b2). Stereographic plots corresponding to the boundaries shown in Figure VIII-8 are given in Figure VIII-10.

The condition of contiguity, that the mating faces of two conjoint crystals must have equal areas and identical three-dimensional shapes, is an essential feature of grain boundary geometry. As will be shown in a later section of this chapter, when the condition of contiguity is violated, other adjustments, such as grain boundary shearing, must occur in order to maintain contact between the mating surfaces of conjoint crystals.

There are two vantage points from which to view grain boundary contiguity. From the first, one considers the formation of a grain boundary in a single crystal and describes the boundary in terms of the tilts of each of the conjoint grains with respect to the plane of the boundary interface. Contiguity of the boundary thus formed requires that the areas of the mating faces of the conjoint grains must be equal. The areas of the mating faces of the conjoint grains are related to the tilts of each grain with respect to the boundary interface. When one grain of the conjoint pair is considered, the area of its mating face in terms of two tilt angles is

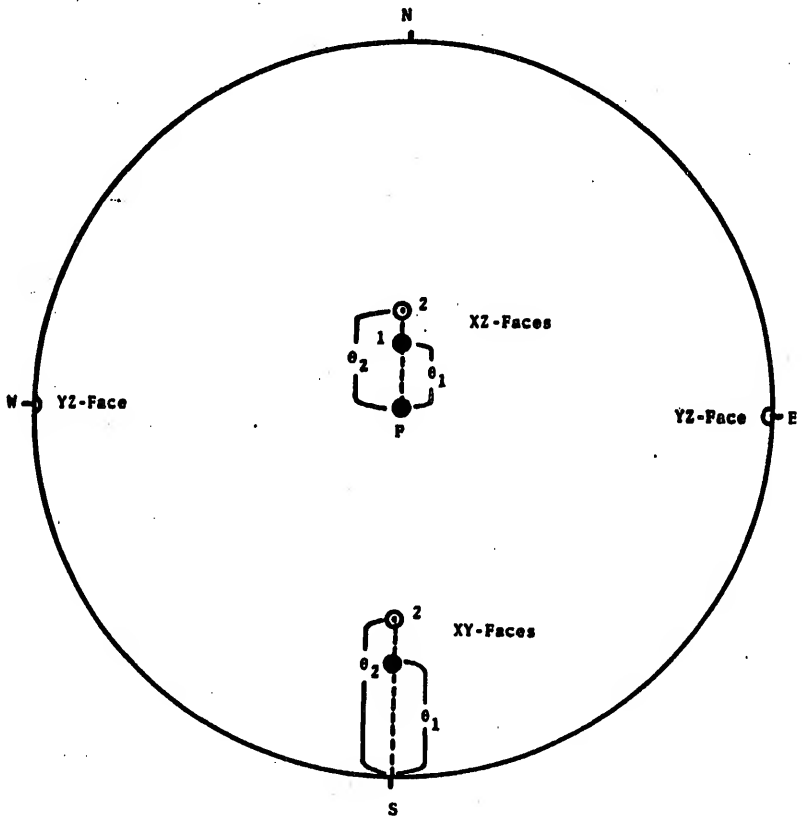

Figure VIII-10. Stereographic plots of grain boundaries corresponding to those shown in Figure VIII-8.

(a1) Single tilt (non-symmetrical) $\theta_1 < \theta_2$.

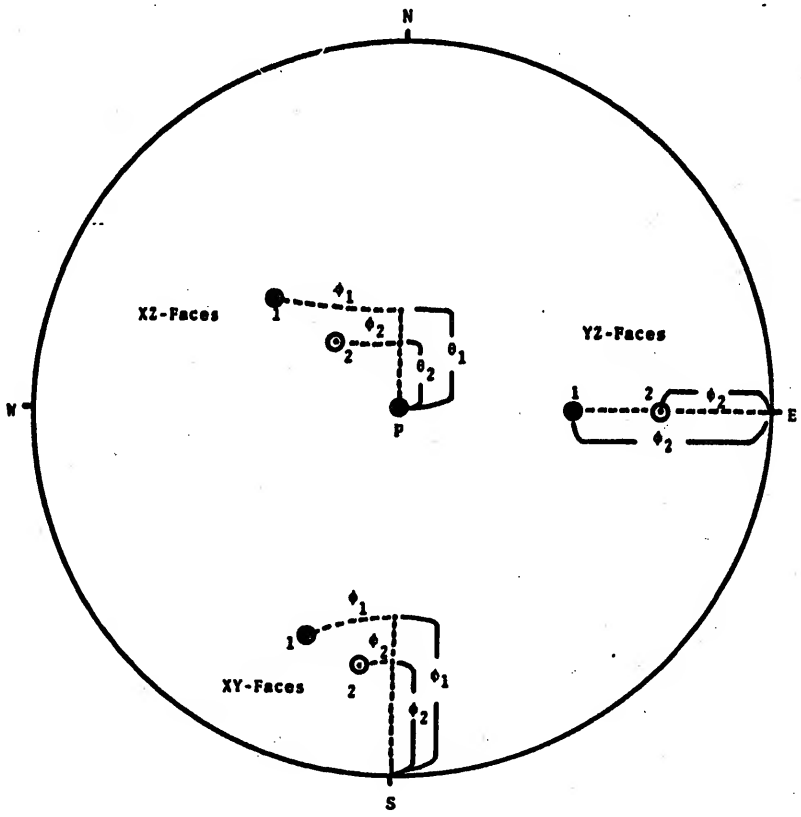

Figure VIII-10. (continued)

(a2) Double tilt (both tilts non-symmetrical) $\theta_1 > \theta_2$, $\phi_1 > \phi_2$.

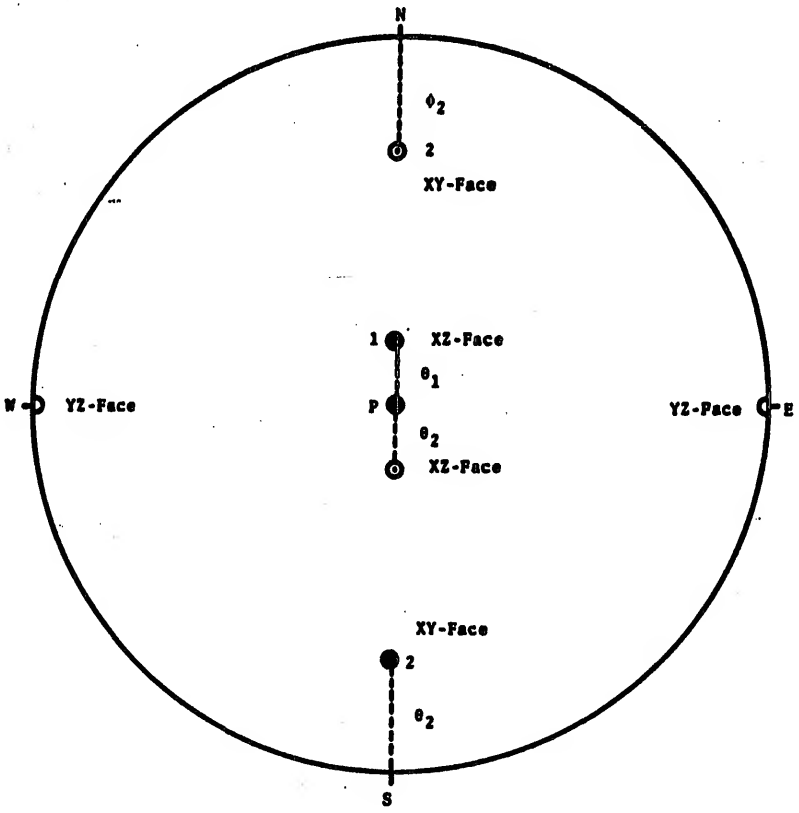

Figure VIII-10. (continued)

(b1) Single tilt (symmetrical) $\theta_1=\theta_2$.

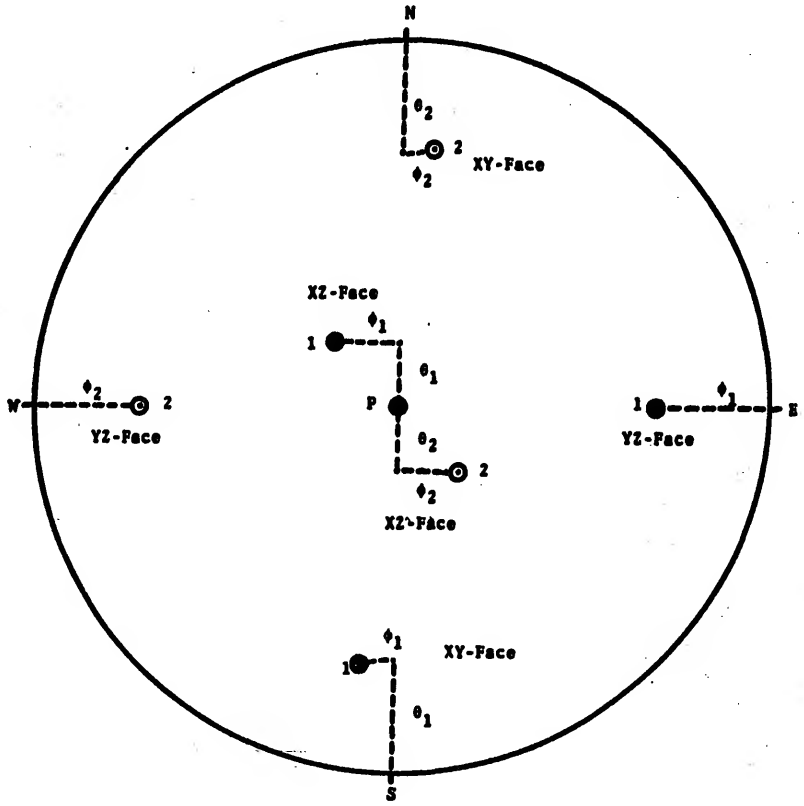

Figure VIII-10. (continued)

(b2) Double tilt (both tilts symmetrical) $\theta_1=\theta_2$, $\phi_1=\phi_2$.

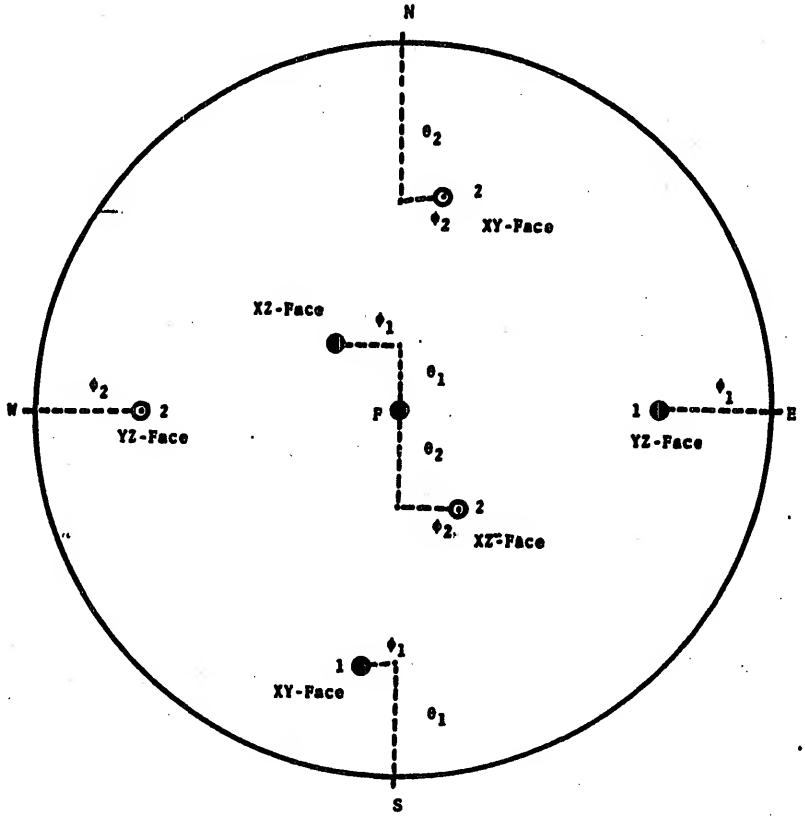

Figure VIII-10. (continued)

(b3) Double tilt (one tilt symmetrical)
$\theta_1 < \theta_2$, $\phi_1 = \phi_2$.

$$A = [\tan^2\theta + \tan^2\phi + 1]^{1/2} , \qquad (16)$$

where θ and ϕ are the tilt angles and A is the area of the mating face. In the derivations of this expression it is assumed that the area of the boundary plane prior to forming the boundary by tilting was equal to unity. The derivation is given at the end of this appendix. The area of the mating face of one of a conjoint pair of crystals is related to the angle α between the pole of the boundary interface and the pole of the cube face (considering a boundary in a cubic crystal) by the expression

$$\cos\alpha = \frac{1}{[\tan^2\theta + \tan^2\phi + 1]^{1/2}} , \text{ or}$$

$$\alpha = \cos^{-1}[\tfrac{1}{A}] , \qquad (17)$$

where θ and ϕ are the tilt angles and A' is the area of the mating face. The angle, α, can be obtained directly from the stereographic plot showing the tilt relations between each conjoint crystal and the plane of the boundary interface. Associated with the tilts of each of the conjoint crystals there exists an angle, α, which corresponds to the area of its mating face. See Figure VIII-11. The angles α_1 and α_2 as shown in Figure VIII-11 are equal, because the conjoint grains are tilted symmetrically with respect to the boundary interface. This implies that the areas of the conjoint mating surfaces are equal.

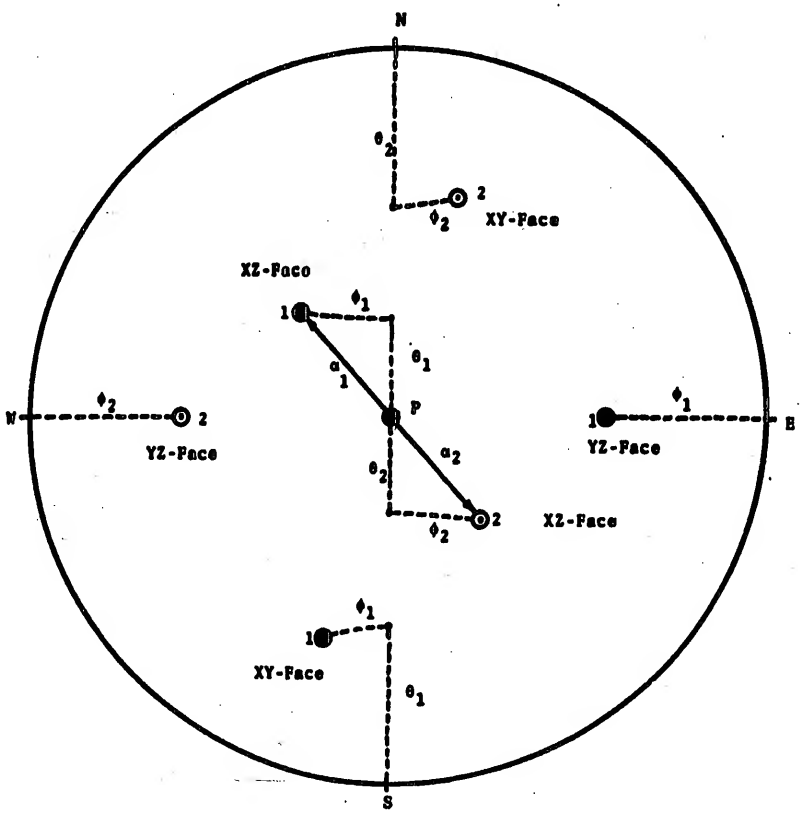

Figure VIII-11. Stereographic plot of the boundary formed between two simple cubic crystals by double symmetrical tilting. Note that $\theta_1=\theta_2$, $\phi_1=\phi_2$ and $\alpha_1=\alpha_2$.

In the case of a non-symmetrical tilt boundary, Figure VIII-12, α_1 and α_2 may not be equal. Such a circumstance, from equation (17), would imply that the mating surfaces of the conjoint grains have unequal areas. According to the foregoing discussions, this is indeed a violation of contiguity. In real polycrystalline metals it seems that non-symmetrical boundaries of this sort must certainly exist, and that their interfaces are certainly contiguous. It is now that the second vantage point from which to view grain boundary contiguity becomes most convenient. From this point of view, one considers that, for a given boundary already in existence, the mating surfaces of its conjoint grains must have equal areas, and that the angles, α_1 and α_2, describe the nature of the boundary in terms of the relative tilts of each grain with respect to the boundary interface. Further, these angles contain crystallographic information because, through equation (17), the angle α for one of a conjoint pair of grains is related to the tilt angles, θ and ϕ. In turn, θ and ϕ can be described by the lattice shears. Similarly, the area of a mating surface computed by equation (16) also contains crystallographic information. When there exists a grain boundary such that α_1 is different from α_2, the factor by which they differ is then related to the crystallographic differences between the mating surfaces of the conjoint crystals provided the boundary is contiguous.

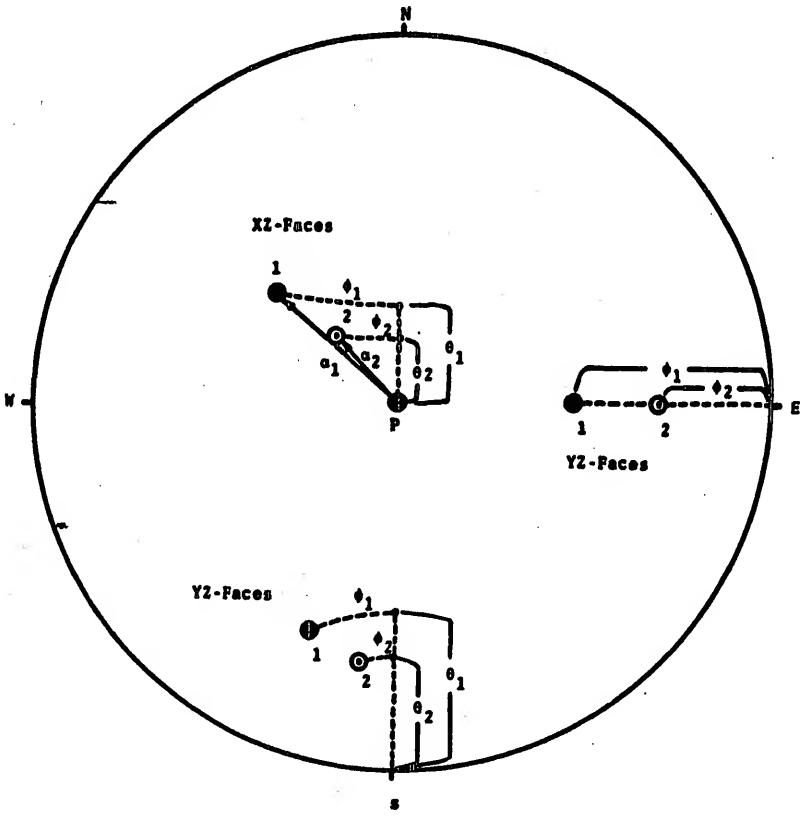

Figure VIII-12. Stereographic plots of the orientations of conjoint grains relative to the plane of the boundary interface. The boundary is doubly tilted so that both tilts are non-symmetrical; therefore, $\theta_1 \neq \theta_2$, $\phi_1 \neq \phi_2$ and $\alpha_1 \neq \alpha_2$.

Equations (16) and (17) hold for non-symmetrical boundaries if the area of the mating surface and the tilt angles of one of the conjoint grains are normalized to those of the other grain.

Since one considers that the pre-existing boundary is contiguous, the areas, A_1' and A_2', of the mating surfaces of its conjoint grains must be equal,

$$A_1' = A_2' \ . \qquad (18)$$

Let $A_1' = c_1 A_1$ and $A_2' = c_2 A_2$, where c_1 and c_2 are unequal constants. Then from the condition of contiguity, equation (18),

$$A_1 = c_2/c_1 \ A_2 \ ,$$

or, replacing the constant ratio c_2/c_1 with the constant ζ

$$A_1 = \zeta A_2 \ , \qquad (19)$$

where the constant, ζ, by its value, gives in degree the non-symmetry of the boundary. The operations above normalize the area, A_2, of the mating surface of grain 2 to the area, A_1, of the mating surface of grain 1.

Now, let v and w be constants such that, from equation (16),

$$\zeta A_2 = [\tan^2 v\theta_2 + \tan^2 w\phi_2 + 1]^{1/2} \ . \qquad (20)$$

By combining equations (19) and (20), and substituting

$[\tan^2\theta_1 + \tan^2\phi_1 + 1]^{1/2}$ for A_1, the following expression is obtained,

$$[\tan^2\theta_1+\tan^2\phi_1+1]^{1/2} = [\tan^2 v\theta_2+\tan^2 w\phi_2+1]^{1/2}. \quad \text{(VIII-5)}$$

Therefore,

$$\theta_1 = v\theta_2 \text{ , and}$$
$$\phi_1 = w\phi_2 \text{ .} \quad (21)$$

In effect, the constants, v and w, normalize the tilt angles of grain 2 to the tilt angles of grain 1. The values of v and w give the degree of non-symmetry between the tilts of the two grains with respect to the boundary interface.

In addition, the angles, α_1 and α_2, are related by the expression

$$\cos\alpha_2/\cos\alpha_1 = \zeta. \quad (22)$$

The constants, ζ, v and w, have significance in that they are not only related to the differences in the tilts between the conjoint grains, but they are also related to crystallographic differences between the mating surfaces of the conjoint grains. Rhines [170] has described the crystallographic nature of the mating faces of conjoint grains in terms of ledges produced upon the mating surfaces of the grains by shearing each of the grains along slip planes.

A special significance is to be attached to the values of ζ, v and w, when one considers passing shear through a

grain boundary. For the condition of contiguity to hold while shear is passed through a grain boundary, the values of v and w, and hence ζ, established for the boundary prior to shear,must not be altered by the shearing process. If the values of v and/or w are altered, then the mating faces of the conjoint grains will not maintain matching shapes. A change in the value of ζ reflects that the areas of the mating surfaces have become unequal.

VIII-1. Derivation of the Relations Between the Area of a Grain Boundary Mating Surface and the Tilt Angles

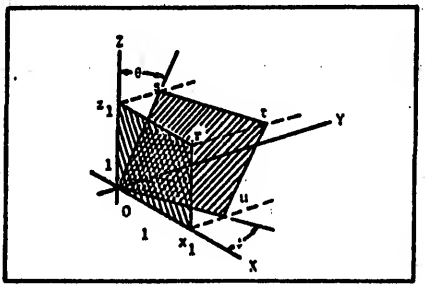

Consider a mating surface to be formed from a unit area A in the xz-plane, rectangle ox_1rz_1, by tilting through an angle θ about the x-axis and through an angle ϕ about the z-axis. The area of the surface A', parallelogram, outs, increases in the process.

Let the sides of the unit area A be given by the unit vectors $\vec{i}$ and $\vec{j}$ on the x- and z-axes, respectively.

Let the sides of the area A' be represented by vectors $\vec{v}_1$ and $\vec{v}_2$ in the xy- and yz-planes, respectively.

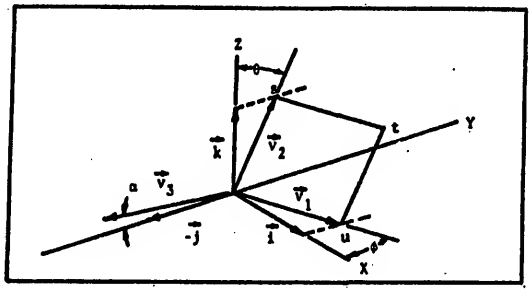

Accordingly,

$$\vec{v}_1 = \vec{i} + \tan\phi\vec{j} \tag{23}$$

$$\vec{v}_2 = \tan\theta\vec{j} + \vec{k} \tag{24}$$

The vector product $\vec{v}_3 = \vec{v}_1 \times \vec{v}_2$ is a vector normal to the plane, outs, and is absolute value in the area, A', of the plane.

$$\vec{v}_3 = \vec{v}_1 \times \vec{v}_2 = \tan\phi\vec{i} - \vec{j} + \tan\theta\vec{k} \tag{25}$$

$$A' = |\vec{v}_3| = |\vec{v}_1 x \vec{v}_2| = [\tan^2\phi+1+\tan^2\theta]^{1/2} \tag{26}$$

Consider now the angle, α, between the vector normal to the plane, outs, and the unit vector normal to the boundary plane, $-\vec{j}$.

Taking the scalar product of $\vec{v}_3$ and $-\vec{j}$

$$\vec{v}_3 \cdot -\vec{j} = |\vec{v}_3|\ |-\vec{j}|\ \cos\alpha \tag{27}$$

$$\cos \alpha = \frac{\vec{v}_3 \cdot -\vec{j}}{|\vec{v}_3||-\vec{j}|} = \frac{1}{[\tan^2\phi+1+\tan^2\theta]^{1/2}[1]} \quad (28)$$

$$\cos \alpha = \frac{1}{A'} \quad (29)$$

$$\alpha = \cos^{-1}\left(\frac{1}{A'}\right) \quad (30)$$

Therefore, the angle, α, is related to the inverse of the area of the plane, outs, formed by tilting the plane ox_1rz_1 of unit area through the angles ϕ and θ.

APPENDIX IX

CALCULATIONS OF THE LENGTH OF DISLOCATION LINE WHICH PRODUCES EXTERNAL SHAPE CHANGE AND THE LENGTH OF DISLOCATION LINE STORED IN SUB-BOUNDARIES

Consider a 1 mm thick slab of material in the center of the gage length of a creep specimen as shown below.

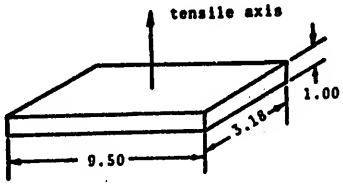

The dimensions given are in mm. The cross-sectional area is

$$A = 30.2 \text{ mm}^2 .$$

The volume of the slab is

$$V = 30.2 \text{ mm}^3 .$$

Consider that the strain produced in the slab of material is the result only of the external shear steps which, on the average, are inclined at 45° to the tensile axis. Then the change in length, Δl, is

$$\Delta l = l - l_o = \sin 45^\circ \, d_s , \qquad (31)$$

where Δl is the change in length, l is the length after creep, l_o is the initial length, and d_s is the shear displacement at 45° to the tensile axis. For unit strain, $\Delta l = l - l_o = 1$, $d_s = 1/\sin 45° = 1.414$ mm.

The average length of the shear displacement, L, is one-half of the perimeter of the cross-section,

$$L = \frac{2(3.18+9.50)}{2} = 12.68 \text{ mm} . \qquad (32)$$

The length of the dislocation line required to produce shear steps of displacement d_s is

$$l_s = \frac{12.68(d_s)}{2|\vec{b}|} , \qquad (33)$$

where $\vec{b}$ is the Burger's vector. ($|\vec{b}| = 2.86 \times 10^{-7}$ mm for aluminum.)

The length of dislocation line in the shear steps, l_s, for unit strain, assuming that the only edge dislocations are involved in producing the shear steps is

$$l_s = \frac{12.68(1.414)}{2(2.86 \times 10^{-7})} = 3.14 \times 10^{7} \text{ mm} . \qquad (34A)$$

For any amount of strain, ε, less than unit strain, equation (IX-4A) becomes

$$l_s = 3.14 \times 10^{7} \, \varepsilon \text{ mm} . \qquad (34B)$$

The surface area of the sub-boundary is the measured or calculated value of sub-boundary area per unit volume times the volume of the slab,

$$S_{(SGB)} = S_{V(SGB)}\, V = 30.2\, S_{V(SGB)} , \qquad (35)$$

where $S_{(SGB)}$ is the surface area of the sub-boundaries in the slab and $S_{V(SGB)}$ is the surface area of the sub-boundaries per unit volume.

Now assume that, on the average, the sub-boundaries represent a misorientation of 5° and that this misorientation is the result of only edge dislocations in a simple tilt boundary. In the range of strains for which these calculations are to be made, the 5° misorientation is not greatly in error.

The spacing between edge dislocations, x_d, for a 5° tilt boundary is

$$x_d = \frac{1/2\ b}{\tan \theta} , \qquad (36)$$

where θ is one-half the angle of misorientation. Substituting in the appropriate values,

$$x_d = 3.28 \times 10^{-6} \text{ mm} . \qquad (37)$$

The length of the dislocation line in sub-boundaries, l_b, is the sub-boundary area, $S_{(SGB)}$, divided by the dislocation spacing, x_d,

$$l_b = \frac{30.2\ S_{V(SGB)}}{x_d} = \frac{30.2\ S_{V(SGB)}}{3.28 \times 10^{-6}} \text{ mm} . \qquad (38)$$

Based upon specimens tested at 200°C under an initial stress of 1,000 psi, values for the secondary creep strain

and the sub-boundary area per unit volume formed in 24 hours of secondary creep testing calculated from the strain rate and rate of subgrain boundary area formation are

$$\varepsilon = 6.66 \times 10^{-2} ,$$

$$S_{V(SGB)} = 1.79 \times 10^{-1} \text{ mm}^2/\text{mm}^3 .$$

The length of dislocation line which has produced shear step at the surface, using equation (34B), is

$$l_s = 2.09 \times 10^{6} \text{ mm} .$$

The length of dislocation line which is stored in the sub-boundaries, using equation (38), is

$$l_b = 1.65 \times 10^{6} \text{ mm} .$$

Using the measurements of strain and subgrain boundary area per unit volume obtained from the data of specimen S1-4 tested at 200°C under an initial stress of 1,000 psi for 95.78 hours ($\varepsilon = 9.8 \times 10^{-3}$, $S_{V(SGB)} = 11.66 \text{ mm}^2/\text{mm}^3$), the lengths of dislocation line resulting in external shape change and stored in sub-boundaries are

$$l_s = 3.08 \times 10^{6} \text{ mm, and}$$
$$l_b = 1.08 \times 10^{8} \text{ mm.}$$

BIBLIOGRAPHY

1. J. E. Stead: J. Iron and Steel Inst., 1898, vol. 53, p. 175.

2. C. H. Desch: Metallography. London: Longmans, Green and Co., 1910.

3. J. C. W. Humfrey: Phil. Trans. Royal Soc., 1904, A, vol. 200, p. 145.

4. W. Rosenhain and J. C. W. Humfrey: J. Iron and Steel Inst., 1913, vol. 87, p. 219.

5 F. Osmond and G. Cartaud: J. Iron and Steel Inst., 1906, vol. 71, p. 414.

6. O. Mügge: N. Jahrb. Min., 1898, p. 71.

7. O. Mügge: N. Jahrb. Min., 1899, p. 55.

8. O. Mügge: Naturwiss. Rundschau, 1900, vol. 15, p. 69.

9. J. A. Ewing and W. Rosenhain: Phil. Trans. Royal Soc., 1900, A, vol. 193, p. 353.

10. J. A. Ewing and W. Rosenhain: Proc. Royal Soc., 1899, vol. 65, p. 85.

11. G. T. Beilby: J. Inst. Metals, 1911, vol. 6, p. 5.

12. W. Rosenhain and J. C. W. Hunfrey: Proc. Royal Soc., 1909, A, vol. 83, p. 200.

13. W. Rosenhain and D. Ewen: J. Inst. Metals, 1912, vol. 8, p. 149.

14. W. Rosenhain and D. Ewen: J. Inst. Metals, 1913, vol. 10, p. 119.

15. W. Rosenhain: Engineering, 1913, vol. 96, p. 509.

16. W. Rosenhain and S. L. Archbutt: Proc. Royal Soc., 1919, A, vol. 96, p. 55.

17. W. Rosenhain: Trans. Faraday Soc., 1921, vol. 17, p. 2.

18. C. Chappell: J. Iron and Steel Inst., 1914, vol. 89, p. 460.

19. H. M. Howe: The Metallography of Steel and Cast Iron. New York: The McGraw-Hill Book Company, Inc., 1916.

20. Z. Jefferies and R. S. Archer: The Science of Metals, pp, 166-167. New York: McGraw-Hill Book Company, Inc., 1924.

21. N. F. Mott: Proc. Phys. Soc., 1951, vol. 64, p. 729.

22. L. J. Vicat: Poggendorfer Annalen, 1834, vol. 31, p. 108.

23. D. Hanson: Trans. AIME, 1939, vol. 133, p. 15.

24. P. G. McVetty: American Soc. Test. Mat., 1943, vol. 43, p. 707.

25. E. N. daC. Andrade: Proc. Royal Soc., 1910, A, vol. 84, p. 1.

26. A. H. Cottrell and V. Aytekin: Nature, 1947, vol. 60, p. 328.

27. F. Garofalo: ASTM Special Technical Publication No. 238, 1960, p. 82.

28. J. de Lacombe: Rev. Met., 1939, vol. 36, p. 178.

29. A. K. Mukherjee, J. E. Bird and J. E. Dorn: Trans. ASM, 1969, vol. 62, p. 155.

30. O. D. Sherby and P. M. Burke: Prog. Mat. Sci., 1968, vol. 13, p. 325.

31. H. J. McQueen: Trans. AIME, 1968, vol. 244, p. 31.

32. J. B. Conway and M. J. Mullikin: Trans. AIME, 1966, vol. 236, p. 1629.

33. I. S. Servi and N. J. Grant: Trans. AIME, 1951, vol. 191, p. 909.

34. O. D. Sherby and J. E. Dorn: Trans. AIME, 1953, vol. 197, p. 324.

35. O. D. Sherby, A. Goldberg and J. E. Dorn: Trans. ASM, 1954, vol. 46, p. 681.

36. C. R. Barrett, W. D. Nix and O. D. Sherby: Trans. ASM, 1966, vol. 59, p. 3.

37. D. Hardwick and W. J. McG. Tegart: J. Inst. Metals, 1961-62, vol. 90, p. 17.

38. J. McKeown: J. Inst. Metals, 1937, vol. 60, p. 201.

39. R. C. Gifkins: J. Inst. Metals, 1953-54, vol. 82, p. 39.

40. F. R. N. Nabarro: Report of a Conference on Strength of Solids. London: The Physical Society, 1948, p. 75.

41. C. Herring: J. Appl. Phys., 1950, vol. 21, p. 437.

42. J. G. Harper, L. A. Shepard and J. E. Dorn: Acta Met., 1958, vol. 6, p. 509.

43. E. N. daC. Andrade: Proc. Royal Soc., 1914, A, vol. 90, p. 329.

44. H. M. Howe: Trans. AIME, 1885, vol. 13, p. 646.

45. A. S. Nemy and F. N. Rhines: Trans. AIME, 1959, vol. 215, p. 992.

46. R. D. Heidenreich and W. Shockley: Report of a Conference on Strength of Solids. London: The Physical Society, 1948, p. 59.

47. D. Kuhlman-Wilsdorf and H. Wilsdorf: Acta Met., 1953, vol. 1, p. 394.

48. D. McLean: J. Inst. Metals, 1952-53, vol. 81, p. 133.

49. A. F. Brown and R. W. K. Honeycombe: Phil. Mag., 1951, vol. 42, p. 1146.

50. W. A. Wood and W. A. Rachinger: J. Inst. Metals, 1949-50, vol. 76, p. 237.

51. I. S. Servi and N. J. Grant: Trans. AIME, 1951, vol. 191, p. 917.

52. D. Hanson and M. A. Wheeler: J. Inst. Metals, 1931, vol. 45, p. 229.

53. D. McLean: J. Inst. Metals, 1951-52, vol. 80, p. 507.

54. R. W. Cahn: J. Inst. Metals, 1951, vol. 79, p. 129.

55. G. J. Ogilvie and W. Boas: Trans. AIME, 1948, vol. 175, p. 102.

56. R. Maddin, C. H. Mathewson and W. R. Hibbard, Jr.: Trans. AIME, 1948, vol. 175, p. 86.

57. R. Maddin, C. H. Mathewson and W. R. Hibbard, Jr.: Trans. AIME, 1950, vol. 185, p. 527.

58. J. Trotter: J. Inst. Metals, 1951-52, vol. 80, p. 521.

59. P. Lacombe and L. Beaujard: J. Trans. Met., 1948, vol. 74, p. 1.

60. G. J. Oglivie: J. Inst. Metals, 1952-53, vol. 81, p. 491.

61. G. K. Davis, E. Teghtsoonian and A. Lu: Acta Met., 1966, vol. 14, p. 1677.

62. G. J. Oglivie: Scripta Met., 1967, vol. 1, p. 79.

63. V. M. Urie and H. L. Wain: J. Inst. Metals, 1952-53, vol. 81, p. 53.

64. C. H. M. Jenkins and G. A. Mellor: J. Iron and Steel Inst., 1935, vol. 132, p. 179.

65. D. McLean: Creep and Fracture of Metals at High Temperatures. N. P. L. Creep Conference (1954), London: (H.M.S.O.), 1956.

66. G. R. Wilms and W. A. Wood: J. Inst. Metals, 1948-49, vol. 75, p. 693.

67. W. A. Wood, G. R. Wilms and W. A. Rachinger: J. Inst. Metals, 1951, vol. 79, p. 159.

68. J. L. Lytton, C. R. Barrett and O. D. Sherby: Trans. AIME, 1965, vol. 233, p. 1399.

69. J. A. Ramsey: J. Inst. Metals, 1951-52, vol. 80, p. 167.

70. A. H. Cottrell and V. Aytekin: J. Inst. Metals, 1951-52, vol. 80, p. 389.

71. C. J. Ball and P. P. Hirsch: Phil. Mag., 1955, vol. 46, p. 1343.

72. A. R. Chaudhuri, N. J. Grant and J. T. Norton: Trans. AIME, 1953, vol. 197, p. 712.

73. A. E. B. Presland and R. J. Hutchinson: J. Inst. Metals, 1963-64, vol. 92, p. 264.

74. D. McLean and M. H. Farmer: J. Inst. Metals, 1956-57, vol. 85, p. 41.

75. R. C. Gifkins: J. Inst. Metals, 1951, vol. 79, p. 223.

76. W. Betteridge and A. W. Franklin: J. Inst. Metals, 1951-52, vol. 80, p. 147.

77. G. Brinson and B. B. Argent: J. Inst. Metals, 1962-63, vol. 91, p. 293.

78. A. Orlová and J. Čádek: Phil. Mag., 1970, vol. 51, p. 509.

79. A. Franks and D. McLean: Phil. Mag., 1956, vol. 1, p. 101.

80. J. J. Jonas, H. J. McQueen and W. A. Wong: "Dynamic Recovery During the Extrusion of Aluminum," in Deformation Under Hot Working Conditions: Iron and Steel Institute Publication 108. London: Iron and Steel Institute, 1968.

81. H. Conrad: Mechanical Behavior of Materials at Elevated Temperatures. Ed. J. E. Dorn. New York: McGraw-Hill Book Company, Inc., 1961.

82. W. A. Wood and J. W. Suiter: J. Inst. Metals, 1951-52, vol. 80, p. 501.

83. G. R. Wilms: J. Inst. Metals, 1954-55, vol. 83, p. 427.

84. O. D. Sherby and J. E. Dorn: Proc. Soc. Expr. Stress Analys., 1953, vol. 12, p. 139.

85. H. J. McQueen, W. A. Wong and J. J. Jonas: Can. J. Phys., 1967, vol. 45, p. 1225.

86. V. V. Voznesensky and V. M. Rosenberg: Metally., 1970, vol. 4, p. 106.

87. D. McLean: J. Inst. Metals, 1952-53, vol. 81, p. 287.

88. D. McLean: J. Inst. Metals, 1954-55, vol. 83, p. 1.

89. D. McLean: Met. Rev., 1962, vol. 7, p. 481.

90. I. S. Servi, J. T. Norton and N. J. Grant: Trans. AIME, 1952, vol. 194, p. 965.

91. F. Garofalo, L. Zwell, A. S. Keh and S. Weisman: Acta Met., 1961, vol. 9, p. 721.

92. F. J. Hammad and W. D. Nix: Trans. ASM, 1966, vol. 59, p. 94.

93. W. V. Green, P. P. Gillis and E. G. Zukus: Acta Met., 1970, vol. 18, p. 43.

94. R. W. Cahn: J. Inst. Metals, 1949, vol. 76, p. 121.

95. A. H. Cottrell: Dislocations and Plastic Flow in Crystals, pp. 181-186. London: Oxford University Press, 1953.

96. W. A. Wood and R. F. Scrutton: J. Inst. Metals, 1950, vol. 77, p. 423.

97. W. A. Rachinger: J. Inst. Metals, 1951-52, vol. 80, p. 415.

98. J. A. Ramsey: J. Inst. Metals, 1952-53, vol. 81, p. 215.

99. R. W. Evans and G. R. Dunston: J. Inst. Metals, 1971, vol. 99, p. 4.

100. A. H. Cottrell: Dislocations and Plastic Flow in Crystals, pp. 162-168. London: Oxford University Press, 1953.

101. C. S. Barrett and L. H. Levenson: Trans. AIME, 1940, vol. 137, p. 112.

102. P. Gay and R. W. K. Honeycombe: Proc. Phys. Soc., 1951, vol. A64, p. 844.

103. R. W. K. Honeycombe: J. Inst. Metals, 1951, vol. 80, p. 45.

104. R. W. K. Honeycombe: Proc. Phys. Soc., 1950, vol. A63, p. 672.

105. N. K. Chen and C. H. Mathewson: J. Inst. Metals, 1951, vol. 191, p. 653.

106. C. S. Barrett: Trans. AIME, 1939, vol. 135, p. 296.

107. R. E. Reed and C. J. McHargue: Trans. AIME, 1967, vol. 239, p. 1604.

108. J. W. Mitchell, J. C. Chevrier, B. J. Hockey and J. P. Monaghan, Jr.: Can. J. Phys., 1967, vol. 45, p. 453.

109. J. S. Ahearn, H. McD. Hobgood and J. W. Mitchell: "The Formation of Bands of Deformation in Single Crystals of Cu-Al Alloys with Polyslip Orientations," in Proceedings of the Second International Conference on the Strength of Metals and Alloys, Vol. 2, p. 416. Cleveland: American Society for Metals, 1970.

110. J. B. Hess and C. S. Barrett: Trans. AIME, 1949, vol. 185, p. 599.

111. S. Petrova, M. Gaidakov and L. Smirnov: Phys. of Met. and Metallog., 1962, vol. 13, p. 59.

112. B. Suitkina and E. Yakoleva: Phys. of Met. and Metallog., 1959, vol. 7, p. 123.

113. F. N. Rhines, R. E. Reed-Hill, C. R. Smeal, L. Lee and W. Converse: "Evolution and Control of Grain Structures in Nickel Alloys During Hot Plastic Deformation." Met. Res. Lab. Univ. of Florida, January, 1962.

114. C. R. Smeal: Structural Evolution in Nickel During Annealing Subsequent to Hot Deformation. Ph.D. Dissertation, University of Florida, April, 1965.

115. K. Malyshev, G. Bogacheva and V. Sadovskii: Phys. of Met. and Metallog., 1959, vol. 7, p. 95.

116. J. W. Suiter and W. A. Wood: J. Inst. Metals, 1952-53, vol. 81, p. 181.

117. F. N. Rhines: Structural Changes Associated with High-Temperature Deformation of Uranium, Report NLCO-998. Cincinnati: National Lead Company of Ohio, April, 1968.

118. D. McLean: J. Inst. Metals, 1952-53, vol. 81, p. 293.

119. H. C. Chang and N. J. Grant: Trans. AIME, 1952, vol. 194, p. 619.

120. H. Brunner and N. J. Grant: Trans. AIME, 1960, vol. 218, p. 122.

121. J. E. Walter and H. E. Cline: Trans. AIME, 1968, vol. 242, p. 1823.

122. G. D. Gemmell and N. J. Grant: Jnl. Metals, 1957, vol. 9, p. 417.

123. N. J. Grant: "Intercrystalline Failure at High Temperatures," in Fracture. Ed. B. L. Averbach et al. New York: John Wiley, 1959.

124. A. W. Mullendore and N. J. Grant: Structural Processes in Creep, Special Report No. 70. London: Iron and Steel Institute, 1961, p. 44.

125. T. S. Kê: Phys. Rev., 1947, vol. 72, p. 41.

126. R. C. Gifkins: Trans. AIME, 1959, vol. 215, p. 1015.

127. W. A. Rachinger: J. Inst. Metals, 1952-53, vol. 81, p. 33.

128. P. W. Davies, J. P. Dennison and R. W. Evans: J. Inst. Metals, 1963-64, vol. 92, p. 409.

129. P. W. Davies, J. P. Dennison and R. W. Evans: J. Inst. Metals, 1964-65, vol. 93, p. 25.

130. V. M. Rosenberg: Phys. Met. and Metallog., 1961, vol. 11, p. 77.

131. B. Fazan, O. D. Sherby and J. E. Dorn: Trans. AIME, 1954, vol. 200, p. 919.

132. O. D. Sherby, R. L. Orr and J. E. Dorn: Trans. AIME, 1954, vol. 200, p. 71.

133. O. D. Sherby and J. E. Dorn: Trans. AIME, 1952, vol. 194, p. 959.

134. C. R. Barrett, J. L. Lytton and O. D. Sherby: Trans. AIME, 1967, vol. 239, p. 170.

135. H. Brunner and N. J. Grant: J. Inst. Metals, 1956-57, vol. 85, p. 77.

136. R. N. Stevens: Trans. AIME, 1966, vol. 236, p. 1762.

137. S. L. Couling and C. S. Roberts: Trans. AIME, 1957, vol. 209, p. 1253.

138. R. C. Gifkins: Proc. Berkeley Conf. on Properties of Reactor Mat'ls and Rad. Damage. London: Butterworth Press, 1960, p. 33[illegible].

139. H. Brunner and N. J. Grant: Trans. AIME, 1959, vol. 215, p. 48.

140. Y. Ishida, A. W. Mullendore and N. J. Grant: Trans. AIME, 1964, vol. 230, p. 1454.

141. R. L. Bell, C. Grame-Barber and T. G. Langdon: Trans. AIME, 1965, vol. 233, p. 1648.

142. P. Feltham: Proc. Phys. Soc., 1953, vol. 64, p. 865.

143. N. F. Mott: Proc. Phys. Soc., 1948, vol. 60, p. 391.

144. C. Crussard and J. Friedel: "Creep and Fracture of Metals at High Temperatures," N.P.L. Creep Conference (1954). London: H.M.S.O., 1956.

145. S. K. Tung and R. Maddin: Trans. AIME, 1957, vol. 209, p. 905.

146. J. A. Martin, M. Herman and N. Brown: Trans. AIME, 1957, vol. 209, p. 78.

147. F. Weinberg: Trans. AIME, 1958, vol. 212, p. 808.

148. R. C. Gifkins: "Mechanisms of Integranular Fracture at Elevated Temperature," in Fracture. Ed. B. L. Averbach et al. New York: John Wiley, 1959, p. 579.

149. M. Biscondi and C. Goux: Mem. Sci. Rev. Met., 1968, vol. 65, p. 167.

150. C. A. P. Horton, N. B. W. Thompson and C. J. Beevers: J. Met. Sci., 1968, vol. 2, p. 19.

151. R. Raj and M. F. Ashby: Met. Trans. 1971, vol. 2, p. 1113.

152. C. J. Beevers, M. D. Halliday and C. A. P. Horton: "Grain Boundary Sliding: Its Relation to Crystal Deformation," in Proceedings of the Second International Conference on the Strength of Metals and Alloys, Vol. 3, p. 1089. Cleveland: American Society for Metals, 1970.

153. C. A. P. Horton: "Characteristics of Grain Boundary Sliding and Slide Hardening," in Proceedings of the Second International Conference on the Strength of Metals and Alloys, Vol. 3, p. 1138. Cleveland: American Society for Metals, 1970.

154. D. McLean: J. Met. Sci., 1970, vol. 4, p. 467.

155. R. N. Stevens: J. Met. Sci., 1970, vol. 4, p. 265.

156. F. N. Rhines, W. E. Bond and M. A. Kissel: Trans. ASM, 1956, vol. 48, p. 919.

157. A. Seeger: "The Mechanism of Glide and Work Hardening in Face-Centered Cubic and Hexagonal Close-packed Metals," in 1957 Report, Lake Placid Conference on Dislocations and Mechanical Properties of Crystals, p. 243. New York: John Wiley, 1957.

158. A. Seeger, J. Diehl, S. Mader and H. Rebstock: Phil. Mag., 1957, vol. 2, p. 243.

159. P. Haasen: Phil. Mag., 1957, vol. 3, p. 384.

160. J. J. Jonas, H. J. McQueen and D. W. Demianczuk: "Interpretation of Extrusion Substructures as Revealed by the Electrolytic Etching of Aluminum," in Deformation Under Hot Working Conditions, Iron and Steel Institute Publication 108. London: Iron and Steel Institute, 1968.

161. H. J. McQueen, W. A. Wong and J. J. Jonas: Acta Met., 1967, vol. 15, p. 586.

162. J. E. Hockett and H. J. McQueen: "The Effects of Strain Rate and Temperature upon the Microstructure and Strength of Aluminum," in Proceedings of the Second International Conference on the Strength of Metals and Alloys, Vol. 3, p. 991. Cleveland: American Society for Metals, 1970.

163. H. J. McQueen and J. E. Hockett: Met. Trans. 1970, vol. 1, p. 2997.

164. F. H. Hammad, C. N. Ahlquist and W. D. Nix: Met. Trans., 1970, vol. 1, p. 2179.

165. J. D. Embury, A. S. Keh and R. M. Fisher: Trans. AIME, 1966, vol. 236, p. 1252.

166. G. Langford and M. Cohen: "Dynamic Recovery of Iron During Severe Plastic Deformation," in Proceedings of the Second International Conference on the Strength of Metals and Alloys, Vol. 2, p. 475. Cleveland: American Society for Metals, 1970.

167. G. Langford and M. Cohen: Trans. ASM, 1969, vol. 62, p. 623.

168. H. J. McQueen and J. E. Hockett: Met. Trans., 1970, vol. 1, p. 2997.

169. G. E. C. Tucker and P. C. Murphy: J. Inst. Metals, 1952-53, vol. 81, p. 235.

170. F. N. Rhines: Met. Trans., 1970, vol. 1, p. 1105.

BIOGRAPHICAL SKETCH

Richard G. Connell, Jr., was born on January 3, 1938, in Richmond, Virginia. He received his elementary and secondary education in the public schools of Richmond and was graduated from Thomas Jefferson High School in 1956. From 1956 to 1960 he attended Virginia Polytechnic Institute in Blacksburg, Virginia, and received the degree of Bachelor of Science in Metallurgical Engineering from that institution in 1960. The following two years he was employed as a Metallurgical Engineer in the Metallurgical Research Laboratories of Reynolds Metals Company in Richmond, Virginia. In 1962 he was appointed as an Instructor in the Department of Metallurgical Engineering at Virginia Polytechnic Institute. He held that position and was enrolled as a part-time graduate student until 1965, when he received the degree of Master of Science in Metallurgical Engineering.

In the Fall of 1965 he entered the Graduate School in the Department of Metallurgical and Materials Engineering at the University of Florida to pursue studies and research leading toward the degree of Doctor of Philosophy, which he received in 1973.

The author is married to the former Linda Dare Lane of Richmond, Virginia, and is the father of two children. He is a member of the American Society for Metals, American Institute of Mining, Metallurgical and Petroleum Engineers, International Society for Stereology, National Association of Corrosion Engineers, Alpha Sigma Mu, Sigma Gamma Epsilon, The Society of the Sigma Xi, and is a Registered Professional Engineer in the State of Florida.

I certify that I have read this study and that in my opinion it conforms to acceptable standards of scholarly presentation and is fully adequate, in scope and quality, as a dissertation for the degree of Doctor of Philosophy.

F. N. Rhines, Chairman
Professor of Materials Science
and Engineering

I certify that I have read this study and that in my opinion it conforms to acceptable standards of scholarly presentation and is fully adequate, in scope and quality, as a dissertation for the degree of Doctor of Philosophy.

E. D. Verink, Jr.
Professor of Materials Science
and Engineering

I certify that I have read this study and that in my opinion it conforms to acceptable standards of scholarly presentation and is fully adequate, in scope and quality, as a dissertation for the degree of Doctor of Philosophy.

R. T. DeHoff
Professor of Materials Science
and Engineering

I certify that I have read this study and that in my opinion it conforms to acceptable standards of scholarly presentation and is fully adequate, in scope and quality, as a dissertation for the degree of Doctor of Philosophy.

J. C. Slater
Professor of Physics

I certify that I have read this study and that in my opinion it conforms to acceptable standards of scholarly presentation and is fully adequate, in scope and quality, as a dissertation for the degree of Doctor of Philosophy.

E. H. Hadlock

E. H. Hadlock
Professor of Mathematics

This dissertation was submitted to the Dean of the College of Engineering and to the Graduate Council, and was accepted as partial fulfillment of the requirements for the degree of Doctor of Philosophy.

March, 1973

Robert E. Uhrig

Dean, College of Engineering

Harry H. Vaughan

Dean, Graduate School

UNIVERSITY OF FLORIDA
3 1262 08666 437 1